Techniques for MIR Rare Earth Doped Waveguide Lasers in Chalcogen based Glasses.

Huma Latif

May 2022

A thesis submitted for the degree of Doctor of Philosophy of

The Australian National University

Quantum Science Technology

Research School of Physics

College of Physical and Mathematical Sciences

The Australian National University

Declaration

The contents of this theses are the result of original research and have not been submitted for a higher degree to another university or institution. This thesis is entirely my own work, unless explicitly stated otherwise.

Huma Latif

May 2022.

I hated every minute of training. But I said don't quit. Suffer now and live the rest of your life as a Champion.

Muhammad Ali.

Acknowledgements

Prior to anyone else, I owe too much to almighty Allah who induced the man with Intelligence, Knowledge, and Wisdom, who bestowed upon me the ability to complete this tiresome task successfully and who is always there to listen to me in every critical phase of my life. Peace and blessing of Allah be upon the Prophet Muhammad (PBUH) who exhorted his followers to seek for knowledge from cradle to grave.

I deem it a rare privilege and source of great pleasure in expressing my profound and cordial gratitude to my supervisors: Prof. Steve Madden, A/Prof. Duk-Yong Choi and Dr KunlunYan not only for providing me with the opportunity to do research work but also for their dynamic elaborate me enlightening, suggestions, illustrious advice, persistent help, and constant encouragement during the whole course of my PhD study and research work.

This is my Pleasure to remember the College Dean (Prof Kiaran Kirk) and Director of the Physics Department (Prof Tim Senden), who allowed us and enhanced our morale to work in the Physics department. I would like to say thanks to the former (A/Prof Matthew Sellars) and current (Prof Andrew Truscott) HOD for their Constant Corporation and guidance. Thanks to Sukanta Debbarma for his unforgettable help in the fabrication and testing of films, and Craig and John for their assistance in fixing lab equipment. I am also thankful of our prior (Sonia Padrun) and current (Nikki Azzopardi) department administrators for their kind help and sincerity. Also, I want to acknowledge CAM staff (Frank, Jeff, and Hua) for providing access to the testing facilities of fabricated films and devices. I would like to thank the HDR team (Prof Patrick Kluth, Liudmila Mangos, and Karen Nulty) for their unforgettable assistance and care. It is hard to forget the

true love and friendship that I gained from the RSPhys store room (Goran and Patrick) and RSPhys kitchen (Gail and Jo) teams. I really appreciate that.

Moreover, I am thankful to Dr.Khu Vu and Dr Pan Ma, Chris Craig from Southampton University, Sean from Angstrom Engineering and Bin Gong from University of NSWs, Prof Jong Chow, Benjamin Young, and Prof Paul Francis for their precious time and support, which is unforgettable. I pledge my thanks to all my friends (in Pakistan and Australia) and colleagues (Choon Kong, Yile Zhong, Harry Dean and Hassan Iqbal). And I can never dare to degrade the help provided by seniors and juniors, CT lab mates, and also from gym members. I also thank all members of the Pakistan Society in Canberra and Pakistan embassy in Canberra for providing a home away from home. I express many thanks to members of Graduate House (especially Rob and Peter) for providing a friendly living environment for the duration I stayed here.

Last but not least I will always be thankful to my adorable parents, and my magnificent siblings for their tremendous help and care. Whole RSPhys is just like my family, so thank you so much everyone for your unwavering support and encouragement.

Abstract

Over the last 20 to 30 years, chalcogen based devices have received significant attention due to their promising properties and potential photonics applications in the MIR wavelength region covering 2 to 20 μm. Emission from rare earth doped materials has therefore been an active field of research, though achieving longer wavelength emission from planar waveguide devices has proven challenging. Several issues have emerged such as dopant clustering from either the deposition process or subsequent thermal processing, contamination, photoinduced absorption, and concentration dependent lifetime, all of which were explored in this work. The use of appropriate chalcogen based glasses as host materials with high rare-earth solubility but without photo induced absorption loss was previously identified as a necessity to get net gain. This work explores improved deposition techniques, film post processing and several tellurite and sulphide based host materials with better rare earth ion solubility to achieve these objectives.

One of the key goals of this thesis was to investigate and mitigate the effects of concentration dependent lifetime in rare earth doped chalcogen films to enable high gain and high-power on chip amplifiers to be built. A significant barrier to this in reactively sputtered films has been achieving good control over the film stoichiometry. The low concentration lifetimes achieved in this work are in fact more than double those of prior results obtained, which was a promising result. Poorer than expected results were observed at high Er concentration, and this coupled with inconsistent outcomes required improvement of the deposition system performance. Therefore, deep studies of issues in reactive sputtering and custom enhancement of the sputtering system were performed and means found to fabricate consistent and good quality undoped and Er doped tellurite films.

Given the previously promising performance of Er:As_2S_3 sputter deposited material, work was conducted to determine if Rapid Thermal Annealing (RTA) could overcome the known limitations of these films. RTA was systematically tested and the morphological and spectroscopic properties of fabricated and annealed films characterised. Post RTA treated samples were green light irradiated to investigate PL performance for comparison with prior results. Unfortunately RTA did not prove able to resolve the known issues with water ingress to the films.

Previous work identified that the doping of thermally evaporated As_2S_3 and other materials with low rare earth solubility needs to be performed with a rare earth doped compound rather than the metal to eliminate clustering from the evaporation source. Evaporation of erbium sulphide was therefore studied in detail. Depositions were performed at a series of crucible temperatures from 1800^{o}C down to 1550^{o}C. Whilst successful with the deposition of Er_2S_3, the work identified several and some unusual challenges which are poorly understood. Therefore another approach seems a better solution.

GeGaS glasses have high rare earth ion solubility and a short enough wavelength bandgap to avoid transient photoinduced absorption issues seen for example in Selenide based materials. Therefore, thermal evaporation of $Ge_{28.5}Ga_{6.2}S_{65.3}$ bulk glass was studied including the flash evaporation regime. Films fabricated at <1100^{o}C displayed significant stoichiometry variation as phase separation occurred in the crucible and the material remaining was pure Ga_2S_3. Even for flash evaporation where better stoichiometry was achieved there was genuine concern that the film does not have uniform composition through its depth. Therefore it was not investigated further.

Gallium Lanthanum Sulphide (GLS) has long been considered as one of the most promising candidates for chalcogenide RE doped devices. RF sputtering was used to fabricate undoped and doped films at varying Er concentrations and lifetime

and PL properties of Er-doped GLS films were systematically investigated. erbium concentrations up to 1.3 x 10^{22} ions/cm^3 were explored. Thermal annealing at different temperatures was carried out to study its impacts on PL properties to optimise the annealing condition. The emission spectra of all Er:GLS annealed films under 1490 nm excitation was measured, which produced extraordinary spectra in terms of the strength and number of peaks in the UV/Vis/NIR region as compared to previously published results. Long lifetimes were observed even into the blue part of the spectrum suggesting these doped films are promising for achieving MIR emission. The films were however found to have a high oxygen content (seemingly present as both oxides and hydroxyl groups) which prevent MIR emission. The most likely source of high oxygen concentration was explored and mitigation strategies discussed. Fabricated films with oxide content identical to the target material and therefore low OH contamination were ultimately fabricated and characterized with attendant care, but it is also clear specifically from fluorescence data that sulphide chalcogenide glasses suffer OH contamination problem to a much greater extent than for example tellurium dioxide sputtered films.

Major outcomes:

- Consistent process to fabricate high quality material, best ever observed lifetimes in Er:TeO_2.
- RTA was systematically tested to overcome known limitations of Er: As_2S_3 sputtered films, shown to be ineffective and results in RE clustering under all conditions that may be of interest.
- Successfully evaporated Er_2S_3, identified many challenges.
- Thermal evaporation of GeGaS glass proven to be infeasible due to phase separation in the glass melt in the crucible and loss of one species before the others. Better stoichiometry was achieved by flash evaporation, but the film likely does not have uniform composition through its depth.

- ❖ Promising results from highly doped GLS fabricated films, best emission spectrum ever seen with good lifetime for many potential IR emissions.
- ❖ GLS deposition strategy for low OH contamination developed and proven, first emission with as deposited room temperature grown films demonstrated.

Table of Contents

Chapter 1: Introduction

1.1 Aim and the Focus of the Project.

Chalcogenide and Tellurite glasses are very well known and recognised materials for MIR emission with rare earth doping. Despite much promise, no amplification or lasing beyond 1550 nm has been achieved to date in chalcogenide glasses in any format, and only recently was 2mm emission achieved in tellurite planar devices. The aims of this project were therefore to experiment with different chalcogen based glasses (TeO_2, As_2S_3, GeGaS, Er_2S_3 and GaLaS) to overcome some of the identified limiting problems with the ambitious goal of demonstrating MIR emission and gain in waveguide devices. The detailed objectives towards this goal were better Er ion solubility, improved fabrication techniques (RF sputtering, thermal and co-thermal evaporation, flash evaporation) and film post processing (Thermal annealing, Rapid film consolidation) to overcome some of the known problems (such as dopant clustering, contamination, photoinduced absorption, and concentration dependent lifetime) faced in the past. Whilst good progress was made against several of these, the emission goal has not yet been achieved for reasons that will be covered later in the thesis

1.2 The Motivation of the Work

1.2.1 Background

The MIR region, spanning wavelengths from 2.5 μm to 25μm [1], covers the key spectroscopic region from approximately 4000 cm^{-1} to 400 cm^{-1} [2]. This coverage (figure 1.1a) makes the MIR important as the strong characteristic vibrational transitions of many important molecules lie here as well as two important atmospheric transmission windows from 3 – 5 μm and 8 – 13 μm. This makes it crucial for potential applications in spectroscopy, remote sensing, medical and

dental diagnostics and procedures, chemical and bimolecular sensing, security, and industrial process control (figure 1.1b), etc. [3].

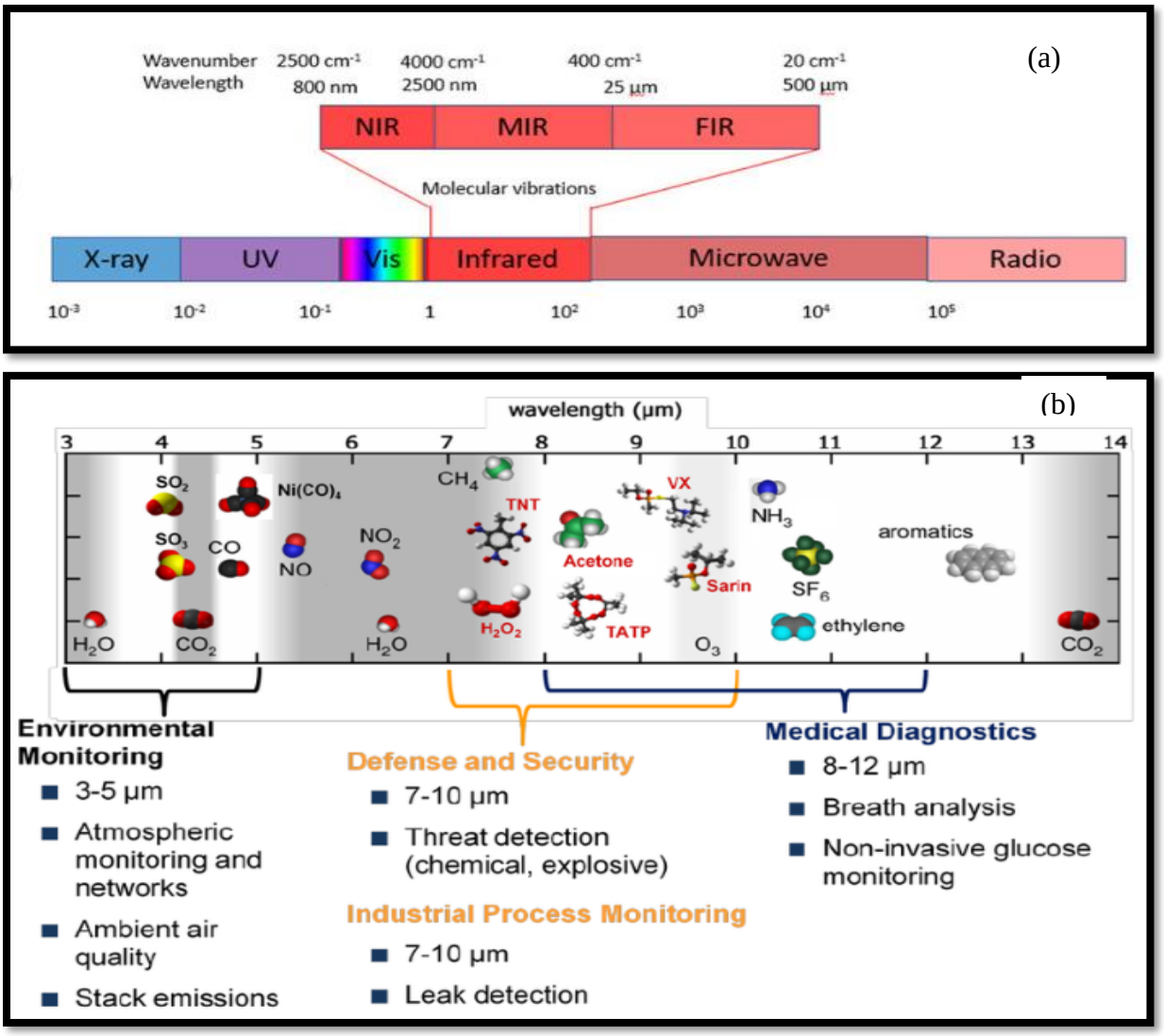

Figure 1.1: (a) Location of mid-infrared (MIR) in electro-magnetic spectrum [4] *and (b) potential applications and vibrational transition of many important molecules within two atmospheric transmission windows [1]* [5].

Though there are some existing and “in development” MIR source options such as fluoride glass fibre lasers [6], solid state lasers [7], quantum cascade lasers (QCL) [8], and optical parametric oscillator (OPO) [9], etc., these are not without their own disadvantages [10] in some cases including power scaling[11], narrow linewidth, tunability, cost, complexity, etc. [12]. QCLs are perhaps the most promising technology in terms of providing wide wavelength access from ~3-15 μm but they are often not widely tunable with narrow linewidth and cannot be mode locked to produce high energy short pulses as is needed for nonlinear processes to generate broadband MIR light or for parametric processes. Rare earth doped systems (fibre and waveguide) can fill this gap because they can offer a wide tuning range and high output power [13]. For example, Pr^{3+} offers a wide emission band in the 3-5 μm region, which has been demonstrated in Pr^{3+} doped GeAsGaSe chalcogenide fibres. This operation made this fibre a potential candidate for ASE sources and mid IR fibre laser amplifiers [14]. Recently, milliwatt level spontaneous emission providing full coverage of the range from 3.5-8 μm has been revealed in Pr^{3+} doped GeAsGaSe chalcogenide fibre under 1470 nm laser diode pumping [15]. Furthermore, , Pr^{3+} doped CW lasers have demonstrated >1W power outputs in the 3μm region [16] and Pr^{3+} doped mode locked fibre lasers also show mode locked operation centered at 2.867 μm [17] and 2.94 μm [18] with 2.5W output power respectively. Mode locked lasers [19] are also quite useful on account of their very large peak powers and femtosecond timescale pulses which enable damage free material processing [20]. In the MIR this makes them especially useful for medical applications such as surgery, dental tissue ablation etc [21].

Photonic integration [22] is rapidly expanding the horizons of optical systems into applications approaching consumer level deployment by leveraging much the same advantages as the silicon electronic circuit has (cost, size, power consumption, robustness, volume production, etc.). Considerable progress has been made in MIR integration utilising low MIR loss materials such as

chalcogenides (GeAsSe, GeAsS etc.) (waveguides with <1dB/cm up to ~10 microns demonstrated) for extremely sensitive sensors [23] and spectrometers [22,23]. Besides chalcogenide, there are several viable materials [26] platforms. For example, Aluminum Nitride (AIN) has demonstrated low propagation loss (0.83 dB/cm) at 2.5 μm [27]. Si based waveguides have been utilised for MIR gas sensors (N_2O) working at 3.7 μm with 69 mV/W responsivity[28], etc. Therefore, planar integratable MIR light sources with small dimensions, simple and robust construction, low price, high efficiency, high output power, broad tuning range and good quality output beams would be strongly advantageous and potentially enable widespread deployment of MIR sensing and other types of systems [29]. Of the options discussed above, only QCLs (integrated by flip chip bonding) [30] or rare earth doped glass devices [31] can potentially accomplish this in an integrated optics environment [32]. Given the other advantages of rare earths already highlighted, they are a natural candidate for deeper study as planar MIR sources.

1.3 Materials for MIR RE Planar Devices

A key requirement for planar integrated rare earth doped devices is the capacity to offer efficient performance at high dopant concentrations as planar devices typically have much higher propagation losses than fibre meaning that amplification typically has to be achieved in shorter lengths, ie higher doping is required than for fibres. In some chalcogen based glasses (e.g. GeGaSe [33] etc), the high solubility of rare earth ions (erbium etc.) > 2 at %, offers the potential of very high gain optical amplification and of achieving long wavelength emission due to very low phonon energy and broad transmission windows that is not possible in other glass host materials.

Generally, IR transmitting glasses are categorised into three groups: Halides (Fluorides and Chlorides), heavy metal oxides (Tellurite and (lead-) Germanate/Bismate) and Chalcogenides [34].

1.3.1 Fluoride Glasses

Fluoride glasses are well known and established materials most prominently used in IR fibres [35]. As materials for active and passive IR optics [36], these glasses are well established [6] due to their known interesting properties such as IR transparency to ~5 μm [37] and the potential doping of rare earth ions with up to 6 mol% [38]. Extensive previous research was focused mainly on fluorozirconate glasses, leading to successful demonstration of efficient MIR fibre lasers [6]. For example, 3μm CW and pulsed lasers have been reported using heavily doped (Er^{3+}) ZrF_4 based glass [33] by several research groups. Ho^{3+} doped ZBLAN fibre can also oscillate at 2.9 μm but with reduced slope efficiency at higher Ho concentrations [39]. Oscillation at 2.9 μm is also observed in Dy^{3+} doped ZBLAN fiber lasers but with low power and slope efficiency [40]. Significant challenges have been faced in prior studies in achieving transitions beyond 3 μm in fibre laser technology (e.g fluoride glasses [6]) [41].Whilst laser transitions at 3.45 μm [42] and 3.95 μm [43] have been achieved by Er^{3+} and Ho^{3+} doped fluoride fibre respectively, decreased output power and slope efficiency problems have been discovered. Many factors based on host material issue such as high phonon energy, high impurity, greater tendency to crystallisation, enhanced heat load with increasing dopant concentration and high quantum defects etc. have been observed, which significantly suppress laser operation beyond 3μm [44] in fluoride glasses. Despite these challenges, there is continuing effort to achieve good performance out of rare earth doped fluoride glasses beyond 3μm [45].

ZBLAN glass is one of the most stable fluoride glass and has a nonlinear refractive index comparable to silica [46]. Fluoride fibre is however brittle without coating and hygroscopic and it requires to be shielded from attack by moisture [6].

Tellurite [47] and chalcogenide [48] glasses are also known as promising materials for planar integration due to their expanded transparency out to potentially 7 microns for tellurites and 25 microns for chalcogenides. Both exhibit

strong nonlinear properties as well [49]. Both are relatively stable, and have high stability to atmospheric moisture, and chalcogenide glasses in particular can be engineered with a low propensity to crystallise [50].

1.3.2 Tellurite Glasses

Tellurite glasses (TeO_2 as the major constituent) are considered good candidates for the fabrication of high gain optical waveguide devices due to their many promising properties. Tellurite glasses have a broad transmission window, which reaches to ~6 μm in the mid IR region and tellurites can have much lower maximum phonon energy than silica [51] and can achieve laser operation well beyond 2000 nm [52] and this spectral region is quite useful for many prospective applications [53]. For example, 2.1-2.3 μm spectral range out of mid IR laser source is effective for deep imaging in biological tissues [54]. Remote gas detection (CO, C_2H_2), eye-safe LIDARs, and material processing can also be achieved with laser sources operating in the 2.2-2.7 μm mid IR spectral region [55].

Compared to other oxide glasses, tellurites have high linear and nonlinear refractive indices [56], low phonon energy, good IR transmittance [49], and greater stability than fluoride glasses [57]. Tellurites have high rare earth ion solubility [56] and an order of magnitude higher Raman gain than fused silica [58]. The low loss index guiding tellurite microstructured fibre achieved a nonlinearity $\gamma = 670\ (W.km)^{-1}$ with a loss of just 0.18 dB/m at 1550 nm [59] telecommunications window, which make tellurite an excellent candidate for the highly efficient and compact parametric devices.

The special case of being all chalcogen component glass, though usually classified as an oxide glass, tellurite glasses are well known to have a range of interesting properties [60] for fibre and planar waveguide devices, especially for optical amplification [61]. Tellurite erbium doped waveguide amplifiers (TEDWAs) can provide high gain (more than 15 dB already demonstrated from a 5 cm long device at 1550 nm) with potential for >10 dB/cm which is advantageous for short pulse

amplification, low cost amplifiers, as gain sections for on-chip mode locked or CW lasers, and for loss compensation in complex integrated optics devices [12]. Such devices are therefore key components in integrated optics [62]. Tellurites offer several advantages as emission hosts for EDWAs: high refractive index (~1.5-2 times higher emission cross section than silica and fluoride glasses [63] and more compact devices) [64], large emission bandwidth [65], low ion to ion cross relaxation [66], comparatively low dependence of the 1550 nm erbium lifetime on concentration, and high erbium solubility as has been demonstrated in tellurite glass and fibre amplifiers [67]. Tellurite is a better erbium host [68] than silica and can still achieve 3000+ nm emission [69]. Tellurites have demonstrated low loss waveguiding e.g ~0.1 dB/cm [70]and 0.6 dB/cm [71] at 1550 nm and 2000 nm respectively. These results make them very appropriate for planar integrated devices [70].

One established issue in tellurites revolves around hydroxyl ion (OH^-) contamination. Achieving sufficiently low OH concentration to prevent quenching of MIR emissions in rare earth doped oxide glasses requires special attention. For example, in the state of the art erbium doped tellurite glass, lasing at 3μm wavelength has been suppressed due to energy transfer from excited erbium ion to OH^- impurity [72], combined with the low radiative efficiency of the upper laser level [44].

1.3.3 Chalcogenide Glasses

Another class of glass hosts that offer good performance for the MIR are the chalcogenide glasses [73]. The chalcogen elements are the column of the periodic table encompassing sulphur, selenium, tellurium, and polonium. Chalcogenide glasses comprise amorphous materials where one of sulphur, selenium, and/or tellurium is alloyed with glass formers and network modifiers such as germanium, silicon, arsenic, or antimony. Such glasses have some of the lowest known phonon energies amongst glasses [74] and are highly transmissive to well beyond 8 microns [75] (figure 1.2, b).

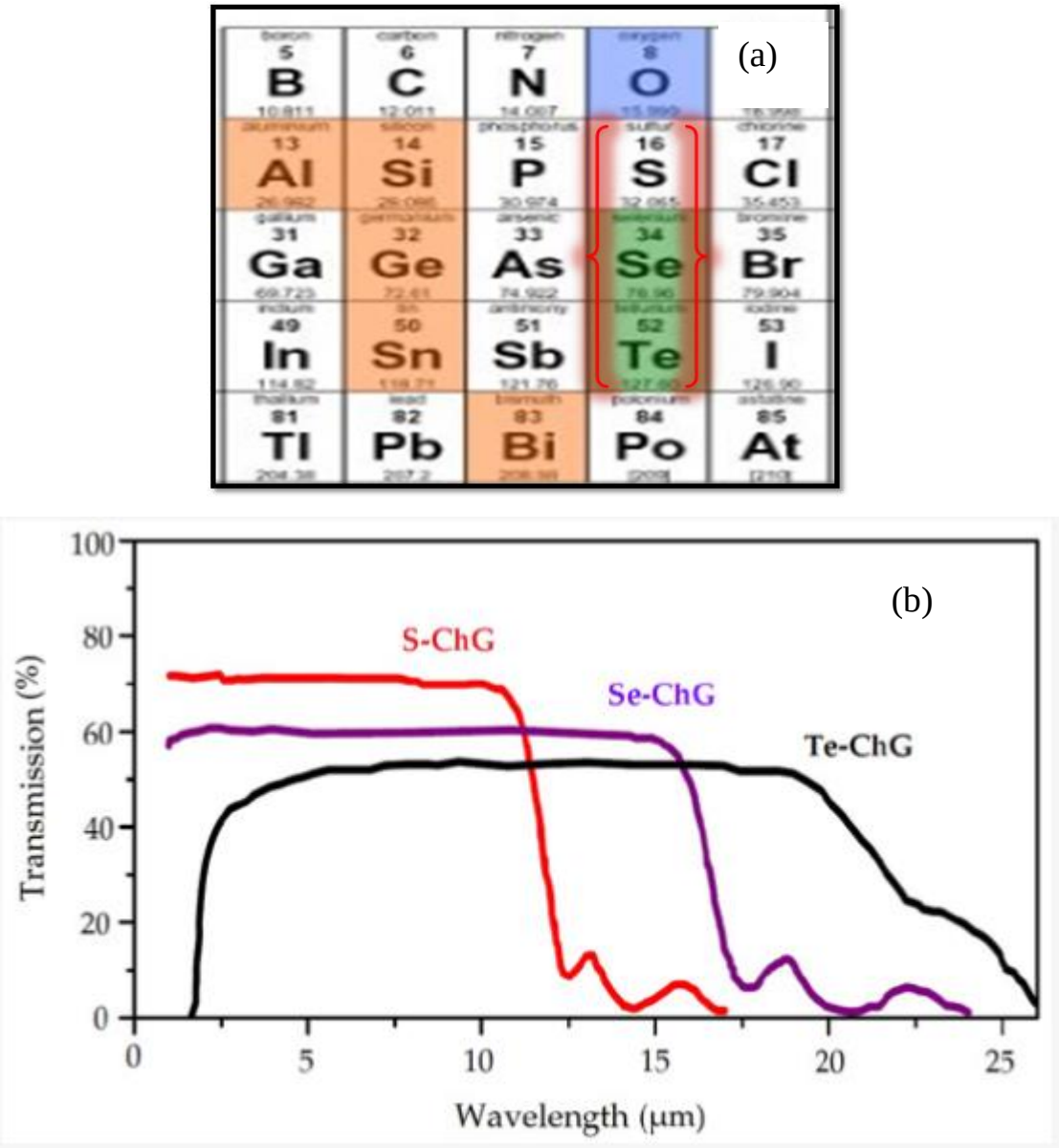

Figure 1.2: (a) Chalcogen elements in periodic table, (b) Typical IR transmission spectra of S, Se, and Te ChG millimeter-thick bulk samples [76].

This makes them of considerable interest for MIR photonic applications and those incorporating rare earth ion (REI) doping to build amplifiers and light sources in the MIR wavelength range [34].

Chalcogenide glasses possess good properties for MIR planar integration such as high (nonlinear) refractive index, low (nonlinear) absorption, the lowest phonon energies amongst glassy materials [3], wide optical transmission windows, relatively straightforward means to fabricate low loss waveguide devices [77], etc.

Chalcogenide glasses (As_2S_3, GeAsSe, and GeSbS in particular) have also received considerable attention for planar photonics MIR applications with several important capability demonstrations including MIR chemical sensing [24], supercontinuum generation [78], etc. The selected applications already described are purely exemplars; there exist many other emerging applications as diverse as more efficient solar energy collection [79], multifunctional optical fibres containing metal, insulator, and semiconductor components [80], or chalcogenide based “taste” sensors that already can distinguish between 29 varieties of wine [81]. As a result of the good potential of MIR transitions in rare earths in low phonon hosts, rare earth doped waveguide devices are therefore an important research area for the MIR.

1.3.4 Properties Comparison

In table 1.1, the basic properties of chalcogenide glass [82] compared to other glasses (silica [83][84], fluoride [85], and tellurite [86]) are displayed.

Table 1.1: Basic properties of chalcogenide glass compared to other glasses.

Property	Silica	Fluoride	Tellurite	Chalcogenide
Refractive Index	1.46 at 525 nm	~1.5	**1.8-2.3**	**2.1-3+**
Phonon Energy (cm^{-1})	1000	600	**~700-800**	**~250-425**
Transmission range (μm)	0.2-2.5	0.2-7.0	**0.4-5**	**0.8-20**
Bandgap (eV)	~10	~10	**~3**	**1-3**
Nonlinear Refractive index (n_2,m_2/W)	$1\text{-}3x10^{-20}$	$\sim10^{-21}$	**$3\text{-}6x10^{-19}$**	**$3\text{-}10x10^{-18}$**
Glass Transition (Tg, ^oC)	~1000	~300	**300-450**	**100-600**
Emission FWHM Bandwidth/nm (Er^{3+})	20	82	**80**	**45**

Chalcogenide glasses have low phonon energies due to large atomic masses and relatively weak bond strengths [87] [3]. The low phonon energies [73] present in chalcogenide glasses permit radiative transitions for rare earth ion dopants that are not possible in oxide and fluoride glasses due to multiphoton quenching or enhanced non-radiative decay [88]. Low phonon energy hosts are necessary to avoid thermal bridging of the emission transitions. For example the maximum phonon energy of chalcogenides glasses (S, Se) is 250-425 cm^{-1} compared to about 1100 cm^{-1} for silica for example. Target emission wavelengths for rare earth ion

laser operation would be up to ~6 μm (~1700 cm^{-1}) for the S glasses, ~8 μm (~1250 cm^{-1}) for Se glasses and ~11 μm (~900 cm^{-1}) for Se/Te glasses. Therefore, 1-2 phonons can effectively bridge the energy gaps for silica in all these emission ranges, whereas in chalcogenide glasses 3-4 phonons are required thereby vastly increasing the emission probability [1].

There are also non-MIR benefits to low phonon energies, which provide usable access to the higher level transitions in rare earth ions. Amplification in the second fibre optic telecom window at 1300 nm in Pr^{3+} is completely quenched in silica due to high non-radiative decay between the necessary rare earth energy levels [88] but high gain is possible in Fluoride fibre.

Tellurite glasses have shown emission at 3 microns [89] but fibre or planar devices have not yet been built [90]. Fluoride glass has been proven as a good host option for only up to 3 microns, Er doped ZBLAN fibre demonstrating the most powerful fibre laser sources built to date at 3 μm [1] achieving 24W continuous wave output [91]. But beyond 3 microns, multiphonon relaxation rates of Fluoride glass compete with the sharp line luminescence [1]. Therefore, host materials with lower phonon energy must be sought to enhance the radiative lifetime of the excited state in the mid IR region beyond 3 microns. The extended mid IR transitions have extensive applications such as below 2.9 μm is known as the molecular fingerprint region and expanded mid IR wavelength range to the 3.5 μm region is also crucial for molecular spectroscopy and material processing etc. [55]

Chalcogenide glasses can withstand temperatures in the range 200-600ºC depending on composition, are non-hygroscopic, chemically and mechanically durable, and have low toxicity [50]. High rare earth ion solubility into many chalcogenide glasses minimises the clustering and quenching effects, which potentially enables the fabrication of efficient MIR lasers and amplifiers [92]. These glasses have proven to be the best glass option for transparency far beyond

Fluoride glasses, allowing many potential mid IR transitions (0.7-6 μm (As-S) and 2-10 μm (GeAsSeTe) [50]) from rare earth ions [93]. Despite this promise, no amplification or lasing beyond 1550 nm has been achieved to date in chalcogenide glass in any format [92]. So further research is needed to obtain the amplification.

1.3.5 Rare Earth ion Choices

The selection of an appropriate rare earth ion for different applications is also important. The original driving force for making RE doped fibres was to make 1550 nm fibre amplifiers for which erbium was an excellent candidate [33].Huge amounts of research in RE doped glasses has been performed, and a lot of that is around erbium [94] so erbium is very well understood [95]. For this reason, erbium was chosen as the ion for study in this project. There is however a range of other RE ions [96] of interest for other (MIR) applications [97] that will be discussed shortly.

Before venturing into MIR transitions, it is worth noting that there are advantages even at 1550 in moving to non silicate hosts. Unfortunately, commercially available silica based EDFAs have relatively narrow bandwidth (~35 nm) compared to the available low loss window [97]. Er^{3+} doped Fluoride fibre has been demonstrated extremely large 3 dB gain bandwidth of 75 nm [98]. However, due to fibre durability problems, this device did not receive much commercial attention [99]. erbium doped tellurite glass has a much larger emission cross section as compared to Er doped silicate and Fluoride glasses because of the large refractive index that impacts the large field correction factor [66]. The higher cross section translates directly to higher gain per unit length and/or high output power capabilities, which coupled with the much higher solubility than silica, enables very short gain sections. Tellurite also supports much wider gain bandwidth (~50 nm) [100], which is appropriate for the future transmission systems [101]. High power on-chip 1550 nm lasing [102] is also potentially useful as a pump wavelength for mid IR cascade supercontinuum generation [103] or for

other MIR transitions [104], which are useful for many potential applications (e.g chemical sensing, absorption spectroscopy etc.) [104].

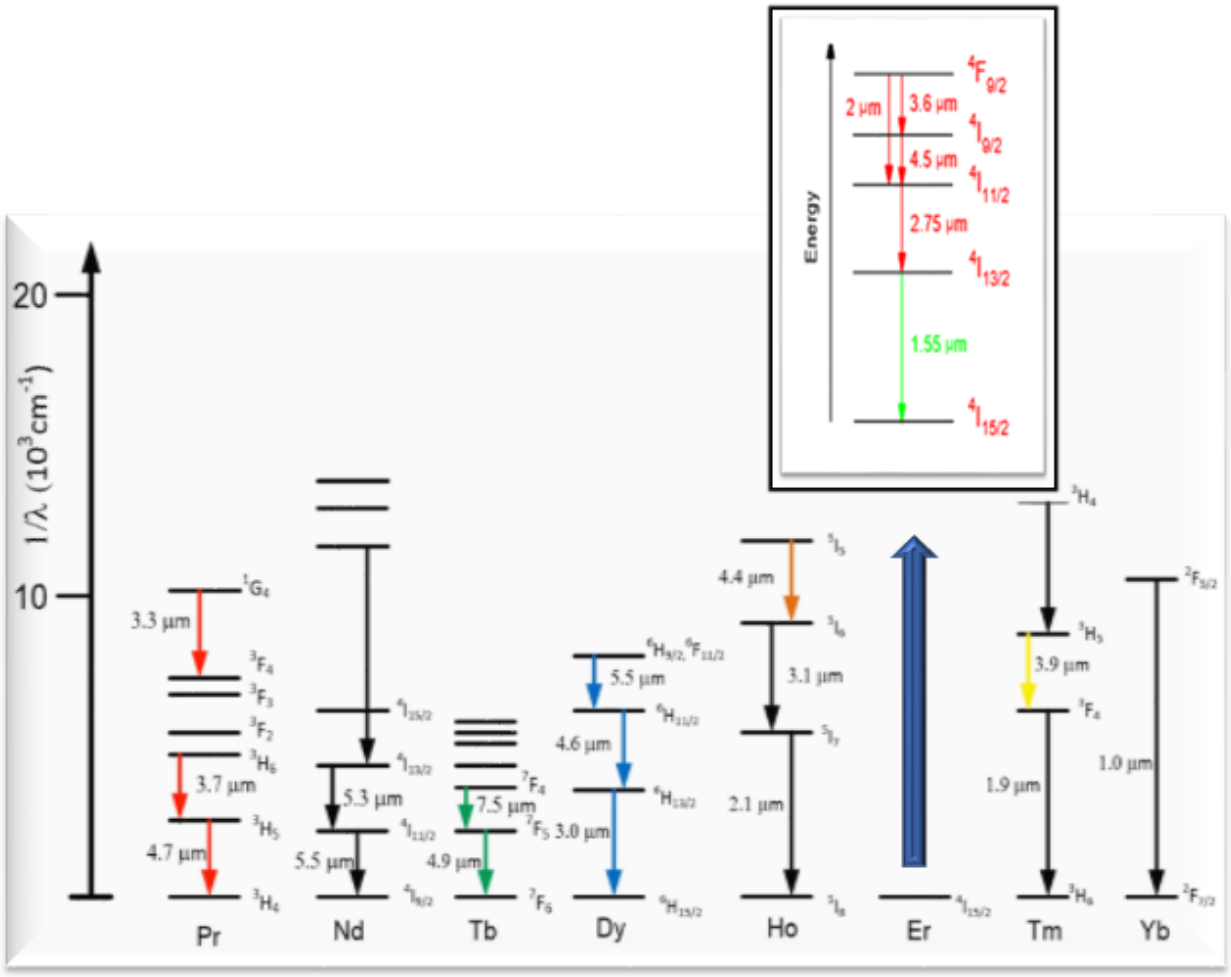

Figure 1.3: Range of MIR emissions of erbium and other REIs [1].

Erbium [105] also offers very useful MIR emissions [106]. Erbium and several of the more interesting REIs with potential emission wavelengths in the MIR region are shown in figure 1.3. Materials such as praseodymium (Pr^{3+}) offer the potential for broadly tunable and cascade lasing of MIR emission in the 3 um to ~ 5 um

range and beyond, offering a MIR equivalent to Ti:Sapphire [107]and so opening the possibility of ultrashort pulse mode locked MIR lasers. As previously realised, ultrashort pulses beyond 4 microns are also extremely useful for pumping direct broadband MIR supercontinuum generation[108]. Moreover, long wavelength transition (7 um) between F_3 to F_2 states has already been reported [109] due to the quadratic upconversion (H_6+ H_6 to F_3 + H_5) process in the low phonon host material, which is useful for commercial and military applications.

Terbium (Tb^{3+}) also has a rich variety of mid IR transitions. The transition from F_3 to F_4 centered at 10.5 micron has been found active in the lower phonon energy glass host due to the small energy gap between these states. Moreover, the transition between F_5 to F_6 and F_4 to F_5 showed high cross section, long lifetime and adequate quantum efficiency in many (sulphide and selenide, etc.) glasses and these properties are highly beneficial for efficient laser operation[110]. Moreover, another active rare earth dopant called dysprosium (Dy^{3+}) ion also have the potential to cover wide (up to 5 um) transmission window in highly doped and having low phonon energy glasses [111], which is beneficial for remote and environmental sensing operations [96].

So, there is a good range of mid IR transitions available (fig 1.3), whereas as discussed earlier that this thesis is focused on erbium, which is the perfect candidate for 1550 nm emission. In terms of using 1550 nm studies as a gateway to longer wavelengths, it is required to choose compatible host material with unique optical properties. Such as low phonon energies, high rare earth solubility, high linear refractive index, and optical nonlinearity [31], etc., which are found in predominantly chalcogenide and tellurite glasses make them very good host materials for rare earth doped planar devices with high efficiency in short length waveguides for amplifiers operating in MIR region. Moreover, High optical nonlinearity is not required for lasers/amplifiers but many MIR applications require broadband sources that can be generated with optical nonlinearity though processes such

as supercontinuum generation. Therefore nonlinearity is useful but not essential for lasers [112].

It is also important to understand the background work to this thesis in particular with erbium doping in thin films in these materials.

1.4 Previous Research Achievements

1.4.1Building on Past Chalcogenide Research

It is important to highlight the history of rare earth doped chalcogenide based glass, fibre and planar waveguides as these provide pertinent background to the work in this thesis.

The first laser action in a chalcogenide glass was reported in neodymium doped gallium lanthanum sulphide (GLS) glass at 1080 nm in 1996 [113]. Here a 1.42 mm thick GLS sample doped with 1.5 mol % ($2.6x10^{20}$ $ionscm^{-3}$) neodymium was pumped with a Ti: Sapphire laser at 890 nm. Laser action from the transition between $^4F_{3/2}$ an$^4I_{11/2}$ levels was observed. It was suggested by the authors that laser results could be improved with a longer pump wavelength. Longer pump wavelength can directly excite the upper laser level without generating heat through the multiphonon relaxation from $^2H_{9/2}$, $^4F_{5/2}$ to the upper laser level $^4F_{3/2}$. At 890 nm pump wavelength, the smaller absorption coefficient reduced the thermal load on the glass and led to a more homogeneous excitation of the sample. The authors also measured the dependence of output power on absorbed pump power, where only 50% pump power was absorbed at 890 nm. The measurements were also repeated at 815 nm pump wavelength where 80% pump power was absorbed. Under this condition, laser action ceased at high pump power (output power dropped to 0.7 mW) illustrating the nature of the thermal effects in the glass. Moreover, it was suggested that improvement in laser action was possible by optimising the doping concentration and the length of the sample. These results were the first step towards the realisation of chalcogenide based lasers operating at new wavelengths and 1300 nm amplifiers for the telecommunication based on

GLS glass fibres. The same authors also subsequently demonstrated a purification scheme [114] to remove loss sources (absorption and scattering) in the GLS glasses to make these glasses the material of choice for various promising applications [115].

Then in 2000, optical amplification was achieved in single mode praseodymium (750 ppm wt) doped gallium sodium sulphide (GNS) fibre at 1340 nm [116] pumped with a laser diode at 1012 nm. The background losses of the fabricated fibre at 1340 nm were ~1.4 dB/m. A gain coefficient of 0.81 dB/mW and a net gain of 30dB at a pump power of less than 100 mW were achieved, performance sufficient for telecoms type applications.

Lasing was also attained in a laser inscribed planar channel waveguide 16 mm long in neodymium doped gallium lanthanum sulphide bulk glass ($5.1x10^{19}$ ions/cm^3) at 1075 nm in 2002 [117]. A maximum laser output of 8.6 mW for an absorbed pump power of 89 m W was observed with 814 nm pumping. A slope efficiency of 17% was attained with attenuation in the fabricated waveguides measured to be less than 0.5 dB/cm. A peak emission cross section of $5.9x10^{-20}$ cm^2 was calculated from a Judd–Ofelt analysis. Thus, it was suggested by the authors that with the combination of high refractive index, low phonon energy, and the relative ease of fabricating high-quality low-loss waveguides, GLS glass is definitely a promising candidate for efficient active Integrated Optic devices.

Thereafter, there was a lot of research trying to obtain gain at longer wavelengths in chalcogenides, and some in planar tellurite devices but no one succeeded in accomplishing this until the work described below at ANU.

1.4.2 Prior Work at ANU

In 2010, net gain (2.8 dB/cm) at 1550 nm was obtained for the first time in 5cm long Er doped ($2.2x10^{20}$ ions/cm^3) tellurite planar rib waveguide amplifiers, also with wide bandwidth operation when pumped at 1490 nm [69]. The measured 1/e lifetime of the film with 1490 nm pumping was 2.1 ms at 1550 nm at 919 kW/cm^2.

Though the measured 1/e lifetime was lower than the ~4 ms 1/e lifetimes reported in some multicomponent tellurite glasses [66], the actual lifetime in pure TeO_2 does not seem to have been previously reported and would be expected to be shorter due to the higher refractive index. Furthermore, it was also reported that with increasing Er concentration the lifetime was decreasing strongly. This was examined and the reason was confirmed after observing the absorption dip centered at 1290 nm, this showing the presence of significant OH contamination in the tellurite films. This was initially found to be due to water contamination in the sputtering gasses which was improved with appropriate gas purification [69]. It was suggested by the authors that more than 30dB of gain could be achievable by doping with a higher Er concentration, improving the lifetime through improved film fabrication to reduce OH contamination and to achieve consistent film stoichiometry, by better waveguide structure, and by using a non-resonant pumping scheme to attain higher inversion levels.

In chalcogenide glasses, in 2015 internal gain at 1550 nm was reported for the first time in low loss erbium doped (1.8×10^{20} ions/cm^3) arsenic tri-sulphide (As_2S_3) strip loaded waveguides 2.8 cm long when pumped at 1490 nm. This glass was used as it has a long history of making very low loss waveguides including the lowest ever reported optical loss at 1550 nm [118] of 0.05 dB/cm. Though it is the first Complementary Metal Oxide Semiconductor (CMOS) [119] compatible chalcogenide waveguide amplifier only low gain [120] was achieved due to erbium clustering during the film deposition [121], and the very limited erbium solubility (below 0.45×10^{20} ions/cm^3) [120] preventing dispersal by annealing.

Later in 2016 strip loaded 26 mm long Er doped germanium gallium selenide (GeGaSe) waveguides were fabricated, this chalcogenide glass overcoming the solubility issues in the prior experiment. High inversion (55%) and good erbium solubility (0.5 to 0.75 mol%) were reported under 1505 nm excitation. However, a big problem that no one ever reported before was encountered, which was high

optically induced absorption from upconverted pump light which was sufficient to counteract the gain, thus no net internal gain was achieved [33].

In the work described, that is why most of the effort was expended on experimentation with different, several significant problems arose that need to be resolved to make these materials into practical MIR gain platforms.

1.5 Details of Obstacles to Attaining Desired Performance.

Table 1.2 lists the significant problems faced in prior work that required to be resolved to fabricate promising IO devices in the MIR wavelength range.

Table 1.2: Emerging challenges from prior work.

Material/s	Challenges	Detail	Result
TeO_2	Contamination Issues	OH group in Tellurite and OH/SH in chalcogenide	MIR emission quenching, reduced lifetime
GeGaSe	Optical Absorption Issues	Up conversion induced Absorption	Quantum efficiency and gain reduced/eliminated
As_2S_3	Film Deposition Issues	Clustering during deposition	
		Columnar structure	
As_2S_3	Solubility and Contamination Issues	Inability to anneal to homogenise dopants	

The work in this thesis explores potential solutions to these issues. Several paths were explored, some successful and some not as is the nature of research. The detail around these issues is now discussed.

- Contamination issues were evident in prior work in the form of OH contamination in deposited films and waveguides. Initial results for tellurite showed that the sputter gas supply was the root of the problem despite this being high purity 99.999% gas. Installation of a gas purifier enabled the first high quality results to be obtained. However, it became clear that this was not the entire story. Hydroxyl groups can also be formed or enter the glass from the source materials, background vacuum leakage or physical water desorption from the vacuum system surfaces, or by in diffusion after film growth. The roles and impact of these mechanisms have not been quantified in the literature, and further work is required to understand and eliminate them.
- The maximum usable doping level is also of particular interest as this ultimately limits the output power potential of propagation loss limited devices such as planar waveguide amplifiers. There are mechanisms such as pairing effects that are inherent to certain deposition processes e.g. [122], and the onset of clustering from exceeding the solubility limit is not necessarily the effect that defines the maximum usable concentration. Despite high gain amplification being demonstrated in thin film waveguides [38], there remain unanswered questions about the performance limits. Maximum usable REI (Er) concentration (without clustering/crystallisation or concentration quenching), pump efficiency, gain dependence on doping are perhaps the main ones. The origins and amelioration of these issues are therefore a part of the work discussed in this thesis.
- Up conversion processes were observed to induce high optical absorption in Er doped GeGaSe films and waveguides [2]. These glasses were initially investigated for their much higher RE solubility and therefore the ability to anneal them to disperse REI clusters. Transient optically induced absorption was previously observed with external light close to or above the bandgap energy. This effect had been observed to be particularly bad

in glasses containing both germanium and selenium, but there is an absence of detailed information as to what drives this process or which materials, in particular, do not exhibit it (though anecdotally it has not been observed in Sulphur glasses used by the group). The high intensity of up conversion related emissions which are trapped within the waveguide can lead to absorption in the 1-5 dB/cm range, enough to nullify the internal gain in the device as was observed in previous studies [12]. Clearly, a solution to this issue is necessary to exploit hosts with higher RE solubility [123]. This means that host materials that do not exhibit this effect have to be found and experimented upon.

- RF sputtered Er doped As_2S_3 films showed great promise in terms of their photoluminescence properties and doping level behaviour, much more so than thermally evaporated films [2]. However, they displayed an unexpected property in that moisture from the air could be incorporated into the glass as hydroxyl groups, this being driven by the presence of upconverted green light. This effect could quench all emissions from the material. Though the films appeared dense under the SEM, the effect was presumed to arise from a nano-columnar structure that formed during deposition as this is not uncommon for sputtered films. Thus, the question of whether post deposition rapid thermal annealing could densify the material without allowing the erbium to precipitate needs to be investigated as the performance is otherwise excellent with a clear path to low loss waveguide devices.

1.6 Proposed Solutions

The use of the appropriate chalcogenides as a host glass with high rare earth solubility without clustering was previously identified as a necessity to get net gain without photoinduced absorption loss. chalcogenide glasses are well known

to have the lowest phonon energies amongst glassy materials and are therefore a key element for emission in the mid and far infrared region.

Three main routes were considered to attempt to overcome the prior issues:

- Improved or alternate deposition techniques (TeO_2, As_2S_3, GeGaS and GLS)
- Rapid film consolidation methods (As_2S_3)
- Modified composition or alternative glass host materials (ErS, GeGaS and GLS)

Given the range of issues identified above and the very different maturities of tellurite and chalcogenide technologies in terms of demonstrations of high performance amplifiers and on chip lasers, a clear set of research tasks were identifiable that form the basis of this thesis.

- Refine RF sputtering of Er doped tellurite films and determine maximum usable concentration and means to eliminate remnant OH contamination to obtain 2700 nm gain and high output power capability for on-chip supercontinuum pumping
- Investigate Thermally evaporated Er:As_2S_3 devices using Er_2S_3 as dopant instead of Er metal to avoid the polyatomic evaporation based clustering.
- Investigate non-precipitating consolidation of RF sputtered Er doped As_2S_3 films
- Research thermally evaporated Er doped GeGaS films which have much higher RE solubility so can be annealed and which also appear to have low transient light induced absorption
- Explore RF sputtered Er doped GaLaS as a host as it has shown promise in other work, has high solubility, and has proven very low transient light induced absorption.

Many people tried; many people failed over the last 30 years to realise gain in RE doped chalcogenides beyond 1300 nm with no results in the MIR. For this reason,

tellurite is pursued as an option to 2700 nm and perhaps 3400 nm as good 1550 nm on chip amplification and lasing has already been achieved. Further high power output at 1500 nm could also achieve MIR supercontinuum generation through the use of cascaded processes and so is also of importance [124] [125]. Emission at ~3000 nm is long enough to enable efficient single stage on chip supercontinuum generation and laser surgery sources [127]. However, tellurite will not extend past this region due to its higher phonon energy. In terms of the chalcogenides which can reach further, the right approach is not clear. Hence several approaches based on the previously promising methods are investigated in this thesis. The two most promising approaches were planned to progress to the next stage where waveguide and amplifier testing will occur.

1.7 Outline of Thesis Chapters

The rest of this thesis is structured as follows:

Chapter 2: This Chapter presents a brief literature review of some of the key papers in the field of chalcogenide based rare earth doped glasses that highlights some of the most important knowledge in the field.

Chapter 3: One of the key goals of this thesis was to investigate and mitigate the effects of concentration dependent lifetime decrease in rare earth doped chalcogen films to enable high gain and high-power on chip amplifiers to be built. Therefore, undoped and tellurite films doped with different Er concentrations were fabricated by RF sputtering where structural and optical properties were carefully characterised. Whilst many issues were encountered in the growth of tellurite and Er doped tellurite films, results were obtained in pure tellurite glass that represent the best ever seen for tellurite films and information was obtained on the concentration dependent doping of tellurite films. Studies of inconsistency from run to run in reactive sputtering and the need for revisions in the deposition

system were also part of the work. Much more consistent sputtering of tellurite and Er doped tellurite was required and ultimately achieved to study concentration dependent effects.

Chapter 4 (part a): Given the previously promising performance of Er:As_2S_3 sputter deposited material, work was conducted to examine the impact of Rapid Thermal Annealing (RTA) on the photoluminescence properties of these films. The goal was to try and develop a process to eliminate the incorporation of OH groups by upconverted light observed in prior studies which was not observed in thermally evaporated materials. In this chapter, RTA was tested systematically (time and temperature based) and the morphological and spectroscopic properties of fabricated and annealed films characterised.

Chapter 4 (part b): The use of appropriate host glasses with high rare earth ion solubility and low photo-induced absorption was previously identified as an alternative route to get good results. GeGaS glasses are anticipated to be good materials for this purpose as well as having a bandgap at short enough wavelengths to avoid transient photoinduced absorption issues. Thus, work was required to develop deposition methods for these materials and is described in this chapter along with the issues encountered.

Chapter 5: Previous work highlighted that the doping of thermally evaporated chalcogenide films needs to be performed with rare earth doped compounds rather than using a pure metal source to eliminate clustering from the evaporation source. Thus, work was conducted on evaporating erbium sulphide, which was previously very problematic. This chapter presents work on extending the initial studies on this and several new and in some cases unexplained difficulties encountered.

Chapter 6: GLS glasses have long been considered as excellent hosts for chalcogenide RE doped devices and this chapter describes work towards building a planar device from GLS. RF sputtering processes are developed and films with

different Er concentrations are studied producing some very interesting results in terms of potential dopant concentration and photoluminescence lifetimes of upper Er levels. It was also found that fabricated films can easily become highly contaminated by oxygen (presumed to be in OH), which was confirmed by XPS and WDS. Moreover, a potential cause of high oxygen concentration in Er doped GLS films is explored and mitigation strategies discussed. Fabricated films with oxygen content identical to the target material were ultimately fabricated and characterised.

Chapter 7: This chapter is comprised of a summary of the main challenges, achievements, and future work required to achieve the desired MIR waveguide amplifier and chip based MIR lasers.

Chapter 2: Literature Review

2.1 MIR emission from Er doped Chalcogenides

Chalcogenide hosts, especially those doped with gallium (GaLaS (GLS), GeGaS, and GeGaSe) have received significant attention [128] because they accept very high [3] rare earth ion concentrations (Er, Dy and Pr, etc) [129] without clustering [130] and showed long PL decay time at 1550 nm emission wavelength [131]. Whilst the gallium containing materials are promising, the more mature platforms should also not be discounted.As_2S_3 is the workhorse material for studies into chalcogenide planar waveguide nonlinear optics with the advantage for rare earth doped applications of a bandgap in the green. Therefore, all tail absorption processes are low at common rare earth pump wavelengths. Furthermore, it has transparency up to 10 µm, a high refractive index, low phonon energy, good chemical stability, is easily patterned into low loss planar waveguides, has a low absorption coefficient of ~ 0.01 cm^{-1} at 1535 nm, and can be formed into fibres [132].

Aside from the papers already highlighted in terms of MIR emissions from chalcogenide hosts, there are a number of other key papers. A literature review of the more important works based on emission at MIR wavelength from Er doped chalcogenide glasses and films/waveguides is now presented.

Bulk glass/fibre

Ye et al [133] in 1996 studied Er doped ($0.94x10^{21}$ ions/cm^3) GLS (70 Ga_2S_3:30La_2S_3) glass to examine the potential of this glass for mid infrared applications. This appears to be the first time 2700 nm emission was observed in chalcogenide glass, this enabled by the long PL lifetime (1.23 ms) and high radiative quantum efficiency (14%) of the $^4I_{11/2}$ level. Five times higher radiative

decay rates, which were calculated based on Judd-Ofelt theory [134], compared to silica [135] was observed due to increased refractive index (2.35), along with three times lower nonradiative decay rates due to lower phonon energy (425 cm^{-1}). Moreover, five times shorter PL lifetime of $^4I_{13/2}$ level (2.3 ms), and 2.5 times higher emission and absorption cross sections ($15.7x10^{-21}$ cm^2) were measured at 1540 nm than the average value for silicate glasses. Thus, this glass can be used as a short wavelength amplifier, saturable absorber, and for long (mid IIR) wavelength lasers as well. Besides this, ion-ion effects have also been uncovered in this work where Er ion cooperative upconversion (Donor: $I_{13/2}$-$I_{15/2}$, Acceptor: $I_{13/2}$-$I_{9/2}$) was stated as the biggest hurdle in achieving amplification at 1540 nm. However, the doped GLS glass having high Er concentration, so the low level of ion-pair up conversion was confirmed due to existence of inverse energy exchange process (Donor: $I_{9/2}$-$I_{13/2}$, Acceptor: $I_{15/2}$-$I_{3/2}$), which dynamically suppressed the dissipative effect of cooperative upconversion. Thus, high solubility and the presence of an inverse energy transfer process were shown to make this doped glass a promising choice for the fabrication of a highly efficient 1540 nm fibre/waveguide amplifiers and lasers.

In 1997 Schweizer et al [105] showed the potential of Er doped ($1.81x10^{21}$ ions/cm^3) GLS glass as a high quality, stable, non-toxic, low phonon energy ($425cm^{-1}$), high solubility, high refractive index (2.4), and non-hygroscopic doped host material for the fabrication of MIR sources. In this work, specific mid IR transitions (2000 nm, 2750 nm, 3600 nm, and 44500 nm) were targeted for gas sensing, atmospheric transmission, and medical applications. For spectroscopic measurements, Er ions were excited first with DCM dye laser diode at 660 nm from ground to $F_{9/2}$ level, and three infrared Er^{3+} emission bands at 2000nm ($F_{9/2}$-$I_{11/2}$), 2750 nm ($F_{11/2}$-$I_{13/2}$), and 3600 nm ($F_{9/2}$-$I_{9/2}$) were detected. Pumping with a Ti:Sapphire laser at 810 nm also revealed the presence of 4500 nm mid IR emission. The radiative decay rates and radiative lifetimes of all transitions were also calculated based on Judd-Ofelt theory and then emission cross sections of

each transition were calculated from the radiative rates. Radiative and measured lifetimes were also used to calculate the branching ratios and quantum efficiencies [133]. It was concluded that the achieved branching ratios of 3600 nm and 4500 nm transitions were 0.4% and 1.0% with the measured lifetimes of 100 µs and 500 µs and cross sections of $0.45\times10^{-20}cm^2$ and $0.25\times10^{-20}cm^2$, respectively. The achieved results were the good agreement with the prior studies [136]. The measured lifetime of the $I_{9/2}$ level (500 µs) was longer than the lifetime of $F_{9/2}$ level (100 µs), which indicated that the non-radiative decay rates are quite low in GLS glass and decay rates are dominated by radiative decay. The branching ratios at 2000 nm and 2750 nm were 3.7% and 14.7% with measured lifetimes of 100 µs and 1230 µs and cross sections of $1.52\times10^{-20}cm^2$ and $1.10\times10^{-20}cm^2$, respectively. Light at 2000 nm, 2750 nm, 3600 nm, and 4500 nm has application in LIDAR systems, medical applications (strong water absorption in tissue), remote sensing and gas sensing of H_2S, NO, SO_2, CO and O_3 respectively. Thus, this paper provided the first analysis of the emission parameters for GLS doped glass and confirmed it as a suitable host for fabrication of mid IR sources.

Low phonon energy and high rare earth ion solubility had already been identified in prior studies as a requirement for Mid IR host materials and chalcogenide glasses were known as the best choice among other vitreous materials [137]. The GeGaS glass system had already been considered as an appropriate option by Zavadil et al [123]in 1999 to achieve good, rare earth ion incorporation in comparison to other sulphide glasses (e.g As_2S_3, $GeS_{2+x,}$ etc.). In 2008, Kasap et al [138] further studied the same glass and examined optical and photoluminescence properties of Er (2.1×10^{20} ions/cm^3) doped $Ge_{28}Ga_{6.2}S_{65.3}$ glass at 1550 nm. The glass used had stoichiometric composition because in 2005 it has been demonstrated by the same authors that stoichiometric glass is more capable of solubility up to ~2 at% Er concentration with the right amount of Ga content[139].The optical absorption spectrum was used to perform Judd-Ofelt (JO) analysis [140] to calculate the fluorescence lifetime and the values of the

intensity or JO parameters (Ω_λ) which allowed the authors to calculate the radiative fluorescence lifetimes. At 1550 nm, the calculated value was 2.6 ms and the low values of JO parameters confirmed that the used glass could be considered to be a strongly covalently bonded, but comparatively flexible host matrix.

In 2010, Seddon et al [1] reviewed the progress and challenges in the fabrication of rare earth doped chalcogenide glass mid IR fibre lasers. The significance of optimising the host material and material processing routes to prevent non-radiative decay and rare earth ion clustering was considered. For the first time the authors explained (i) the failure in developing GLS glass mid IR fibre lasers despite the very promising earlier experiments and measurements and (ii) recognised impurity multiphonon relaxation based processes as a previously unacknowledged barrier to MIR emission processes. The wide potential window (equal or less than 11000 nm) for rare earth ion laser operation was concluded for chalcogenide glasses due to minimum lattice phonon energy as compared to silica and Fluoride glasses. It was suggested that both glass quality and the lattice multiphonon relaxation rates were important in the lack of MIR lasing in rare earth doped GLS glasses, the former from impurities and the latter due to compositional decisions made to make fibre drawing easier. RE-doped gallium-lanthanum–sulphide-based glass fibres are made by preform-drawing and according to Hruby parameters [141], large T_x-T_g difference (where: T_x is the crystallisation onset temperature [142]) and T_g is glass transition temperature] is key here. The inclusion of high levels of oxide provides a high probability of effectively preventing crystallisation. Unfortunately, the oxide inclusion also has a relatively high maximum phonon energy and as the purpose of using GLS is to exploit low phonon energy to lase in the mid-IR, this could be problematic. It was not previously appreciated how damaging the oxide inclusion was in this respect, for example, fluorescence was measured at ~5000 nm (~2000 cm^{-1}) in Nd^{3+} doped GLS glasses but not in GLSO glasses due to increase in phonon energy close to 8.6 μm (1163 cm^{-1}) on adding of La_2O_3 to GLS glass [143]. Moreover,

the prediction was that fluorescence beyond 2100 nm (~4760 $cm^{-}1$) would not be possible in GLSO due to multi-phonon quenching. Thus, this paper exposed for the first time why prior research over a long period have failed to achieve Mid IR lasing in GLS glasses. After studying the optical loss spectrum of different doped chalcogenide glasses, it was also shown that extrinsic vibrational impurities such as O-H and S-H have the potential to create unwanted multiphonon fast relaxation from the excited state and damage the overall performance of mid IR laser devices.

In 2017, chalcogenide glasses $Ga_xSb_{(40-x)}S_{60}$: Er_y (GSS), where x = 4, 6, 8, 10, 12 mol% and y= 0, 0.1, 0.2, 0.3, 0.5, 1.0 mol% were studied to show the relationship between the structure, optical properties and composition of the glass by Jiao et al [144]. They also discussed the effect of the introduction of gallium and erbium content into the glassy network to investigate the relationship between glass structure and attaining useful mid IR emissions. Under 980 nm laser excitation the infrared emission spectra displayed two obvious emissions centered at 1550 nm and 2700 nm, and the emission intensity of these two transitions increased with increasing Ga content (fixed 0.2 mol% Er concentration). This was considered to be a consequence of the associated increase in edge sharing tetrahedral structures [145], which significantly improved the Er ion solubility in the chalcogenide glass matrix [146]. A drop in emission intensity at 1550 nm and 2750 nm wavelengths was observed due to clustering effects for a fixed 8 mol% Ga concentration when the Er concentration exceeded 0.5 mol% [147]. In prior studies [148] it was recommended to use Ga: RE ratios≥ 10:1 to enhance rare earth ion solubility and dispersal in Ga introduced sulphide glasses. The effects of exceeding critical Ga:RE limit were also confirmed by far infrared absorption spectra and high resolution transmission electron microscopy (HRTEM) images in the undoped films at varying Ga content (from 4 mol% to 12 mol%). In the far infrared absorption spectra the introduction of Ga kept the basic framework with no change of glass structure in the short range. However wide vibration band

(330–375 cm^{-1}) appeared in the films having more than 8 mol% Ga concentration, which belongs to [GaS_4] tetrahedron. The formation of same vibration unit was also identified with HRTEM images where a uniform amorphous state was seen in the lower Ga concentration sample (4 mol%) and gradual formation of [GaS4] units was observed with higher Ga concentrations. The vibration mode changes implied a change of the microstructure inside the glass host. So under the critical Ga:RE limit, the rare earth ions were dispersed evenly after connected with [GaS_4] structure. Thus the quenching effect was prevented and improvement in the infrared emission was observed. However, with exceeding critical Ga:RE limit when more erbium ions connected with [GaS_4] units, in which the latter cluster is inclined to generate concentration quenching. The paper therefore clearly identified the need for a balanced Ga:Er ratio in chalcogenide glasses to optimise the emissions in the MIR region.

In 2020, the highest doping level to date was investigated by Chen et al [149] in xEr_2O_3-$25La_2O_3$-$(75-x)Ga_2O_3$(x=0, 1, 3, 5, 10 mol%) glasses considered as a potential material for high power lasers or waveguide amplifiers. In terms of emission intensity, authors observed the strongest luminescence band at 1550 nm and weakest one at 2750 nm. Generally, it is hard to measure the emission at 2700 nm ($I_{11/2}$ to $I_{13/2}$ transition) due to self terminating process because of the shorter lifetime of the upper laser level ($I_{11/2}$) than the lower laser level ($I_{13/2}$) [150]. However, in the low phonon energy hosts the population inversion between the $^4I_{11/2}$ and $^4I_{13/2}$ levels can be increased with reducing absorption coefficient of OH and increasing Er concentration due to the occurrence of the Energy Transfer Up conversion (ETU) processes among the $I_{13/2}$ level. The ETU processes ($I_{13/2}+I_{13/2}\rightarrow I_{9/2}+I_{15/2}$, $I_{11/2}+I_{11/2}\rightarrow F_{7/2}+I_{15/2}$) occurred between two or more neighboring erbium ions, which depopulated the $I_{13/2}$ state and repopulated the $I_{11/2}$ state [151] as shown in figure 2.1.

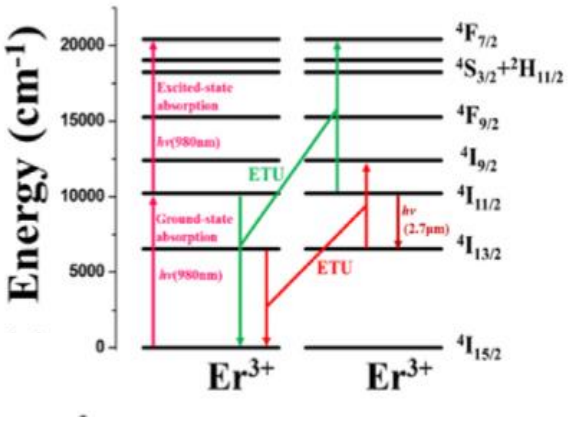

Figure 2.1: Energy level diagram of erbium doped GLSO glasses.

Thereby increasing 2750 nm inversion and emission. Moreover, authors detected the decrease in intensity of 1550 nm ($I_{13/2}$ to $I_{15/2}$) emission band and fluorescence lifetime (ms) with increasing Er concentration (equal or more than 5 mol%) due to concentration quenching at higher Er concentration. However, the longest lifetime (5.91 ms) of $I_{13/2}$ level at 3 at% ($3.01x10^{20}$ ions/cm^3) of Er concentration compared to other glasses having low phonon energy was observed [152]. Thus, these studies make this doped glass as a potential substrate material especially for the fabrication of C-band EDWA or high-power laser.

Overall it is concluded from above studies that chalcogenide glasses can satisfy the requirement for MIR emission due to potential properties such as high are earth ion solubility, high refractive index, low phonon energy and long fluorescence lifetime etc. for the fabrication of high power laser sources.

Thin films /deposited waveguides

Relatively little published work exists on rare earth doped chalcogenide films and waveguides. In 1998, photoluminescence properties at 1550 nm were studied for the first time in thin films, which were fabricated from Er doped chalcogenide glasses using sputtering (Ramachandran et al [153]) and co-evaporation [154] methods. Later in 2000, Fick et al [155] followed already published work [156] and enlarged their prior work by fabricating Er doped As_2S_3 films by thermal evaporation followed by ion implantation. According to prior studies[157], the evaporation of rare earth doped chalcogenide glass leads to nearly undoped films and therefore, the authors decided to use the ion-implantation technique for rare earth ion doping (Er: $5.2x10^{18}$ ions/cm^3) in the fabricated films. The films were thermally annealed at 165^{o}C for 2 h after implantation with subsequent cooling at a rate of 1^{o}C/min. The spectroscopic properties of the fabricated and annealed films were characterised under 983 nm pumping. The prior work [158] was used to calculate the absolute emission cross-section value ($13x10^{-21}$ cm^2) of as implanted As_2S_3 film. Though a small decrease of emission cross-section value ($11x10^{-21}$ cm^2) was confirmed in annealed films, these values are two times higher than the Er peak emission cross section value of Er doped Al/P doped silica or Fluorophosphate glass fibres [158] due to the higher linear refractive index of As_2S_3 glass (n=2.41). Additionally, PL intensity increased numerously in thermally annealed implanted films as compared to as implanted films. The PL intensity increase was attributed to the "activation" of erbium ions as already reported for soda lime silica fibre [157].The measured lifetime of $I_{13/2}$ level of as deposited implanted film was 1.9 ms, which increased after annealing to 2.3 ms. The measured $I_{13/2}$ state lifetimes was ~ five times lower than for Er doped silica [159]. This is again because of the higher refractive index of chalcogenide glasses, which increased the oscillator strength of the radiative ($I_{13/2}$-$I_{15/2}$) transition. Importantly, in an annealed film 2700 nm emission was detected and the $I_{11/2}$ to $I_{13/2}$ level lifetime measured at 0.28 ms. This represents the very first

measurement of MIR emission from a chalcogenide thin film and with acceptable lifetimes and indicates that there is real potential for planar MIR lasers.

Fuchs et al [160] discussed spectral properties of RF sputtered Er ($2.2x10^{20}$ ions/cm^3) doped As_2S_3 films from where non-columnar structures were confirmed by AFM of the sputtered films in 2004. The doping was achieved by placing an Er foil piece on top of the As_2S_3 target surface. It is well known that As_2S_3 has low REI solubility[3]that is why before thermal annealing, the PL intensity was hardly measurable due to clustering issue. However, after thermal annealing (at 165°C for 2 hours, just below the T_g of As_2S_3 at 172°C), PL intensity increased up to 40x at 1550 nm in a slab waveguide geometry due to lack of clustering. It was suggested that annealing "activated" the Er ions leading to improvement in Er $^4I_{13/2}$ lifetime (4 ms) was observed when pumped at 977 nm, though the nature of this activation was not discussed. It was suggested by the authors that PL intensity and lifetime will be further improved with decreasing Er concentration (< $2.2x10^{20}$ ions/cm^3) as PL intensity depends upon the distribution of Er ions in the films.

Frantz et al [161] in 2006, studied RF sputtered thin films ($70Ga_2S_3$:$23La_2S_3$:$6La_2O_3$:$1Er_2S_3$ doped target) where the substrate temperature was maintained at 100°C during deposition to study the surface quality and fluorescence lifetime of the 1550 nm and 2700 nm emissions at 1480 nm pump wavelength. The sputtered films were glassy, without crystalline diffraction peaks and apparent bulk scattering losses. Waveguides were fabricated via the lift off technique. The first demonstration of a measured enhancement factor (ratio of output with pump on and pump off) at 2.8 dB/cm was achieved for a 1550 nm signal in an Er doped chalcogenide glass waveguide. However, the achieved enhancement was insufficient to overcome waveguide fabrication induced side wall scattering losses and the Er absorption loss in the waveguide so no internal gain was observed. The fluorescence lifetime at 1550 nm was 1.1 ms but unfortunately, no measurement was possible at 2700 nm the precise reasons for

this not being entirely clear. This paper thus demonstrated the potential for making rare earth doped waveguides in GLS that should, after further development, ultimately be able to have actual gain.

In 2011, Yan et al [162] investigated Er (0.1, 0.2 and 0.4 mol%) ion implanted, thermally evaporated $Ge_{11.5}As_{24}Se_{64.5}$ thin films to study the photoluminescence properties of pre and post thermally annealed films (up to 10 hrs at 180^{o}C). Based on prior studies, authors claimed that $Ge_{11.5}As_{24}Se_{64.5}$ are the best glasses in this ternary system for waveguide applications and displays excellent structural stability against thermal or optical annealing [163]. Moreover, this glass was used for doped films fabrication because of low enough absorption coefficient around 0.05dB/cm at 1550nm [164], which will be beneficial for the fabrication of low loss waveguides ultimately suitable for all optical processing. Furthermore, a damaged glassy network caused by implant was confirmed by lowered values of refractive index, but this drop was eliminated by thermal annealing with recovery to the bulk value after sufficient annealing. Thermal annealing at 180^{o}C for 3 hours improved the PL intensity and lifetime values of films having 0.4 mol% Er concentration. After such thermal annealing, PL intensity increased threefold and PL lifetime increased from 1.04 ms to 1.35 ms, respectively, due to activation of Er ions [165] and removing the local phonon sources (defects), which coupled to doped ions dropping their lifetime. Thus, it is concluded from photoluminescence results that Er doped $Ge_{11.5}As_{24}Se_{64.5}$ could be a useful material for the fabrication of laser sources at telecom wavelengths.

The effect of deposition temperatures on the MIR lifetime of $70Ga_2S_3{:}23La_2S_3{:}6La_2O_3{:}1Er_2S_3$ integrated optic waveguides was investigated by Frantz et al [166] in 2014. RF sputtered Er doped GLS films were fabricated at two different deposition temperatures (25°C and 525°C) then converted to rib waveguides of 5 μm and 10 μm width. The fluorescence lifetime at 1550 nm and 2700 nm of waveguides were then measured for the two different substrate temperatures. The 1550 nm fluorescence lifetime of the waveguide deposited at

25°C was 1.1 ms which increased to 2.2 ms with increased deposition temperature (525°C) though the lifetime definition was not discussed. In terms of comparison to JO known data for doped GLSO, the derived fluorescence lifetime value using Judd-Ofelt analysis is 3.3 ms [152]. The discrepancy in lifetime values can be explained by considering many factors such as different dopant concentrations, dependency of film stoichiometry on deposition technique, impurity effects, and effective energy transfer in Er system etc [3]. No emission was detected at 2700 nm on the 25°C waveguide, but was observed with a lifetime of 0.7ms for the 525°C waveguide. The different results were concluded to be due to differences in Er incorporation as a function of substrate temperature, which needs further investigation, whereas this work represents the first observation of MIR emission in a rare earth doped chalcogenide waveguide device and with good life time in addition which bodes well for the attainment of gain.

RF sputtered Er ($1.55x10^{20}$ ions cm^{-3} and $4.66x10^{20}$ ions cm^{-3}) doped $Ga_5Ge_{20}Sb_{10}S_{65}$ films and waveguides were fabricated to study the luminescence properties at 1550 nm and 2700 nm emission wavelengths by Nazabal et al [167] for infrared applications in 2016. This work was inspired by Frantz's prior study [166], where an obvious emission band centered at 2760 nm was obtained from doped GLS sputtered waveguides which showed their potential for use as mid-IR incoherent fluorescence sources. The thin film growth process induced some changes in the structure; thus, defects were formed and were analyzed by Raman spectroscopy. Some differences emerged in the low frequency region of the Raman spectra with new bands at 163, 208, and 253 cm^{-1}. A slight shift of the dominant Raman band (260-450 cm^{-1}) to lower frequencies was observed as well. The whole band was broadened in the case of films also. Moreover, in the low frequency domain, the shape of Raman spectra of sputtered thin films was closer to those observed for S-deficient glasses than to stoichiometric $Ga_5Ge_{20}Sb_{10}S_{65}$. The attained results illustrated the significance of deposition parameters on the reproducibility and control of optical and spectroscopic properties induced

through the composition and structure of the films [168]. Structural defects can lower the fluorescence lifetime and so thermal annealing was investigated to eliminate the defects in the sputtered films. Fluorescence lifetime measurements of the $^4I_{13/2}$ state in $3.11x10^{20}$ ions/cm^3 Er doped GeGaSbS film were made. Whilst the lifetime definition was not explained in the paper, before annealing the lifetime was 1.57 ms which increased to 1.88 ms after annealing at Tg-20°C (60 mins) and the measured lifetime showed very good agreement with the corresponding calculated radiative lifetime (1.90 ms) of bulk glass by Judd-Ofelt analysis [169]. The same protocols applied to films with $9.33x10^{20}$ ions/cm^3Er concentration also showed an increased lifetime from 1.12 ms to 1.32 ms. Moreover, 975 nm pumping was used to study the amplification in waveguides at 1540 nm and a 4.4 dB pump on/off enhancement factor was recorded from etched chalcogenide waveguides (undefined length of the waveguide). By subtracting the Er absorption contribution, the Authors claimed 0.3 dB/cm internal gain value, which was greater than the first 1550nm gain achieved in Er:As_2S_3 waveguides in prior studies [120]. The achieved internal gain was however still too low to overcome scattering and absorption losses. Nonetheless, the high doping levels attained with good radiative lifetimes are still promising attainments towards the goal of planar chalcogenide MIR lasers.

Conclusion

Chalcogenide hosts have received significant attention for the fabrication of low loss mid infrared waveguides and rare earth doped sources due to their promising properties. The demonstrated high rare earth ion solubility without clustering in selected bulk glasses, low nonradiative decay rate due to lower phonon energy, planar processibility, compositional tunability, minimal energy transfer quenching processes at longer wavelength due to absence or low level of available contamination etc. make them attractive materials for planar MIR devices. In planar form, initial works have shown promise and one clear element is that

thermal input is often required to ensure good fluorescence lifetime and PL intensity.

2.2 MIR emission from Er doped Tellurites

Tellurite glasses are well known candidates for the fabrication of high gain optical waveguide devices to have range of interesting properties such as broad transmission window (~6 μm), much lower maximum phonon energy than silica [51], high linear and nonlinear refractive indices [56], greater stability than Fluoride glasses [57], high rare earth ion solubility [56], large emission bandwidth [65] etc. Moreover, high erbium solubility as has been demonstrated in tellurite glass and fibre amplifiers [67]. Tellurite erbium Doped Waveguide Amplifiers (TEDWAs) can provide high gain (more than 15 dB already demonstrated from a 5 cm long device at 1550 nm) with potential for >10 dB/cm, which is advantageous for short pulse amplification. Tellurites have demonstrated low loss waveguiding e.g ~0.1 dB/cm [70] and 0.6 dB/cm [71] at 1550 nm and 2000 nm respectively. These results make them very appropriate for planar integrated devices [70].

In 1990, Romanowski [170] studied Er doped (ranging from 8.1 x 10^{19} ions/cm^3 to 1.5 x 10^{21} ions/cm^3) multicomponent tellurite (85.6% TeO_2, 8.4% BaO, 4.0% Na2O, 1.0% MgO, 1.0% ZnO, wt%) glass in the 20-473 K temperature region when pumped with a nitrogen laser pumped tunable dye laser (undefined wavelength). The pure radiative lifetimes were calculated using Judd-Ofelt theory at 3.44 ms ($I_{13/2}$-$I_{15/2}$), 2.92 ms ($I_{11/2}$-$I_{15/2}$), 2.57 ms ($I_{9/2}$-$I_{15/2}$), 0.27 ms ($F_{9/2}$-$I_{15/2}$), 0.29 ms ($S_{3/2}$-$I_{15/2}$), and 0.006 ms ($H_{11/2}$-$I_{15/2}$) [171]. Experimentally the author only studied the effect of concentration and thermal effect on the transition from $S_{3/2}$ and $I_{11/2}$ levels. At an Er concentration of 8.1 x 10^{19} ions/cm^3, luminescence decay of the $S_{3/2}$ and $I_{11/2}$ levels was governed by radiative transitions and multiphonon relaxation involving the highest energy Te-O vibrations. However, luminescence quenching was observed in a more heavily doped sample (1.5 x 10^{21} ions/cm^3), which occurred due to nonradiative energy transfer processes (e.g

excitation energy migration and cross relaxation). For example, quenching of the $S_{3/2}$ level was consistent in more heavily doped samples ($\geq$ 6.1 x 10^{20} ions/cm^3) via cross relaxation to intermediate level ($S_{3/2}$-$I_{9/2}$ and $I_{15/2}$-$I_{13/2}$) and the quenching rate increased at 145 K and room temperature depends quadratically on Er concentration. Conversely, quenching from the $I_{11/2}$ level in heavily doped samples ($\geq$ 6.1 x 10^{20} ions/cm^3) was attributed only to nonradiative energy transfer from Er ions to the structural defects and OH groups present in the glass.

In 2002, Shen et al [172] proposed tungsten-tellurite ($40WO_3$:$40TeO_2$:$20Li_2O$) glass as the promising host and studied an Er concentration of 3.11x10^{20} ions/cm^3.The spectroscopic properties were measured and a broad 1550 nm emission spectrum at 85 nm FWHM was measured using Ti-Sapphire pumping at 800 nm. The measured lifetime of $I_{13/2}$ level was 5.1 ms, and the authors also measured the $I_{13/2}$ level lifetime as a function of Er concentration, which is shown in figure 2.2. It was concluded that the doping level producing the longest lifetime (5.1 ms) at 3.11x10^{20} ions/cm^3; while at 0.62x10^{21} ions/cm^3 Er concentration the lifetime is reduced to 4.5 ms and further reduced to 2.9 ms at 0.93x10^{21} ions/cm^3, this is due to non-radiative effects from concentration quenching but authors did not mention the dominating effects.

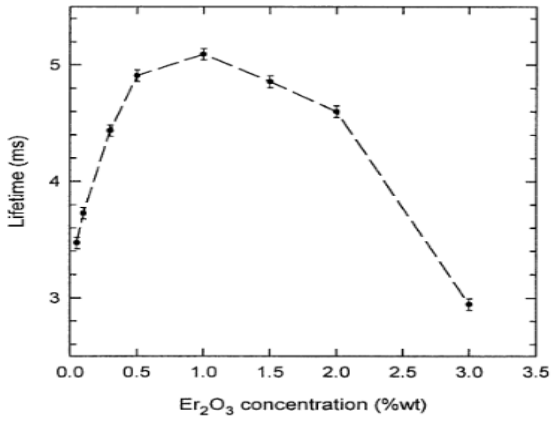

Figure 2.2: 1/e lifetime of $I_{13/2}$ lasing level of erbium in tungsten tellurite glass doped at varying Er concentration [172].

The Raman spectra of this glass showed the highest phonon energy at 920 cm^{-1}, which is higher than pure tellurite glass (770 cm^{-1}). Moreover, the calculated lifetime at $I_{11/2}$ level using the empirical formula [173] was 0.002 ms, compared to that in pure tellurite glass of 0.02 ms and silica at 0.001 ms. The short $I_{11/2}$ lifetime (comparable to silica) produced by the higher phonon energy indicates that 980 nm pumping will be very efficient in this glass [174] for the $I_{13/2}$ state, but of course will prevent MIR emission. The broad emission demonstrated however indicates tungsten-tellurite glass has the potential for broadband erbium doped amplifiers with extended L-band gain.

In 2003, Rolli et al [175], studied Er doped ($4.405x10^{20}$ ions/cm^3) $75TeO_2$:12ZnO:$10Na_2O$:2PbO glass in absorption and emission and used Judd–Ofelt and McCumber theories to obtain radiative transition rates and stimulated emission cross sections. The calculated radiative lifetime of $I_{13/2}$ level was 3.50 ms with 94% quantum efficiency [176] and stimulated emission cross section with 63 nm effective bandwidth of the transition between $I_{13/2}$ to $I_{15/2}$ states was $9x10^{-21}$ cm^2 and these values are very large as compared to silicate and phosphate

glasses [177]. Moreover, the measured 1/e lifetime of $I_{13/2}$ level upon excitation by 514.5 nm excitation sources was 3.3 ms. Authors suggested that the large spectral bandwidth of the stimulated emission cross section makes this glass a promising host material for broadband amplification in the third telecommunications window.

Dai et al [65], in 2006 presented the concentration quenching in $75TeO_2–20ZnO–(5–x)La_2O_3–xEr_2O_3$(x=0.05, 0.1, 0.3, 0.6, 1.0,2.0 and 3.0) in mol% glasses. They used a model based on energy transfer and quenching by hydroxyl (OH) groups to fit their measurements, where it was it estimated that ~15% of OH groups in the tellurite glass are coupled to the Er ions, which caused the concentration quenching. They did not attempt to purify the glass to remove remnant OH groups during fabrication. The $I_{13/2}$-$I_{15/2}$ fluorescence properties were measured for different Er concentrations upon excitation at 980 nm and Infrared spectra were measured to estimate the exact OH content in samples. With increasing Er concentration, significant broadening of the $I_{13/2}$-$I_{15/2}$ emission was observed due to radiative trapping. This trapping always occurs in a typical 3-level system when the absorption and fluorescence spectra overlap [178]. Furthermore, the emission intensity of Er: $I_{13/2}$-$I_{15/2}$ transition drastically increased till $4.44x10^{19}$ ions/cm^3 Er concentration and decreased with the further increase in the Er concentration (figure 2.3, a). The reduction in the 1/e lifetime of $I_{13/2}$ level was observed with increasing Er concentration such as at lowest Er concentration ($0.22x10^{19}$ ions/cm^3) the measured lifetime and OH concentration values were 3.4 ms and $5.3x10^{19}$ ions/ cm^3 respectively. However, at the highest Er concentration ($13.2x10^{19}$ ions/cm^3) the lifetime value dropped to 0.7 ms, whereas OH concentration increased to $5.8x10^{19}$ ions/cm^3 (figure 2.3, b).

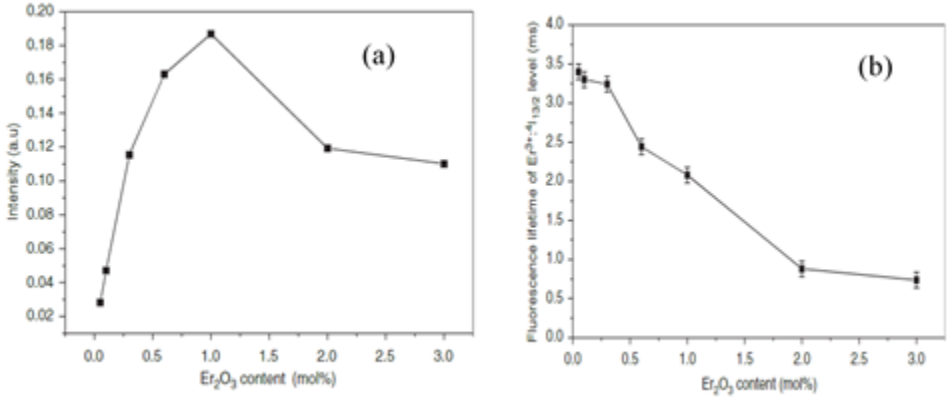

Figure 2.3: (a) Measured PL intensity and (b) PL lifetime of erbium in TZL glass doped at varying Er concentration [65].

The reduction in lifetime indicated the rise of the energy transfer rate involving both Er ions and the quenching center (OH groups) [179]. IR absorption spectra showed strong absorption in the range 2800–3200 cm^{-1}, this band being ascribed to the stretching vibration of OH in tellurite glasses, which are incorporated as $Te(OH)_6$ and H_2TeO_6 [180].

Cacho et al [181] in 2014 demonstrated pedestal waveguides produced with Yb^{3+} ($4.18x10^{20}$ ions/cm^3)/Er^{3+} (0.05×10^{20} ions/cm^3) codoped Bi_2O_3-WO_3-TeO_2 thin films deposited from bulk glass by RF magnetron sputtering for optical amplifiers at 1530 nm. The definition of the pedestal waveguide structure was made using conventional optical lithography followed by plasma etching of the undercladding (SiO_2) in order to define the sidewalls before deposition of Bi_2O_3-WO_3-TeO_2 core waveguides. Propagation losses in the multimoded 20-100 μm width range bottomed out at around 2.0 dB/cm and 2.5 dB/cm at 633 and 1050 nm, respectively. The authors suggested an internal gain of 5.6 dB at 1530 nm was

achieved for 1.5 cm waveguide length (~3.7 dB/cm) in a waveguide under 980 nm excitation, with only 9 mW of pump power, probably because of the use of Yb^{3+} as a sanitiser. However the definition of internal gain and the method of measurement was not provided, and the gain curve showing zero gain at zero pump power instead of a net loss suggests the use of the enhancement factor rather than actual gain (propagation losses at 1550 nm not reported either which are a component of internal gain). However the results indicate that an alternative waveguide structure could be useful and that the sputtering of already doped glasses can also be considered as a viable route to making rare earth doped tellurite devices

In 2018, Motorin et al [182] studied the photoluminescence properties of Er_2O_3 (0.5 mol%) doped high purity TeO_2-ZnO based tellurite glasses, prepared by melt quenching with a fundamental OH group absorption at 2800 nm below 0.01 cm^{-1}. The lower absorption coefficient value reflected the high purity of the fabricated glass. Under 980nm pumping, broad luminescence bands were recorded at 1550 nm and 2700 nm corresponding to Er transitions from $^4I_{13/2} \rightarrow {}^4I_{15/2}$ and $^4I_{11/2} \rightarrow {}^4I_{13/2}$ respectively. The photoluminescence lifetimes of both $^4I_{13/2}$ and $^4I_{11/2}$ excited levels were measured, which were 3.5 ms and 250 μs respectively. The measured $I_{13/2}$ level lifetime was quite comparable to the calculated lifetime value using JO data in prior work[175].However, the measured $I_{11/2}$ level lifetime is higher than that calculated and measured in heavy metal tellurite (like tungsten Tellurite) glasses [172], which make zinc tellurite glass of considerable interest for emission at 2700 nm wavelength. These results show promising photoluminescence properties for MIR region applications with tellurite glasses confirming the high potential for use as an active media for EDWAs and lasers in the 3 micron region. Minimizing OH absorption is however a matter that needs careful attention.

Huang et al [183] achieved highly efficient 3400 nm emission in bulk (100-x)TeO_2-xEr_2O_3 (x = 2, 4, 6, 8, 10 mol%) glasses for the first time in 2020, where

increase of emission cross section at 3400 nm was increasing with increasing Er concentration. This paper is of particular relevance to the current work as it is one of very few that use the same pure TeO_2 formulation. The glasses were prepared by the conventional melt quenching method. A maximum Er concentration of 3.8×10^{21} ions/cm^3 was used and beyond 6 mol% Er concentration ($2.29x10^{21}$ ions/cm^3), a new crystal phase precipitated from the glass, which lowered the thermal stability significantly. The fluorescence in the 2000-4500 nm range were measured for different Er concentrations upon excitation at 976 nm and the range of possible radiative emissions of Er are shown in in figure 2.4. Emissions centered at 2716 nm and 3430 nm were observed corresponding to transitions from $^4I_{11/2} \rightarrow {}^4I_{13/2}$ and $^4F_{9/2} \rightarrow {}^4I_{9/2}$ in erbium respectively. Stark splitting was observed in the $^4I_{13/2}$ transition, thus the emission band at 2716 nm was split into three sub-bands (2650, 2716, and 2790 nm) and the 2716 nm intensity started to decrease with increasing Er concentration beyond 6 mol% due to cross relaxation between the Er^{3+} ions. Four cross relaxation processes were identified as being active: $[^4I_{13/2} \rightarrow {}^4I_{15/2}]$:$[^4I_{13/2} \rightarrow {}^4I_{9/2}]$,$[^4I_{13/2} \rightarrow {}^4I_{15/2}]$:$[^4I_{9/2} \rightarrow {}^2H_{11/2}]$,$[4I_{11/2} \rightarrow {}^4I_{15/2}]$:$[^4I_{13/2} \rightarrow {}^4F_{9/2}]$,$[^4I_{11/2} \rightarrow {}^4I_{15/2}]$:$[^4I_{13/2} \rightarrow {}^4F_{7/2}]$.

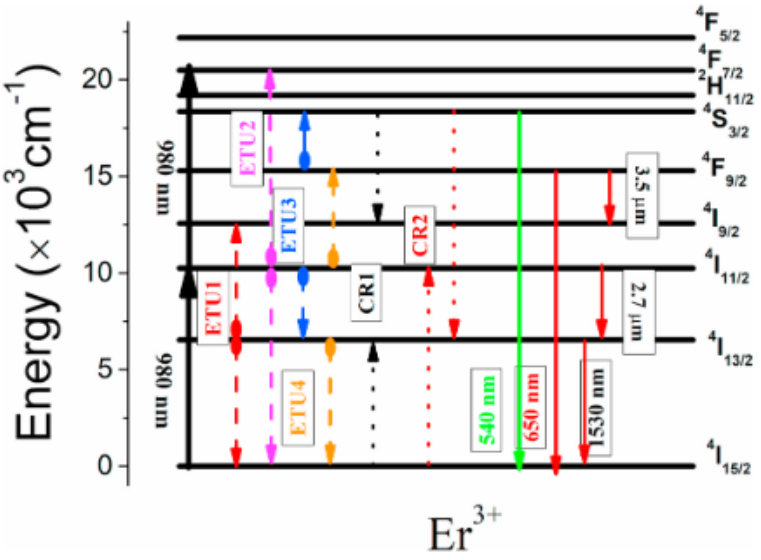

Figure 2.4: Energy level diagram, energy transfer and cross relaxation process of Er doped tellurite based glass [183].

The cross relaxation reduced the $^4I_{13/2}$ population but enhanced the $^4I_{9/2}$ and $^4F_{9/2}$ populations. These processes may open an effective route to achieving efficient ~3400 nm emission in Er^{3+}doped Tellurium dioxide. The 3400 nm emission intensity gradually increased with increasing Er concentration this being believed to be a result of the transition of TeO_4 trigonal bipyramids structure (tbps) into TeO_3 trigonal pyramid structure (tps), this also leading to the broadening of the emission. Both emission and absorption cross sections were also increasing at 3400 nm with increasing Er concentration. For example at maximum Er concentration ($3.79x10^{21}$ ions/cm^3), highest emission ($2.53x10^{-21}$ cm^2) and absorption ($1.47x10^{-21}$ cm^2) coefficient values were calculated. The NIR emission spectra were also studied in all the glasses, the emission intensities here being seen to decrease with increasing Er concentration indicating the different optimisations that may be required for 1550 nm emission vs MIR emission. Due

to cross relaxation between Er ions, the fluorescence lifetime at 1530 nm decreased from 2.02 ms to 0.28 ms with increasing Er concentration. Up conversion fluorescence spectra of the glasses at 550 nm and 670 nm from the $^4S_{3/2} \rightarrow {}^4I_{15/2}$ and $^4F_{9/2} \rightarrow {}^4I_{15/2}$ transitions, respectively were also investigated. In samples with up to 6 mol% erbium ion concentration, the up-conversion fluorescence intensity increased with Er concentration. However, beyond that (6 mol%) concentration (also the concentration at which the new phase precipitated), fluorescence intensity started to decrease, and 550 nm ($S_{3/2}$-$I_{15/2}$) lifetime dropped from 38.7 μs to 20.8 μs and 670 nm ($F_{9/2}$-$I_{15/2}$) lifetime decreased from 93.1 μs to 38.5μs respectively. Several non-radiative processes were occurring between Er^{3+} ions, such as cross relaxation between Er^{3+} ions, excited state absorption, and energy transfer, etc. These processes either become more efficient with increased Er^{3+}concentration (reduced inter ion separation) or because of the changed material structure in the newly precipitated crystal phase. In summary, highly doped Tellurium dioxide was shown to be promising as an emission medium at ~3400 nm and may provide applications in mid infrared EDWAs. This paper is also significant in that it shows crystallisation during high temperature treatment (from room temperature to 800^{o}C with the heating rate of 10 ^{o}C/min in a flowing nitrogen atmosphere) is suppressed at concentrations up to at least ~$7.6x10^{20}$ ions/cm^3 and that performance is good there also, which suggests that sputtered Er doped TeO_2 films with this or more concentration should be annealable.

In terms of waveguide based tellurite devices, the field is very much more restricted. Pietralunga et al [184] presented the technological approach to the realisation of channel optical waveguides in 2008 with a lithographic process and sputter etching recipes. Authors have started from reactively sputtered tellurite glass thin films of sub-nanometre surface roughness, homogeneous structure, and controlled optical properties, which were fabricated on thermally oxidised silicon (TOx) wafers. Variable angle spectroscopic ellipsometry in the 260nm - 1700nm range was used to study the optical parameters (n and k) for sputtered films at

different compositional (O/Te) ratio ($1.9<x<2.15$). Negligible absorption in the third telecommunication optical window was detected, while a 1.5 % spread in refractive index was measured, as the O/Te ratio was varied (2.06 to 2.03). Particular care was required during the development process in the photolithography step as the films were very soluble in the aqueous alkaline developer. The fabricated rib waveguides displayed 5.7 dB/cm propagation loss at 1550 nm and this represents the first TeO_2 waveguides reported in the literature.

Madden et al [70] reported fabrication and optical properties of pure tellurite planar rib waveguides in 2009. For the first time, the authors achieved very low propagation loss using a newly developed reactive ion etch process based on Hydrogen as the active species. Optical losses below ~0.05dB/cm in most of the NIR spectrum (1000-1450 nm) and ~0.10dB/cm at 1550nm were accomplished. Furthermore, they also achieved strong spectral broadening of 0.6ps pulses in fabricated waveguides, and did not observe optical damage or photorefractive effects at GW/cm^2 intensities. The available properties such as low losses, zero dispersion waveguide designs and high damage thresholds indicated significant potential for future waveguide devices.

In planar form, Vu et al [62] fabricated thin film based Er doped ($2.2x10^{20}$ $ions/cm^3$) tellurite waveguide amplifiers using RF sputtering, UV lithography, and reactive ion etching and demonstrated high internal gain when pumped with laser diodes at both 1480 nm and 980 nm in 2010 and 2015. They obtained internal gain from 1500 nm to 1640 nm providing coverage for most of the S, C, and L telecommunications bands. As the pump power was increased, the device began to lase at 1535 nm off the end facet reflections at an estimated 15dB gain (3dB/cm) preventing further measurement of the gain response. Gains exceeding 20dB appeared possible compared with a maximum possible 35 dB with 100% inversion of the ~4cm long waveguide. Excited state absorption (ESA) was indicated by inversion in the gain spectrum from 1640 nm to beyond 1700nm and it was increasing with increasing pump and signal gain. Significant green up conversion

was also observed from 3 pump photon absorption and other processes exciting the ions to the $^4S_{3/2}$ and $^2H_{11/2}$ states. This reduces pump efficiency and maximum achievable inversion. Some prior studies using Er/Ce co-doping with 980 nm pumping however displayed 100% inversion [185].

Conclusion

It is concluded that tellurite has high potential to be used as an active media for EDWAs and lasers in the mid infrared region up to ~3000 nm because it has high erbium solubility, promising PL properties in the MIR region, and has already demonstrated high performance waveguide amplifiers and planar waveguides at 1550 nm. It thus seems a good complimentary option to chalcogenide glasses given its higher glass stability for 3 micron applications.

Chapter 3: RF Sputtered Er Doped Tellurite Films.

This chapter reports on the appeal, opportunities and limitations of tellurite glass as a planar gain medium for MIR light generation, before delving into the details around achieving potentially high power emission. Given the need for high doping in planar devices, especially for high output power, the experimental section is primarily focused on researching the nature of the concentration dependence of the luminescence properties in Er doped thin films and comparing these to bulk glass properties. Key findings were that despite achieving some of the best luminescence properties ever reported for thin films, the films show much worse concentration dependence than bulk glass. Further, the film deposition was not stable enough to make repeatable stoichiometry/structure films to enable reliable investigation of these properties nor to look at ameliorating deleterious effects. Consequently, solutions were sought to overcoming film growth issues with a successful outcome where repeatable and stable control of stoichiometry has been obtained to enable the future investigation of how to make high power planar amplifiers.

3.1 Why Tellurite?

Tellurite glass is a promising optical material for integrated optics because of good transmittance (vis-mid IR region), good chemical stability, low phonon energy, high rare earth ion solubility, and high linear and nonlinear refractive indices [186].These properties make this glass a good candidate material for both fabrication of high power output planar laser/amplifier devices and for fully on-chip supercontinuum (SC) generation up to 6000 nm [187]. SC offers great

potential for optical telecommunication, remote sensing, atmospheric pollution monitoring, molecular spectroscopy, medical diagnosis, hyperspectral imaging, etc. [188]. This glass has been studied for more than 150 years [189] and due to the relatively broadband gain spectrum, initial research in rare earth doped tellurite glass was concentrated around erbium doped tellurite fibre amplifiers. Research interest in tellurites has persisted up to the present [189] and significant progress has been achieved over the last 10 years [190].

Tellurite offers two routes to MIR light generation, firstly as a MIR capable rare earth host in its own right for 2700 nm emission, and secondly as a platform that can integrate both a NIR pump laser and a highly nonlinear waveguide for SC generation up to 6000 nm. Mode locked sources are essential for SC generation, and achieving short pulses requires large optical gain bandwidth, something native to tellurite amplifiers in the NIR. Whilst wideband MIR supercontinuum is generally more simply generated using pump wavelengths at or beyond 2700nm, successful MIR SC has also been generated using 1550 nm pumps. As previously noted, Tellurium dioxide is a good candidate for planar waveguide lasing at 2700nm, and waveguide lasing has already been demonstrated at 1550nm. The major challenges are output power, and achieving 2700 nm waveguide lasing. It was, therefore, natural to examine these topics further.

3.1.1 Background

In the SC generation process, a nonlinear optical medium is pumped with high peak power laser pulses, which result in the emission of a much wider bandwidth spectrum than the spectrum of the launched pulses due to a cascade of nonlinear optical interactions driven by the high peak power. Further, when performed in a guided mode device, the generated light has high spatial coherence and Gaussian like mode profile meaning it has many of the characteristics of a laser beam leading to diffraction limited focusing and high collimation. The first SC generation in a guided wave device was obtained in 1976 in an optical fiber pumped by a nanosecond pulsed dye laser [191]. Forty six years later, this field

remains active in both the research and commercial sectors, primarily because there are many potential applications for such light and because it is still not a low cost light source. The applications lie in fields such as medicine particularly in the detection of skin cancer [192], Molecular finger printing of gases, solids, and liquids (greenhouse gasses, explosives, toxic agents, etc) [193], infrared spectroscopy [194], and MIR LIDAR systems [195], etc. The required SC source properties depend significantly upon the application. Whilst commercial fibre based sources exist they are expensive and this has spurred ongoing research into on chip SC sources beyond 2000 nm, e.g. [55]. A key component of such devices is an integrated mode locked laser.

In the visible and NIR region, silica fibre based SC sources are already commercialised and robust due to the favourable properties of silica (low loss, high strength, and high damage threshold, etc.) [196]. The high maximum phonon energy of silica ($1000cm^{-1}$) and the resulting short wavelength cut off and attendant dispersion properties in the MIR however do not allow silica to achieve SC generation in MIR region. High power SC generation in the Mid and Far Infrared regions is more difficult because glasses with transmission to 10+ μm have their zero dispersion point deep into the MIR and so without either multi-material cascaded architectures or exotic structures MIR pump sources are vital to SC generation [197]. For MIR SC generation, glasses are needed which offer high nonlinearity with high transparency at longer wavelengths and good optical power handling [198]. Efficient pump sources[10]are also required at wavelengths ideally in the 3-5 micron range to make architectures simpler for planar integration and therefore cost reduction. Alternatively, and perhaps less preferably, a high power ~1550nm pump source and a cascaded/tapered waveguide approach could also be realised in a single chip implementation at the expense of higher fabrication complexity.

Over the last decade, many glasses such as ZBLAN, InF, Chalcogenides, and Tellurites, etc have been investigated in the MIR region. ZBLAN or InF, has a

low material zero dispersion wavelength (ZDW) of 1600 nm and much research has been undertaken on ZBLAN and InF fibres for SC sources with extended MIR spectra, for example up to 4.75μm [199] and 5 μm [200] respectively. Whilst interesting in their own right, fluoride glasses have not been successfully planar integrated beyond femtosecond direct writing in bulk glass blocks to date and so are not considered further.

SC in chalcogenide glasses such as As_2S_3 [201] and GeAsSe [202] etc. have been reported from 2 μm to 15 μm due to the ~1000 times higher nonlinearity and low loss transmission up to 15 μm as compared to ZBLAN and InF glasses [198]. Planar sources with extension to 10 μm have also been demonstrated with high polarisation purity and stable operation for spectroscopic applications [203]. Whilst this is clearly a promising route forwards to chip based SC systems, pump laser development has lagged considerably in chalcogenides as previously discussed. However, the promise is a key reason for this thesis further examining rare earth doped gain in chalcogenides. A more mature pump laser technology that is closer to fruition in the MIR range yet that can be easily co-integrated with chalcogenide waveguides is then also of interest.

Tellurites present more than 15 times higher non-linearity, higher optical damage threshold, comparable transmission window, and established planar capabilities compared to ZBLAN and InF glasses, and shorter ZDW with proven rare earth capabilities when compared with chalcogenides [204]. This makes them good candidates for pump lasers, SC generation up to ~5 microns, and first stage SC generation before a transition to a chalcogenide waveguide for wideband MIR SC generation. In several studies, MIR SC generation from 900 nm to 3900 nm has been explored from small core sized tellurite fibres to enhance nonlinearity and to down shift the ZDW (well below 2000 nm) [205]. SC from 790-4900nm with a total power of 90 mW has been achieved from an 8mm long tellurite fibre, when pumped at 1550 nm [206]. However, the broadest SC bandwidth has been obtained up to 5000 nm with a total power of 150 mW from a 9cm long tellurite fibre

pumped at 2400 nm [207], which can be taken as the best example where high nonlinearity permitted the use of short piece fibre to compensate the high losses beyond 4000 nm.

3.1.2 Tellurite-based (TeO_2) glasses

Oxide glasses have higher chemical, mechanical, and thermal stabilities than chalcogenide and Fluoride ones. High thermal stability against crystallisation when doped and processability with standard very large-scale integration (VLSI) techniques makes them good candidates for the fabrication of low loss optical waveguide devices [208]. Among oxide glasses, tellurites exhibit low maximum phonon energy (~750cm^{-1}) [209], and thus low nonradiative decay rates with the potential for rare earth doping to achieve longer wavelength emission (beyond 2000 nm) as compared to silica [210]. Further, high quantum efficiency [211] is also attainable leading ultimately to better laser performance. Tellurite glasses possess a reasonably wide transmission region (400-6000 nm at the ultimate limits), high linear and non-linear refractive indices, low linear and nonlinear absorption, and higher absorption and emission cross-sections [53] when rare earth doped than silica and most other oxide glasses. Tellurites also have the broadest emission cross section amongst silica and Fluorides[63]and also offer high rare earth ion solubility [212], which makes them attractive for broadband optical amplifiers [211]. Tellurite glass so glass transition temperature >350^{o}C, a high optical damage threshold (15–20 GW/cm^2) [213],reasonable mechanical strength and corrosion resistance [214], high nonlinearity (n_2=3.9x10^{-19} m^2W^{-1}) [215], and lower intrinsic losses compared with chalcogenide glasses [213] making it an undeniably interesting material for active planar waveguide devices. Tellurite material offers great promise for planar optic devices with further development [216]. In prior work [101]internal and net gain was demonstrated in Tellurite planar waveguide devices. Up to 14 dB gain was measured in a 5cm long Er (~2.2x10^{20}ions/cm^3) 1490 nm pumped doped tellurite planar rib waveguide amplifier (2.8 dB/cm) at 1530 nm. Further increases in gain are certainly

achievable by using non-resonant 980 nm pumping to attain higher inversion, and by further increasing the doping level. In these devices, input power dependent gain compression was observed and the saturated output power was estimated at somewhere in the 10-20 mW range, not enough for generating technologically useful broadband MIR supercontinuum for practical applications. Therefore, higher Er concentration and/or tapered amplifiers are required to achieve sufficient output powers, ideally perhaps up to the 1 W level. To provide some context around this, 1 Watt at 1550 nm corresponds to ~$7x10^{18}$ photons/sec from which some rough estimation of the doping concentration required can be made. A full amplifier/laser model is required to arrive at a correct figure, but to within an order of magnitude some simplifying assumptions ease calculations. Assuming that 60% of ions overall contribute to the gain process, considering a waveguide of say 20 cm length with a 4 square micron cross section, and assuming sufficient pump power is available to reinvert all ions within a radiative life time of ~1 ms then ~$1.5x10^{22}$ ions/cm^3 Er concentration are needed to supply the photon flux. This figure can be reduced by using tapered waveguides to increase the cross section at the output in particular, but the amplifier cannot likely be lengthened significantly due to the higher passive propagation losses if 980 nm pumping were used. Pumping at 1480 nm would avoid this issue and allow longer structures but at the expense of lower inversion, and again a full model is required to determine the better choice. Therefore concentrations in the high 10^{21} to low 10^{22} /cm^3 range are the necessary target.

As testing at concentrations this high was not undertaken previously in thin film devices, then the original aim of the work discussed in this chapter was to investigate and characterise highly doped tellurite films using fabricated using the RF sputtering technique, with the goal of obtaining suitable structural and optical properties to enable high output power chip based amplifiers/lasers.

3.2 Motivation of this Work

The motivation of this work was to build a high output power planar waveguide amplifier (>500 mW) with a small footprint which requires high erbium doping concentration in a planar device [217] and overcome the integration based challenges and engineering issues [218]. So, the main planned focus for this work was to investigate the limits imposed by concentration dependent lifetime in rare earth doped tellurite glass films and to determine if there are suitable mitigation techniques to enable concentrations up to 10^{22} ions/cm^3.

3.2.1 Following on from Previous Fabrication work

A prior Ph.D. student fabricated good quality tellurite films and working waveguide amplifiers at varying Er concentrations using reactive RF magnetron sputtering in a load locked deposition chamber (AJA, ATC-2400-V) [219]. However, this was a shared system in a national facility and was frequently not available for experiments as well as suffering from temporally indeterminate contamination from the sputtering of a wide range of other materials including metals. Thus, a move to a different sputtering system operated solely by the group (Angstrom EvoVac Series) was made to fabricate undoped and doped tellurite films with different Er concentrations and study their PL properties before trying to build a suitable waveguide amplifier demonstrator.

Somewhat unexpectedly, many significant issues were encountered in the growth of tellurite and Er doped tellurite after making this switch, mainly related to balancing the number of tellurium atoms and oxygen atoms to achieve the required stoichiometric oxidation. In this chapter the details surrounding this, its resolution, and results finally obtained will be discussed.

3.2.2 Objective and Initial Studies

In prior work [69], it was confirmed that the Er doped tellurite films fabricated in the AJA chamber had significant OH contamination which significantly shortened the lifetime. This was initially thought to arise from impurities in the

sputter targets and leaks/chamber wall water desorption in the vacuum system. Subsequent work also showed significant water contamination from the sputter gases as observed from RGA measurements. Further, the potential issue of multi-atom cluster sputtering from the erbium target was apparent, this leading to a level of Er clustering in the as-grown film that could significantly increase as the doping level increases as more sputtering power is required to raise the concentration. It was therefore required to improve the 1/e lifetime of $I_{13/2}$ level by reducing the OH contamination in the fabricated films and also to reduce multi-atom clustering at high doping. That this is potentially possible to yield the desired performance in tellurite glass can be gauged by examining the work of Jha et al [220] as shown in figure 3.1. Here good lifetime was obtained in glasses with even 10^{23} /cm^3 doping and indications of the required water absorption can be inferred from the data. The glasses with lowest OH concentrations (~0.7 cm^{-1}absorption peak at 2700nm) were melted in dry air, while the higher OH (~1.7 cm^{-1}) glass samples were fabricated in the laboratory air atmosphere. Note that these absorption figures are very much lower than observed in thin films (typically > 100 cm^{-1} [219]).

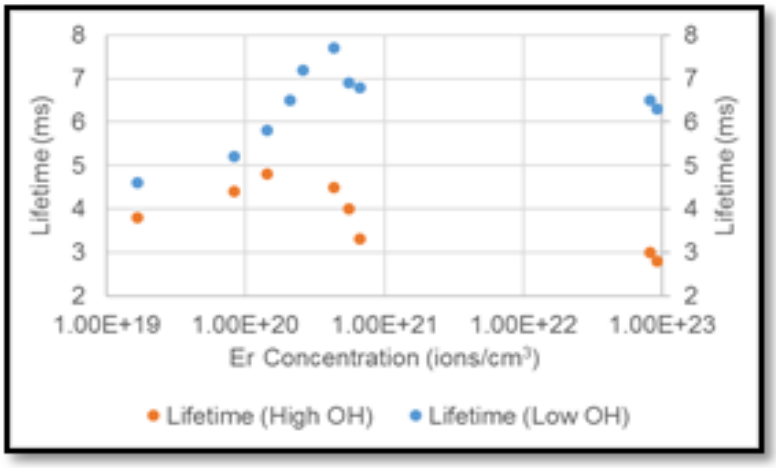

Figure 3.1: Dependence of the measured 1/e lifetime of $I_{13/2}$ level on the Er concentration at two different OH concentrations in Er doped multicomponent tellurite glass [220].

Whilst ion-ion based effects were observed to become significant at high doping, the data of figure 3.1indicate that tellurite glass as a host is intrinsically capable of delivering the performance required for high power planar devices with low enough OH contamination and dopant clustering. Clearly even small amounts of OH contamination can degrade performance significantly, and an OH contamination resulting in optical absorption of < 1 cm^{-1} at 2700nm is desirable. To achieve this requires work on both the deposition process and through post processing the films. Thermal post processing has been demonstrated to be an effective means of removing OH contamination from glasses and films and to assist in rare earth doped materials (e.g. [221], [179]). Further it is known that it can improve the PL properties by decreasing clustering provided that the rare earth solubility is high enough thereby potentially easing the polyatomic sputtering issues. Therefore, it was planned to systematically study the effects of

thermal annealing on PL lifetime in films of varying Er concentration in tellurite films, which has not been previously studied.

Initial studies were undertaken on doped films left from the prior student's studies, which were fabricated on thermally oxidized silicon substrates and multicomponent glass microscope slides (Livingstone, plain) in an Ar/O_2 atmosphere (but no gas purifiers on the input lines). The targets (Te and Er) were pure (>99.95%) commercially available materials sourced from AJA International. The AJA sputtering system was equipped with A330 RF magnetron guns. The Ar flow was 9.5 sccm and O_2 was 5.5 sccm. The chamber pressure was maintained at 5 mTorr during the deposition process. The power supplied to the Te gun was 150W (25% of the 600 W maximum power of the gun) and the Er gun powers were in the range of 5% to 15% (30W to 90W) varied to obtain different Er concentrations. This chamber has a load lock, and is normally pumped to a base pressures < $3x10^{-7}$ mTorr and the distance between the substrate holder and the target was 10cm [219].

A dual angle spectroscopic reflectometer (SCI Filmtek 4000 [222]) with 350 nm to 1700 nm wavelength range (normally operated with 450-1650 nm limits) was used to measure the refractive indices and thicknesses of the deposited films. This reflectometer calculates the properties of the films using normal incidence and polarized 70 degree reflection data. A Tauc band edge + multiple Lorentz oscillator model was then used to simulate the refractive index dispersion. The instrument uses nonlinear least squares fitting to find the best fit parameters in the Tauc-Lorentz model and the film thickness that provide minimum deviation from the measured film interference spectra to obtain the thickness and refractive index as a function of wavelength.

The resultant thicknesses for the available films were 1140, 1150, 1160 ±1.1 nm and refractive indices at 1550 nm were 2.05, 2.045, 2.048 as measured with the Filmtek 4000. The refractive index of bulk tellurite glasses at 1550 nm is around

2.08 [223] and it is expected in the literature that high quality fabricated films should have refractive indices in this range. The dark field surface morphological images of the as deposited doped films showed smooth amorphous surfaces with a few particulates as shown in figure 3.2.

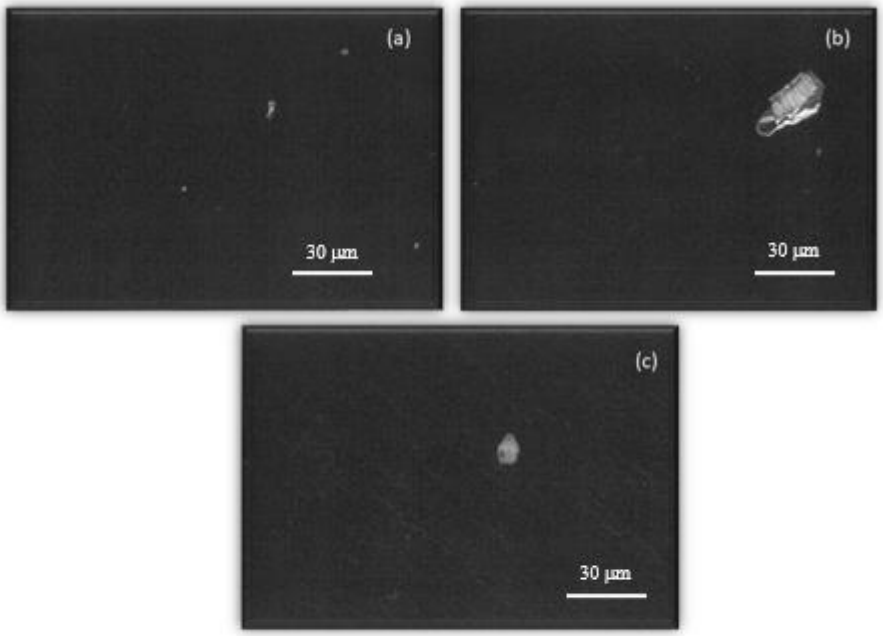

Figure 3.2: Dark field image of as deposited Er doped tellurite films# (a) 1, (b) 2, and (c) 3 showing smooth amorphous surface.

After confirming the quality of the films, the Er content in all sputtered films was measured with an electron probe micro analyser (EPMA, JEOL JXA-8530F). EPMA is an add-on instrument in a scanning electron microscope which enables precise non-destructive compositional analysis principally by wavelength-dispersive spectroscopy (WDS) [224] of the x-ray emission stimulated by the

incident electron beam. The erbium concentration was measured at $3.85x10^{18}$, $2.35x10^{19,}$ and $6.59x10^{19}$ ions/cm^3 in each film (#1, 2 and3) respectively.

3.2.3 Photoluminescence Lifetime of Er doped Tellurite films

Fluorescence lifetime ($^4I_{13/2}$ metastable state of Erbium ion) as a function of Er concentration of the as-deposited films on glass slides were then measured. It was decided not to cleave the thermally oxidised silicon substrates and keep them for device fabrication as the waveguides were already etched; thus the glass slide samples were used for initial photoluminescence lifetime measurements. All PL measurements were made with a semi-confocal fibre based system [225] where the 2.5 μm $1/e^2$ diameter spot of a lens tipped fibre was aligned to the edge of the glass slide sample to couple in the 1490 nm pump diode and to collect the 1550 nm emission. A chain of three 1490 nm/1550 nm wavelength division multiplexers (WDMs) was used to reject back reflected and back scattered pump light and the fluorescence at 1550 nm was detected with an InGaAs photodiode (Fermionics Inc. FD150SC) and a fast, low noise Signal Recovery Inc. transimpedance amplifier (model number 5402). The voltage vs time signal was captured using a 16 bit National Instruments analog to digital convertor and custom Labview software that allowed ~100 traces per second to be averaged to an arbitrary degree enabling the detection of extremely weak signals and the accurate measurement of 4-5 decades of decay with moderate signal intensity.

Fluorescence lifetime is usually characterised by the 1/e decay time which is also usually pump intensity dependent for all but very low doped films. Thus maintaining clarity about the intensity at which a lifetime is measured is important. However the underlying radiative lifetime, defined as the intrinsic radiative lifetime measured on the low intensity single exponential part of the PL decay curve, depends neither upon the pump intensity nor the population dependent energy exchange processes. Typically the decay curve would become a single exponential decay at two decades down from the initial decay intensity, but the measurement was adjusted according to the circumstances to be on the single

exponential region. The underlying radiative lifetime (hereafter just referred to as radiative lifetime) is a true measure of the host dependency including multi-phonon effects and the impacts of energy exchange processes that are not population dependent. It is therefore also a useful means of characterising material quality.

The as-deposited films were pumped with a 1490nm laser diode and the observed 1550 nm emission signal ($^4I_{13/2}$ to $^4I_{15/2}$ transition)measured at 1305.15, 1109.65, and 957.56 kW/cm^2 pump intensity for each film (#1, 2 and 3) respectively is described in table 3.1 below.

Table 3.1: PL properties at 1550 nm wavelength of fabricated Er doped tellurite films

Film	Applied Er power (W)	Er Concentration (ions/cm^3)	1/e Lifetime (ms)	Radiative Lifetime (ms)	Pump intensity (kW/cm^2)
1	30	3.85x10^{18}	1.041	1.83	1305.15
2	60	2.35x10^{19}	1.275	1.877	1109.65
3	90	6.59x10^{19}	0.919	1.709	957.56

The above results show an improvement relative to the lowest doped sample in 1/e lifetime value at 2.35x10^{19}ions/cm^3 Er concentration, whereas a drop in 1/e lifetime from 1.275 ms to 0.919 ms was observed at highest Er concentration (6.59x10^{19}ions/cm^3). The reasons for these variations are unclear and are likely related to the structure, stoichiometry and OH contamination level of the individual films as was observed in lifetime measurements on films previously fabricated in this machine which were essentially driven only by the OH

concentration [65], [69]. Contamination of sputtered films by OH turned out to be a serious issue in other aspects of this work and further detailed investigation of OH contamination of sputtered films is separately discussed in detail in Chapter 6.

For the 1550 nm transition only, there are additional demonstrated methods that can be adopted to improve the PL properties such as co-doping of Er doped tellurite films with tungsten [172] or titania and alumina [226]. Pure tellurite glass has low maximum phonon energy ($770cm^{-1}$) therefore, $I_{11/2}$-$I_{13/2}$ nonradiative decay is too slow to allow very efficient pumping at 980 nm. Therefore Shen et al [172], considered Tungsten doping to increase the phonon energy ($920cm^{-1}$). Authors also observed a higher (85 nm) FWHM of 1550 nm peak, high refractive index (2.1) and shorter calculated lifetime of $I_{11/2}$ level (0.002 ms) at $3.11x10^{20}$ ions/cm^3 Er concentration as compared to pure tellurite glass [227]. For a high power 1550 nm device co-doping may be a useful method but care is needed to avoid non-uniform etching if the material is to be plasma etched.

Amongst other approaches, one useful method of improving PL for sputtered films is thermal annealing [228]. Thermal annealing can activate Er ion mobility [229] and enable the dissolution of Er clusters, homogenise the doping, and allow re-bonding of Er atoms into the glass matrix in a more optimal configuration. It can also reduce the effects of some local phonon sources (e.g OH contamination)in the deposited films [230], which couple to the Er ions decreasing their lifetime [162]. Thus, thermal annealing of the deposited films was investigated to determine any beneficial effects on the photoluminescence properties and to ascertain any limitations particularly around crystallisation which is strongly favoured in undoped TeO_2 films.

3.2.4 Anneal Temperature and Time dependence of Emission Properties

In prior work [219], the impact of annealing on PL properties was not studied. Thus a systematic thermal annealing study (temperature and time based) was conducted on Er:TeO_2 films. An aluminium dish with a built in handle was fabricated, which is thermally more stable and can sustain high temperatures and more rapid cooling thanthe commonly used glass petri dish. A new high vacuum ($7.6x10^{-6}$ Torr) annealing oven was built which comprised of a stainless steel chamber, turbomolecular and rotary mechanical vacuum pumps, and a PID controlled ceramic cartridge heater based vacuum hotplate to accomplish annealing processes at temperatures potentially up to 600^{o}C.

Though the T_g of pure TeO_2 is thought to be about 305^{o}C, testing began with lower annealing temperatures (200^{o}C) followed by higher temperature tests to look for further improvement in emission properties and determine the optimum temperature without clustering or crystallisation [231]. At 200^{o}C annealing temperature, all three films were annealed for 35 hours but no change in PL performance was observed. Thus subsequent tests were performed at 300^{o}C and 350^{o}C.

Annealing at 300^{o}C

Pieces of all three films were annealed at 300^{o}C for 2, 4, 8, 16, 32, 64, 128, 256, and 512 hours in a multiple step process with the 1/e lifetime measured at each time interval. The results for fluorescence lifetime are shown in figure 3.3.

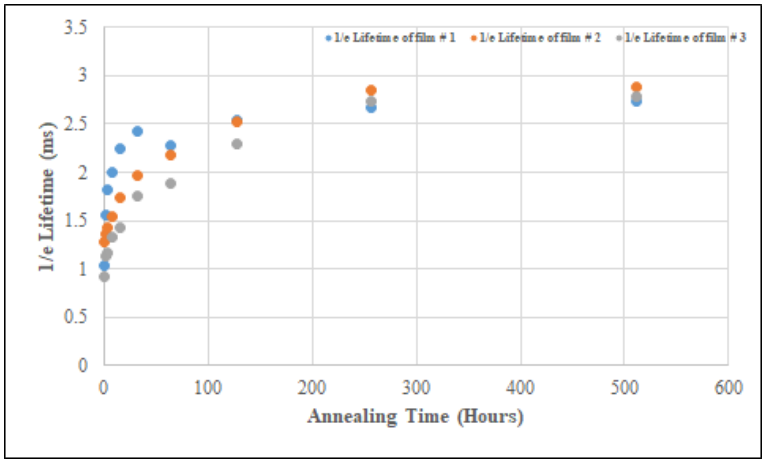

Figure 3.3: PL lifetime of Er doped TeO_2 films# (1) $3.85x10^{18}$, (2) $2.35x10^{19}$ and (3) $6.59x10^{19}$ ions/cm^3 annealed at 300C for 2 to 512 hours.

The films showed significantly improved lifetime with the lifetime in all films eventually asymptoting to about the same value of ~2.7 ms after sufficient annealing. Similar behaviour was observed in a prior study [232] on zinc-fluorotellurite thin films fabricated by pulsed laser deposition. The films in that study were optimally annealed close to the glass transition temperature (315°C annealing vs 320°C T_g) and it was proven via IR spectroscopy that the improvements resulted from a prominent reduction of the free and weakly bound OH concentration.

Later, bright and dark field micrographs of all annealed films after 512 hours were taken (figure 3.4) showing clear signs of crystallisation in the lowest doped film and different types of defects (particles, striations, and dewetting).

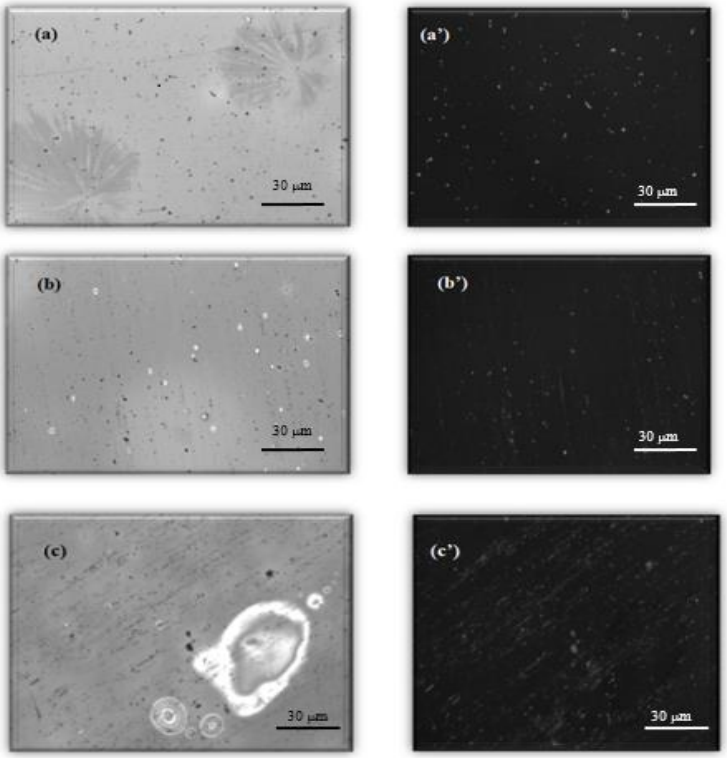

Figure 3.4: Bright and dark field images of annealed Er doped tellurite films # (a) 3.85x10^{18}, (b) 2.35x10^{19} and (c) 6.59x10^{19}ions/cm^{3}at 300^{o}C for 512 hours.

The surface of the annealed film (figure 3.4, a) having the lowest Er concentration (3.85x10^{18} ions/cm^3) has visible signs of crystallisation [221] and particles. The smooth surface with few particulates of as deposited films have already been shown in figure 3.2, which confirmed that the particles on the surface of the annealed films have grown during the annealing process or were deposited on the wafer during handling as this process was not carried out in a clean room. As per prior studies [233], a longer annealing time could be one of the reasons for surface degradation and the formation of obvious defects [234]. Thermal treatment at higher temperatures enhances the surface atom mobility and surface diffusion,

which permits migration and either crystallisation or formation of different types of structures [235]. No crystallisation was apparent in the higher Er concentrations ($2.35x10^{19}$ ions/cm^3 and $6.59x10^{19}$ ions/cm^3), prior studies [236] indicating crystallisation depends upon the film composition, surface oxidation, heating rate, internal stress and film thickness, etc. [237], [238]. However, obvious surface defects such as particles, striations, and dewetting were observed. The dynamics of the dewetting process depend upon the annealing temperature and annealing time and it becomes more prominent with increasing annealing time [239]. Many authors [240] have studied this process where theoretical and experimental work confirmed that the early stage film roughening is the result of spinodal decomposition [241], which is driven by the amplification of thermal fluctuations. Rupturing finally led to the breakup of the films and once this stage is established further heating does not produce any additional changes [239].

Annealing at 350°C

Er doped tellurite films were next annealed at 350°C for 2, 4, 8, 16, and 32 hours and the fluorescence lifetime results are shown in figure 3.5. Shorter annealing times were studied as the annealing temperature is higher than the expected T_g of the film.

.

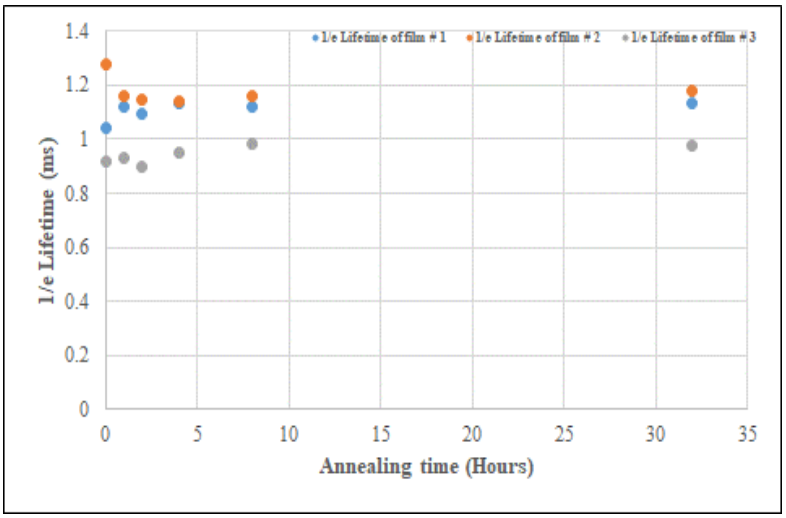

Figure 3.5: PL lifetime of Er doped TeO_2 films# (1) $3.85x10^{18}$, (2) $2.35x10^{19}$ and (3) $6.59x10^{19}$ ions/cm^3 annealed at 350C for 1 to 32 hours.

Unfortunately, the obtained 1/e lifetime results do not show the same or better improvement as those at 300°C. Below T_g (200°C) and above T_g (350°C) showed similar results. Similar studies in multicomponent tellurite thin films [232] also showed only a narrow band of temperatures around T_g where significant improvement occurred.

In terms of surface morphology in annealed films up to 32 hours at 350°C, no crystallisation was observed but surface degradation was quite prominent as shown in figure 3.6. Different types of defects such as striations, particles, and dewetting were observed in all annealed films. Tests were also conducted at 400°C and 500°C, but these were equally unsuccessful in terms of PL property improvement and led ultimately to complete film destruction above 400°C.

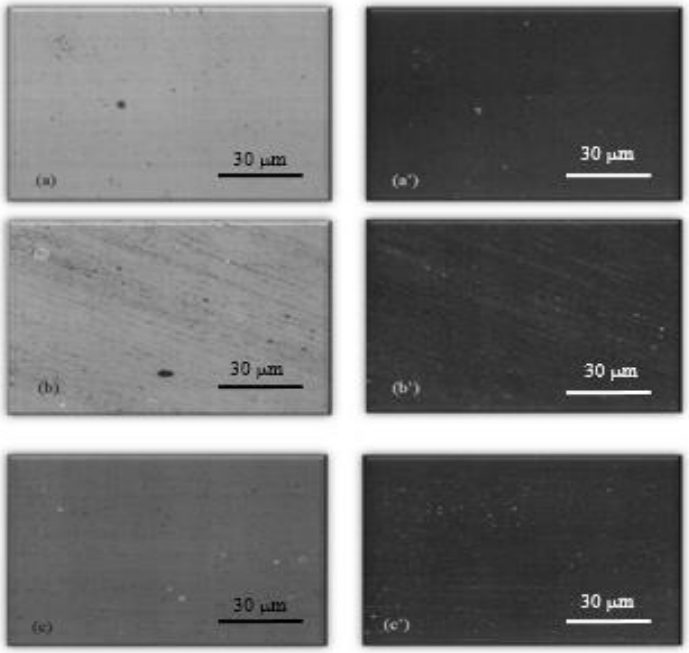

Figure 3.6: Bright and dark field images of annealed Er doped tellurite films # (a) $3.85x10^{18}$, (b) $2.35x10^{19}$and (c) $6.59x10^{19}ions/cm^3$ at 350^oC for 32 hours.

Conclusion

Based on the results above, 300 ^oC appears to be the best annealing temperature as it optimised lifetime for all three Er doped TeO_2 films. Crystallisation was prominent in long duration annealed films at low ($3.85x10^{18}ions/cm^3$) Er concentration, and this is not entirely surprising given the known crystallisation tendency of pure TeO_2. Addition of ZnF_2 [242] or YF_3 [243] in the glass matrix can increase the stability of the glass against crystallisation and achieve high homogeneity of erbium dispersion through thermal diffusion [244], whilst maintaining the advantages of high rare earth solubility and reduced phonon energy and also beneficially reducing OH concentration [245]. Thus, this glass

could be a promising material for fabrication of amplifier devices at 2700 nm. The only potential downside relates to the plasma etchability with the fluoride inclusions and this would need researching.

Having seemingly found the best annealing conditions, doped waveguides (7.5 cm long) on Thermal oxide (TOx) (5000nm), which were fabricated [101] by the prior student from the same films discussed above were used to repeat the annealing experiment with the intention of studying the PL and gain properties.

3.2.5 Emission properties of Thermally Annealed waveguides

The available waveguides were first examined using a light microscope (figure 3.7). Having determined they were in good condition, transmission measurements were made before proceeding with the annealing process.

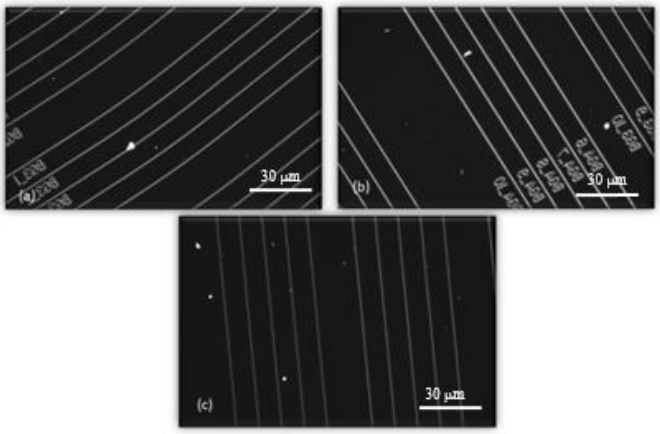

Figure 3.7: Dark field images of as deposited Er doped tellurite waveguides # (a) $3.85x10^{18}$, (b) $2.35x10^{19}$and (c) $6.59x10^{19}$ions/cm^3

Annealing at 300°C

Based on the results of the film annealing studies, the waveguides were initially annealed at 300°C for 256 and 589 hours as further improvement in PL properties was then expected. The measured 1/e lifetime values of all three annealed waveguides as compared to the as deposited waveguide results are shown in figure 3.8.

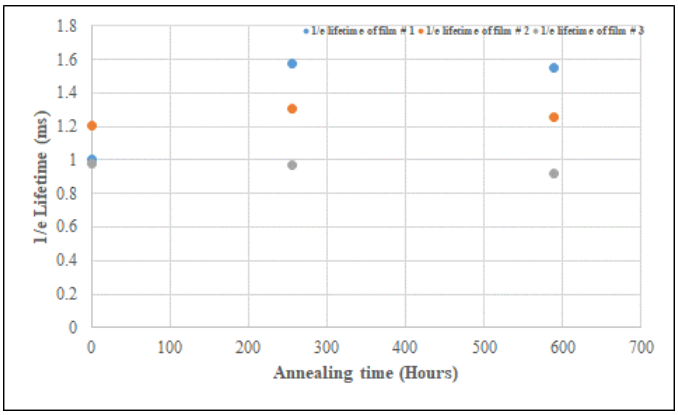

Figure 3.8:1/e lifetime of Er doped TeO_2waveguides# (a) $3.85x10^{18}$, (b) $2.35x10^{19}$and (c) $6.59x10^{19}$ions/cm^3annealed at 300C for 256and 589 hours.

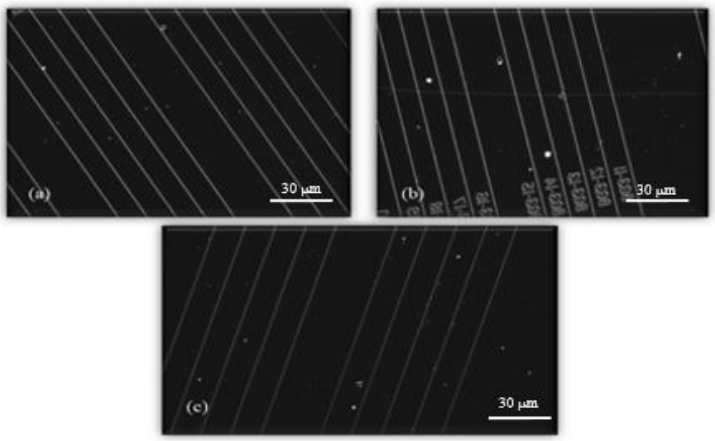

Figure 3.9: Dark field images of annealed Er doped tellurite waveguides # (1) $3.85x10^{18}$, (2) $2.35x10^{19}$and (3) $6.59x10^{19}$ions/cm^3at 300C for 589 hours.

Given the improvements seen on the glass slide samples, the results are disappointing. Only the low doping sample showed any significant improvement, and the highest doped sample (still well below what is needed for planar devices)

actually got slightly worse. PL intensity followed the same relative trends with little change in amplitude (<10% reduction relative to unannealed for the higher doped films). The observed PL lifetime reduction with little corresponding change in PL intensity in the highest doped film could also reflect an increase in the film refractive index during annealing (from structural densification, new species formation, etc) which would result in a drop in lifetime. As this was a processed waveguide wafer, unfortunately the refractive index could not be measured on the SCI Filmtek. The only plausible reason why the behaviour was so different to the glass slide samples relates to the multicomponent nature (sodium, potassium etc.) [246] of the glass used with relatively low T_g [247], which may have allowed diffusion of the more mobile species [248] into the TeO_2. This would lower the refractive index and raise the maximum phonon energy thereby enabling a longer $I_{13/2}$ lifetime.

Annealing at 350^oC

Next,the impact of raising the anneal temperature to 350^{o}C (likely above T_g) for 24 and 48 hours was assessed. The 1/e lifetime values are shown in figure 3.10. The PL results are not better than the unannealed films with the1/e lifetime first fell slightly then stabilised with increasing annealing time. PL intensity fell relative to the unannealed films by ~20% at the longest anneal times in all films.

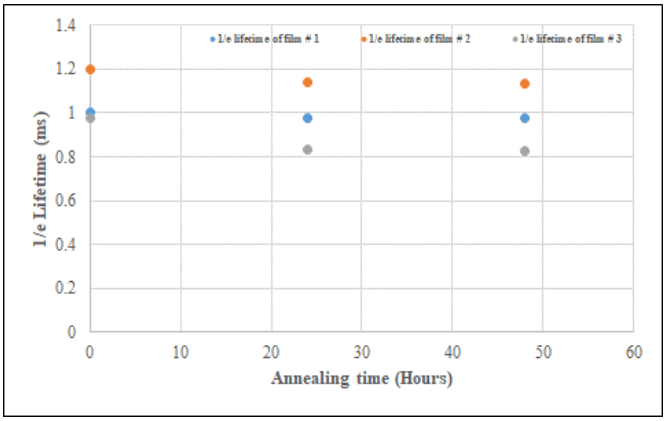

Figure 3.10: 1/e lifetime of Er doped tellurite waveguides # (1) $3.85x10^{18}$, (2) $2.35x10^{19}$and (3) $6.59x10^{19}$ions/cm^3 at 350C for 24 and 48 hours.

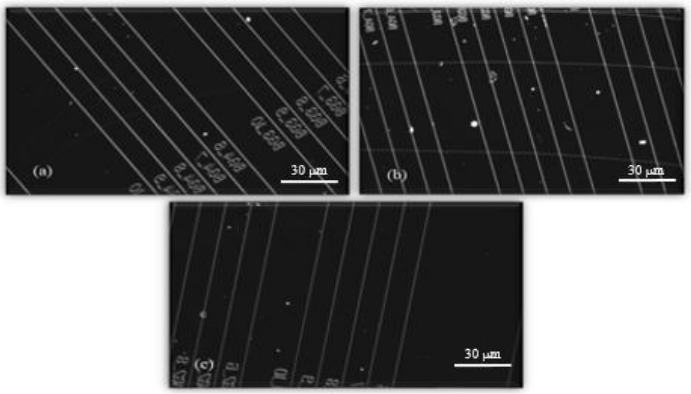

Figure 3.11: Dark field images of annealed Er doped tellurite waveguides # (a) $3.85x10^{18}$, (b) $2.35x10^{19}$and (c) $6.59x10^{19}$ions/cm^3at 350C for 48 hours.

After annealing for 48 hours (fig 3.11) some cracks in the film are quite noticeable as compared to as deposited (fig 3.7) or annealed at 300°C (fig 3.9) waveguide surfaces. This may be related to the cooling rate for the samples, but no further investigation was performed. No sign of crystallisation is apparent in all annealed waveguides (fig 3.9, 3.11). Annealing was also tested at 400°C with much the same PL results, cracking being more apparent, but importantly no film degredation or crystallisation was observed. At 500°C, total film destruction occurred.

Discussion

The prior annealing study on tellurite films [232] appeared to prove that annealing is a promising remedy to drive out OH from doped tellurite films with commensurate significant improvements in PL properties. Thus, the results obtained here seem somewhat surprising in terms of the lack of improvement especially given the known OH contamination in the films. However, the films presented in the referenced study were shown to be quite porous with a highly granular structure with large surface area that was not seen in reactively sputtered films fabricated here. This likely allowed far more significant penetration of free/unbound OH into the film (and so close to the erbium) which also appears to have been quite weakly bonded and could be driven off by relatively low temperature annealing. Similar behaviour was also observed in magnetron sputtered Er:As_2S_3 films [3]. The weakly and strongly bound OH absorption dips were little affected by the annealing regime tested and were still > 100x that the bulk glass from which the films were fabricated.

Further carefully constructed experiments are required in the current case to determine how the OH contamination in the films was affected by the thermal annealing. The results obtained imply it was not which further implies that the deposition process needs to be significantly improved to prevent OH contamination occurring.

Whilst there was no evidence of improved PL performance in the waveguides tested, there is a net positive in that the films were not destroyed even after being annealed well above the glass transition temperature and that the PL properties were not significantly degraded in that process. This may come to be of significant value with very highly doped films where multi-atom clusters are known to occur and degrade performance, and high temperature annealing is a known route to dissociating these and improving doping uniformity.

Cracking of the TeO_2 film is clearly an issue for high temperature regimes likely due to thermal shock and thermal expansion mismatch with the silicon substrate. Tellurite glass has a larger thermal expansion coefficient (typically of the order of $10^{-5o}C^{-1}$) [249] compared with silica ($5.5x10^{-7}\ ^oC^{-1}$) and silicon ($2.6x10^{-6o}C^{-1}$). This can lead to tensile stress getting built into the film upon cooling and subsequent cracking. The furnace used for the studies had no ramping option and it is possible that the cracking could be avoided by using a controlled temperature ramping at low ramp rates (< 5 ^oC/min) on both heating and cooling.

3.3 Concentration Studies.

Given the need to get to very high erbium concentrations, a key need was to optimise undoped and Er doped tellurite sputtered films [250] and investigate the PL properties at varying Er concentrations. The objective was to undertake this study using the Angstrom EvoVac system over which we had complete control to limit contamination and guarantee access. Of particular relevance as will become apparent, the Angstrom system is “box coater” style system with a door that has to be opened after venting to change substrates. The internal schematic of sputtering chamber manufactured by Angstrom Sciences is shown in figure 3.12.

Initial studies were made with pure tellurite depositions, where a 3-inch Tellurium target (< 99.95% pure) was loaded into one target holder, and a metallic erbium target (> 99.95% pure) into another sputter gun for later use. The target was mounted 45° off vertical and facing upwards with a 10 cm distance between the

centres of the target and substrate (100mm diameter wafers). The power of the erbium gun was varied to change the Er ion concentration in the deposited films. The chamber was initially pumped to approximately 2 x 10^{-6} Torr using a cryopump (Brooks Automation CryoTorr CT-10) before commencing deposition.

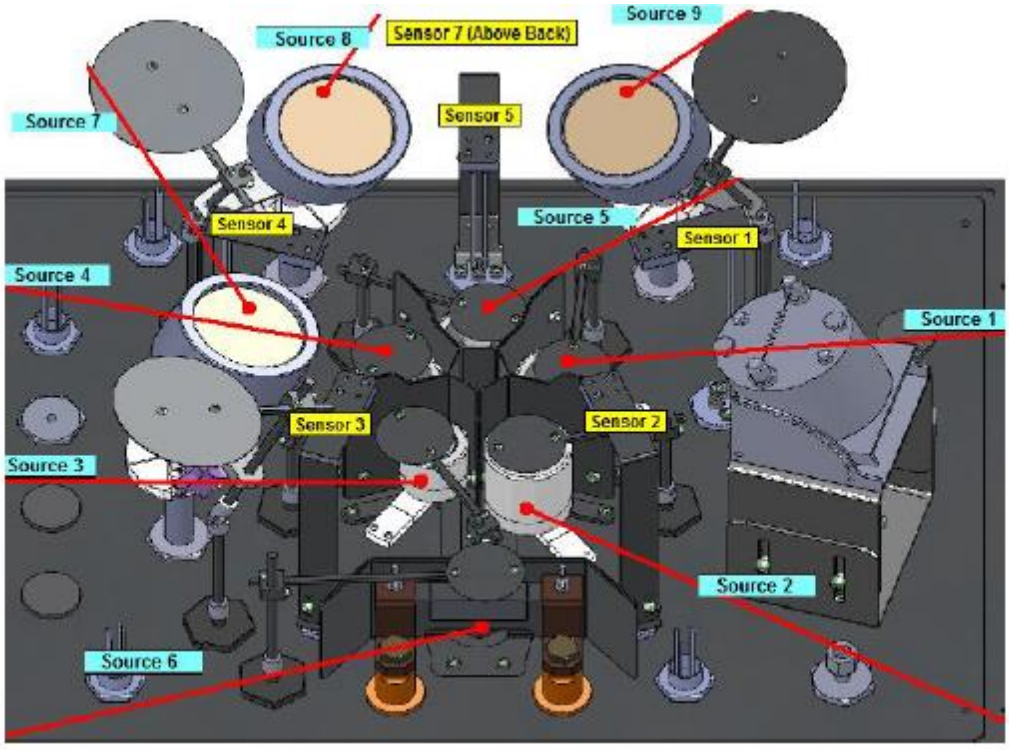

Figure 3.12: Internal view of Angstrom chamber manufactured by Angstrom sciences: 6 sources for co-thermal evaporation, and 3 guns for RF sputtering.

For the tellurite only sputtering, a silicon wafer (525 µm thickness) was mounted and different Argon to Oxygen flow rate ratios trialed with a total gas flow of 11 sccm (standard cubic centimeter per minute) in order to get the desired stoichiometric refractive index (2.07-2.08 at 1550 nm). The starting purity of the gasses was 99.999% and it was then passed through gas purifiers (NuPure IIII, 9924, 250 PSIG MAX) to reduce contamination to the ppb level. Moreover, this flow was chosen by following prior work [219]. Sputtering was carried out at a pressure

of 5.1 mTorr via an automatic pressure control system operating on the cryopump gate valve. During the deposition process, the applied sputtering power was set to 75 W (25% of full power), deposition rates in the system being monitored by a quartz crystal microbalance mounted in the deposition plane and adjacent to each sputter gun. The thickness and refractive index of the prepared films were measured using a dual angle spectroscopic reflectometer (SCI FilmTek 4000).

3.3.1 Films Growth issues.

The measured refractive indices, film thicknesses, and deposition rates corresponding to varying Ar/O_2 ratios are shown in table 3.2. The ratio was varied to achieve the required stoichiometric oxidation by balancing the number of Tellurium atoms sputtered with oxygen atoms available for reaction in the sputtering atmosphere.

Table 3.2: Measured refractive indices, deposited tellurite films thickness, and rates corresponding to applied gases ratios.

Argon (Sccm)	Oxygen (Sccm)	Ar/O Ratio	Refractive Index	Thickness (nm)	Deposition Rate (A/s)
6	5	1.2	1.98	1530	2.7
6.5	4.5	1.44	2.05	1522	2.6
7	4	1.75	2.08	1092	2.86
7.1	3.9	1.82	2.08	1500	2.95

After achieving refractive indices (and by extension tellurite composition) close to the refractive index of bulk TeO_2 [219] at 1.75 and 1.82 Ar/O_2 ratios, erbium doped films were deposited with the Er gun power set to 5% (12 W) on a TOx wafer (5000 nm thickness). Two ratios (1.75 and 1.82) were tested. The measured properties are stated in table 3.3.

Table 3.3: Measured refractive indices, deposited Er doped tellurite films thickness, and rates corresponding to applied gases ratios.

Argon (Sccm)	Oxygen (Sccm)	Ar/O Ratio	Refractive Index	Thickness (nm)	Deposition Rate (A/s)
7	4	1.75	2.03	1300	3.32
7.1	3.9	1.82	2.06	1500	3.3

A result consistent with the prior work [219] at 2.06 was achieved at a 1.82 Ar/O ratio. Then, erbium concentrations were increased by raising the power of the erbium sputter gun to study the concentration dependent refractive index and lifetime as high doping is needed for planar power amplifiers. The Refractive indices and film thickness of all films were measured with the Filmtek 4000 and WDS analysis was used to measure the Er concentration in each fabricated film. The measured refractive index, thickness, Er concentration, and 1/e lifetime at 1550 nm with 1490 nm pumping corresponding to each fabricated film are listed in table 3.4. The relationship between refractive index and 1/e lifetime vs Er concentration is also shown in figure 3.13.

Table 3.4: Measured refractive indices, deposited Er doped tellurite films thickness, rates, Er concentration and 1/e Lifetime values corresponding to applied gases ratios.

Er Power (%)	Refractive index at 1550 nm	Thickness (nm)	Rate (A/s)	Er Concentration (ions/cm^3)	1/e Lifetime (ms)	Pump Intensity (kW/cm^2)
5	2.06	1710	3.0	$4.29x10^{18}$	2.146	838.56
10	2.06	1590	3.3	$5.30x10^{19}$	1.909	871.59
15	1.99	1504	2.82	$2.95x10^{20}$	0.692	885.19
15	1.91	1009	1.86	$2.09x10^{20}$	0.351	1095.35

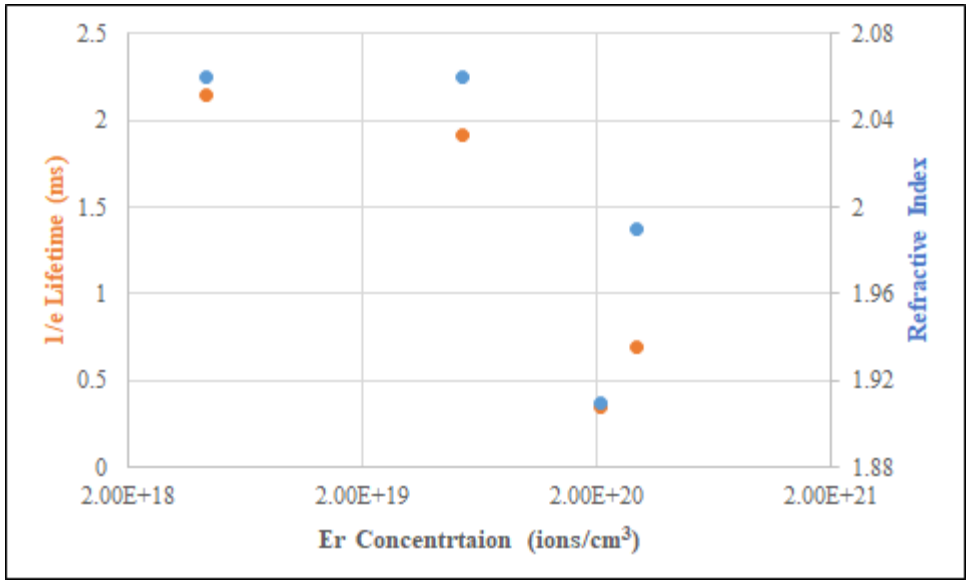

Figure 3.13: Effect of varying Er concentration on refractive index (@1550 nm) and 1/e lifetime.

The results do not show a consistent trend and show poor repeatability for the 15% power setting. Prior work [219] did not study the expected effect of Er concentration on measured refractive index values. Huang et al [183] studied the effect of varying Er concentration on the refractive index (at 632 nm) of pure tellurite based glasses, which is shown in figure 3.14.

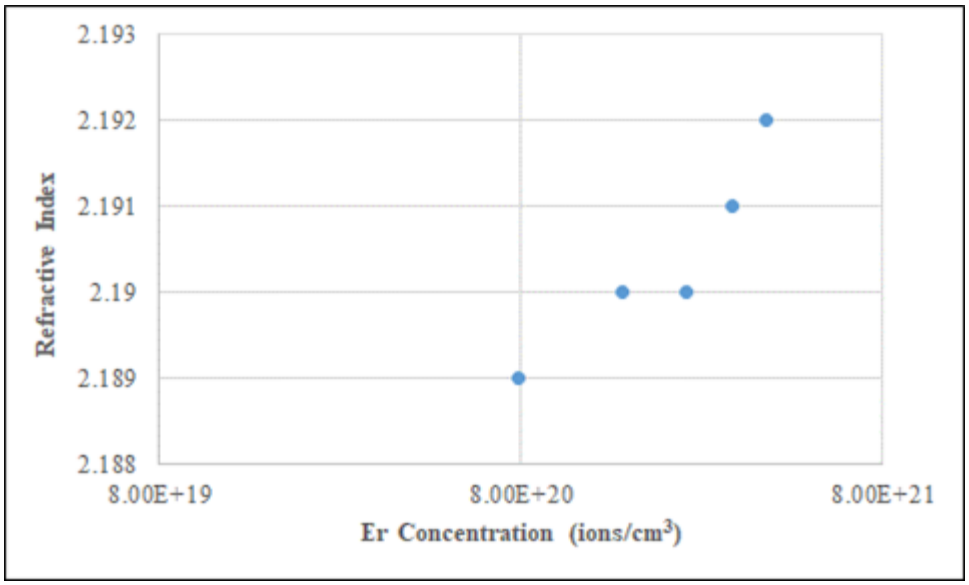

Figure 3.14: Measured refractive index versus Er concentration in doped Tellurite based glasses [183].

The refractive index increased with increasing Er concentration, but only quite weakly (~0.001 per 10^{20}/cm^3). Similar behaviour was observed by Dai et al. in Er doped (0.22-13.4 x10^{19} ions/cm^3) multicomponent tellurite glasses (TZL) [65]. Therefore, in deposited films (figure 3.13) it was expected to achieve a similar relationship between refractive index and Er concentration. In contrast, the measured refractive indices in the fabricated films were decreasing with

increasing Er concentrations and faced inconsistency while repeating the same deposition recipe. Non repeatability issues were frequent beyond 10% (26W) Er power. At 15% (43W) erbium gun power, a significant drop in deposition rate (table 3.4) was recorded and alteration in film stoichiometry is inferred due to significant reduction in the refractive index and 1/e lifetime values. It is possible that with increasing Er power, more metal is sputtering into the system and there could be more oxygen needed to achieve the consistent refractive index value at varying Er concentrations. The stoichiometry variation can easily lead to changes in film structure and host environment, and in fact significant variation in lifetime with film stoichiometry was previously observed [219].

Based on prior studies [65] the reduction of $I_{13/2}$ level lifetime [226] at higher Er concentrations could also occur due to both increases in the probability of polyatomic sputtering and the energy transfer rate involving both Er ions and quenching centres (OH groups). The current measured lifetime results can be compared with prior studies.

The photoluminescence decay vs concentration was also studied by Agazzi et al [251]in reactively sputtered Er doped aluminium oxide waveguide samples with different Er concentrations ($0.27x10^{20}$ to $4.22x10^{20}$ ions/cm^3), where ion clustering, available defects within host material and undesired impurities were concluded as the sources of the concentration quenching process.As Er concentration increased beyond $2x10^{20}$ ions/cm^{3}a rapid decline in 1/e lifetime was evident with the curve indicating a fall in lifetime from 7.5 ms to below 1 ms at ~7 $x10^{20}$ ions/cm^3. Dai et al [65] also observed a reduction in lifetime in Er doped tellurite glasses at varying Er concentration, in this case driven by OH concentration in the glass. Shen et al [172] measured the longest lifetime of $I_{13/2}$ level (5.1 ms) at $3.11x10^{20}$ ions/cm^3; while at $0.93x10^{21}$ ions/cm^{3}Er concentration the lifetime is reduced to 2.9 ms, this is due to non-radiative effects from concentration quenching but authors did not mention the dominating effects. Contrary to the above results is however the data presented earlier in Figure

3.1from Jha et al [220]. This indicates unambiguously that it is possible to obtain long lifetimes at very high concentrations provided that the OH concentration is low enough (< 1 cm^{-1} optical absorption at 2750 nm) and that the rare earth is uniformly distributed, and the works just discussed highlight some of the issues that need to be overcome.

Despite the evident lifetime quenching and undesireable refractive index drop, it should be noted that the results of figure 3.13 are significantly better than prior pure TeO_2 film measurements [219] when considering the highest doped film. Previously films were deposited in a different deposition system (AJA International chamber), which does not have a gas purifier and a 1/e lifetime value of 0.31 ms was obtained for a film with $2.9x10^{20}$ ions/cm^3 Er concentration compared with 0.7 ms here. In the AJA film, the film stoichiometry did not appear to change at higher Er concentration (up to $2.9x10^{20}$ ions/cm^3) as the measured refractive index of the deposited films remained in range 2.06-2.07 at 1550 nm. However, due to high levels of OH contamination in the deposited films [227] quenching in PL lifetime was observed [219] that was consistent with the OH contamination.

As the Tellurium target was completely eroded at this stage, it was possible that the non-repeatability exhibited could have been related to this. The target was therefore replaced and the concentration study repeated. Initial depositions revealed an issue with thermal contact as the Indium solderbond between the Tellurium puck and the copper backing plate failed. From this point on all subsequent runs a silver particle impregnated silicon rubber thermal pad was used behind the Tellurium target to ensure good thermal contact to the water cooled electrode.

Before proceeding with doped fabrications, an undoped film on silicon was deposited as a test run at 1.82 Ar/O_2 ratio. The measured refractive index value of 2.07 indicated stoichiometric conditions and that the chamber was in stable

condition and ready to fabricate films. Doped films were next deposited and the measured Er concentration, thickness, refractive index, and deposition rate of deposited films corresponding to applied Er powers are listed in table 3.5 below:

Table 3.5: Measured Er concentration, refractive indices, thickness, deposition rates corresponding to applied Er powers.

Applied Er Power (%)	Er Concentration (Ions/cm^3)	Thickness (nm)	Refractive Index	Deposition Rate (A/s)	Pump Intensity (kW/cm^2)
5	$3.35x10^{18}$	1612	2.07	3.4	802.98
10	$7.2x10^{19}$	1522	2.06	3.3	795.15
12.5	$1.82x10^{20}$	1513	2.02	3.3	805.21
15	$2.23x10^{20}$	1432	2.03	3.3	846.72
17.5	$3.04x10^{20}$	1574	2	3.1	772.23
20	$3.35x10^{20}$	1467	2.03	3.4	823.15
15	$2.09x10^{20}$	1459	2.02	2.7	828.28
17.5	$2.21x10^{20}$	1640	1.98	3.4	800.03

At high Er concentrations, again the film refractive index was reducing and non-repeatability setting in, indicating issues in the film growth. The measured 1/e lifetime of the $I_{13/2}$ level was also decreasing with increasing Er concentration as shown in figure 3.15.

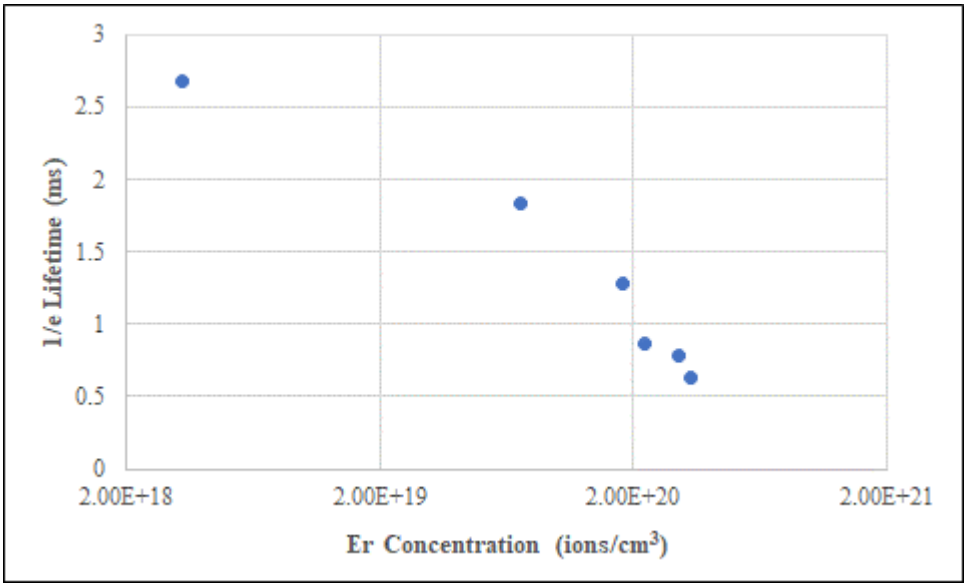

Figure 3.15: Measured 1/e lifetime values w.r.t measured Er concentrations.

The results show some improvement over Fig 3.13, the low concentration result in particular showing a lifetime of 2.67 ms which to the Author's knowledge is the highest ever demonstrated in pure TeO_2 exceeding that of even recent work on Er doped pure TeO_2 bulk glass [183]. The same work performed a JO analysis on the Er:TeO_2 glass which indicated the $^4I_{13/2}$ transition fundamental radiative lifetime to be 3.6 ms, so the result here is approaching that indicating good material quality. There is however still a strong decline in lifetime with increasing Er concentration. The result at 3 x 10^{20} /cm^3 is superior to Fig. 3.13 but still represents a significant decline especially in the context of the results of Jha et al [220]. It is also clearly not good enough to get to the concentrations required for high power on chip devices. Deposition repeatability and overall refractive index values were also still not good for the higher concentration samples, and

none of these issues could be addressed without consistency in the deposition technique so that an optimised process could be developed. Thus attention turned to improving process stability so that the underlying causes of the lifetime drop with concentration could be studied and rectification attempted.

3.3.2 Improvements to Custom Sputtering System

The refractive index is varying almost randomly in table 3.5, which is unacceptable in terms of both optimising the process and getting repeatable results. The question is why? The Angstrom system had some observable issues in its operation and a lack of monitoring systems, so modifications were made to the system to try to improve performance. Table 3.6 outlines the measures taken.

Table 3.6: Revised Custom Sputtering System.

Machine Impediments	Infrastructure Development
Inconsistency from run to run	Logging System, DC bias monitor
Unreliable machine Control/readouts	Higher precision gas flow controller, revised wiring to reduce noise
Inconsistent RF matching to Plasma	Monitoring and control system
Building process cooling variable conductivity -DC bias on target	Self-contained high impedance water cooling system for sputter guns

A desired feature was in-situ optical monitoring, but unfortunately there were no ports in the vacuum system that would enable this.

Inconsistency from run to run of Tellurite.

Inconsistency from run to run was addressed by implementing a comprehensive logging system to monitor all process parameters (sputter gun DC biases, Forward power, Reverse power, Load and Tune capacitor positions, magnitude and phase outputs from auto-match unit, etc.) as reactive sputtering relies upon stability in these parameters. DC bias monitoring kits for the sputter guns were purchased and installed in the Angstrom, and full monitoring system software implemented in Labview using a LabJack 80 port analog input card enabling the logging of many signals at any time interval from 0.3 seconds to 100 seconds. Results were logged to disc for further analysis.

Unreliable machine Control/readouts

Issues were observed with the process data coming back to the control computer from the Angstrom system not being reliable or fluctuating. This affected the mass flow controllers in particular at the +/- 0.2 sccm level, and given the known sensitivity to gas ratio, something needed to be done to ensure gas ratio stability. High precision (+/- 0.01 sccm) controllers were installed which also featured readouts on the MFC of the actual gas flow measured at the head. Wiring inside the machine was also modified and some screening installed to prevent noise pickup within the tool on control lines and read backs.

Inconsistent RF matching to Plasma.

Issues were apparent with the auto-matching RF networks with the system sometimes unable to lock onto the low reflected power state and in some cases strike a plasma. These were mostly resolved when the monitoring system allowed logging of data to see the issues and allow fine tuning of the control pots on the units.

Variable conductivity of cooling water-DC bias on target

The building process cooling water used on the Angstrom system was found to be affecting the gun DC bias as its conductivity changed due to routine maintenance and periodic replenishment/depletion of antifouling agents. This was in direct

contravention to what we had been told by the system vendor, and to overcome this a separate self-contained cooling loop was built. This used a Neslab M700 chiller with an electrically floating three port manifold using longer and larger plastic supply pipes to increase water flow rates and >1 MΩ-cm resistivity water fill as a solution to stabilize the discharge conditions. This resulted in an immediate 50 V increase in gun DC bias.

Backup Plan

Given the issues being faced, a backup plan was also actioned that involved building a small load locked Ion Beam Sputtering system using a chamber and 6 cm ion gun donated by CSIRO. Here high rate deposition from already homogeneously doped targets (available through the University of Adelaide glass facility) could be non-reactively sputtered to achieve the film quality and repeatability IBS is well known for. The system came together over a period of 18 months and is fully computer controlled (see Fig. 3.16)

Figure 3.16: Ion Beam Sputtering (IBS) Chamber.

Multiple COVID lockdowns meant the system and source glass was not available when needed or in time for this project, and this technique will be used in the future for further testing and comparison.

3.3.3 Further Research findings from Modified Sputtering System

After modification of the sputtering system, the goal was to re-optimise the process whilst examining the monitoring data to determine how to attain a more repeatable process.

The first step was to work on the pre-deposition part of the process. For each process run, the Tellurium target was cleaned by sputtering in pure Argon for a period to remove any contamination/atmospherically induced oxidation layers on top of the target surface before switching to the desired gas mix and conditioning the target before commencing deposition. With the new monitoring system it was possible for the first time to see how much time was required to attain stability

in these two pre deposition phases rather than arbitrarily assigned fixed (2 minute) timings to these phases. Before commencing the sputtering, it was observed that almost ten minutes were required to attain stability.

Next, work recommenced on optimising the gas ratio in the hope that this could be better studied and stabilised with the new gas controllers. It was found these offered improved stability and accuracy close to the controller specifications and that the numbers presented in the software did actually match what the display on the controller head was measuring. As this chamber did not have a load lock, then to speed up the testing of different gas ratios, an Aluminium mask with one triangular sector shaped hole was mounted as close as possible to the wafer to get five depositions on one silicon wafer without breaking the vacuum (see Fig. 3.17) The wafer was rotated between depositions by manually turning the drive motor to index to a fresh piece of silicon.

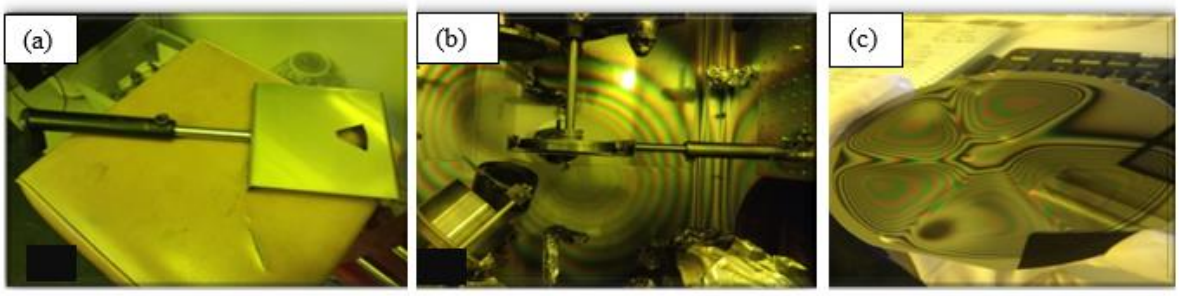

Figure 3.17: (a) Aluminium mask for consecutive five runs without breaking vacuum, (b) Mounted mask between target and substrate in the chamber and (c) deposited films on one wafer.

Sputtering of undoped tellurite was then resumed with the initial goal of exploring the gas ratio dependence with better resolution than previously possible with the new high resolution MFCs and by making many more depositions based on the

masking setup. Many depositions were carried out, and again huge inconsistency observed particularly around the desired operating point.

Cutting a long and arduous story very short, there were several findings that emerged from the study. Firstly, DC Bias was not found to correlate in any way with film stoichiometry and so was not a useful control parameter. It did however provide a linear measure of target erosion and so is useful for monitoring target health and to provide input to long term process tuning as the target ages. As previously noted it was also very useful in determining how long the preconditioning steps need to be to achieve stability. The second finding was that there was a clear tendency for the system to become unstable in terms of refractive index control when the chamber was vented. The major issue here relates to the partial pressure of oxygen in the chamber not being stable because of unoxidized tellurium the quantity of which depends upon; when it was last vented, how long it was vented for, whether metallic sputtering occurred and when, how much metal was in the chamber, etc.

Reactive sputtering processes can often follow a hysteresis loop concept [252] as shown in figure 3.18 where achieving a stable oxide mode sputtering state requires direct control over the oxygen partial pressure in the chamber rather than the oxygen flow [253].

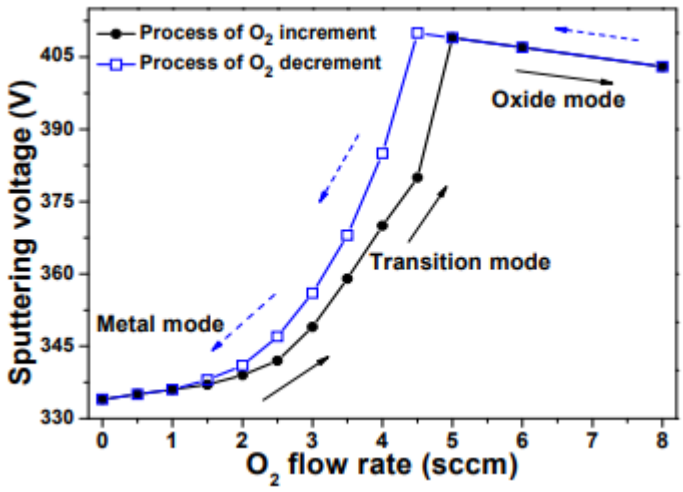

Figure 3.18: Hysteresis effect during sputtering [254].

3.3.4 Further machine Development and Success

As noted above, the only solution to the instability problems was to control the chamber oxygen partial pressure. There is a very delicate balance between the available oxygen in the camber and the rate at which metallic Tellurium is sputtered off the target. For ideal stoichiometry just enough oxygen is needed to oxidise all the Tellurium that comes off but no more to prevent higher oxidation states previously shown to slowly degrade performance [225].

An oxygen measuring tool (Zirox, SS27/MS27, figure 3.19) was therefore sourced, installed and calibrated from 1-95 mTorr using a 20 sccm oxygen flow and the capacitance manometer on the chamber to enable accurate detection and control of the oxygen partial pressure.

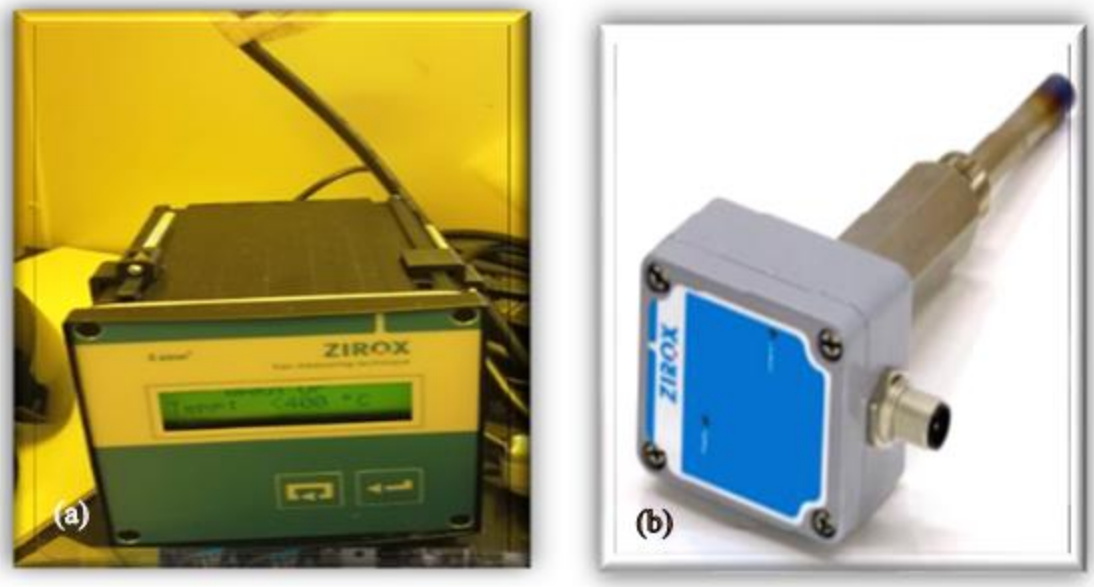

Figure 3.19: Oxygen sensor: (a) monitor and (b) Probe.

The calibration process was repeated five times to ensure consistency as this was a key parameter. The oxygen sensor requires half an hour to warm up before deposition can be commenced. The initial data is presented in Table 3.7, where applied sputtering power of Te gun was set to 71 W (25% of full power) and wafer monitor was used to report the sputtering rate.

Table 3.7: Measured promising values corresponding to applied gases ratios and partial pressure of oxygen.

Ratio (Ar/O)	Rate (A/s)	O_2 pressure (mT)	DC Bias (V)	Refractive index
1.36	0.67	1.04	-207	2.01
1.36	0.69	1.02	-209	2.04
Break the vacuum, Chamber opened loaded new Si wafer				
1.42	0.66	1.08	-204	2.01
1.42	0.68	1.07	-205	2.04
1.44	0.74	0.95	-201	2.05
Break the vacuum, Chamber opened loaded new Si wafer				
1.62	0.84	0.88	-190	2.05
Break the vacuum, Chamber opened loaded new Si wafer				
1.72	0.86	0.84	-185	2.04
Break the vacuum, Chamber opened loaded new Si wafer				
1.86	0.8	0.82	-184	2.04

The decision of sensor installation was quite useful because after a bit more process development now consistency in required results as stated in table 3.8 is achievable. The stability in results after breaking the vacuum and switching the ratio randomly from low oxygen concentration (1.86) to high oxygen concentration and vice versa was also checked. This time, consistent results were obtained. Even with the oxygen sensor, care is required in the sputter process set up and control/reaction to the sputter rate and oxygen pressures are key parameters to achieve consistency in each run. For example, it was tried to balance the oxygen pressure with the sputtering rate by rebalancing gas composition (Adjustment of Argon flow) to achieve consistency. Based on the reading from

the sensor, tried different Ar/O ratios to come back to something in the range of 0.8 to 1 mT of oxygen. Moreover, as the chamber got oxygen rich that is why the oxygen partial pressure value went away from the range of 0.8 mT to 1.0 mT of oxygen. After achieving consistent results it was decided to proceed with concentration studies.

3.3.5 Consistent and Stable Results

The oxygen partial pressure has been controlled to about 0.6 mT, which just happened to correspond to 1.8 ratio (set 5sccm oxygen and 9 sccm Argon), fabricated undoped and doped tellurite films on Tox wafers and so far, consistent, and stable results are shown in Table 3.8 below:

Table 3.8: Deposited undoped and doped tellurite films with persistent promising values of each parameter.

Run #	Te/Er Gun Power (W)	Te/Er monitor Rate (A/s)	O_2 pressure (mT)	DC Bias (V)	Refractive index
1	Break vacuum, Chamber opened, new TOx wafer loaded				
	71, 0	0.93	0.61	-183.82	2.07
2	Break vacuum, Chamber opened new TOx wafer loaded				
	71, 14	0.85,0.51	0.59	-185.59	2.07
3	Break vacuum, Chamber opened, new TOx wafer loaded				
	71, 29	1.07,1.01	0.57	-186.82	2.061

Moreover, the deposition rate of Te and Er was monitored by microbalance mounted in the deposition plane and adjacent to Er sputter gun respectively.

Deposition recommendations

A few important conclusions were reached from the above work to assist in obtaining high quality close to stoichiometric films and are listed below:

- Use 0 sccm oxygen and 15 sccm Argon to strike the plasma because it has been determined experimentally that pure Ar struck more reliably than Ar/O mixture. Therefore, initially set Ar only to strike the plasma.
- After striking the plasma, immediately switch to the sputter gas mixture and set the selected gas ratio (Oxygen: 5 sccm, Argon: 9 sccm) manually during soak 2 time.
- During soak 2 time, the deposition rate and oxygen pressure values should be in the range 0.75- 1.0 A/s and 0.55 -0.75 mTorr respectively to get stoichiometric results in both undoped and doped films.
- To obtain the suggested ranges for oxygen partial pressure and deposition rate, adjustment of Argon flow during the soak 2 control time is the recommended route to achieve consistent results.
- Then start the program after completing the soak 2 (600 secs), which set initially.

Hence, the oxygen sensor proved a key element for the repeatable fabrication of good quality stoichiometric undoped and doped tellurite films. However, because of multiple COVID interruptions, the opportunity to get the end results and investigate and optimise the concentration testing was lost.

Conclusion

After deep studies of significant issues in reactive sputtering and custom enhancements to the sputtering system (MFC, water cooling system, monitoring system, oxygen partial pressure control etc.), a stable and repeatable process to fabricate high quality undoped and Er doped tellurite films was achieved with the resultant films having apparently the best ever lifetime for Tellurium dioxide.

The stable sputtering process developed for the fabrication of doped reactively sputtered tellurite films can now be used to finally and scientifically study the impact of high Er concentrations in pure TeO_2 films and allow the development of processes to match the outstanding performance achieved in highly Er doped pure and multicomponent TeO_2 glasses. This would then allow a high saturated output power optical amplifier to be built on chip, a key technological milestone. It is however clear that further development work around adding dedicated vacuum water vapour pumping is necessary as part of this study to reduce OH incorporation because rare earth lifetimes are significantly affected by OH contamination in particular.

Chapter 4: (part a) RF Sputtered Er doped As_2S_3 films.

4.1(a) Why Arsenic Trisulphide (As_2S_3)

As_2S_3 is a promising host glass for planar MIR rare earth doped devices as it has already been proven to be fabricated into low loss waveguides [120]. Arsenic trisulphide was therefore studied further despite the issues previously identified in prior research elsewhere and at ANU, to see if there were adequate means to resolve these issue as the waveguiding is already well advanced.

Arsenic trisulphide is a chalcogenide glass, comprised of covalently bonded arsenic and the chalcogen element, Sulphur [256]. It is a naturally occurring substance in crystalline form as orpiment and realgar frequently occurring in proximity to volcanic activity. In glassy form it has a transmission range from ~500 nm to ~9 μm [257], high refractive index (2.43 at 1550 nm) [258], high optical nonlinearity (2.5×10^{-14} cm^2 W^{-1} at 1550 nm, about 100x that of silica) [259], very low two photon absorption (TPA) coefficient (three orders of magnitude lower than silicon) [260], a high material nonlinear figure of merit (FOM) [261] from NIR to MIR, low propagation loss [262], and low processing temperature [263], and can exceed rare earth (Er^{3+}) ion solubility (~4%) [264][265] in unannealed As_2S_3 films [120] with 3x higher emissions at 1550 nm, compared to similarly doped GeGaS bulk glass. Additionally, high purity As_2S_3 bulk glass can be produced by melt quenching with less than 0.01 dB/cm loss in the telecommunications band. These spectral properties make it an ideal alternative to silicon [266] for NIR nonlinear optical applications and a good

candidate for many MIR applications [267] in the field of (low loss) integrated optics [268].

4.2 (a) Motivation of this Work

In prior studies, a previous PhD student had tested thermal evaporation and RF sputtering for the fabrication of Er doped arsenic trisulfide films. Relatively low loss rare earth doped waveguides (0.35 dB/cm) were fabricated from thermally evaporated Er doped arsenic trisulfide films using an undoped As_2S_3 "loading strip" to make a rib waveguide. Unfortunately, the fabricated waveguides had very limited internal gain due to Er ion clustering [120] that was intrinsic to the deposition method itself. However, RF sputtering is widely considered as a device-quality films deposition technique [3]. So following on prior research [269], previous student attempted to use this technique as a promising alternative [69] to eliminate erbium ion clustering from the deposited films and successfully achieved significant PL performance out of sputtered films as compared to thermally deposited ones [3]. Thus, given these and other successes [270] with sputtering [160], it is considered that RF sputtering produces material with much less Er clustering than thermal evaporation [3]. In contrast, the sputtered films displayed an unexpected property, where all emissions from them have been quenched. The effect was presumed to arise from a formation of nano-columnar structure during deposition and RF sputtering can be responsible for that. Though thermal annealing has proven to be the promising remedy to partially overcome deposition based issues but failed to completely destroy the columnar growth. The failure was confirmed with green light annealing test on thermally annealed films where PL intensity got completely quenched after green light treatment. Thus, the question of whether rapid post deposition treatment can densify the material without allowing the erbium to precipitate needs to be investigated as the performance is otherwise excellent with a clear path to low loss waveguide devices.

4.2.1 (a) Effect of Thermal annealing on Photoluminescence Results

It is widely known and reported in the literature that columnar structures are frequently formed in magnetron sputtered dielectric films due to the growth habit of RF sputtering [271] and moisture can easily be trapped from the air into a sputtered film along the columnar boundaries. However, according to prior studies, up to 40x [160] improvement in PL emission has been observed in thermally annealed RF sputtered Er doped As_2S_3 films. Therefore, prior student decided to investigate the impact of thermal annealing (130^{o}C for 24 hours) [265] on the photoluminescence properties of 848 nm thick Er (0.1 mol%) doped As_2S_3 sputtered film. The previously studied PL emission results of as deposited and annealed films are restated in table 4.1 [3].

Table 4.1: 1/e Lifetime and Photoluminescence intensity of thermally annealed (130 degrees for 24 hours in Vacuum) Er doped As_2S_3 sputtered film [3].

$I_{13/2}$ state of Er under 1490 nm pumping	As deposited sputtered film	Annealed sputtered film
1/e Lifetime (ms)	1.18	~1.82
PL intensity (mV)	120	~440

Clearly, annealing [160] enables some of the doped erbium ions to re-bond in a proper way as well as activate more erbium ions optically [272]. That is why improvement in 1/e lifetime and PL results of annealed film as compared to as deposited sputtered film was observed.

4.2.2 (a) Photo Degradation in Rare Earth doped Waveguide

In previous experiments, almost total quenching of emission was observed when the RF magnetron sputtered waveguides were pumped at 1490nm [219]. It was clearly established that the reason for this was the intense upconverted green light in the core of the doped As_2S_3 waveguide [3]. Green light (2.31 eV) is above the bandgap (2.2 eV) of As_2S_3, and it was established that this causes bond rearrangement and incorporates OH^- already in the matrix due to the nanoporous structure of RF sputtered As_2S_3, which results in the quenching of the erbium emission effectively [3]. Light annealing experiments at 550 nm wavelength with ~10 mW/cm^2 intensity in ambient air for 48 hours almost completely quenched the PL intensity of annealed films. The evidence of water diffusion in waveguide was confirmed in undoped RF sputtered As_2S_3 film, which was later patterned into waveguide [3]. After repeatedly each thermal and light post-treatment on 2um wide waveguide, the propagation loss was recorded [3]. From this recording, it was concluded that after each light post- treatment an evident absorption band at 1430-1480 nm showed up but disappeared after each thermal post-treatment (figure 4.1). The observed absorption band at this wavelength was considered to be appeared due to moisture in the air. The moisture in the air is highly presumed one of the main reasons contributing to overtones of the O-H stretch vibration near 3600cm^{-1} [273] in the fabricated waveguide [3].

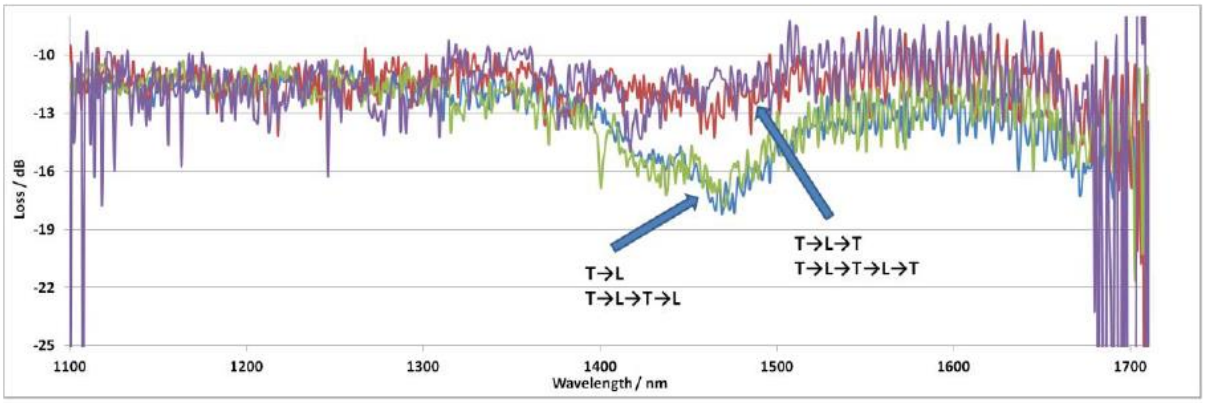

Figure 4.1: Loss spectra of RF sputtered As_2S_3 waveguide after thermal (T)/ light (L) post-treatment [3]*. These spectra were recorded with OSA and using SC source as probe source.*

Proposed Approach

Aside from switching to another completely different deposition technique (unavailable at the time of this thesis), the logical means to prevent the OH incorporation is to prevent it from penetrating in the first place. This would require sealing the pores or eliminating them completely. One option to accomplish this is to exploit the low melting temperate of As_2S_3 and flash melt the glass using rapid thermal annealing (RTA). RTA was originally developed in the semiconductor industry to offer an annealing process that was too fast to allow for thermally driven diffusion of dopants. Thus there appears to be a reason to believe it could seal the pores without allowing sufficient time for Er ion diffusion and clustering to occur [265] in sputtered films.

4.3 (a) Film Fabrication for RTA experiments

A 3-inch As_2S_3 glass target was loaded into the target holder which was mounted 45° off vertical and facing upwards with 10 cm distance between the target and wafer (substrate). A piece of erbium foil was stuck onto the As_2S_3 target surface

with carbon tape to act as an erbium ion source. The Angstrom EvoVac chamber was initially pumped down to $1.5x10^{-7}$ Torr and the pure argon gas was introduced through a mass flow controller with a flow rate of 20 sccm was used for the creation of the sputtering plasma. During the deposition process, the sputtering power was set at 43 W, resulting in a sputtering rate of ~0.1 nm/s in our system. The obtained films were coated with a 100 nm SU-8 layer for protection purposes. Then, film thickness, refractive index, and bandgap of the films were measured at the film center and the edge, to check the uniformity of the whole film, using the FilmTek 4000. The measured thickness, bandgap, and refractive index (at 1550 nm) of the obtained film were 1100 nm, 2.2 eV, and 2.4 respectively. The photoluminescence properties of doped films were measured using the fibre quasi-confocal setup. In addition, the PL measurement results in a detected voltage from the photodiode induced current through the use of a transimpedance amplifier. Given all the uncertainties in the amount of collected light, the detected voltage is a somewhat arbitrary measure of the total emitted intensity and cannot be easily compared meaningfully between different film depositions. It is not an absolute measure nor even a reliable relative measure between different depositions. The results were therefore left in raw Volts.

4.3.1 Rapid Thermal Annealing (RTA) Results

Two different types of RTA were tested, isochronal at 190, 220, 250, 270, 288 ^{o}C, for 1 minute and isothermal at 200^{o}C with 2, 4, 8, 16, 32, 64 mins. Testing was performed on two RF sputtered Er doped As_2S_3 film samples (cleaved from same wafer) and it was implemented in ambient atmosphere. Due to malfunctioning of the designated RTA furnace, it was decided to use a standard oven for the rapid heating and cooling process. The annealing was performed in a pre-heated oven at the desired temperature for a specified duration time. When the furnace achieved the preselected RTA temperature then quickly loaded the furnace with the sample. The samples were on the glass tube and that tube was pushed

immediately into the flat surface of the furnace. After the annealing process, samples were slowly pulled out and naturally cool down under the ambient air as well. The PL intensity and 1/e lifetime of the $^4I_{13/2}$-$^4I_{15/2}$ transition of erbium ions at 1490 nm excitation with 1136.96 kW/cm^2 excitation power were measured before and after RTA treatment. The results are displayed in Figures 4.2 (a) and 4.2 (b). In the isothermal tests at 200^{o}C of figure 4.2 (a), the PL intensity dropped rapidly with time, from 0.43 V (without annealing) to almost zero (completely quenched) in the 64 minutes annealed sample. Besides, the prominent fall in lifetime in the samples annealed over 6 mins from 1.9 ms to zero (completely quenched) in and over 32 mins annealed samples was observed as well. It is well known that $I_{13/2}$ state lifetime is a sensitive measure of interactions of Er ions with defects and ion ion interactions [274]. The drop in lifetime might be due to activation of cross relaxation process between the ions, which is facilitated by the magnetic or electric dipole interaction [275]. Thus, majority of Er ions might experience nonradiative transitions more frequently and that relaxation might be via defects linked with Er ions. Therefore, the concentration of optically active Er ions significantly changed during the isothermal test and annealing for longer times significantly increased the nonradiative transitions. In the 60s isochronal samples (figure 4.2 (b)), PL intensity dropped from 0.43 V to 0.145 V in the 190^{o}C treated sample, and to almost zero in the samples treated over 250^{o}C. The considerable drops in PL intensity shown in RTA treated films indicated that rare-earth ion clusters [229] were formed during RTA treatment. The abrupt decrement might be attributed to the formation of closely-spaced erbium ions such as Er clusters or precipitates [276], thus strong Er-Er interaction, resulting in the nonradiative relaxations [274].

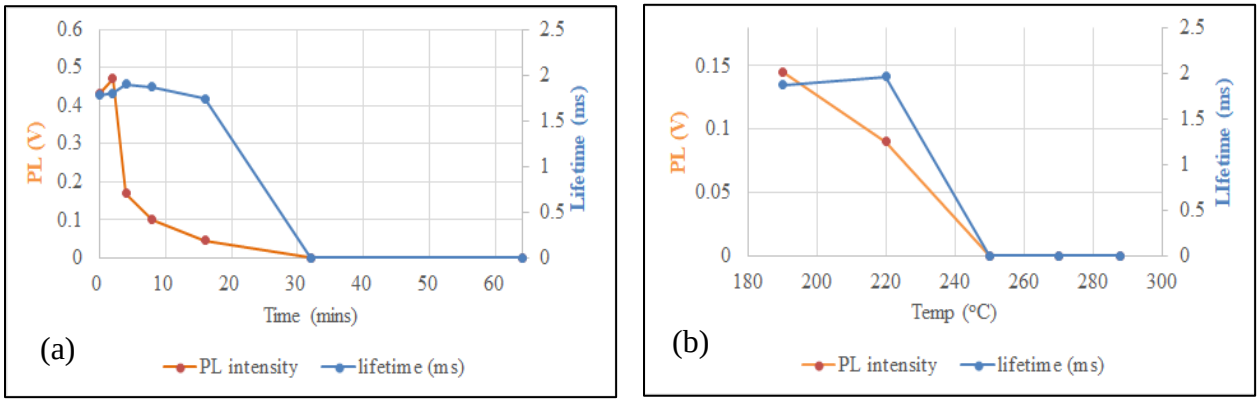

Figure 4.2: (a) Variation in PL intensity and 1/e lifetime at a fixed temperature (200°C), (b) Variation in PL intensity and 1/e lifetime at a fixed time (the 60s).

4.3.2 Film Quality of Pre-and Post-Annealed Films

The film quality of pre- and post- annealed samples were examined using dark-field microscopy. No obvious melting was observed in all isothermal films, whereas melting signs started to appear in the isochronal film annealed at 270°C and got prominent in the film annealed at 290°C for 60 secs. Cross-section images of as deposited and the 290°C for 60s RTA treated film were captured and are displayed in Figures 4.3 (a) and 4.3 (b) respectively. Signs of softened or melted surface and resultant reflow an evident in annealed film at 290°C for 60s. However, the film surface was softened when annealed above Tg but it could not seal it up enough to achieve better PL without diffusing the erbium, as the results are shown in figure 4.2.

Figure 4.3: (a) Cross-sectional view of Er doped As_2S_3 film on Tox with a top layer of SU-8 (100 nm), (b) Melted surface of Er doped As_2S_3 film at 290°C for 60s thermal annealing.

4.3.3 Two Days Green Light Annealing Effects

After RTA treatment (isochronal and isothermal), all samples were placed under green light (550 nm) illumination at ~10 mW/cm^2 for two days. Pre and post the green light exposure, repeated PL and 1/e lifetime testing at 1550 nm emission wavelength under same conditions (section 4.3.1). PL properties in all films got quenched due to the nanoporous structure of RF sputtered As_2S_3 films, where green light did bond rearrangement and incorporated the OH^- in the matrix, thus quenched the Er emissions.

These observations are similar to previous investigations where PL degradation in waveguides occurred overtime with green light annealing, plus transmission spectra exhibiting an OH dip in green light annealed samples, but loss recovery after thermal annealing [3] as reproduced in figure 4.1.

Thus, this observation implying RTA is not an effective remedy to remove the nanoporous structure in the RF sputtered Er doped As_2S_3 films.

Conclusion

Rapid thermal treatments still allowed erbium to thermally cluster at treatment times beyond 2 minutes or temperatures beyond 200°C for 1 minute. Whilst film melting was observed with the presumption that the glass is densified, this results in clustering and emission quenching. At temperatures where the emission is still

active, the treatment was shown to be ineffective in preventing green light activated OH induced quenching. Therefore, RTA is not an effective solution to the problem at hand.

Recommendations

RTA cannot solve the porosity problem, and it is clear that magnetron sputtering is not a viable way forward without further measures to alter the film growth habit such as bias sputtering or ion gun bombardment for example [277]. Alternatively, the adoption of an entirely different method is needed. Coating a moisture barrier layer on the film and hermetic sealing to protect it could be an option though this is difficult and relatively costly at the device scale. Other film deposition methods that do not have an intrinsically columnar growth habit, like ion beam sputtering (IBS) should also be investigated.

Chapter 4: (part b) Thermally Evaporated Er doped GeGaS films.

4.1(b) Why GeGaS

The known clustering problems from the thermal evaporation of Er and the low solubility in As_2S_3 indicate that it is required to use a glass with high solubility [120]. Gallium containing glasses are long established to have high rare earth solubility e.g. [278] and were previously investigated.

Though GeGaSe also has very good Er solubility and up to 55% inversion has already been achieved. However, photoinduced absorption was encountered in GeGaSe which presented a new hurdle to realising net gain [33]. Unfortunately, most of the intense up-conversion related emissions (at 980, 800 nm, 670 nm, 540 nm, and 520 nm from radiative decay from the $^4I_{11/2}$,$^4I_{9/2}$, $^4F_{9/2}$, $^4S_{3/2,}$ and $^2H_{11/2}$ states respectively to the ground state) are situated in the bandgap or the strong part of the Urbach tail in Ge-Ga-Se host material. Photon energy close to or higher than the bandgap energy of the glass matrix can directly excite Er ions by electronic processes [279]. In addition, the reverse process is also possible, so both higher level excitation and upconverted light can create free electrons and so absorption in the host material. Furthermore, the intensity of the up conversion related emissions in the waveguides could be increased due to the small mode area (~2 μm^2) of fabricated waveguides and these emissions can generate the photoinduced absorption loss [33]. It is strongly suggested in the literature [3] that this high intensity upconversion related emissions can increase the insertion loss by coupling with the insensitivity to high power 1490 nm (pump) light as well. Thus, these processes could be the contributor to the observed photoinduced loss in GeGaSe waveguides [280].

Photoinduced absorption issues in GeGaSe due to upconverted light were already observed in unpublished investigations by the prior PhD student. As shown in figure 4.4, exposing a GeGaSe waveguide to green light (~550 nm) significantly increases the waveguide propagation losses. Such increases in propagation loss can completely destroy the performance of the GeGaSe amplifier.

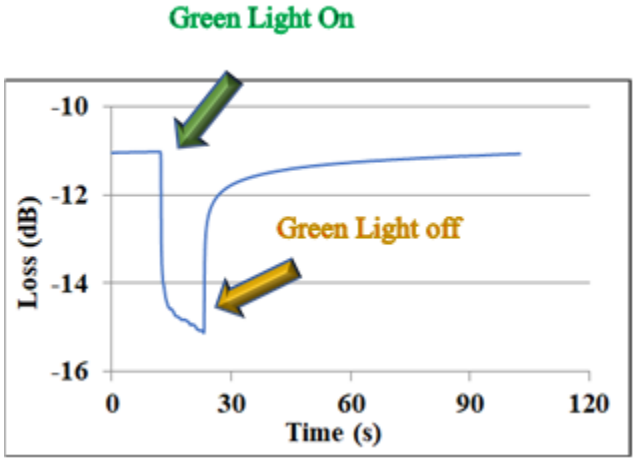

Figure 4.4: Photoinduced loss (at 1550 nm) change with time with green light in a 28 mm length $Ge_5Ga_{20}Se_{75}$ waveguide [3].

Sulphide glasses typically have a somewhat shorter wavelength band gap [281] than their Selenide analogs [282], and so they are potential candidates to avoid this problem [283]. For example, GeGaS glasses are anticipated to be good materials for this purpose due to their short band gaps at short enough wavelengths to avoid photo-induced absorption issues. In addition, photoinduced absorption is not observed in GaLaS films and the shorter wavelength bandgap of sulphide has suppressed the photoinduced absorption effect, which will discuss in detail in chapter #6.

Moreover, the glass composition $Ge_{28.5}Ga_{6.2}S_{65.3}$ was chosen based on prior work [3] identifying an optimum Ga content to achieve high dopant concentration as well as being a candidate for low photoinduced absorption.

4.2 (b) Evaporation Methodology

Initial tests were carried out in the previously described Angstrom EvoVac system but now configured for thermal evaporation. An alumina coated crucible with baffle was used initially for the evaporation of $Ge_{28.5}Ga_{6.2}S_{65.3}$ bulk glass. The crucible was half filled with high purity (5N) bulk glass with a baffle on top to avoid the material spitting and causing defects and loaded the crucible into one of the heated sources. The distance between the used Si wafer substrate and the loaded crucible was 40 cm. The evaporation rate and film thickness were monitored by two quartz crystal microbalance that were mounted adjacent to heated source and in the deposition plane respectively. A shutter was placed between the substrate and the source to avoid deposition before achieving stable conditioning of the deposition process. The deposition process started when the chamber was fully pumped down to $2.2x10^{-6}$ Torr. The melting temperature of the used GeGaS bulk glass was unknown so it was decided to evaporate GeGaS bulk glass at different evaporation temperatures beyond the minimum that achieved a stable evaporation rate. Different evaporation temperatures were achieved by manually operating the source power. The shutter was opened after achieving a stable evaporation rate. The required temperature was then set in the monitoring system to run the evaporation process for a few hours to deposit thick enough film for further studies.

4.2.1 Successful Evaporation and Encountered Problems.

First experiments showed that there was no deposition whatsoever at a source temperature of 450°C. Beyond 450°C, a stable deposition rate (2.8 A/s) was achieved at a source temperature of 677°C and a film was deposited, but the glass remaining in the crucible after the process went from being a yellow clear glassy

material to a material that was white and chalky in appearance as shown in figure 4.5 (a). The compositional analysis (WDS) of the deposited film at 677 °C set temperature is illustrated in table 4.2.

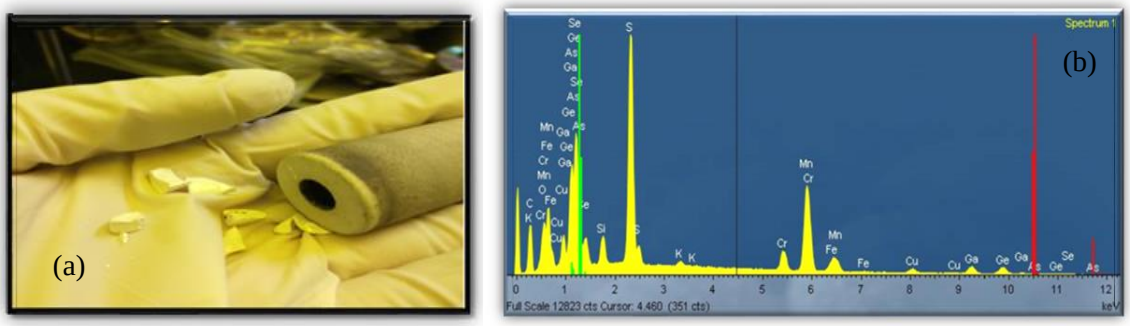

Figure 4.5: (a) White and Chalky leftover glass in the crucible, (b) EDS Spectrum of thermally evaporated GeGaS glass film on Si wafer.

At high operating temperatures (~900 °C) no stability in deposition rate was achieved so it was decided to keep increasing source power to attain deposition at higher temperature. However, beyond 950°C no evaporation rate was recorded by the gold electrode quartz microbalance sensors in any circumstances so the evaporation process was trialled at 1300°C. At high temperatures (~1300°C) the glass appeared to react with the alumina and melted through the bottom of the crucible thereby destroying the furnace, crucible, and thermocouple connection as well. High resolution, non-destructive elemental analysis of deposited film was measured with energy-dispersive xray spectroscopy (EDS, Hitachi 4300 SE/N Schottky) [284]. An EDS investigation of the evaporated material at 1300 °C showed the presence of GeGaS in deposited film (on Si wafer), the spectrum of which is shown in figure 4.5 (b). However, the deposited film was not thick enough for

compositional analysis (WDS) and the stoichiometry of the deposited film could not be determined.

Table 4.2: Atomic% of Ge, Ga, and S in fabricated films at 677°C operating temperatures.

Set Operating Temp(°C)	Thickness (nm) of the film	Deposition rate (A/s)	Ge (at%)	Ga(at%)	S(at%)
Bulk Glass			28.5	6.2	65.3
677	1556	2.8	38.02	0	61.97

4.2.2 Research Impediments

During the initial evaporation experiments, more major issues that caused significant delay were encountered. These included: Issues with the power controllers in the Angstrom system and issues with the insulation in the furnace connection.

The power controllers in Angstrom system for evaporation furnaces constantly blowing fuses at lower temperatures due to the low resistance of the sources and the power supply having no current limit. These fuses were not of a commonly held type and it took over a month to source replacements from overseas. This had to be done twice. It was found that the problem could only be avoided by using an appropriate cleaning procedure. The parts of the used furnace such as Cu disk, the ceramic washer, and the ceramic insulation as shown in figure 4.6 (a) were submerged in (10%) KOH solution overnight, rinsed in hot water dried using a clean cloth, and placed in an oven at 120°C to release any trapped moisture from the washed components. The ceramic washer and ceramic insulation were sand

blasted as well to completely remove any deposited layer of contamination. Before cleaning there was a resistance of 0.3 ohm between the Cu connections and there was an open circuit between one of the Cu connections and the base of the furnace. After the cleaning and reassembly, the resistance value was 1.3 ohm between the Cu connections.

Another commonly known reason for frequent blowing fuses is a loose connections. The power leads can be pushed too far through the Cu connection disks, and touching the furnace body will result in a blown fuse. While reassembling the furnace, no loose connections were noticed. Checks, such as confirming the wire tie connections at the top of the filament were tight and set screws in the Cu disk were held away from the leads of the furnace so that in the event they came loose they would not cause a failure.

To improve the efficiency of the thermocouple, its wires were put out of contact with the Cu disk and the baseplate. The wires were also shortened such that any twisting would be impossible. This is relevant because this is where the temperature is measured from, and the source potentially over drive to correct for any temperature deviation, which may result in temperature in a catastrophically high region.

The furnace connections insulation was also a potential source for a blown fuse. The connectors in the vacuum are bolted to the leads on the feedthrough and need to be insulated. If they are twisted or pushed together a short may occur, or if the connectors are not fully insulated and a connection becomes loose it could arc and blow the fuse. Insulation can wear and fray over time increasing the probability of a short. After consultation with Radak (the manufacturer), glass weave sleeves were used to cover the furnace lead wires to overcome degradation issues. As shown in figure 4.6 (b) the wires are not touching the Cu disk or the base plate of the chamber.

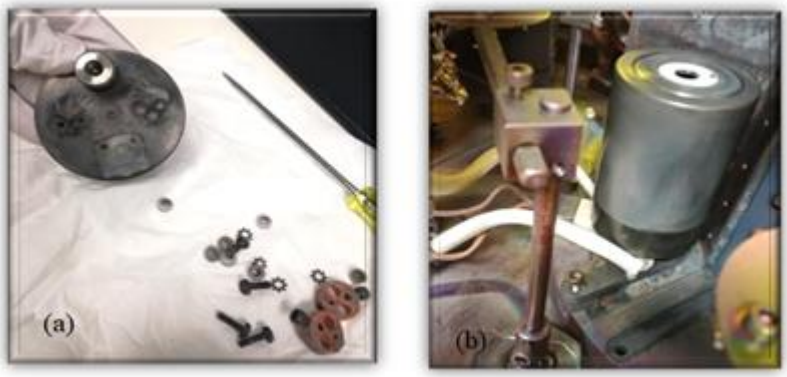

Figure 4.6: (a) Cu disk, ceramic washer, and ceramic insulation for cleaning, (b) Glass weave on lead wires, which are connected to the base of the newly installed furnace.

After modifying the furnaces and employing the insulation procedure, the issue of blowing fuses was resolved and proper experimentation could commence.

In addition, to improve the monitoring of the evaporation rate, at high operating temperatures alloy crystal sensors were used instead of gold quartz crystals. This is the result of no deposition recorded by the Gold electrode quartz microbalance sensors at a 1330^{o}C operating temperature despite a thin film appearing on the Si substrate. Further details will be explained in Chapter#5.

A final precaution was that the replacement alumina crucibles contained no exposed metal on the outside to limit the risk of short circuiting the filament.

4.2.3 Modified System

Attempt#1:

After updating the furnace, tests resumed and no deposition rate at all was observed until 490^{o}C operating temperature. Further increasing the furnace temperature led to an observed deposition rate of 2.77A/s at 650^{o}C, a typical figure in the Angstrom system. After achieving a stable rate of 3.0 A/s at 677^{o}C,

a film was deposited for two hours with a measured thickness of 1556 nm and refractive index of 2.41 (at 1550 nm), which was obtained using the Filmtek 4000 (discussed previously).

The remaining material in the crucible after the deposition had the same white and chalky appearance as with the previous experiments but with black flakes which peeled off the inner side of the crucible. The composition of leftover material was tested by EDS analysis and shown in figure 4.7. This shows that evaporation began from the bulk glass at or below 677°C, which is believed to be GeS_2 evaporating out of the glass matrix (table 4.2).

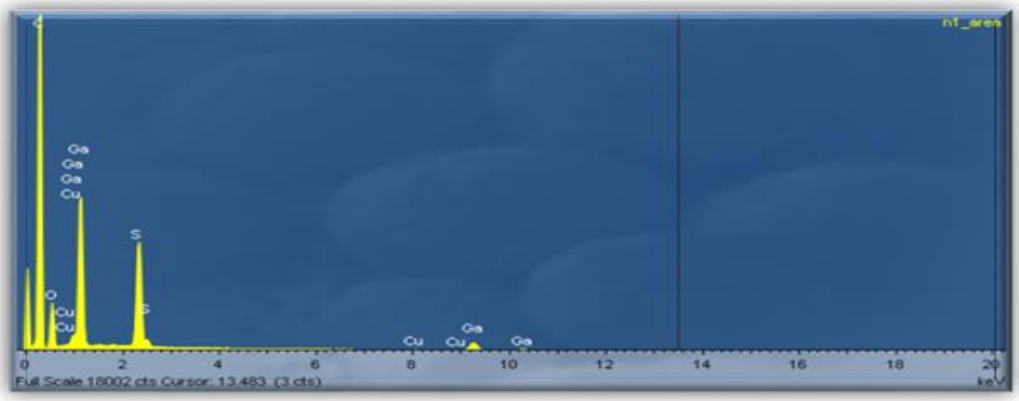

Figure 4.7: Confirmed Ga and S content availability in leftover powder in the crucible.

Analytical Study of the deposited films

EDS analysis of the remnant material in the crucible was carried out (figure 4.7) showing that the white material had a chemical composition predominantly Ga_2S_3. A reason for this is due to the difference in the melting temperatures of GeS_2 and Ga_2S_3. The melting temperature of GeS_2 is 615°C whereas Ga_2S_3 melts at 965°C. Secondly, according to prior studies [286], generally, chalcogenides have lower

field strengths and weaker chemical bonding [287]. This is why they are transmissive at long wavelength regimes, at the cost of poor physical and chemical properties. Additionally, it is mentioned in literature based on sulphide glasses containing germanium that due to excess GeS_2, the phase separation has been investigated in the system. The molecular liquid issue is a well-known problem in chalcogenide glasses that is, which describes how a single phase can evaporate off from the bulk. The proposed solution is the addition of lanthanum (La) as a glass modifier in the glass matrix to increase the thermal stability of the chalcogenide glass without compromising the transmission properties at a longer wavelength [286]. Instead of adding La, it was decided to evaporate the glass at a temperature where Ga_2S_3 would melt (>950^{o}C). The starting temperature was set to 677^{o}C at which point the deposition process would be allowed to start by opening the substrate shutter.

Attempt#2:

The evaporation process was initially started with the set 677^{o}C operating temperature, which was achieved at 21% applied operating power of the used source. The monitored rate at 677^{o}C operating temperature was 1.36 A/s. As stated above, it was decided to increase the power of the source to 28% applied operating power. The achieved operating temperature was 980^{o}C with 1.10 A/s evaporation rate. At 980^{o}C the material was evaporated for two hours. The measured film thickness was 600 nm with a 2.26 refractive index at 1550 nm. However, the available amount of leftover white material in the crucible indicated that the deposited film is not going to have uniform composition through its depth. According to literature, it is a common issue for evaporation deposition to be unable to achieve ideal stoichiometry [270]. The alternative method to achieve ideal stoichiometry could be RF magnetron sputtering but instead of moving toward different technique preferred to try a different method of evaporation using the same technique.

4.2.4 Flash Evaporation

It was clear from the data presented above that simple evaporation was not effective at depositing a uniform $Ge_{28.5}Ga_{6.2}S_{65.3}$ film, and that the only means of using thermal evaporation to circumvent phase evaporation/distillation was to trial flash evaporation. Flash evaporation aims to rapidly raise the temperature to a level above that of the highest component evaporation temperature such that all components are evaporated together [288].

The first attempts were made using a PID controller to drive the temperature ramping at 100^{o}C per minute. The plan was to start deposition at 455^{o}C after 2000 seconds of soak time and then set 980^{o}C as a required operating temperature. The set temperature was achieved in nine minutes due to fast controller ramping. The furnace and substrate shutters were opened simultaneously once the set operating temperature had been reached. The recorded rate at 980^{o}C was 63A/s and the deposition process was stopped after two minutes. The final deposited film thickness was 1210 nm with a refractive index of 2.29 at 1550 nm as measured with the Filmtek 4000. The digital quartz crystal thickness monitor accepts the density of material, acoustic impedance and the tooling factor as inputs before starting the measurement. In current work, tooling factor has been around 100 %. The density of the material is 3.75 kg/m^3 and the acoustic impedance is 1.00. The tooling factor between the crystal position and the substrate position was not calibrated. That is why the difference in calculated and measured thicknesses was observed. The final composition of the deposited film was confirmed by WDS analysis, where film stoichiometry ($Ge_{29.61}Ga_{1.82}S_{68.57}$, table 4.3) did not match with the stoichiometry of the used bulk glass ($Ge_{28.5}Ga_{6.2}S_{65.3}$).

In the deposited film the Ga concentration was the key difference between what was expected. Likely due to the already stated high melting point of Ga_2S_3 compared to Ge_2S_3. To account for this it was decided to rapidly raise the temperature to achieve already stated goals with off ramping of PID controller at different set temperatures. Two different temperatures were selected to fully

understand the flash evaporation effect on the final composition of deposited film, 980°C and 1100°C. 980°C was selected as this temperature is closer to the melting temperature of Ga_2S_3. For the sake of comparison, this temperature was used twice with the 'on' and 'off' ramping of the PID system to compare the stoichiometry results between these two settings. 1100°C was chosen to investigate the effect of higher temperatures on the final stoichiometry of the deposited film.

For these experiments, the glass is heated to a temperature just below the point where GeS_2 is liberated from the bulk material and then ramped to the desired evaporation temperature as fast as was possible (typically two minutes) to ensure that both components are evaporated together.

For the experiments with 980°C set as the operational temperature, which was achieved in five minutes, the deposition rate was quite variable and decreased with the increasing thickness of the film. The resulting surface of the deposited film was full of particles, which is the common spitting issue of flash evaporation at high temperatures [289][288]. The process finished in three minutes and the measured thickness of the deposited film on the silicon wafer was 1100 nm with a 2.32 refractive index at 1550 nm, the stoichiometry of which is included in table 4.3.

In the absence of PID ramping, the film composition was closer to the bulk material.

For this 1100°C temperature experiments, a new (Alumina) crucible and (Tantalum) baffle was used to possibly prevent the material from spitting during deposition. The set temperature (1100°C) was achieved in two minutes and again the deposition rate was variable and could not be monitored reliably. Moreover, no material was left in the crucible. The measured thickness and refractive index of fabricated film was 1184 nm and 2.260 respectively. The film had fewer visible defects after the deposition than the previous experiments indicating that the fitting of the baffle cap is vital in avoiding defects due to spitting. As mentioned

earlier, there are many issues in achieving the ideal stoichiometry in the deposited films with evaporation processes, but the elemental results at 1100°C are quite promising as compared to 980°C operating temperature experiments (table 4.3).

The composition of the deposited films was measured with WDS and recorded in table 4.3.

Table 4.3: Atomic% of Ge, Ga, and S in fabricated films at different flash evaporating temperatures.

PID controller ramping status	Operating Set Temperature (°C)	Deposition Rate(A/s)	Deposition process duration (~mins)	Thick (nm)	Ge (at%)	Ga (at%)	S (at%)
On	980	63	2	1210	29.61	1.82	68.57
Off	980	-	3	1100	29.73	3.05	67.21
Off	1100	-	2	1184	28.49	9.99	61.54

The film evaporated at 1100°C without PID ramping has a composition quite close to the bulk glass ($Ge_{28.5}Ga_{6.2}S_{65.3}$). Despite this, the flash evaporation method cannot be used to fabricate Er doped films due to the short evaporation time, lack of controllability (such as rate, thickness, etc.) and repeatability of the deposition of films including erbium doping level, so, this line of experimentation was discontinued.

Conclusion

Standard thermal evaporation method has proven not a viable way forward for evaporation of $Ge_{28.5}Ga_{6.2}S_{65.3}$ powder. Flash evaporation was considered as a successful strategy. Film deposited in this manner at 1100°C has a composition

of $Ge_{28.49}Ga_{9.99}S_{61.54}$ in less than two minutes, which is quite close to the composition of the used $Ge_{28.5}Ga_{6.2}S_{65.3}$glass. The issues with this method are the difficulties to observe the rate during experimentation when the controller ramping status was set to “Off” in the PID system, which leads to difficulties in controlling the thickness of the film. Furthermore, no consistency in compositions was observed in the fabricated films (<1100^{o}C) and the material remaining in the crucible was pure Ga_2S_3. As a result, there was a genuine concern that the film is not going to have uniform composition through its depth. This method would not be compatible with fabricating Er doped GeGaS films due to the shortest interval of time of evaporation. The lack of controllability, repeatability, and Erbium doping level is also a consideration.

It is proposed to move to co evaporation of GeS_2 and Ga_2S_3 from separate rate-controlled furnaces in the future to get consistent composition. It is estimated that 90% GeS_2 and 10% Ga_2S_3 can be used to fabricate one micro thick uniform film with the required atomic ratio ($Ge_{28.5}Ga_{6.2}S_{65.3}$). It is also recommended to use Pyrolytic Boron Nitride crucible and baffle for further thermal evaporation process.

Chapter 5: Thermally Evaporated As_2S_3 +Er_2S_3 films.

5.1 Why Erbium Sulphide (Er_2S_3)

It was previously identified that the doping of thermally evaporated chalcogenide films needs to be performed with a rare earth doped compound (Er_2S_3, $ErCl_3$) rather than metal (Er) to eliminate clustering from the evaporation source [121].

The condensation of evaporated material vapour onto a cold substrate is non-equilibrium process, which provides inadequate time for the material to restore its metastable equilibrium state. On the one hand, this provides opportunities to incorporate more dopant than the material's solubility limit allows, as there is insufficient time for diffusion and clustering to occur. This is one of the potential upsides of planar integrated rare earth doped structures. However, for this to be of value it is critical that the dopant is not already clustered when incorporated into the film. It was realised in past studies [3] that due to polyatomic evaporation from Er metal sources, the emission properties of rare earth doped films having low solubility were severely compromised. Furthermore, as As_2S_3 has already limited erbium solubility due to the available significant fraction of clustered Er ions in Er doped As_2S_3 thin film based waveguide amplifiers, no improvement in gain (from 1570 nm to 1630 nm) with increasing pump (1490 nm) power has been reported in prior work [120]. Thus, the use of a rare earth compound which can be directly incorporated into the host matrix (i.e. already bonded with S for As_2S_3) should avoid the issue of deposition induced clustering in evaporated films. As previously noted in detail in chapter 4 of this Thesis, despite its poor solubility, As_2S_3 is a good host candidate due to its good waveguiding and low photoinduced absorption properties and so is worthy of further attempts to optimise the rare earth doping process.

5.2 Challenges

Prior unpublished fabrication work by a previous PhD student [3] already observed that once the wafer temperature rises much above 70°C during deposition, the As_2S_3 film quality degrades rapidly. This was a problem for doping with Er_2S_3 as the melting temperature is stated as 1730°C, meaning the evaporation source is likely to heat the wafer substantially. Thus, work was initially conducted on thermally screening the source to avoid overheating of the deposited films.

5.2.1 Evaporation Process

The high melting temperature of Er_2S_3 is beyond the normal recommended range for the Radak furnaces in the Angstrom EvoVac system and so initially evaporation from open boats was trialled. There is no information available in the literature about evaporation temperatures, processes, vapour pressure etc. for Er_2S_3 and so there was much uncertainty about the requirements. Therefore, attempts were made to thermally screen the boat from the wafer using copper heat shields ultimately bolted back to the water cooled copper heat isolator between the Radak sources in the bottom of the chamber to avoid reaching the unacceptable temperature (> 730°C) where the copper shield starts to melt in a vacuum system.

Attempt #1

The first attempt was made using a Tungsten open boat filled with pure Er_2S_3 powder (5N) with a 1mm thick copper heat shield as is shown in figure 5.1. Thermocouples were mounted to the boat and heat shield to monitor the temperature as the boat temperature was manually raised. At a boat temperature of 1300°C, the shield became unacceptably hot at 680°C. After opening the chamber it was clear that the erbium sulphide had not evaporated but some material had melted and reacted with the base of the chamber. Though the chamber base was not damaged, the copper shield was dissolved due to attaining the high temperature.

Figure 5.1: Post Evaporation condition of (a) Loaded Tungsten boat (b) Cu shield and (c) damaged base of Cu shield.

Next, it was decided to use a thicker copper shield, which was bolted back to the water cooling system to successfully achieve the evaporation of used powder.

Attempt #2

A thicker 3mm shield was therefore constructed which was connected back to the water cooled copper heat isolator between the Radak sources in the bottom of the chamber. The rest of the setup was the same as the first attempt. With this configuration the boat temperature reached 1232°C before the copper was at risk of evaporating and no signs of Er_2S_3 evaporation at this temperature were observed. Upon opening the chamber, it was found that the Tungsten boat had

broken and so a change was made to heavier duty Molybdenum boats. However, it proved difficult to keep the thermocouple in contact with the base of the boat as the boat bent at higher operating temperatures breaking the thermal contact to the thermocouple.

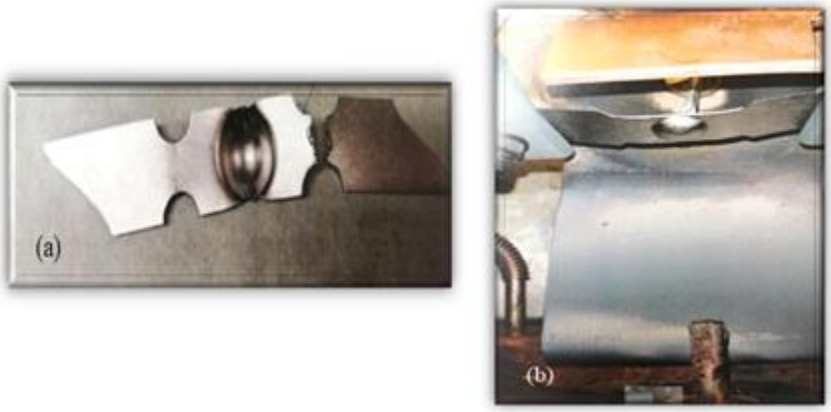

Figure 5.2: (a) Broken Tungsten boat and (b) bent Molybdenum Boat with untouchable thermocouple.

Attempt #3 and Successful Deposition

Given the challenges with open boats then after consultation with Radak, it transpired that the furnaces can be operated at higher temperatures though with risk of damage. The Radaks already have multi-layer heat shielding built in and so provide a usable alternative. The deposition software however had to be upgraded to allow operation at higher temperatures (1800^{o}C) because the prior set point limit was 1550^{o}C. One of the Radak sources with an Alumina crucible was filled with pure erbium sulphide powder (5N) and the crucible was covered with a Tantalum baffle to prevent spitting. Depositions were performed at a series of

temperatures from 1800°C down to 1550°C. Deposition of erbium sulphide was observed on the silicon wafer substrates. The existence of Er_2S_3 was confirmed by EDS Analysis. Figure 5.3 indicates the refractive index and thickness vs operating temperature for a further series of run, which were measured with the Filmtek 4000. The deposition time was not fixed, as it was decided to set the temperature and source power manually, so time was varied according to set values. The deposition rate and thickness could not be recorded or controlled because the gold crystal sensor used was unable to read these values. Besides that, the slight variation in measured refractive indices occurred due to poor fitting in the Filmtek with such thin films.

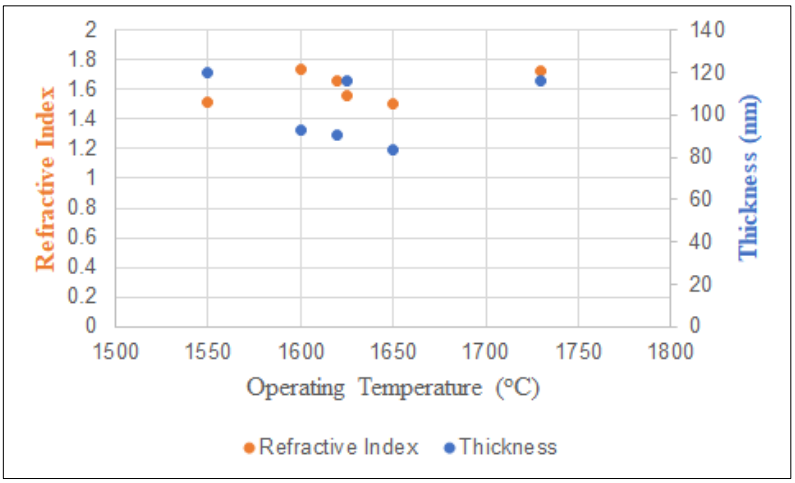

Figure 5.3: Refractive index and thickness vs operating Temps

At the end of this run sequence, the Er_2S_3 material supply was exhausted, so it was not possible to go lower than 1550°C operating temperature.

5.2.1.1 Research Impediments

During the series of deposition runs, many issues were faced. Such as:

No reading by the Gold electrode sensors

No deposition was recorded by the Gold electrode quartz microbalance sensors in any circumstances, but films were noted on some substrates. That led to much wasted time whilst discovering this problem. Further research (INFICON application note) revealed that at high temperatures the normal gold contacts on the crystals do not work acceptably and Alloy (Ag/Al) crystal sensors, which are meant for higher stress applications, are required. This was a very useful discovery and not a previously observed problem in the local environment. These were sourced, and after a considerable wait, work recommenced.

Blown Fuses

At higher temperatures requiring beyond 55% on the input power, the fuses blew on a number of occasions. The temperature at which this occurred was typically ~1200^{o}C. The reason for blowing the fuses was finally evident after opening the chamber and removing the furnace. It was observed that material that had deposited on the walls of the heat shield (figure 5.4) had melted and also dropped on the base of the chamber. This had likely accumulated over a long period of time as the furnaces were not normally run above typically 600^{o}C in routine depositions performed in this system. Further, loose connection of thermocouple lead wires was observed into the ceramic plug which inserts into the furnace, presumably due to additional thermal expansion compared to previous operation at lower temperatures. After retightening the screws, cleaning the base of the chamber, and also ensuing the lead wires did not short to the furnace body, the issue was resolved.

Figure 5.4: Melted erbium sulphide, which sticks with the walls of the vapor shield.

Destroyed Furnace

Prolonged operation at high temperatures resulted in one furnace burning out. The Alumina crucible and Radak furnace were fine for 3-5 runs at higher operating temperatures, but later, the used powder first turned dark, burnt, and stuck on the base of the crucible. Ultimately the crucible cracked whilst stuck to the heater cage and destroyed the whole furnace including the heat shielding. At this point the only option was a complete furnace replacement which had a two month lead time.

Carousal Assembly failure

The wafer carousel assembly in the Angstrom system failed several times at higher temperatures in several failure modes not previously seen at lower operating temperatures. This required several mechanical fixes of varying durations until ultimately the drive shaft was sheared off. At this point the whole system had to be removed, disassembled, and rebuilt. This was a month long process to resolve and ensure that this would not happen again.

Erbium Sulphide Supply Issues

After exhausting the supply of Er_2S_3, there were issues reimporting it as no MSDS existed that meets Australian standards. Unfortunately, that imposed a further 8-week delay in getting more material.

5.2.2 Resumed Evaporation Process

After sourcing new furnaces and new 99.9% Er_2S_3 material from Angstrom Engineering and American Elements respectively, the evaporation process was restarted aiming at a series of temperatures from 1450^{o}C down. Unexpected evaporation behavior at low temperatures was however observed. In the first run, a high evaporation rate (4.86 A/s to 10.07A/s) was observed at 200^{o}C operating temperature which did not occur with the previous batch of Er_2S_3. The temperature was nonetheless ramped to 1450^{o}C and a decreasing deposition rate (0.04 A/s) was observed with increasing temperature. Over the 2 hour deposition time at 1450^{o}C, the deposition rate fluctuated between 0.04 to 0.10 A/s. An erbium sulphide film was however deposited on the TOx wafer but the surface of the deposited film was full of particles. In the second run, a high deposition rate (2.71 A/s) was again observed this time at just 155^{o}C along with the same decreasing trend in deposition rate with increasing operating temperature. At 1400^{o}C the deposition rate was almost zero (-0.006 A/s). After a 2 hour deposition, upon opening the chamber, it was confirmed that there was no deposition on the wafer and that there was unevaporated but melted material in the crucible, which is shown in figure 5.5 (a). There was also a powdery deposit on the base of the chamber as shown in Figure 5.5 (b).

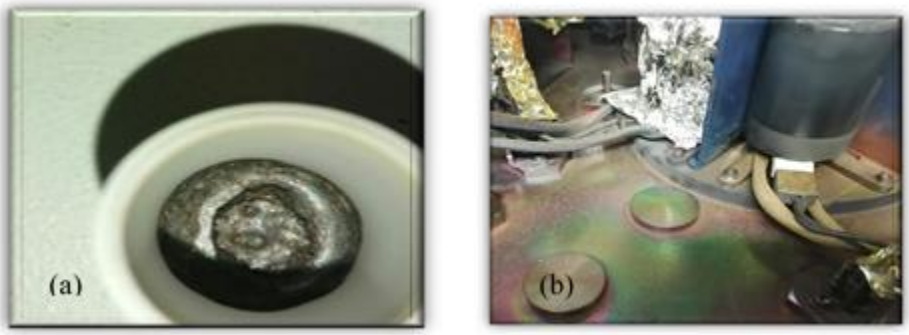

Figure 5.5: (a) Melted and stuck erbium sulphide in the crucible and (b) spread material on the base of the chamber.

The existence of Er_2S_3 in the deposited film at 1450°C was confirmed by EDS Analysis. The atomic percentage content in the fabricated film, the erbium sulphide source powder, and the powder spread in the chamber base were also measured with the same technique. Though WDS could give an exact elemental composition, the deposited thickness was quite low (50 nm) so the conditions were not appropriate for WDS testing. The EDS results are presented in Table 5.1.

Table 5.1: Measured available content (at%) in the deposited film, used powder, and spread powder in the chamber.

	Oxygen (at%)	Erbium (at%)	Sulphur (at%)	Si (at%)
Deposited Film	39.83	3.01	7.87	49.29
Source Powder	2.09	35.10	62.81	No Silicon
Spread powder in the chamber	5.13	37.80	57.07	

As the deposited film is quite thin and the used substrate was a TOx wafer, it was not possible to avoid penetration of electron beam toward the substrate during EDS analysis. That is why high oxygen concentration in the deposited film was recorded. Furthermore, for the elemental analysis of powder, a thin layer of used powder was spread on carbon tape, which acted as the substrate. The measured elemental results do not correlate with the expected values (40% Er 60% S) for Er_2S_3, because of the addition of the oxygen inclusion. The used powder is 99.9% pure and it is well known that sulfur easily gets oxidised in an atmosphere. Therefore, the availability of oxygen concentration in the used source powder, and the powder spread in the chamber was recorded. However, the spread powder in the chamber had a higher oxygen concentration as compared to the source powder. The most convincing possibilities behind this reason will be explained in detail in chapter # 6.

So far, no other element was detected in the film to inform the reasons behind evaporation at low temperature out of the new source powder. The promising thing was looked for in this analysis is that if erbium sulphide can evaporate at a low temperature, then it will be very beneficial to achieve the required goal such as fabrication of co-evaporated film without degrading the quality of As_2S_3 film.

5.2.3 Further Research Findings

Though the melting temperature of Er_2S_3 at atmospheric pressure is 1730^{o}C the apparently high evaporation rates observed from the above experiments at low temperature (between 150^{o}C to 200^{o}C) suggested trialing lower temperature evaporation. This also had the benefit that it could avoid the raising wafer temperature issue as well. Thus, a co-evaporation process at lower temperatures was first set up.

Co Thermal Evaporation on Tox wafer

280^{o}C set temperature.

The co-evaporation process utilised two different sources: Radak furnace for erbium sulphide powder and a resistive boat for arsenic trisulphide glass. After setting 280^{o}C temperature for Er_2S_3, the rate was quite high but kept fluctuating between high values (0.90 A/s to 1.1 A/s). The deposition continued for two hours and a thin film was fabricated with 5000 nm thickness. The film was then spin-coated with ~100 nm thick SU-8 (Microchem) layer and ultraviolet-cured (UV) to prevent As_2S_3 evaporation and crystallisation during the vacuum annealing required to restore structural and optical properties [265] of the film.

345^{o}C set temperature.

To provide a low dopant reference point, a further film was deposited with the deposition rates set at 0.02 A/s and 2.33 A/s for erbium sulphide and arsenic trisulphide, respectively. The deposition was again continued for two hours and a thin film was fabricated with 4500 nm thickness. This same protective coating was applied after deposition.

Issues

Unfortunately, no erbium was detected in both deposited films by EDS analysis. The WDS analysis result of the deposited film at 345^{o}C is listed in table 5.2.

Table 5.2: Measured available content (at%) in the film, which deposited at 345°C on silicon wafer.

O(at%)	Si(at%)	Er(at%)	As(at%)	S(at%)	Ga(at%)
22.506	0.2	0	20.379	56.884	0.031

It is well known that the Su8 polymer has a large amount of oxygen content. This polymer was deposited on top of the fabricated film as a protective layer. Therefore, beside the other reasons that have been discussed earlier, this polymer layer could be the main reason behind the presence of oxygen in the deposited film. The existence of a small amount of Ga in the film could be due to residuals from prior fabrication processes in the chamber.

As the main goal, evaporation of erbium could not be achieved. However, after opening the chamber of each Co-thermal evaporation, it was confirmed that erbium sulphide powder tried to evaporate but could not reach to the silicon substrate and spread on the base of the chamber. Unlikely, sensors were showing evaporation of something else at both set temperatures that was not identified to be erbium sulphide. Thus, further tests of only Er_2S_3 evaporation at low temperatures were carried out.

Er_2S_3 Only evaporation on Silicon wafer

After consecutive failures, it was decided to just evaporate erbium sulphide first with set rate value (0.02A/s) on the silicon wafer then move to co-evaporation testing for further analysis. The first evaporation test was done at 300°C. During the whole evaporation process, the sensor showed rate values between 0.02A/s to 0.06A/s. However, no evidence of deposited film on the silicon wafer was found, which was confirmed with Filmtek. The operating temperature was then increased to 500°C and again failed to achieve film deposition.

After facing an unexplainable problem, a decision was made to revert to a high operating temperature (1400°C) to evaporate only Er_2S_3 powder. At 600°C operating temperature, the deposition rate shown by the sensor was 0.03A/s but with increasing temperature, the rate started to drop and first reached 0.01A/s then 0.0A/s at 1400°C. However, as the temperature reached the set point value (1400°C), the thermocouple showed a disconnection error and the process halted with no deposition. Upon opening the chamber, the thermocouple was indeed found to be broken. Thermocouple wire from thermocouple plug was not touching the base of the crucible and had sucked in the thermocouple. The source powder was found in the base of the furnace as well.

After adjusting the thermocouple installation, the crucible was refilled with source powder to continue testing at high temperature. At 1200°C, the monitored deposition rate was 0.06A/s however the temperature started to drop and again the same thermocouple disconnection problem occurred. To be certain a brand new Radak furnace was installed to hopefully avoid thermocouple disconnection issues and further evaporations were performed at 1450°C operating temperatures. The monitored value of the deposition rate at 960°C was 0.02A/s and this value was consistent until 1450°C applied temperature. However, after 30 minutes of set temperature value (1450°C), deposition rate dropped to zero and the process was stopped. Upon opening the chamber, clustered erbium sulphide powder was observed in the crucible. It is still uncertain if this is why the deposition rate dropped to zero. Moreover, at 1450°C set temperature, no film was deposited, whereas the evaporation process ran normally without thermocouple disconnection issue.

Co-evaporation on TOx wafer

Next it was decided to start co-evaporation at 1500°C applied temperature because previously (section 5.2.1) it was expected to achieve deposition at this operating temperature. Therefore, the crucible was half filled with the source powder and after achieving a required deposition rate value (0.02 A/s) of erbium sulphide, the

arsenic trisulphide resistive source was tuned on, with a set rate of 0.26A/s. The deposition rate appeared to complete successfully for 2 hours at 1550°C. However, the deposition rate of both sources was not stable (fluctuating between 0.19A/s to 0.29A/s and 0.04 A/s to 0.08 A/s of arsenic trisulphide and erbium sulphide respectively).

After opening the chamber, it was apparent that erbium sulphide powder was spread everywhere in the chamber and found in the base of the furnace as well. Used powder was melted and stuck to the crucible. Some melted material spilled inside the furnace and the crucible adhered to the furnace heater cage such that it could not be removed. The crucible base stuck to the thermocouple as well. The Tantalum baffle was broken and had dropped inside the crucible, and the thermocouple casing was broken with the thermocouple disconnection again. Images of the furnace interior are shown in Figure 5.6.

Figure 5.6: (a) Melted and stuck erbium sulphide in the crucible (b) melted material outside of the crucible and (c) glued crucible with the heater cage of the furnace.

After depositing Su8 layer (100nm) on top of fabricated film, it was decided to measure the available content in the deposited film on the silicon wafer, using WDS. The results are shown in table 5.3.

Table 5.3: Measured available content (at%)in the deposited film at 1500^{o}C.

O (at%)	Si (at%)	Er (at%)	As (at%)	S (at%)	Al (at%)	Ga (at%)	Te (at%)
36.73	0.324	0	10.513	44.24	8.156	0	0.02

Unfortunately, no Er was detected in the deposited film. The huge amount of oxygen in the deposited film was detected due to Su8 polymer, which was deposited on top of fabricated film as a protective layer. Al was detected due to alumina crucible being used, which was damaged during the evaporation process. The tiny amount of Te content in the deposited film was due to contamination of prior deposition processes in the chamber. So far, no information is available in literature regarding the spitting issue of erbium sulphide during the evaporation. However, according to prior studies, detailed investigations regarding spitting of metals (e.g Gold) during evaporation have taken place. The behavior where ejection of liquid droplets from the molten pool of metal instead of the smooth transfer of material through evaporation, is known as spitting and Gold can be prone to this behavior [290]. Therefore, from these studies it was concluded that two major factors can predominately affect the spitting. These are (i) material quality and (ii) process conditions including power input, heat transfer, crucible liner user, ramp profiles and deposition rates. Material quality is determined by both purity and cleanliness. The used source powder is 99.9% pure. According to the issued certificate of analysis of erbium sulphide powder by the manufacturer, it became apparent that the used powder had other additives such as Y, Tm, Ho,

Dy, Yb, Lu, Fe, Si, Al, Ca, Mg, Ni, W, C and Cu. Normally, researchers prefer to use minimum 3N powder but due to availability of resources, it was decided to purchase this powder to restart the pending research work.

Secondly, liner was not used in the crucible and deposition rate was not recorded during evaporation. That is why an understanding of the critical process parameters could not be developed, which would have informed how to adjust to minimise the possibility of spitting issue.

After reviewing the results, it was concluded that evaporation of erbium sulphide is difficult, and that further work is required to establish the correct means to do this. Observations and suggestions include:

- The minimum evaporation temperature appears to be between 1450 and 1500^{o}C
- Several furnaces (including ceramic casing of thermocouples) were destroyed despite the temperature being inside the operating range of the Radak furnaces (attempt # 3, figure 5.3). Results such as molten Er_2S_3 cannot be removed from the crucible and the major furnace damage and "gluing" of alumina elements from "spilt" Er_2S_3 e.g. figure 5.6, b suggest erbium sulphide may have reacted with Alumina. No data is available in the literature.
- The apparent evaporation of erbium sulphide at low operating temperatures for the second batch of material (section 5.2.3) as indicated by the rate monitor is not a real effect. However, it could have been some kind of contamination in the Er_2S_3.
- The cause of the erbium sulphide (second batch of material) being ejected from the crucible (spitting behavior) could be controlled by improving material quality and adjusting process parameters.
- The base of the Alumina crucible was found to be cracked because it had molten erbium sulphide material (sublimable material in the form of chunks

or pellets). The molten material may be evaporated but if the residual charge is too large then the difference in the expansion coefficient can result in the Alumina crucible cracking upon reheating. It is better to use a metal crucible liner in future to avoid cracking issue.

- The repeatedly observed thermocouple disconnection issue with the second batch of erbium sulphide is also unexplained and a major issue. This could be related to reactions between Alumina and Erbium sulphide, and spitted powder and thermocouple lead wire as well.

Conclusion:

Multiple attempts at high or low evaporation temperatures have proved that the evaporation of Erbium Sulphide is difficult. Much more work is required to overcome issues faced such as several furnaces being destroyed due to the reaction of Erbium Sulphide with Alumina, evaporation of contamination in the Erbium Sulphide at low temperature, ejection (spitting effect) of Erbium Sulphide from the crucible, cracking of Alumina crucible and repeated thermocouple disconnection, which have never been discussed in the literature. It has been suggested that improving material quality, adjusting process parameters, and using a metal crucible liner can overcome these issues in the future. However, it is still uncertain whether co-evaporation is a viable technique without a huge investment of effort.

It may be much more sensible to adopt another approach such as E-beam co-evaporation for the fabrication of Erbium Sulphide co-doped films or otherwise depositing already doped glasses by methods such as ion beam sputtering etc.

Chapter 6: RF sputtered Er doped GLS films.

After facing the issues discussed in evaporated GeGaS films, attention was instead focussed on another promising sulphide host with known high solubility for rare earths, GaLaS. This has proven high rare earth ion solubility without clustering and no detrimental photoinduced losses as well as established prior laser demonstrations at 1 micron [113].

6.1 Motivation of this Work

For fabrication of IR transmitting fibers and waveguides, to date, ZBLAN [291], sulphides, selenides [292], and tellurides/tellurites are known as the potential candidates [293], each of these glasses having related advantages and disadvantages dependent on the application [294]. Gallium Lanthanum Sulphide (GLS) has been considered as one of the most promising potential chalcogenide materials for use in rare-earth-doped waveguide amplifiers [295] due to its excellent properties. These include low phonon energy (425 cm^{-1}) [96], high glass transition temperature (~580^{o}C) [296], good chemical stability (non-hygroscopic) [129], high refractive index (2.4) [297], wide IR transmission window (0.5 um to 10um) [298], low toxicity [129], and especially high rare-earth solubility due to the presence of La [115]. According to prior studies [299], it is possible to obtain a glass with even ($9.66x10^{21}$ $ions/cm^3$) doping of erbium sulphide. Compared to Er doped silica glasses, GLS glass has 2.5 times higher emission and absorption cross section, two orders of magnitude stronger third order nonlinear index [300], and five times higher radiation transition rate because of a higher refractive index. Moreover, due to much lower maximum phonon energy and other phonon related properties, this glass has three order lower multiphonon nonradiative decay rate

[133]. Therefore, high RE ion doping, combined with wide IR transparency and low phonon energy, make this glass a favorable candidate for IR devices.

Spectral properties of rare earth doped GLS glasses have been investigated since the 1990s, e.g. [133]. Praseodymium doped and dysprosium doped GLS glasses and fibers showed fluorescence at wavelengths which are useful for sensing the two most important greenhouse gases (i.e. Methane and Carbon dioxide) at 3400 and 4300 nm respectively. Thulium doped and Holmium doped glasses and fibers emitting at 3800 nm and 3900 nm wavelengths, could be suitable for remote sensing applications [301]. Furthermore, Judd-Ofelt analysis was also performed to calculate the radiative lifetime and branching ratios of mid IR radiative levels in Er ($1.81x10^{21}$ ions/cm^3) doped GLS glass [105], see table 6.1.Emissions at (2000 nm, 2750 nm, 3600 nm, and 4500 nm) wavelengths with corresponding calculated radiative lifetimes (0.14, 1.53, 0.14, and 1.2) ms and branching ratios (3.7, 14.7, 0.4, and 1.0) % respectively.

Table 6.1: Radiative properties of Mid IR transitions in Er doped GLS glass [115].

Wavelength (nm)	Measured Lifetime (ms)	Radiative Lifetime (ms)	β (%)
2000	0.1	0.14	3.7
2750	0.1	0.14	0.4
3620	0.59	1.2	1
4530	1.23	1.53	14.7

The computed radiative lifetimes showed good agreement with the measured results, and these properties make this glass useful for many promising applications.

The first laser action in a chalcogenide glass was reported in neodymium doped gallium lanthanum sulphide (GLS) glass at 1080 nm in 1996 [113]. Dysprosium doped GLS [302] and praseodymium doped gallium sodium sulphide [116] glasses subsequently demonstrated emission at 1300 nm wavelength. Emission at 1300 nm with 58% quantum efficiency was recorded in praseodymium doped GLS [303] with potential for practical telecom based applications and inferred but not measured MIR capability.

So far, despite ongoing studies [304]–[308] and the progress made [309], no optical gain was achieved in erbium doped GLS fibres or planar waveguides [295]. Several essential questions are unanswered, such as, what is the optimum Erbium ion concentration in GLS films, how does thermal annealing affect the lifetime/PL performance in erbium doped GLS films, and how are the lifetime/PL/gain properties affected by different dopant and excitation intensities, etc.

In this work, Er-doped GLS films with different erbium concentrations were fabricated by magnetron RF sputtering using Angstrom EvoVac system. The lifetime/PL properties were systematically investigated and thermal annealing at different temperatures was carried out to study its impacts on PL properties to optimize the annealing condition. The lifetime/PL properties under different excitation intensities, wide range PL spectra and the effect of light annealing on PL properties were carefully investigated. Following compositional studies by EDS/WDS and the realisation of significant OH contamination, and the relationship between deposition start chamber pressure, chamber water partial pressure under sputtering conditions and OH contamination in the deposited films as also investigated.

6.1.1 Fabrication of Undoped and Doped Films

Er-doped GLS films were fabricated by using radio frequency (RF) magnetron sputtering. A 3-inch gallium lanthanum sulphide target (ChG Southampton Ltd) with the nominal molar composition of Lanthanum (III) Sulphide (70 %): Gallium

(III) Sulphide (30%), was loaded into the target holder, which was mounted 45° off vertical and facing upwards with 10 cm distance between the centers of the target and substrate (usually 100mm diameter silicon wafers on a rotating holder). Initial studies were made with only the GLS target, later ones achieved erbium doping by placing a piece of erbium foil (AlfaAesar, 0.62 mm Thick, 99.9% purity) on the top of the GLS target surface as an erbium source. The area of the Er foil was varied to change the Er ion concentration in the fabricated film, the location of the foil being constant as shown in figure 6.1.

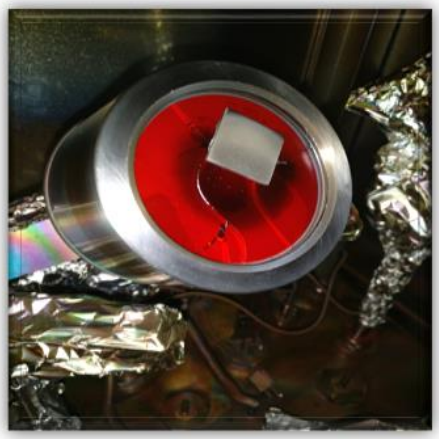

Figure 6.1: Er foil on top of GLS target as an Er source. Unfortunately, the target cracked and blackened in some area due to an electric field enhancement effect [310].

Four different sizes of Er foil were trialed to get four different Er concentrations in the doped films. The chamber was initially pumped into the high 10^{-6} Torr range using a cryopump before commencing deposition. Argon (99.999% and

further purified by in-line gas purifier) with a flow rate of 20 sccm was used to sputter the target at a pressure of 5.1 mTorr via an automatic pressure control system operating on the cryopump gate valve. During the deposition process, the applied sputtering power was set to 20% of the available 300W (which resulted in a measured forward power of 56 W), corresponding to a deposition rate of ~0.9 Å/s on the substrate as monitored by a quartz crystal microbalance. The initial parameters and fabrication method were guided by following prior sputtering work on sulphides [3], [161]. Issues with the target such as the target cracking and blackening of some areas due to electric field enhancement effect were also observed [310].

Characterisation of undoped and doped films quality

Dual-angle spectroscopic reflectometry (SCI FilmTek 4000) was used to determine the refractive index of the as-deposited undoped film, where the values of the measured parameters such as film thickness, refractive index, and bandgap were uniform across the full surface of the thermally oxidised silicon substrate with ten points at a wavelength of 1550nm. The results are illustrated in table 6.2.

Table 6.2: Measured thickness, refractive index, and bandgap value of the as deposited undoped film.

Material Parameters	Film
Thickness (nm)	400±1.1
Refractive index	2.05
Bandgap (eV)	3.48

According to the literature, at 1550 nm the refractive index value of bulk GLS glass is 2.41 [311], which is significantly higher than the current measurements (table 6.2). Prior studies [312] indicate it is not necessarily unusual to see this

much difference in refractive indices between used bulk glass and deposited film in chalcogenides. It was initially suspected that the poor morphology of the deposited films could be the reason for the decreased refractive index values. A similar issue is routinely observed in the deposition of As_2S_3 films within the group and has been investigated in $Ge_{33}As_{12}Se_{55}$ films for example by Fuchs et al [160] where porosity was calculated by the relation given by Kinishita and Nishihori [313] in the deposited film due to the formation of the columnar structure while sputtering. Porosity of 20% was calculated in a 100 nm thick film, which increased with increasing film thickness, thus a further reduction in refractive index was measured in thicker films. Therefore, the surface morphology of as-deposited film using was investigated using scanning electron microscope (SEM) but the existence of columnar structures was not observed (Fig 6.2).

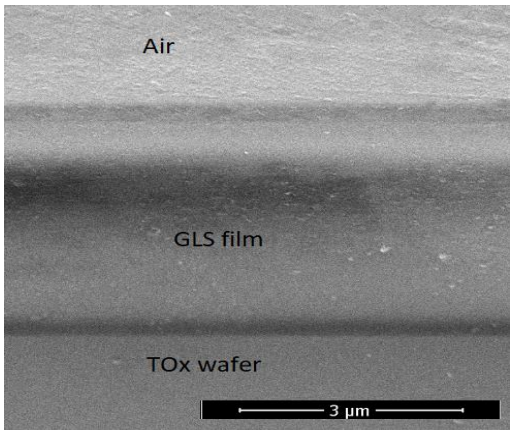

Figure 6.2: Surface Morphology of sputtered film analysed by SEM.

The propagation loss in the undoped film was measured using a Metricon 2010 prism coupler, with a tunable laser source (1550 nm) and an InGaAs camera. A laser beam with 1mW power was coupled into the film and the scattering streak was recorded with an InGaAs camera. Custom image processing software was used

to calculate the propagation loss by analysing the background-corrected scattering streak versus distance. The calculated film loss was at the limit of detectability (~0.1dB/cm), which indicated good film quality and the absence of particles on top of the sputtered film.

The Er concentration in each film was measured with Electron Probe Micro Analyser (EPMA). The results vs the erbium foil size and the measured thickness, refractive index, and bandgap values of deposited doped films at varying Er concentrations using the Filmtek are reported in table 6.3.

Table 6.3: Refractive index and bandgap values of as-deposited doped films.

Film No.	Sizes of Er foil (cm^2)	Er Concentration ($ions/cm^3$)	Thickness (nm)	Refractive Index	Bandgap (eV)
1	2.5 x 2.5	1.27E+22	662±2.1	1.91	2.74
2	1.4 x 1.1	4.97E+21	400±2.2	1.90	2.69
3	0.6 x 1.1	1.65E+21	658±2.2	2.11	2.88
4	0.7 x 0.7	0.76E+21	1042±3.1	2.18	3.14

In Er doped GLS samples the mean concentration values (two to three replicate experiments) had relative error within ±3% to ±5%. Moreover, the dopant concentrations achieved here are quite high, certainly sufficient for all low power applications and even potentially for high power devices as previously discussed. The maximum dopant concentration achieved could lead to hundreds of dB/cm gain if all the Er is inverted.

In terms of thickness, all four deposited films were uniform in thickness with minor variation (662±2.1, 400±2.2, 658±2.2, and 1042±3.1) nm respectively as analysed across the full surface of a TOx wafer with ten points. Same conditions were used to deposit each film, whereas for final one (film#4) the deposition process was run for longer time. However refractive index appears to decrease with increasing Er concentration, the reasons for which were unclear at the time. As previously noted, chalcogenides often deposit with refractive index considerably different from bulk and annealing is then required to normalize the film structure. The scattering loss in the doped films was investigated using the Metricon film coupler at 1310 nm, and again a very low loss was calculated (0.06dB/cm) again indicating good film quality.

6.2 Photoluminescence Properties

As deposited films.

The photoluminescence properties of doped films were next measured using the fibre quasi-confocal setup [3] previously described. A 300mW 1490nm grating stabilised pump laser diode was used. Unfortunately, in all four films, emission at 1550 nm was completely quenched [314] to the detection limit using this system. There could be many reasons for this [315] such as concentration quenching, Hydroxyl contamination, ion to ion interaction, or clustering [53], [210], [211].

It is well known that PL intensity strongly depends on the uniformity of the distribution [316] and the concentration of Er ions in the film [212], [213]. All the fabricated films had very high Er content (minimum $0.76x10^{21}$ ions/cm^3), leading to the possibility of strong energy exchange processes such as upconversion, cross-relaxation, etc, which are predominantly responsible for the degradation of the 1550 nm PL signal [251].

However, more likely the Hydroxyl group(-OH) [317] has a significant influence on near and Mid IR fluorescence [318].The -OH impurity can be easily trapped

through environmental water (H_2O) [101]. The quenching effect originates due to the resonant energy transfer process between Er ions and OH impurities, which is well known as a quenching center[319]. The coupling of the Er ion $^4I_{11/2}$ and $^4I_{13/2}$ excited states with OH vibrational bands around 2.9 and 1.45 μm can significantly reduce the quantum efficiency if sufficient OH is present to provide a quenching center for each ion by increasing the non-radiative relaxation rate.

As other groups reported PL in high temperature deposited Er-doped GLS films[320], post deposition heat treatment was trialed to see if this would lead to PL appearing after increasing solubility and overcoming Er clustering issue.

Thermal Annealing.

As has already been mentioned earlier, PL intensity strongly depends on the distribution and the concentration of the Er ions in the film and all deposited films here had very high Er concentrations. Further, annealing studies elsewhere in the group had shown that high temperature annealing was also successful in driving out OH groups in chalcogenide films and if this was the cause of quenched emission, it would therefore enhance PL properties. Other research groups reported PL in high-temperature deposited films [161], but it was not possible to heat the substrate during deposition with the available setup. Thermal annealing was therefore trialled. Thermal annealing is known to diminish stress and defects/homopolar bonds in PVD deposited chalcogenide films and can enhance the PL properties up to ~50% in different Er-doped chalcogenide sputtered films by increasing Er ion mobility and creating atomic rearrangement, which leads the film towards equilibrium conditions [321].

In terms of selecting annealing temperatures, the available glass specifications indicated a T_g of 560 ^oC for the glass used. Annealing temperatures from 530 ^oC to 630 ^oC were therefore trialed for a fixed annealing time of 2 hours initially using film #3. The thermal annealing process was undertaken in a 2 inch diameter quartz tube annealing furnace where Argon gas was continuously purging while

annealing with 5 L/min flow rate. The ramp up and ramp down rate of the furnace was set to 5 ^{o}C per minute using a programmable temperature controller to control the annealing process to try and prevent film cracking from thermal stress/shock. After annealing the PL intensity and 1/e lifetimes were measured with a 1490 nm pump at 724 kW/cm^2 pump intensity. The measured values are shown in figure 6.3.

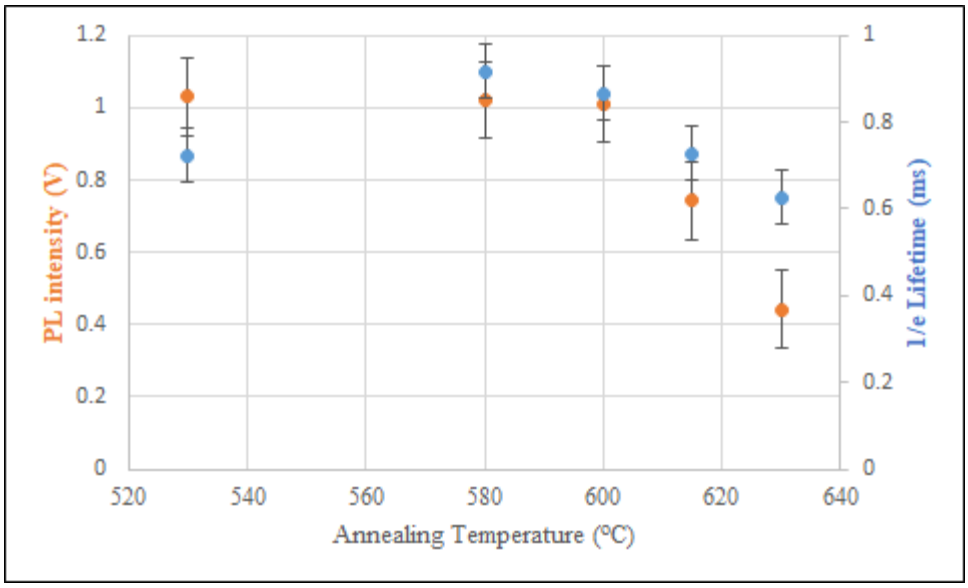

Figure 6.3: 1/e lifetime and PL amplitude for films at 1550 nm with 1.65x10^{21} ions/cm^3 Er concentration at various thermal annealing temperatures for 2 hours.

Photoluminescence was easily observed in all the samples, indicating a radical change in film properties. From the annealing test, it was concluded that 580 ^{o}C was the optimum annealing temperature to essentially maximise both lifetime and PL intensity. One prior study [229] indicated that sufficiently high temperature

annealing can drive a significant fraction of Er to interstitial sites of the glass matrix where Er-Er cross-relaxation is favourable in a film having a high Er concentration. Thus, enhanced Er diffusivity at high annealing temperature may be responsible for the degradation of PL signal (figure 6.3) above 580^{o}C. Another study [308] showed that at higher annealing temperatures the Er ions can be incorporated into a crystalline phase present in the glass. This activation can lead to ion to ion interaction and self-quenching of PL properties in films having high Er content. Therefore, based on the above results, 580 ^{o}C was selected as the required annealing temperature as it optimised lifetime and likely PL intensity within uncertainty limits.

The annealing behaviour of the films with other doping levels was then evaluated. The results of 1/e, Intrinsic radiative lifetime, and PL intensity of other films at varying Er concentrations after thermal annealingat 580 ^{o}C for 2 hours are illustrated in table 6.4. Thermally annealed film # 1 having highest Er concentration (1.27 x 10^{22} ions/cm^{3}) still failed to show PL at the detection limit of the confocal setup.The lack of detectable PL is likely a combination of the extremely high Er concentration which may have led to clustering/many energy exchange effects [322] and potentially also the available OH contamination. This was not investigated further as the concentration is higher than needed initially for MIR device studies.

Table 6.4: Measured 1/e, Intrinsic radiative lifetime, and PL intensity of all doped films at varying Er concentrations at 580 °C for 2 hours thermal annealing, pumped with 1490 nm laser diode.

Film #	Er Conc (ions/cm^3)	Pump Intensity (kW/cm^2)	1/e Lifetime (ms)	Radiative Lifetime (ms)	PL Intensity (V)
1	1.27E+22	0			
2	4.97E+21	1255.18	0.476	1.565	0.494
3	1.65E+21	724.901	0.916	1.952	0.919
4	0.765E+21	503.68	1.259	2.161	1.039

It is concluded from above results that thermal annealing activated the PL properties of the films having Er concentration less than 1.27 x 10^{22} ions/cm^3 Er concentration. PL properties improved with decreasing Er concentration due to increasing population inversion between $I_{13/2}$ state and ground state [323]. The highest fluorescence 1/e lifetime (1.259 ms) and PL intensity (1.039 V) were measured in the film having lowest Er concentration (0.765x10^{21} ions/cm^3). In terms of comparison to JO known data for doped GLS, the derived fluorescence radiative lifetime value using Judd-Ofelt analysis was 2.75 ms [152]. The discrepancy in radiative lifetime values likely arose from factors such as dependence of film stoichiometry/structure on deposition technique, effects of energy transfer processes in Er system etc [3]. Nevertheless, the lifetime is comparable to the expected values in the lower doped (but still highly doped) films.

6.2.1 PL properties vs Pump power

The PL properties were next investigated as a function of applied 1490 nm pump power. All annealed films (#2 to #4) were used for these studies and the results are shown in figure 6.4.

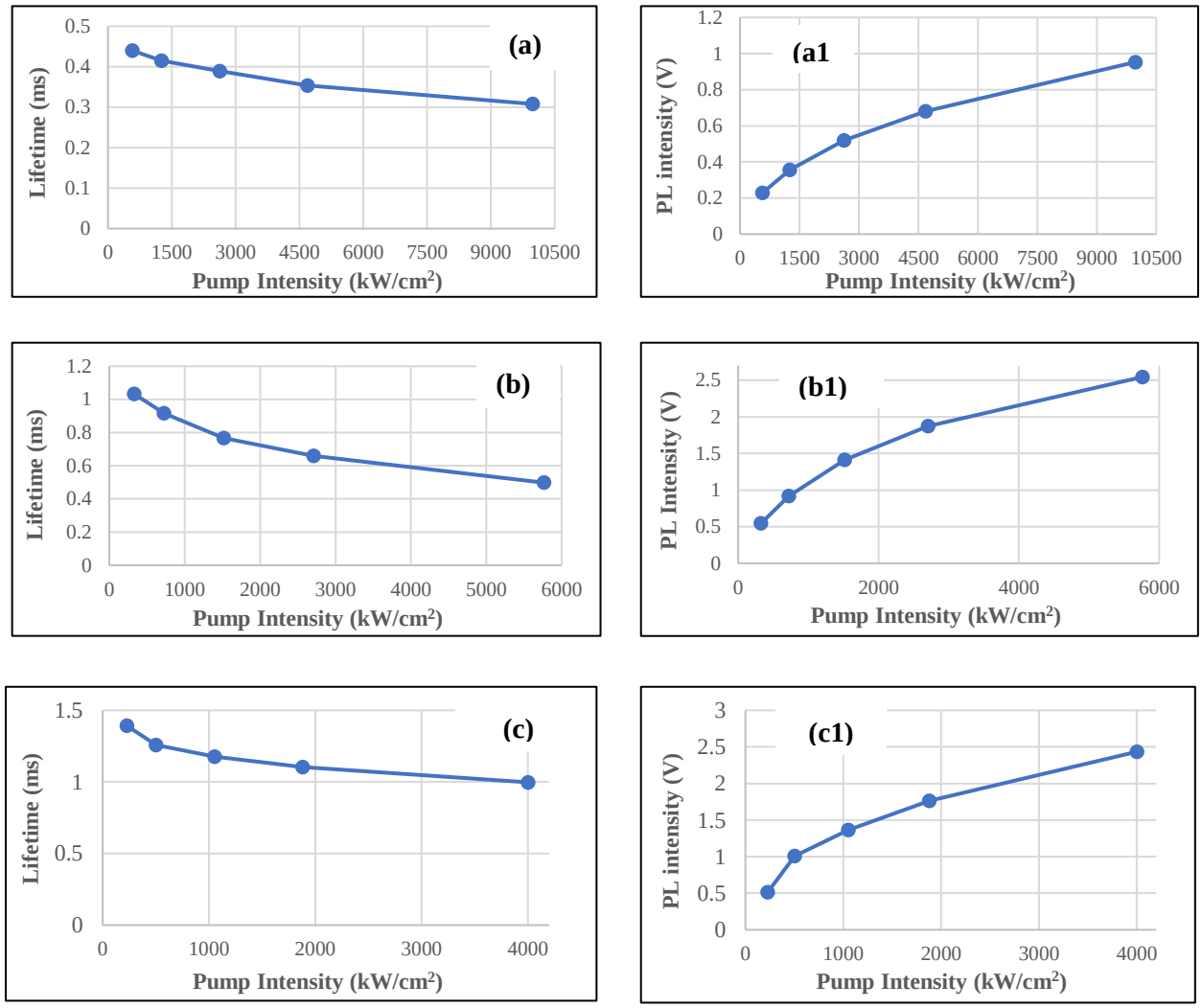

Figure 6.4: 1/e lifetime Vs pump intensity of annealed film # (a) 2,(b) 3 and (c) 4 and PL intensity Vs pump intensity of annealed film # (a1) 2,(b1) 3 and (c1) 4 with 4.97, 1.65 and 0.76 x10^{21} ions /cm^3 Er concentration, pumped at 1490 nm.

For example, from the results of the annealed film having $1.65x10^{21}$ ions/cm^3 Er concentration, where the measured 1/e lifetime (fig 6.4 (b)) is 1.034 ms at low pump power (328.25 kW/cm^2). Even with this much high Er concentration, the lifetime is quite promising, and other people got this much value in the glass, as per prior studies [105]. However, with increasing pump power the lifetime dropped down from 1.034 ms with a 328.25 kW/cm^2 pump intensity to 0.916 ms when the pump intensity reached 724.90 kW/cm^2. Thus, under the influence of high excitation power, energy exchange effects and excited state mechanisms got activated [3], which indicated the dependencies of the 1/e lifetime on the pump power. Furthermore, the energy transfer processes depopulating the metastable state ($I_{13/2}$). Therefore, the rate of up conversion depends upon the number of ions in the metastable state, quadratically. Though 1/e lifetime goes down but still quite good enough to get good performance out of this device.

At high Er concentration, the distance between neighboring ions decreases towards a critical separation where a number of energy exchange processes become very important in the PL behavior [149]. Energy exchange effects between two or more Er ions in $I_{13/2}$ level do not allow the excited ions to contribute in the desired radiative transition ($I_{13/2}$ to $I_{15/2}$) and therefore reduce PL efficiency [324] and result in $I_{13/2}$ level lifetime decrease as well [314].

Given the large difference between measured radiative lifetime and 1/e lifetime in Table 6.4 and the 1/e lifetimes in Figure 6.4, the measurements of radiative lifetime were checked against pump power to ensure their accuracy using the procedure described earlier to determine a radiative lifetime. The difference between radiative and 1/e lifetimes shows the existence of ion-ion interactions and multiphoton effects. Table 6.5 shows that the expected independence of radiative lifetime on pump power was observed indicating the measurements were indeed true representations of the radiative lifetime. Both 1/e and radiative lifetime values however clearly showed dependence on the Er concentration.

Table 6.5: Independency of radiative lifetime on pump intensity of all annealed film (#2 to #4).

Film# 2		Film# 3		Film# 4	
Pump Intensity (kW/cm^2)	Radiative Lifetime (ms)	Pump Intensity (kW/cm^2)	Radiative Lifetime (ms)	Pump Intensity (kW/cm^2)	Radiative Lifetime (ms)
568.375	1.683	328.25	1.98	228.07	2.14
1255.18	1.654	724.90	1.952	503.68	2.161
2628.79	1.646	1518.19	2.057	1054.89	2.163
4689.22	1.606	2708.14	2.09	1881.70	2.205
9977.64	1.625	5762.34	2.04	4003.86	2.174

In terms of PL intensity with excitation power (figure 6.4, b), all films show a saturation type behavior. There are multiple potential mechanisms for this, such as bleaching of the erbium absorption, upconversion and other ion-ion based processes, excited state absorption, etc. Deconvoluting out all the processes and determining which are dominant is a difficult process in a thin film geometry and required further carefully constructed detailed measurements if it is possible at all with any degree of certainty due to issues like accurate estimation of the interaction volume etc. Some of the potential energy exchange processes will be discussed in detail later in section 6.2.2 based on detailed wideband PL measurements which shed some light on processes occurring.

While measuring the PL emission at different excitation pump intensities green and red light emissions were observed from all annealed films with the naked eye. It was also observed that with increasing excitation pump intensity, the green light was also getting brighter. For example, clear green and red emission from the top surface of annealed film# 3 is shown in figure 6.5. Consequently, a more detailed investigation was considered necessary to try to determine which

processes (upconversion, excited state absorption, etc) are participating. This will be reported in section 6.2.2.

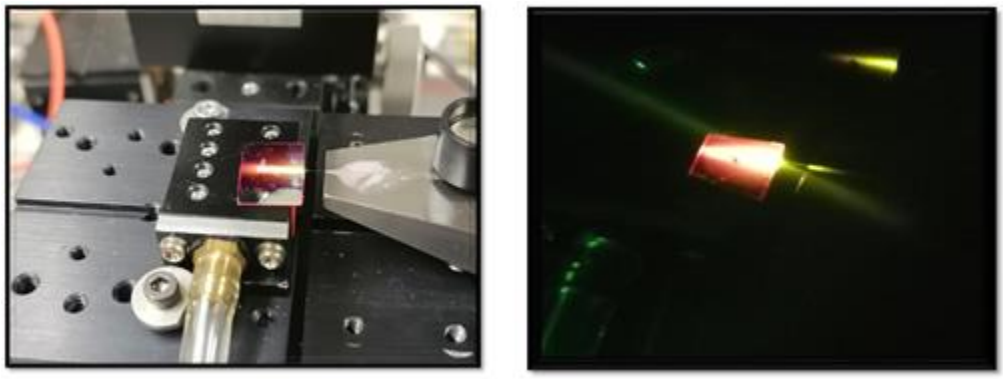

Figure 6.5: Strong Visible light emission from top of the surface of the annealed film with 1.65x10^{21} ions/cm^{3} Er concentration.

Thus, it is concluded from the above results that 1/e lifetime decreasing and PL intensity increasing with increasing pump intensity but with the same quadratic trend even at different Er concentrations. As all films have high Er concentration so quadratic trend resulted from radiative and non-radiative ion-ion energy exchange interactions due to the diminished average distance between ions, which allowed the number of energy transfer process to become relevant.

6.2.2: 380 nm to 1750 nm Broad Wavelength Range of PL

All three annealed films had their wide band emission spectra under 1490 nm excitation measured. The wavelength range from 350 nm to 1750 nm was measured by combining two optical spectrometers, an Ocean Optics HR4000 diode array spectrometer covering 200-1100 nm and an Ando AQ6137Optical spectrum analyser covering 600-1750 nm. The emission was collected with a 400 micron multimode fibre from the top surface of the excited film in a position as close to

the excitation spot as possible. The instrumental spectral response of the HR4000 was flattened using a calibrated white light source, and the intensities between the two spectrometers were leveled using emission features in the overlap zone from 650-1000 nm. Before examining the effect of doping levels, it is instructive to first examine the emission spectrum of all three films, which is shown in figure 6.6.

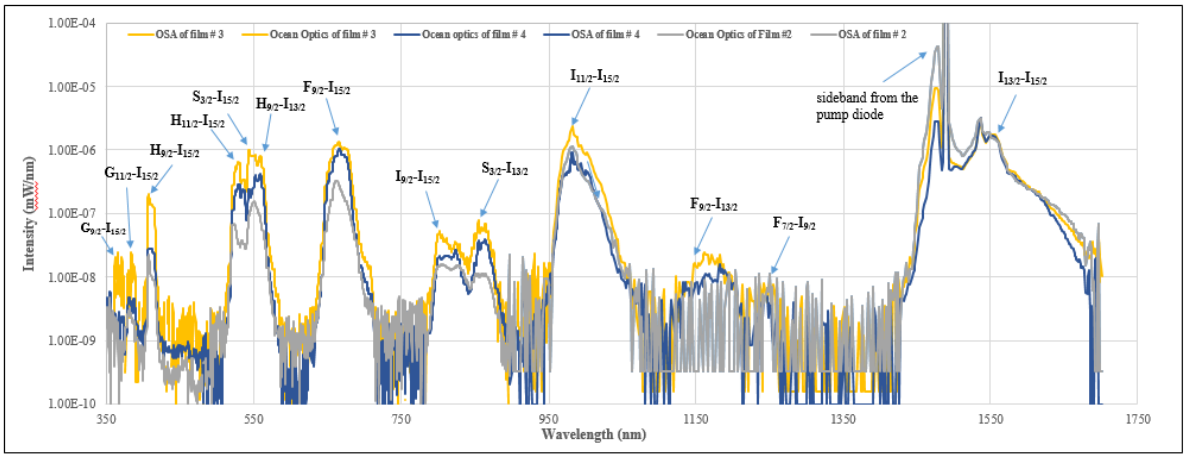

Figure 6.6 Emission spectrum of Er:GLS annealed films (#2:4.97x10^{21}, #3: 1.65x10^{21} and #4: 0.76x10^{21} ions/cm^3) from UV to NIR , pumped at 1490 nm with 15608.64 kW/cm^2 pump intensity, respectively.

The emission spectrum is extraordinary in terms of the strength and number of peaks in the UV/Vis/NIR region as compared to previously published results [3], these arising from the occurrence of excited state, multi-photon, and energy exchange processes.

The most intense luminescence peaks are observed from various excited levels to the ground state; around 1550 nm (transition $I_{13/2}$ to $I_{15/2}$), 980 nm (transition $I_{11/2}$-$I_{15/2}$), 660 nm (transition $F_{9/2}$-$I_{15/2}$, red) and overlapped spectral signals near 530 and 550 nm (transition $H_{11/2}$-$I_{15/2}$ and $S_{3/2}$-$I_{15/2}$, green) respectively. Interestingly the ground state terminated transitions around 800 nm are very much weaker. There are several weaker emission bands in the UV (at 385 and 410 nm, transitions $G_{11/2}$-$I_{15/2}$ and $H_{9/2}$-$I_{15/2}$ respectively, violet) and NIR (overlapped bands at 805 nm, transition $I_{9/2}$-$I_{15/2}$), and interestingly emissions that terminate on another excited states, namely at 824 nm ($F_{3/2}$-$I_{11/2}$), at 855 nm ($S_{3/2}$-$I_{13/2}$), 1003 nm ($F_{5/2}$-$I_{9/2}$), 1150 nm ($F_{9/2}$-$I_{13/2}$)and 1252 nm ($F_{7/2}$-$I_{9/2}$).However, the emission band from 1003 nm to 1214 nm got completely quenched in film #2, this having the highest Er concentration. Emissions at 410 nm and 660 nm wavelength in oxide glasses are only possible with high Er concentration, where the $H_{9/2}$ and $F_{9/2}$ levels get populated by energy exchanges processes [325]. In particular, 410 nm was observed because GLS glass is resistant to concentration quenching, having low phonon energy thus low multiphoton relaxation rates i.e. less non radiative depletion of the excited states [326] and high Er solubility facilitated the 410 nm emission in the films.

Moreover, it has been observed in prior studies that oxide containing GaLaS (GLSO) has better UV transparency as compared to pure sulphide glass (GLS) [309], [327] as per author's knowledge.

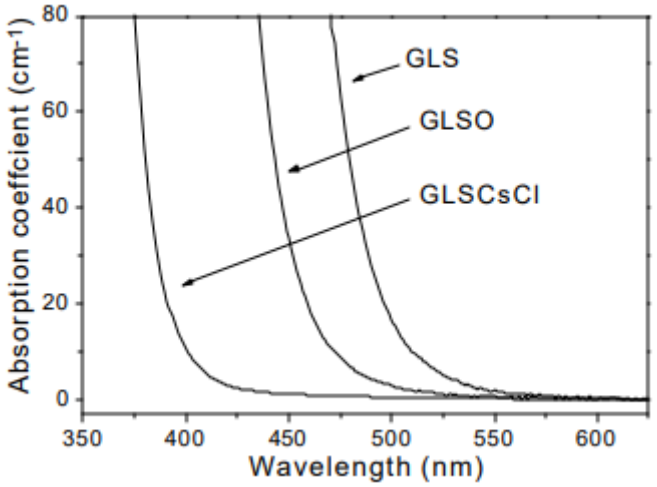

Figure 6.7 UV absorption edge of pure, La_2O_3 modified, and CsCl modified GLS glasses [328].

The observation of short wave Blue or UV emission from pure GLS glass is surprising on account of reabsorption by the intense glass absorption at shorter wavelengths. However, it is eminently possible from modified GLS glasses with better transparencies in the UV region as shown in figure 6.7 [328]. The figure indicates that only chalcohalide variants can move the bandgap low enough for UV transparency. The shortwave transitions were however captured by the 400 micron multimode fibre from the top of the excited film and so pass through a minimal thickness of GLS, therefore, minimizing UV/Blue absorption, leading to it being detectable. The range of possible radiative emissions of Er from UV to near IR region in film #3 is shown in figure 6.8 and a detailed study based on each radiative transition will be discussed later in this section.

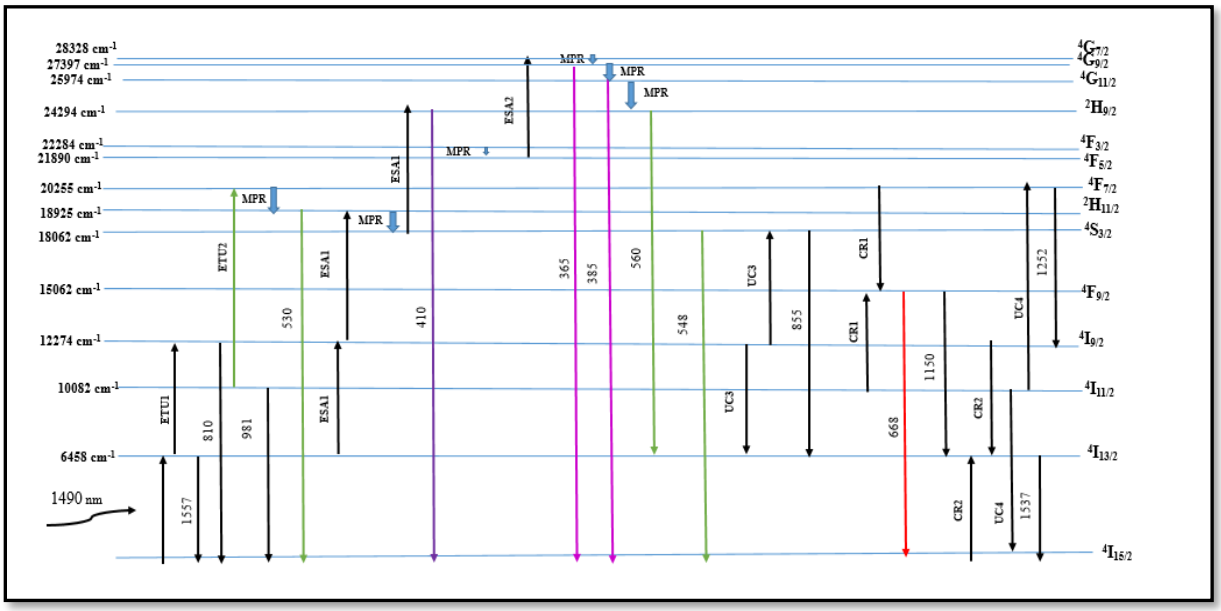

Figure 6.8: Range of possible radiative emissions of Er from UV to NIR region in film # 3.

Lifetime measurements were next sought for the higher level transitions. The light collected by the fibre was passed through high isolation thin film bandpass filters (>OD6 blocking for out of band light) with ≤ 20 nm bandwidth and centre wavelengths corresponding to the ground state transitions. The filters were placed between a pair of fibre collimators before the light was detected using a silicon or InGaAs detector to measure the lifetimes of the states. The measured lifetimes and PL values are tabulated in table 6.6 along with the calculated lifetime and radiative quantum efficiency (ratio of the radiative decay rate of the transition to the total decay rate of the initial energy level, %) from the initial level ($I_{13/2}$, $I_{11/2}$, $I_{9/2}$, $F_{9/2}$, $S_{3/2}$, $H_{11/2}$,and $H_{9/2}$) to ground state for bulk Er:GLS by Judd-Ofelt (JO)

analysis [133]. Moreover the JO parameters are largely independent on concentration unless some major structural change within the glass occurred [329].

Table 6.6: Measured PL properties of detected radiative peaks at 1255.18, 724.90, and 503.68 kW/cm^2 pump intensity, respectively, with the calculated radiative quantum efficiency (QE, %), JO calculated lifetime (ms) based on 1.58 at% Er_2S_3doped GLS glass[133].

	Film # 2 with 4.97x10^{21} ions/cm^3			Film # 3 with 1.65x10^{21} ions/cm^3			Film # 4 with 0.76x10^{21} ions/cm^3				
Central Wavelength (nm) of used Filter	Measured 1/e Lifetime (ms)	Measured Intrinsic Lifetime (ms)	PL Intensity (V)	Measured 1/e Lifetime (ms)	Measured Intrinsic Lifetime (ms)	PL Intensity (V)	Measured 1/e Lifetime (ms)	Measured Intrinsic Lifetime (ms)	PL Intensity (V)	QE (%)	JO Calculated lifetime (ms)
1550	0.415	1.654	0.357	0.916	1.952	0.919	1.259	2.161	1.009	100	2.03
985	0.122	0.564	0.1017	0.784	1.016	3.22	0.915	1.113	1.736	81	1.53
810	0.047	0.304	0.0045	0.194	0.893	0.091	0.193	0.97	0.063	22	1.20
660	0.067	0.258	0.005	0.263	0.547	0.376	0.26	0.633	0.311	87	0.14
550	0.057	0.58	0.005	0.21	0.44	0.048	0.245	0.486	0.023	68	-
530	0.028	0.17	0.002	0.24	0.422	0.012	0.246	0.494	0.0089	-	-
410 at 9977.64 kW/cm^2	0.053	Noise	0.00	0.191	0.82	0.006	0.161	0.814	0.0037	-	-

All films measured have higher Er concentration than prior work [133]. The reason behind decreasing of PL properties (for example, shorter lifetime) with increasing Er concentration could be a quenching possibility, which affects the forthcoming measurements of the upper state lifetime. So the involvement of various energy mechanism (ion-ion, defect, multi-photon etc.) [330][331] due to shortage of adjacent distance between ions thus decreased the generation of photons in the preferred state. Based on prior work [316] the selection of the optimal Er concentration for a particular (often 1550 nm) transition is one of the major factors which requires detailed investigation. PL radiative lifetimes in the

lower doped films was observed to be in reasonable agreement [133] with the calculated values of lifetime with the Judd-Ofelt analysis (JO) [330] for the 1550 and 980 nm transitions, but diverging for the shorter wavelength emissions. The measured radiative lifetimes for even the blue light are surprisingly long, unfortunately there is no JO data to compare them to. These long lifetimes likely give rise to an array of complex excitation and emission processes especially in highly doped highly pumped samples. The long lifetimes observed for the $I_{11/2}$ level and the high emission intensity also suggest these doped films are promising for achieving 2700 nm emissions as observed in prior work [133].

The reason that the PL emission spectrum can support emissions above the band gap is that these can be pumped by a variety of energy exchange processes and multi-photon absorptions possible only in a highly doped low phonon energy host such as GLS. The low phonon energy enables a longer lifetime for upper levels enabling absorption of a further pump photon, and the energy transfer exchange mechanisms provide pumping opportunities to transition upwards between excited states which do not involve photons. Energy transfer mechanisms include mechanisms such as energy transfer up conversion (ETU) or Co-operative up conversion (CUC), excited State absorption (ESA), and cross-relaxation (CR) or Inverse Energy Transfer (IET), etc. Several of the possible ion to ion interactions in Er-doped GLS film # 3 are shown in figure 6.9 [332].

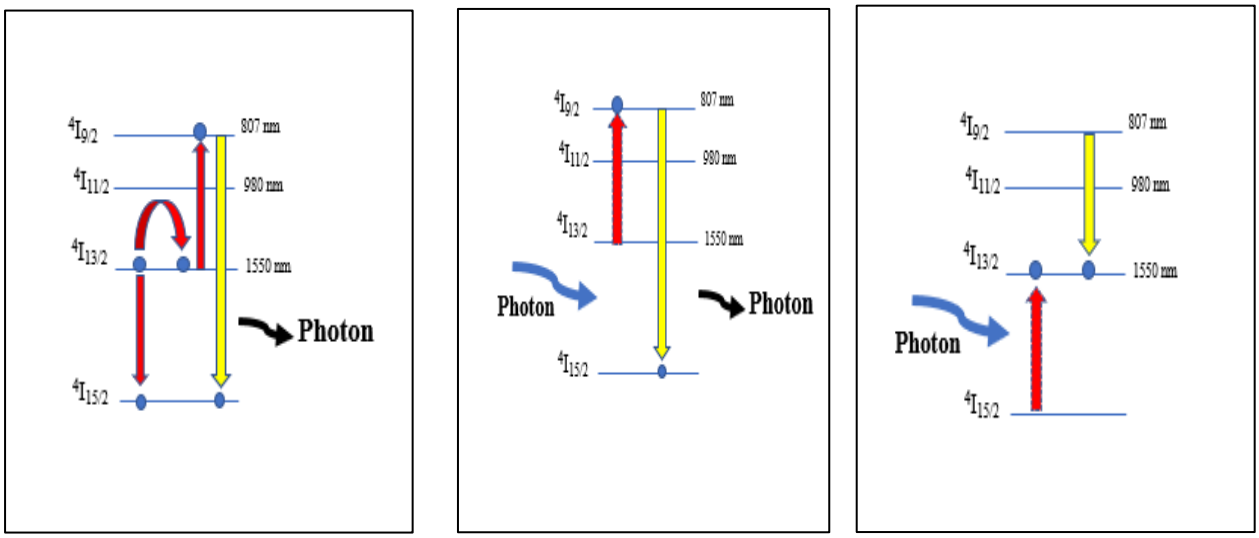

Figure 6.9: Schematic diagram of (a) energy transfer up conversion (UC), excited State absorption (ESA), and cross-relaxation (CR) processes.

Possible Ion to Ion interactions in Er doped GLS film:

As the doped films have high Er concentration so more luminescence bands were observed in the broadband PL spectrum (fig 6.6) due to the large contribution of energy exchange and multi-photon processes. In considering the many emission processes observed, it is useful to split the transition diagram of fig 6.8 into two parts (a, emissions arise from excited states to ground state, and b, emissions arise between excited states) for a better understanding of all possible ways to populate energy levels to achieve all detected radiative transitions, which have been shown in figure 6.6. The detail is given below.

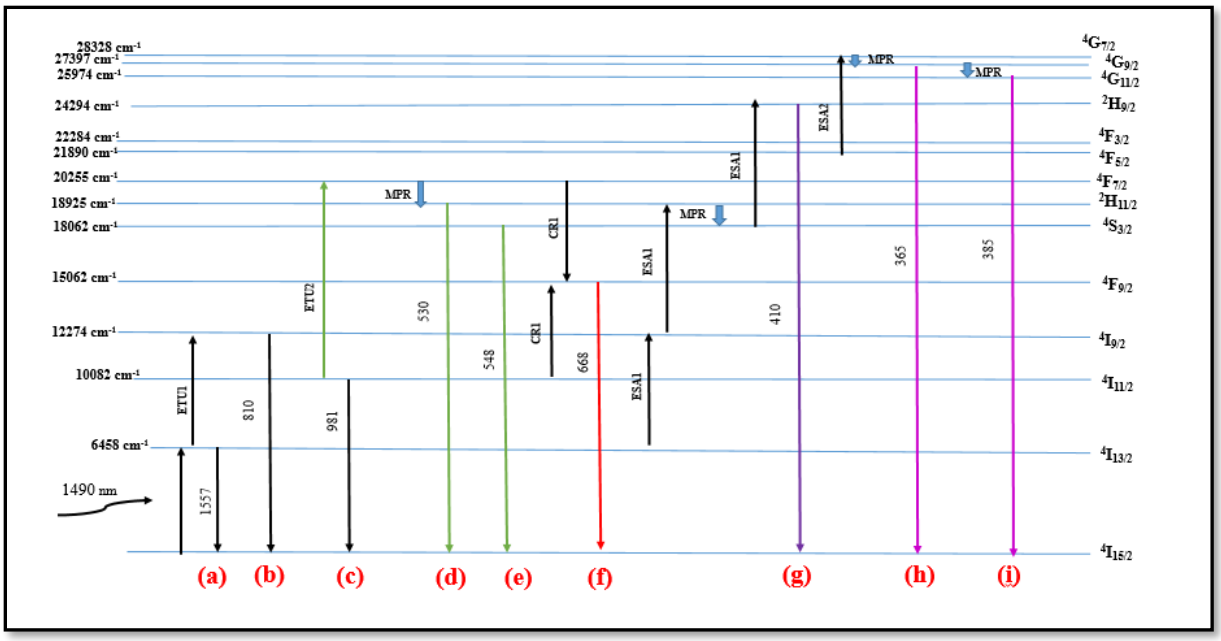

Figure 6.8 (a): Range of possible radiative transitions (to ground state) of Er from UV to NIR region in film # 3 due to Up conversion and Excited state absorption effects.

Figure 6.8 (a) depicts the erbium energy levels up to that of the shortest wavelength emission observed. On this, the most probable routes of exciting the upper levels and achieving the observed radiative transitions upon excitation at 1490 nm are shown.

a. **1550 nm emission from $^4I_{13/2}$ to $^4I_{15/2}$ state transition**: Ions are excited to the metastable $I_{13/2}$ state from the $I_{15/2}$ ground state after absorption of a pump photon. Thus, the most intense emission band is observed at 1550nm after the depopulation of ions back to the ground state. The measured 1550nm 1/e lifetime at 724.90 kW/cm^2 is 0.916 ms (1.952 ms radiative lifetime) and is longer than other levels

in the measured films. Being directly pumped, this level will have a high population of excited ions, and with high concentration/long lifetime can also serve as the base level for upconversion/multiphoton effects. Moreover, $I_{13/2}$ state can be depopulated by upconversion process where in result of energy transfer process between two excited ions in $I_{13/2}$ level, one ion deexcite to ground state and another ion further excite ion to $I_{9/2}$ state [333].

b. **810 nm emission from $^4I_{9/2}$ to $^4I_{15/2}$ state transition**: As the $I_{13/2}$ level has a long lifetime and a high inversion level from being directly pumped, both excited state absorption of another pump photon and ETU will likely be quite efficient in highly doped material. This will lead to high population in the $I_{9/2}$ level, and at first glance strong emission from this level would be expected. Er ions at the $I_{9/2}$ level can radiatively decay to the $I_{11/2}$ state with 4562 nm emission, back to the $I_{13/2}$ level by emitting a ~1700 nm photon, or to the ground state by emitting an 810 nm photon. Based on prior studies, the radiative quantum efficiency (QE, %) from the $I_{9/2}$ level to the ground state in GLS is 22% (table 6.6), to the $I_{13/2}$ state is 5 % and to the $I_{11/2}$ state is less than 1% [133].

c. **981 nm emission from $^4I_{11/2}$to$^4I_{15/2}$ state transition**: As mentioned earlier that Er ions at the $I_{9/2}$ level can radiatively decay to the $I_{11/2}$ state with 4562 nm emission. Furthermore, ions at $I_{11/2}$ level can radiatively decay to either $I_{13/2}$ state or $I_{15/2}$ state with 2750 nm and 980 nm emissions respectively. The transition probability to $I_{13/2}$ is 14% from prior Judd-Ofelt analysis, meaning the majority of emitted photons from this level will be at 980 nm thereby explaining the strong 980 nm emission observed. Moreover emission intensity of 980 nm wavelength is stronger as compared to 805 nm, which indicated that more ions are involved in the radiative transition from

$I_{11/2}$ to ground state. The OSA limit was 1750 nm and so mid IR emissions (4562 nm and 2750 nm) were not detectable with the current setup. However based on prior studies [69] OH contamination is also energy resonant with the $I_{11/2}$ to $I_{13/2}$ transition and would be expected to both dampen the emission and potentially shorten the lifetime of the $I_{11/2}$ state. However, the observed improvement in lifetime values with decreasing Er concentration (table 6.6) confirming three things: first, it could be the possibility that the water contamination just happens to be lower in the lower doped films, secondly, UC related effects will be useful for the population of higher excited states and thirdly, longer lifetime and high radiative QE of $I_{11/2}$ level can make these films ideal for amplifier devices at 2700 nm.

d. **530 nm emission from $^2H_{11/2}$ to $^4I_{15/2}$ state transition:** As the $I_{11/2}$ level has a long lifetime and the samples are highly doped so the $I_{11/2}$ to $F_{7/2}$ ETU process may be efficient especially given the strong 980nm emission observed in all samples suggesting a high population of excited ions here. Furthermore, excited ions at $F_{7/2}$ level non-radiatively decayed to $H_{11/2}$ state due to small energy difference (1330 cm^{-1}) between these states and further relaxed to ground state produces 530 nm radiative emission.

e. **548 nm emission from $^4S_{3/2}$ to $^4I_{15/2}$ state transition:** As there is a small energy gap (863cm^{-1}) between $H_{11/2}$ and $S_{3/2}$ levels so ions can decay nonradiatively to $S_{3/2}$ level. Based on prior studies [133], the transition probability of ions from $S_{3/2}$ level to ground state is 68%, it means more ions in $S_{3/2}$ further decayed to ground state with strong 548 nm radiative emission.

f. **668 nm emission from $^4F_{9/2}$ to $^4I_{15/2}$ state transition:** $F_{9/2}$ level is populated by cross relaxation (CR) process (between $F_{7/2}$ to $F_{9/2}$ and $I_{11/2}$ to $F_{9/2}$). However, ions in $F_{9/2}$ level further decayed to ground

state with strong 668 nm radiative emission. Based on prior studies, the radiative QE from $F_{9/2}$ level to ground state is 87% [334]. Thus, strong emission band at 668 nm was observed due to high probability of radiative transition from $F_{9/2}$ level to ground state.

g. **410 nm emission from $^2H_{9/2}$ to$^4I_{15/2}$ state transition:** $H_{9/2}$ level triplet is three pump photons above the ground state and given the long observed and theoretical lifetimes of the intermediate states, multi-photon pumping is a potentially efficient excitation route to populate the $H_{9/2}$ level. For example, through the excited state absorption (ESA) process the excited ion in the $I_{13/2}$ level further excited to $I_{9/2}$ and $H_{11/2}$ levels respectively. However, excited ions from $H_{11/2}$ level non radiatively first relaxed to $S_{3/2}$ level due to small energy gap (863 cm^{-1}) between two states ($H_{11/2}$ and $S_{3/2}$) and further excited to $H_{9/2}$ level via ESA process. Moreover, the excited ions in $H_{9/2}$ level decayed radiatively from $H_{9/2}$ level to ground state with 410 nm weak emission (fig 6.6, table 6.6) [332].The strong 530 nm (from $H_{11/2}$ to ground state) and 548 nm ($S_{3/2}$ to ground state) radiative emissions assured that less ions involved in transition from $H_{9/2}$ level to ground state, thus weak emission at 410 nm was detected. Moreover, possible CR process ($H_{9/2}$ to $S_{3/2}$ and $I_{15/2}$ to $I_{13/2}$ levels) would also be increase the possibility to diminish the transition from $H_{9/2}$to ground state.

h. **365 nm emission from $^4G_{9/2}$ to $^4I_{15/2}$ state transition:** Multi-photon pumping is a potentially efficient excitation route to populate the $G_{7/2}$ level just like $H_{9/2}$ level, which has already been described before. Ions in $F_{5/2}$ state got excited to $G_{7/2}$ level via ESA process. The excited ions in $G_{7/2}$ can radiatively decay to the ground state with 353 nm emissions [335] or nonradiatively decay to $G_{9/2}$ level due to small energy gap (931 cm^{-1}) between the states. Moreover, ions in the $G_{9/2}$ level can decay directly to the ground state with 365 nm

radiative emission or nonradiatively to $G_{11/2}$ due to a small energy gap (1423 cm^{-1}) between the states [336]. Furthermore, ions in $G_{11/2}$ level also radiatively decayed to ground state with a 385 nm weak emission (**i**). Though 353 nm radiative emission was not detected, whereas the weak emission peaks at 365 nm and 385 nm were observed in PL spectra (fig 5.6), which indicated the involvement of less fraction of Er ions in the transition from $G_{9/2}$ level and $G_{11/2}$ level to ground state. As these emissions are above the band gap of the material so apart from involvement of less fraction of Er ions, the emission intensity is likely reduced due to absorption by the electronic edge [330].

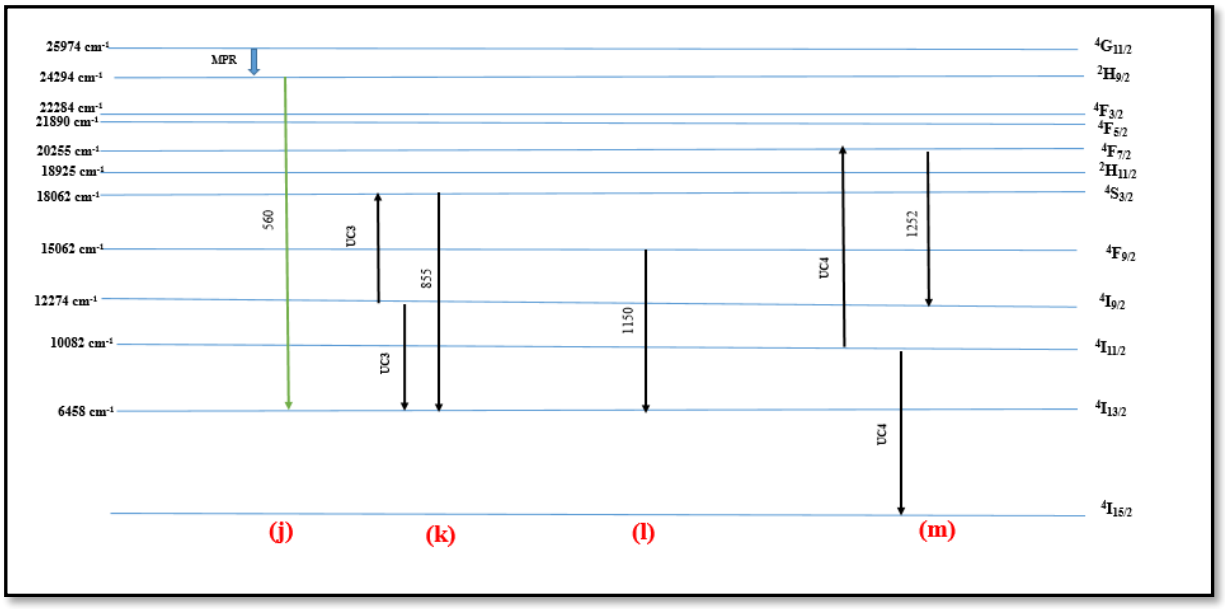

Figure 6.8 (b): Range of possible radiative transitions (interband) of Er from Vis to NIR region in film # 3 due to Cross relaxation and Up conversion processes.

Figure 6.8 (b) shows the erbium energy levels up to that of the visible to near IR emissions observed. On this, the most probable routes of exciting the upper levels and achieving the observed radiative transitions upon excitation at 1490 nm are shown. In detail:

j. **560 nm emission from $^2H_{9/2}$ to $^4I_{13/2}$ state transition**$H_{9/2}$ level can be populated by nonradiative decay of ions from $G_{11/2}$ state due to a small gap (1680 cm^{-1}) between them ($G_{11/2}$ to $H_{9/2}$) and then further decay to $I_{13/2}$ state with strong 560 nm radiative emission. Moreover, the PL intensity of this radiative emission at 560 nm is stronger (fig 6.6) than 385 nm due to involvement of more Er ions in the transition from $H_{9/2}$ to $I_{13/2}$ as compared to transition from $G_{11/2}$ to ground state. Moreover, the available overlapped peaks (e.g 500 wavelength region) in the PL emission spectrum (fig 6.6) are linked with the varying transition schemes ($H_{11/2}$- ground state, $S_{3/2}$ – ground state and $H_{9/2}$ –$I_{13/2}$) with 530, 548, and 560 nm strong radiative emissions, respectively [337].

k. **855 nm emission from $^4S_{3/2}$ to $^4I_{13/2}$ state transition:**$S_{3/2}$ level can be populated by up conversion process ($I_{9/2}$ to $I_{3/2}$ and $I_{9/2}$ to $S_{3/2}$) between the ions in $I_{9/2}$ level or by nonradiative decay of ions from the $H_{11/2}$ level. Further excited ion in $S_{3/2}$ level decayed to $I_{13/2}$ state with weak 855 nm radiative emission. Based on prior studies, radiative QE from $S_{3/2}$ to $I_{13/2}$ level is 22% [133]. Therefore, this radiative emission is weaker than the transition from $S_{3/2}$ to ground state with strong 548 nm emission.

l. **1150 nm emission from $^4F_{9/2}$ to $^4I_{13/2}$ state transition:** $F_{9/2}$ level is populated primarily by cross relaxation process (between $F_{7/2}$ to $F_{9/2}$ and $I_{11/2}$ to $F_{9/2}$). The excited ions in $F_{9/2}$ level decayed to $I_{13/2}$ level with weak 1150 nm radiative emission. It was also observed in PL

spectrum that PL intensity completely got quenched in the film having highest Er concentration ($4.97x10^{21}$ ions/cm^3), whereas improvement in intensity is observed with decreasing Er concentration. Overall, it is concluded that more ions are involved in the transition from $F_{9/2}$ to ground state with strong 668 nm emission as compared to $F_{9/2}$ state to $I_{13/2}$ state.

m. **1252 nm emission from $^4F_{7/2}$ to $^4I_{9/2}$ state transition:** $F_{7/2}$ level can be populated by up conversion process between the ions in $I_{11/2}$ level ($I_{11/2}$-ground state and $I_{11/2}$ to $F_{7/2}$ state). High concentration and long 1/e (0.784 ms) and radiative (1.016 ms) lifetimes of $I_{11/2}$ state at 725 kW/cm^2 pump intensity can serve as the base level for up conversion effects. The excited ions in $F_{7/2}$ level decayed to the $I_{9/2}$ level with weak 1252 nm radiative emission. Only a small fraction of Er is involved in the transition from $F_{7/2}$ to $I_{9/2}$ [332]. Thus, weak emission band was observed (fig 6.6).

It has been concluded from the above analysis that different types of energy exchange processes such as ESA, UCs and CR, etc. were considered as efficient ways to populate energy levels to achieve mid IR emissions out of the annealed films. All radiative peaks showed improvement in PL properties with decreasing Er concentration. Radiative emission at 1150 nm was completely quenched in the film having the highest Er concentration could be due to concentration quenching effect. Overall, due to long lifetime of mid IR levels, a good range of radiative emissions from 350 nm to 1750 nm was measured in all annealed films.

6.2.3: Anneal time dependence of emission properties

As all annealed films used the same 580 ^oC 2 hour anneal, the behavior of the emission properties with longer annealing time (2 hours to 36 hours) was studied on film#3 (Er concentration ($1.65x10^{21}$ ions/cm^3) to determine if longer times

were detrimental or stimulated clustering. The results of annealing for up to 36 hours are shown in figure 6.10.

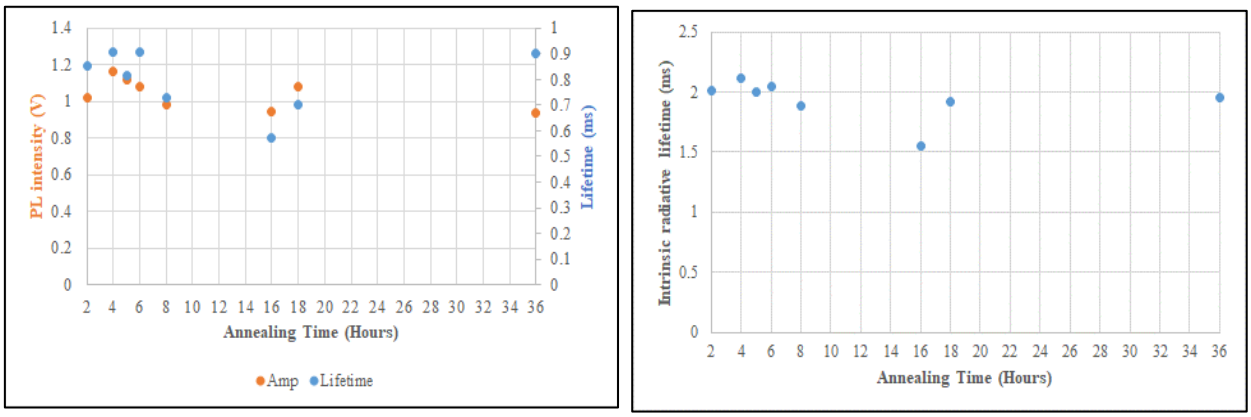

Figure 6.10: Time dependence emission properties of film#3 annealed at a fixed temperature (580°C) for varying annealing hours (2 to 36).

It is determined that Er-doped GLS films are quite stable thermally and show no propensity to cluster, at least at up to 1.5 x 10^{21} /cm^3 doping. Lifetime and PL intensity values did not significantly drop even after long annealing times and the film surface was not damaged. The 1/e and intrinsic lifetimes showed a small drop beyond 6 hours of annealing. According to prior studies, the reason behind the lifetime drop after 6 hours could be due to the formation of surface defects within the glass network, which acts as a local high intensity phonon source. These sources couple to Er ions, thus reducing their lifetime [162]. However, lifetime values recovered after 36 hours, potentially due to improvement in internal crystallisation of the film [338] and reduction in defect density [339]. The measured PL intensity results are stable over the range of annealing times tested within the bounds of experimental error and film edge quality variation.

6.2.4: Photo Degradation

Previous experiments [3] showed that the presence of above bandgap light (green and UV) from either up conversion or external sources significantly and permanently dropped the PL intensity of magnetron sputtered Er-doped As_2S_3 films. Consequently, light exposure tests with green and UV light were conducted on thermally annealed (580°C for 2 hours) Er doped GLS film (#3). Green light exposure was undertaken for 27, 51, and 171 hours using green LED sources (550 nm center wavelength with ~10 mW/cm^2 intensity integrated across the emission spectrum, known to significantly affect other sulphide films). The results are summarized in figure 6.11.

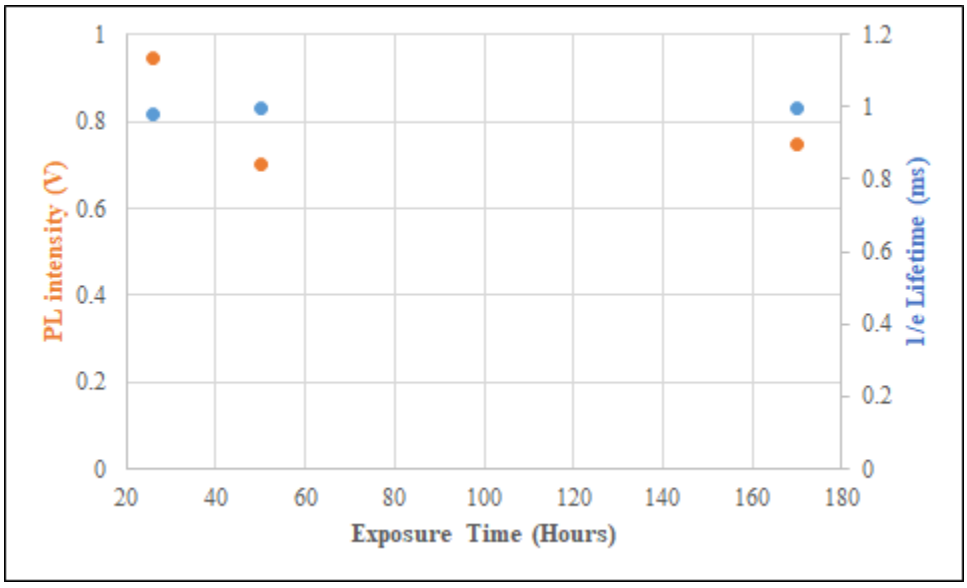

Figure 6.11: Effect of green light (10mW/cm^2) exposure on PL intensity of thermally annealed (580°C for 2 hours) film # 3 having 1.65x10^{21} ions/cm^3 Er concentration.

Lifetime was unaffected, and PL intensity displayed an apparent ~20% drop somewhere between 22 and 50 hours of light exposure but this could still be within the bounds of film edge quality variation. The results are however very promising as compared to prior studies where the PL signal dropped to zero in green light exposed sputtered films. Following the green light exposure, the film was next exposed to intense UV light (500W broadband spectrum Hg:Xe arc lamp) for 3 hours (at an intensity of 58 mW/cm^2 measured narrowband at 365nm, so overall a high intensity exposure factoring in the other emission lines and black body spectrum). The resultant lifetime and PL intensity values were 0.98 ms and 0.768 (V), which is comparable to the green light annealing results above. The UV light has lines well above the bandgap so the glass is stable to high power above bandgap radiation. Therefore, it is concluded from both light exposure conditions that sputtered GLS films are stable to high intensity bandgap light exposure which augurs well for their application in waveguide amplifiers in comparison to prior studies in other chalcogenide materials.

After getting promising results in films, moving to a waveguide geometry (figure 6.12) for further studies seemed the next natural step. However, there is as yet no established means to plasma etch GLS glass, so a strip loaded approach as previously was considered [3]. The most compatible approach at that time was to use As_2S_3 for the loading strip, as it has an almost similar refractive index (n_{1550nm}=2.41), and its waveguiding and plasma etching properties are well understood. Moreover, the reason behind deposition of Su8 polymer on top of As_2S_3 was to protect the As_2S_3 film from oxygen to prevent film quality degradation by oxidation or surface diffusion [340].

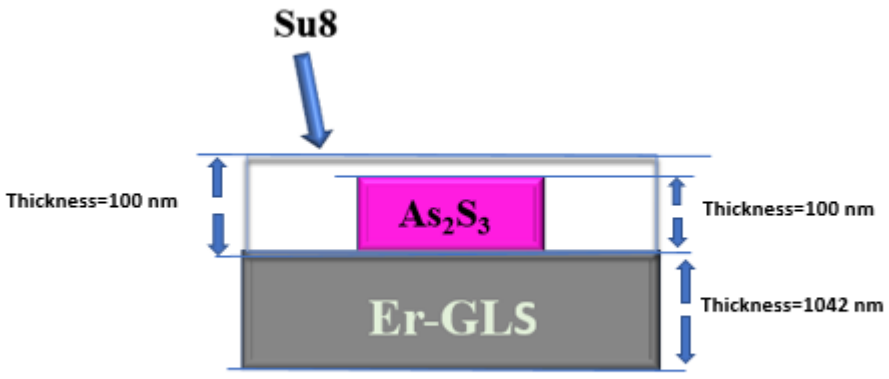

Figure 6.12: Design of required fabrication of strip loaded with 2μm-4μm strip width Er doped GLS waveguide.

As previously noted, as-deposited films did not show PL properties and required annealing at 580 ^{o}C to obtain good PL properties. Whilst this is acceptable for the GLS, As_2S_3 has a melting point of 312 ^{o}C and so the GLS cannot be annealed with the As_2S_3 in place. Therefore, the whole wafer had to be annealed at 580^{o}C for 2 hours before proceeding to As_2S_3 deposition and waveguide fabrication. Normally this would not be problematic, but the large tube furnace at LPC was unavailable for a prolonged period and no other furnace that could take a 100 mm wafer was available to be used to anneal chalcogenides. A large oven that could reach 600 ^{o}C was available (Nabertherm [341], RD 30/200/13), but it was not designed for fully purged operation and so not well sealed. Thus, it was not feasible to use a gas cylinder to continuously flow sufficient Argon through it to ensure an oxygen free atmosphere. Nitrogen was however available in large quantities from the liquid Nitrogen tank boil off. Thus, it was decided to first try a test run of annealing at 580^{o}C for 2 hours under a Nitrogen environment then compare the results with Argon annealing.

For this test, one Er-doped GLS film (700 nm thickness with refractive index 2.01 at 1550 nm) was deposited on a TOx wafer using the same recipe as used for film #3. Two pieces were cleaved from the wafer to thermally anneal (at 580^{o}C for 2 hours) one under Argon in the small tube furnace and the other in a Nitrogen environment in the large oven (50L/min nitrogen gas flow rate and temperature rate was set constant at 5^{o}C/min). PL results of the two annealed films are presented in table 6.7.

Table 6.7: Lifetime and PL intensity of annealed films at 1550 nm wavelength with *1367.14* kW/cm^2 pump intensity when pumped the film edge via 1490 nm pump diode.

PL Properties	Annealed under Argon	Annealed under Nitrogen
1/e Lifetime(ms)	1.072	1.10
PL Intensity(V)	1.492	1.28
Radiative Lifetime (ms)	2.244	1.95

The results show perhaps a 10% degradation in PL intensity properties which is acceptable given the circumstances. A plan was formulated to fabricate a new doped film on a TOx wafer (n=1.44) using the same recipe and used for film# 4 and to fabricate strip loaded waveguide.

The film# 4 recipe was chosen because it has the lowest Er concentration and better PL properties as compared to the rest of the films. According to plan the uniform doped film# 5, with measured 2.12 refractive index and 1042 nm film

thickness at 1550 nm was deposited on a TOx wafer. Unfortunately, it was not possible to carry out the experiment due to the sudden failure of several of the heating elements in the large oven, and the long COVID-19 induced lead time in replacing them (> 6 months) prevented the experiment from being completed during the research period.

6.2.5: Detection of MIR emission

After achieving promising results for visible and NIR emissions, mid IR emission at 2700 nm wavelength was investigated in the annealed films.

Approach # 1

For this experiment, annealed film # 3 was tested using the same optical setup which was utilised to measure PL properties from UV to NIR. However, this time to achieve MIR collection and detection, InF_3 fibres and a thermoelectrically cooled InAs photodiode (J12TE4-3CN-R01M, Teledyne Judson Technologies) were used. The detector has a 1 to 3.8 microns wavelength range, active size 1 mm (diameter), operating temperature -85^{o}C, peak responsivity of 1.5 A/W at 3450 nm. The maximum D* at peak responsivity and 1 kHz of this detector is $7x10^{11}$ Jones (compared to ~3 x 10^{12} Jones for room temperature InGaAs at 1550 nm [342] and the maximum NEP under the same circumstances is 0.43 pW/Hz1/2.The detector is therefore quite sensitive and should be able to detect even small amounts of MIR fluorescence. The schematic diagram of the detection setup and the detectivity curve of the detector is shown in figure 6.13.

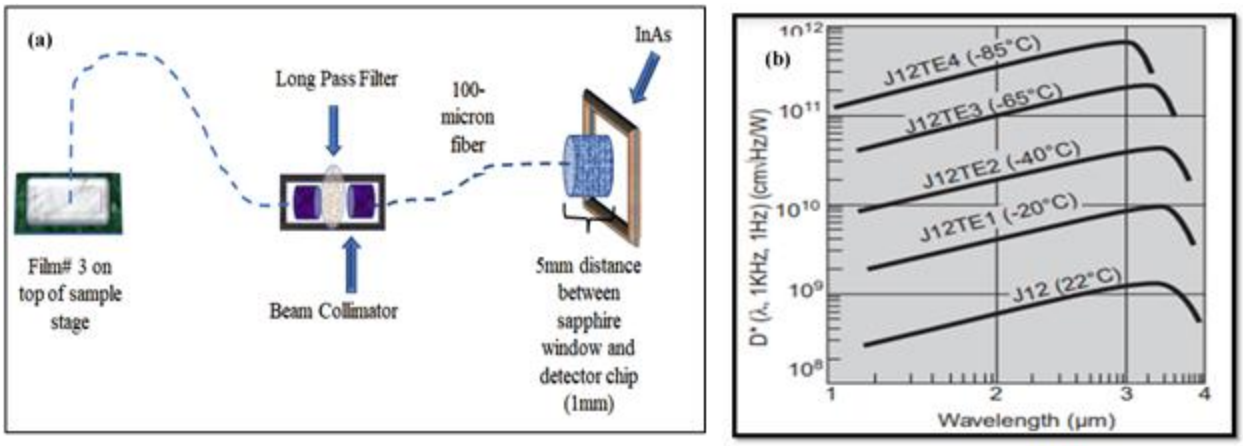

Figure 6.13: (a)Schematic diagram of detection of MIR emissions using high-quality InAs photodiode (The manufacturer of fibre (MF12L2) and collimator (F028FC -3450)is Lastek Photonics Technology Solutions) and (b) detectivity curve of the detector [343].

Pumping the film with a 1490 pump diode at full power, however, revealed no MIR emission.

Approach # 2

The same experimental setup was then trialed replacing the 1490 nm pump diode with 980 nm pump diode as this can excite the Er ion directly to $I_{11/2}$ level and the probability to achieve emission at 2700 nm will be higher than pumping at 1490nm [344]. Before testing for mid-IR emission, the PL properties dependencies for annealed film# 3 were assessed (pump power dependency and wide band emission spectra). The obtained PL properties and broadband emission spectrum are shown in figure 6.14.

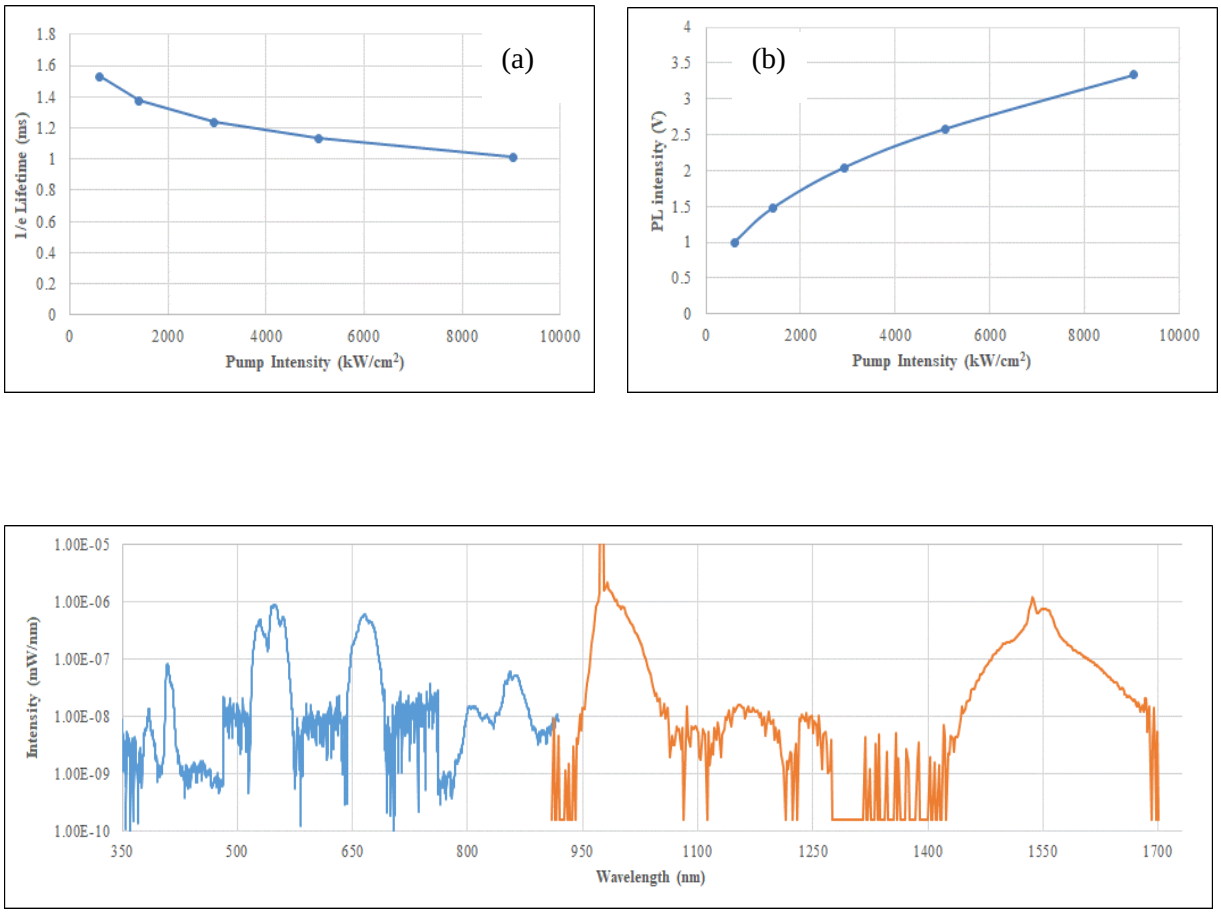

Figure 6.14: (a) 1/e lifetime of $I_{13/2}$ (b) PL intensity of $I_{13/2}$ vs applied 980 nm pump intensity, (c) broad emission spectrum from UV to NIR under 980nm pumping (29023.12 kW/cm^2).

With increasing 980 nm pump power, the lifetime and PL intensity trends at 1550 nm showed similar dependencies on pump power to the 1490 nm pumping discussed earlier in section 6.2.1. A similar broadband emission spectrum was also observed as recorded when the same film (#3) was pumped with 1490 nm pump diode, which have already been discussed in section 6.2.2. However, improvement in measured lifetime and PL intensity values of $I_{13/2}$ level was

observed as compared to PL results under the 1480 nm pump diode. It was expected to detect 2700 nm emission out of this film on account of the improvement in $I_{13/2}$ level PL properties (fig 6.14, a, b) compared to the prior results (fig 6.4). Improvement in PL properties of $I_{13/2}$ level is indicated that more ions involved in radiative transition from $I_{11/2}$ to $I_{13/2}$ level. The population inversion between $I_{11/2}$ - $I_{13/2}$ states was also expected to be enhanced via the ETU process: $I_{13/2}+I_{13/2}$ to $I_{9/2}+I_{15/2}$ as observed in prior studies[151]. ETU will depopulate the $I_{13/2}$ level and repopulate the $I_{11/2}$ level through radiative transition from the $I_{9/2}$ level. This process results in energy reutilisation from $I_{13/2}$ to $I_{11/2}$, which promoted the population inversion between these states. Repeating the mid-IR detection experiment using 980 nm pumping, however still resulted in no light being detected at 2700nm.

Approach # 3

Then it was decided to mount a deep cooled (77 K) Mid-Wave InSb Infrared Xenics camera above the film surface and to try to detect the MIR emissions out of the annealed film directly. Without a long-pass filter (2000 nm), the camera detected strong 1550 nm emission out of the annealed film but with the filter, no emission beyond 2000 nm was observed. As a last attempt, an optical spectrum analyzer with a range from 1800 to 5000 nm (SIR-5000 from Sandhouse) was used to monitor the emission spectrum. A 200-micron core InF_3 fibre (NA ~0.26, transparent up to 5.5um, THORLABS) was positioned just above the top of the film surface to collect and direct light to the Sandhouse spectrometer. Again, no emissions up to 5000nm were detected. All the above approaches were also trialed on film # 4 without success.

Conclusion

It was necessary to investigate the reason behind the lack of mid IR emission. Therefore, it was decided to deeply study the fabricated films.

6.2.6: Elemental Stoichiometry

It was decided to deeply study the fabricated film (undoped and doped) because change in film composition [345] is also known as a potential reason behind the difference in optical properties between the target and the fabricated film. Thus, the fabricated composition of all films was measured using an Electron probe microanalyser (EPMA), where an electron beam irradiates the film surface with sufficient energy and current to generate X-rays characteristic of the elements in the film so enabling elemental analysis. The ideal film thickness for this analysis should be >2000 nm to enable high acceleration voltages to be used whilst avoiding beam penetration to the substrate. As the films were not this thick, the beam acceleration voltage was reduced to ~7 keV, and the beam current obtained was 20.50 nA. The maximum penetration depth of electrons was also confirmed by CASINO Monte Carlo simulations [346], where drop in penetration energy of electrons was observed with increasing thickness of the GLS film and only a small number of electron trajectories could be transmitted through 400 nm the thick film to the TOx substrate as shown in figure 6.15 (a) and (b) respectively.

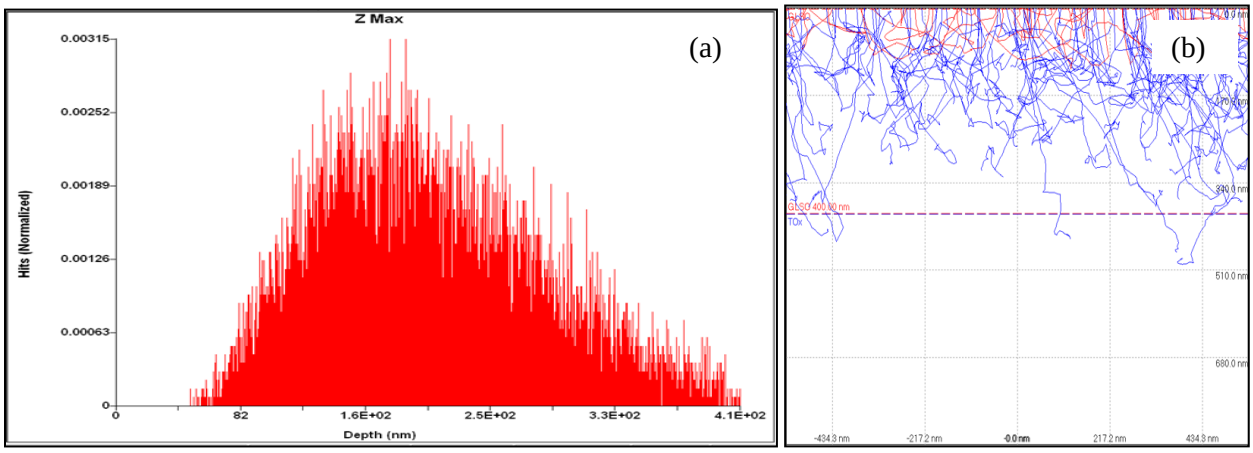

Figure 6.15: (a) Maximum penetration depth histogram in the undoped 400 nm GLS film of the electron trajectories, (b) number of electron trajectories transmitting through film to the TOx wafer.

The measured elemental values of the undoped deposited film measured under these conditions are tabulated in table 6.8.

Table 6.8: Elemental stoichiometry of as deposited GLS film.

O (at%)	Ga (at%)	La (at%)	S (at%)	Si (at%)
37.21	15.50	15.66	31.30	0.29

The known composition (glass sample passport) of the target glass is Gallium (III) Sulphide (70 mol%): Lanthanum (III) Sulphide (30 mol%). From the compositional data (Table 6.2), it is most likely that the 0.29 at% Si component arose from marginal film thickness to prevent substrate irradiation (only 400 nm), so some corresponding oxygen concentration would also be expected. However, the contribution of Si in the film composition is small whilst the oxygen concentration is large, and there are likely other reasons behind the higher oxygen

concentration in the deposited film, which could certainly change the film properties considerably. For example [347], a reduction in refractive index from 2.41 (Gallium (III) Sulphide (70 mol%): Lanthanum (III) Sulphide (32 mol%): Lanthanum (III) Oxide (3 mol%)) to 2.25 (Gallium (III) Sulphide (70 mol%): Lanthanum (III) Oxide (30 mol%))at 1550 nm was observed in GLS glass due to the addition of a higher amount of oxygen in the glass composition.

The prime question is how the fabricated film got such a high concentration (37.2 at%) of oxygen. There could be two possibilities behind high oxygen concentration in the fabricated film either (i) GLS films get oxidised when exposed to air or (ii) water contamination in the sputtering chamber could be incorporated as oxides or –OH groups. The former seems unlikely as GLS is used to make optics commercially and this would then be a widely known issue [303]. Therefore, investigation in more detail was required.

Variations in physical properties (e.g refractive index) were also observed in doped films. Prior studies in Er doped GLS thin films saw a variation in refractive index from 2.5-2.7 at varying Er concentrations and the refractive index (±0.1) was increasing with increasing Er concentration [348]. However, expected dependencies of refractive index such as lower than expected refractive index value on film stoichiometry [349] or different Ga:La and Ga:S ratios [348], the presence of Er_2O_3 phase [350], and incorporation of excess oxygen in the glassy network [347] were also discussed by the authors.

The stoichiometry of the doped films was therefore investigated to determine the reason behind mismatches of the refractive index (RI) compared to expected values. The elemental stoichiometry results of all doped films are shown in table 6.9.

Table 6.9: Elemental stoichiometry of all four doped films at varying Er concentration (at%).

	Film Thickness (nm)	Ga (at%)	La (at%)	S (at%)	Er (at%)	O (at%)	Si (at%)
Film # 1	662±2.1	10.32	7.08	46.30	14.71	21.5	0.09
Film # 2	400±2.2	11.36	14.39	20.57	4.87	48.63	0.18
Film # 3	658±2.2	14.42	14.72	41.28	1.54	28.17	0.10
Film # 4	1042±3.1	17.74	12.18	51.96	0.75	17.3	0.07

All films contain considerable amounts of oxygen, and the amount is approximately inversely proportional to the film thickness. As noted earlier, the measured oxygen content in the films can potentially be higher in thinner films due to greater penetration of the electron beam into the underlying substrate (TOx) in the measurement. This should however be accompanied by a corresponding increase in the Si content. Film#2 has the highest Si concentration (0.18 at%) due to the thinner thickness of the deposited film as compared to the rest of the deposited films. However, this would imply only 0.4 at% of oxygen coming from the TOx, far less than observed.

The huge variation in composition of four doped films was observed and unfortunately this case does not have good explanation. It was suspected that much water in the plasma could be affecting the sputtering condition or may be oxidising the films.

Furthermore, the stoichiometry of the target was then investigated by WDS, which is illustrated in table 6.10.

Table 6.10: Elemental stoichiometry of target.

	Ga (at%)	La (at%)	S (at%)	O (at%)
Target	27.48	13.46	53.96	5.1

The results in table 6.10 indicated that the sputtering target is not pure GLS but has 5.1 at% of oxygen concentration. The glass was apparently prepared from chalcogenide compounds synthesised from high purity elements (99.9999%) but absorption of moisture from the air and oxidation can occur in the glass due to the large surface area of the starting material [330] and with time it can change the composition of the glass as well. According to one prior study [351], this conversion process can quickly introduce oxide, water, or organic impurities into the glass.

A key question here is in what form the oxygen is incorporated into the films, as oxides or Hydroxyl groups. The study of Hydrogen incorporation was unfortunately beyond the mass detection limit of the machine used. Infrared transmittance spectrum is the easiest way to study OH impurities in glass or films due to the very strong absorption of the Hydroxyl group around 2.9 μm. Unfortunately, all four films and the glass target were not suitable for that measurement as the GLS glass was glued to a Cu backing plate and all fabricated

films were thin enough that the absorption measurement would be marginal and on ground back side wafers that scatter IR light strongly.

Therefore one of the surface analytical techniques called Xray Photoelectron spectroscopy (XPS) was used to investigate the elemental composition of unetched and etched (sub-surface analysis) films and the binding configuration of elements such as what the Ga, La, S, and Er were bonded to. XPS technique bombarded the films with photon (low-energy (~1.5 keV) X-rays) to excite the emission of electrons and high resolution electron spectrometer was used to determine the energy spectrum of transmission of photoelectrons. One undoped and two doped films (# 1 and 3) with 37.21 at%, 25.22 at%, and 28.64 at% oxygen concentrations (WDS results), respectively were studied under the best achievable vacuum conditions (typically ~10^{-10} torr) [352]. The detail of measured spectra of unetched and etched films are shown in the figures below, which cover the entire useful range of binding energies available with the used Xray source. The binding energy is indication of specific electron orbital in specific atom and it is just the difference between the final and initial state energies of target atom [352]

From the XPS analysis of the unetched films, it is determined that the binding energies of the elements such as C1s, Ga2p3, La3d5, O1s, S2s, and Er4d photoelectron peaks are located at 284.8, 1118.26, 835.31, 530.52, 225.72, and 168.34 eV respectively, which are shown in the Survey/wide Scan (figure 6.16).

The Carbon peak in the survey spectrum is due to surface chemisorbed atmospheric volatile organic compounds and is quite strong due to the very short penetration depth in XPS. The carbon peak is commonly used as the reference energy peak for binding energy calibration. The survey scan only gives a brief or general analysis of peak structure, so detailed XPS data (proposed chemical bond configuration) is tabulated in table 6.11 and high resolution, narrow region scans of the O1s,and La3d5 regions (multiple peaks) are displayed inset in figure 6.16 as well. It is noteworthy to mention that the values of the measured atomic

percentage in the films could not be real because no standard material have been used for quantitative analysis. However, the relative comparison of the measured films looks quite sensible.

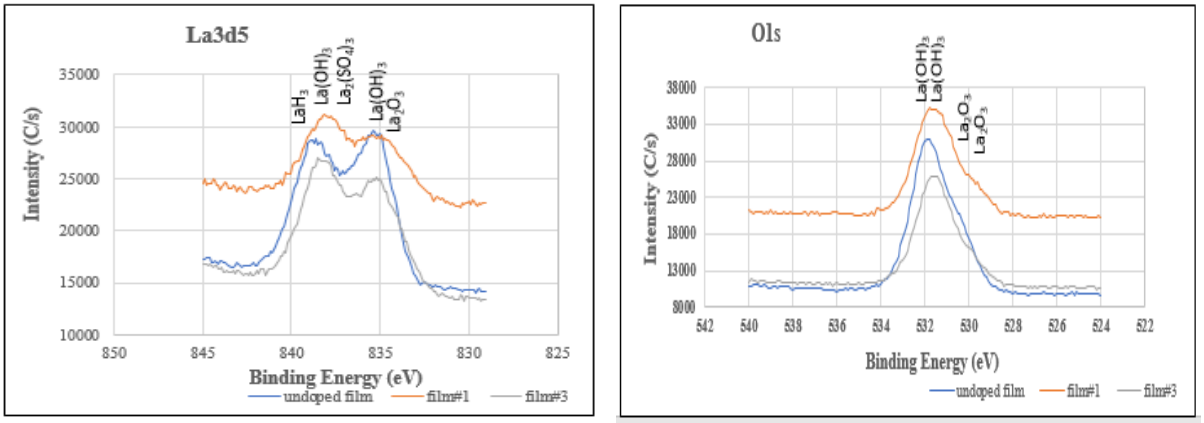

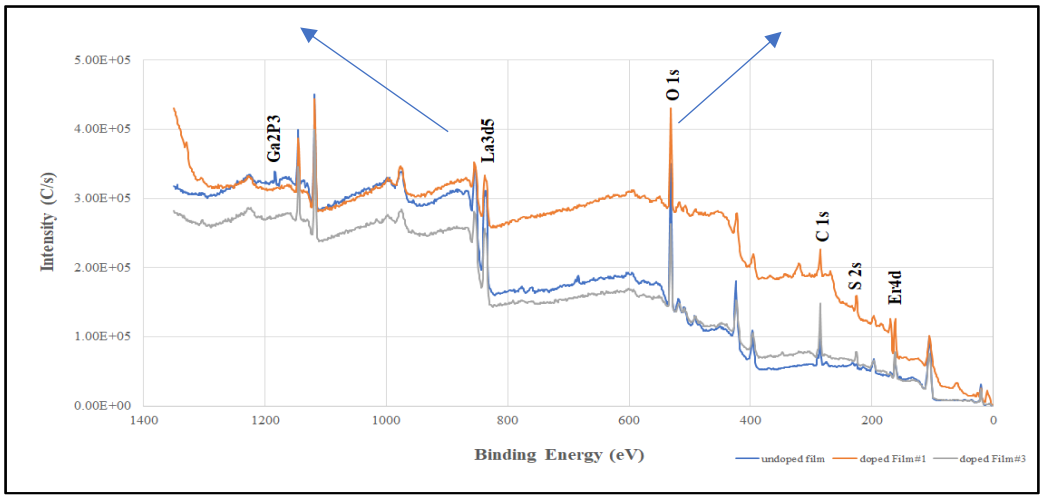

Figure 6.16: Measured XPS spectrum of survey (bottom) and narrow scans of O1s and La3d5 core-level spectra from as deposited undoped and Er doped GLS films.

Table 6.11: Quantitative analysis of as deposited undoped and Er doped GLS films

Peak ID	Peak BE (eV)	Atomic % in as deposited undoped film	Atomic % in as deposited doped film #1	Atomic % in as deposited doped film # 3	Proposed Chemical Bonding
C1s	284.8	19.3	18.4	28.36	C-C
	286.43	2.38	2.6	2.65	C-O-C
	287.8	0.87	0.76		O-C=C
	288.83			3.87	O-C=O
O1s	529.92		7.94	6.82	La_2O_3
	530.52	15.72			La_2O_3
	531.69		34.94	30.86	$La(OH)_3$
	532.03	39.52			$La(OH)_3$
Ga2p3	1118.26	10.21			Ga_2O_3
	1117.86		12.47	9.4	Ga-O
La3d5	834.03		0.98		La_2O_3
	834.4			1.44	La_2O_3
	835.31	3.56	1.28	2.04	$La(OH)_3$
	837.38	1.44			$La_2(SO_4)_3$
	838.24		1.99	2.98	$La(OH)_3$
	839.06	2.79			LaH_3
Er4d	168.34		1.36		Er
	170.25		0.58	0.25	Er_2O_3
S2s	226.32	4.218	16.29	11.3	Ga_2S_3

Hydrogen cannot be detected by XPS because it has no core electrons so core-electron XPS analysis is impossible. It is also hard to distinguish between H1s valence electrons and valence electrons of other elements. However, according to

prior studies [353], it is possible to register the Hydrogen containing compounds and the effect of Hydrogen on different elements (e.g Ga, La, S, O, C and Er) in XPS [354] by an increase in the binding energy of the different elements attached to the Hydrogen.

The detailed XPS data of all elements corresponding to each film (undoped and doped) is provided in table 6.11 for the top surface XPS results, where the above mentioned argument holds true for all elements. The first element in the table is Carbon, where several types of C-O bonded systems are identified on all films and in forms that typical volatile organic species would possess. By default, the binding energy of the C-C component is 284.8 eV [355]. However, peak shifting to higher binding energy was observed after the bonding of C to one electronegative oxygen atom. Further shifting is evident after being bonded to more electronegative atoms. Moreover, the higher atomic percentage of Carbon in film#3 (table 6.11) indicated that the deposited layer of Carbon on this film (#3) is thicker as compared to rest of the two films. That is why even after etching (table 6.12), the Carbon layer could not be removed fully. Therefore, normalised atomic percentage (at%) in film #3 has been mentioned (table 6.12) next to the measured values.

The O1s peak is de-convoluted to four peaks. Two oxygen peaks located at 529.92 eV and 530.52 eV are assigned to the lattice oxygen of La_2O_3 [356], which confirms the effective incorporation of oxygen on the surface of measured samples. Moreover, the presence of water and hydroxide species [357] was confirmed with the increased [356], [358] binding energies of oxygen [359] such as 531.69 and 532.03 eV corresponding to corresponding to $La(OH)_3$ bonding [360], indicated the presence of covalency of the O–H bond [278] in the irradiated [353]. Beside this, as the undoped film has high amount of oxygen concentration (37.21 at%) as compared to doped films that is why high concentration (15.72 at%) of La_2O_3 in undoped film was measured. Effective incorporation of oxygen in the measured samples was again confirmed through Ga2p3 peak locations. The

binding energy of Ga element is 1116.7 eV [361], whereas the increase in binding energy values to 1118.26 and 1117.86 eV is attributed to the presence of Ga-O bond in the films [362].

Next, the highly reactive element called Lanthanum usually found in an oxidised state [363]that is why the binding energy of two peaks such as 834.03 eV and 834.22 eV [359] are suggesting the existence of La_2O_3 bond on the surfaces of measured films [364] Moreover, the higher binding energy values such as 835.31, 837.38, 838.24 and 839.06 eV corresponding to the $La(OH)_3$, $La_2(SO_4)_3$ and LaH_3 bonds are associated to the absorbed water and hydroxide [365] on the surface of the tested films. Moreover, the measured binding energy values for erbium exceed the binding energy of the Er component (167.5 eV [366]), likely as a result of bonding of Er to electronegative atoms (e.g oxygen, etc.). As the film#1 has higher Er concentration ($1.27x10^{22}$ ions/cm^3) than film#3 ($1.65x10^{21}$ ions/cm^3) that is why more concentration of Er_2O_3 (0.58 at%) in film#1 was measured. Beside this, the measured binding energy value (226.32 eV) of S2s indicated the presence of Ga_2S_3 in all films. Though it was expected to measure chemical bonding of La-S and Er-S in all films but failed to find these chemical bondings in tested films.

Thus, it is concluded from above analysis that oxides, hydrides, hydroxyl and also sulphide are present in the fabricated films.

After evaluating the as deposited films the films were etched for the 30 seconds with Ar plasma to explore the sub-surface analysis. The film surface etching was performed to eliminate/investigate surface contamination/oxidation [367]and chemical stability [368], respectively. The extracted spectral data (figure 6.17) indicated the same elemental peaks and consistent increases in binding energies (Table 6.12) of the elemental orbitals C1s, Ga2p3, La3d5, O1s, Er4d, and S2s as observed in all three unetched films (figure 6.17)

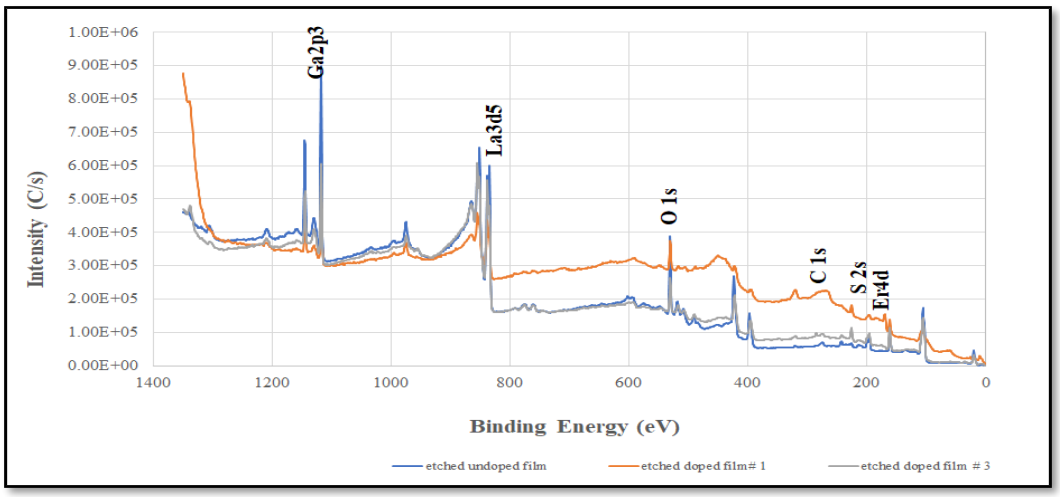

Figure 6.17: Measured XPS (survey) spectrum of as deposited undoped and Er doped GLS films (after Ar etching).

Table 6.12: Quantitative analysis of as deposited undoped and Er doped GLS films (after Ar etching).

Peak ID	Peak BE (eV)	Atomic % in etched undoped film	Atomic % in etched doped film #1	Measured and normalised Atomic % in etched doped film # 3	Proposed Chemical Bonding
C1s	284.8			6.0 (0)	C-C
O1s	529.92		29.6	26.2 (28)	La_2O_3
	530.03	41.9			La_2O_3
	531.69	6.4	7.07	5.4 (5.7)	$La(OH)_3$
	531.63				$La(OH)_3$
Ga2p3	1117.86	28.6	18.0	19.4 (20.7)	Ga-O
La3d5	833.99			8.3 (8.8)	La_2O_3
	834.23	8.5	4.9		La_2O_3
	836.36	3.0	2.2	4.0 (4.2)	$La(OH)_3$
	838.61	6.9	5.1	9.6 (10.2)	$La(OH)_3$
Er4d	168.34		3.9	0.3 (0.3)	Er
	170.6		0.64		Er_2O_3
S2s	226.32	3.8	28.4	20.3 (21.7)	Ga_2S_3

From the etched film results, it is concluded that oxygen is available on the surface and tightly bonded with other elements throughout the film depth as well. This coherency shows strong chemical stability between each available element throughout the film depth.

Though overall XPS results of etched and unetched films confirmed that all films contain oxide, hydrides, hydroxyl and sulphide [327].However, incorporation of the OH impurity could be one of the major reasons for the complete emission quenching of as-deposited doped films [369] and also for the absence of the 2700 nm emission. Similar results were present in prior work [101] where high Er

concentration ($6.0x10^{20}$ ions/cm^3) combined with OH groups was proved to be a serious quencher[179] for effectively damping the erbium 1550 nm transition (0.3 ms 1/e lifetime of $I_{13/2}$ level) in Er doped tellurite films. Moreover, 2.7um emission has been observed in Ga-La oxide glasses, so the problem is not oxide contamination [149].

Discussion

Considering prior studies and the excellent emission properties in the UV-Vis-NIR, the absence of mid IR emissions could be specifically due to the presence of OH- [370]in the films because it is known to be a critical factor in the emission efficiency at 2700nm [334]. The definitive evidence for the presence of OH in the films has already been discussed in the XPS discussion section, where the presence O-H bonds was identified because of the increased binding energy of elemental peaks (e.g. Lanthanum etc.).OH^- has also previously been identified to have a considerable effect on the erbium $I_{13/2}$ level in as-deposited films[371].In the previous studies, annealing improved the IR emission efficiency because of decreasing the probability of non-radiative transitions after diminishing stress and defects and bond rearrangement between OH and Er doped sulphide films [3].

As mentioned earlier, the OH groups are known to quench the $I_{11/2}$ level through a resonant energy transfer process [150]. It is crucial to reduce the OH concentration to obtain efficient emission at 2700 nm. The current fabricated films have quite a high Er concentration so it would be expected to detect 2700 nm emission out of these films, but it did not happen. Based on the discrepancy between measured (1.01 ms) and calculated (1.53 ms) lifetime values of $I_{11/2}$ level and XPS results, it was may be inferred that lack of mid IR emission was occurred due to strong absorption from OH^- group contamination.

Thus, the main problem here is likely the very high OH contamination in the films. As the GLS target was a sintered powder formation [372] the large surface area of the target can absorb much water from the atmosphere and water can also be

carried by the Er metal on top of GLS target [151]. However, there is a more likely source which is desorption from the vacuum system.

6.2.7: Starting Chamber pressure vs OH^- contamination

One major potential source of OH contamination in the deposited films is the vacuum system. It is well known that at vacuum levels below ~1 mTorr that the vast majority of the remaining gas in a leak free system is water vapour which originates from outgassing of the adsorbed water on all the internal surfaces of the vacuum system from exposure to humid air during venting. In many sputtering processes, it is a common assumption that the process can begin once the chamber has pumped to somewhere in the low 10^{-6} Torr range, even more so as during sputtering the system is operated in the milli-Torr range with high gas flows. However, it is also normal practice to throttle the high vacuum pump to attain the desired process pressure, which also vastly reduces the pumping of water vapour from the chamber surfaces. The fast clean pumping of all gases at pressures below10^{-2} Torr was provided by a Brooks Cryogenics CTI Cryo Pump (Model CT-10, 3000 liters/sec Air, 9000 liters/sec water, 5000 liters/sec Hydrogen and 2500 liters/sec Argon) [373], which is connected to the 36x23 inch Angstrom chamber. Four times higher pumping speed for water of the Cryo pump than any other vacuum pump with the same inlet diameter allows faster evacuation of the sputtering chamber[374] as well. The essential question then is the quantity of water present in the sputtering gas under sputtering conditions.

To make an assessment of the potential content, a Residual Gas Analyser (RGA), was used to monitor the partial pressure of the vacuum components (air, water, carbon dioxide, etc). As the RGA will not operate safely at pressures above 1 mTorr, and not well in the presence of oxygen (filament degrades rapidly) an approximation was made by closing the gate valve to the cryopump to the position normally used for sputtering (gate valve reading on VAT auto pressure controller of 110). RGA spectra were then taken at a range of initial starting chamber

pressures over a two week period and recording both the final stabilised total pressure on the chamber Penning gauge (calibrated on nitrogen vs almost entirely water in the vacuum) and water partial pressure on the RGA. Over the two weeks, the chamber pressure fell from $9.3x10^{-6}$ Torr to $4.0x10^{-7}$ Torr. Prior data showed the best achieved base pressure value could be as low as $6.0x10^{-8}$ Torr but only with a freshly cleaned and baked chamber and with the cryopump in optimum condition.The collected data for water pressure in the vacuum chamber with gate valve throttled using the Penning gauge and RGA w.r.t to chamber pressure is shown in figure 6.18.

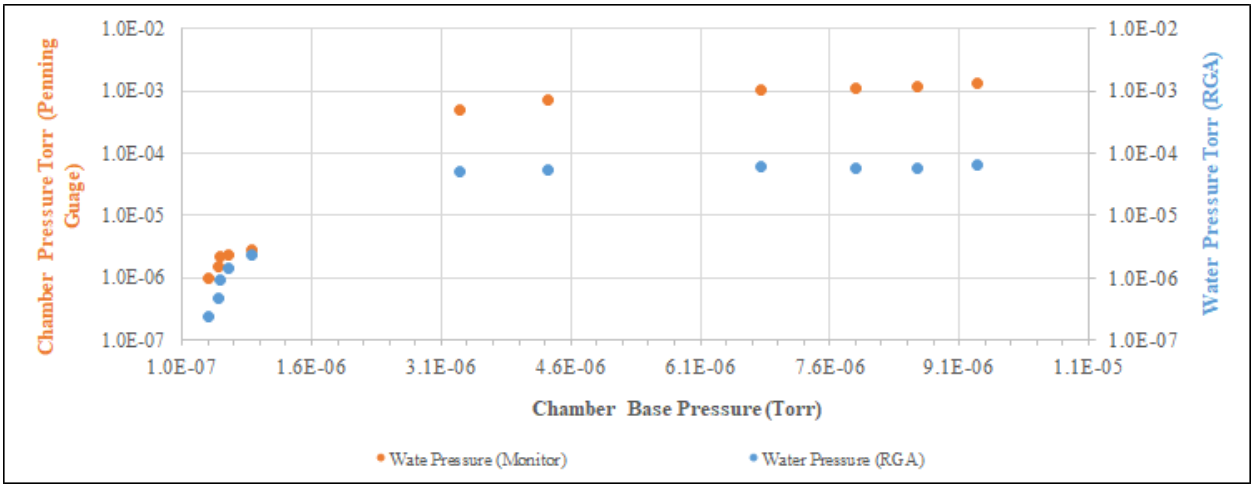

.

Figure 6.18: Measured water pressure using penning gauge and RGA respectively w.r.t set chamber base pressure.

Given that the sputtering process was conducted at 5 mTorr, then it is clear that a chamber base pressure before commencing sputtering of even $3x10^{-6}$ Torr is grossly inadequate with 10-20% of the pressure then potentially being water vapour.

Silicon wafers were then used to deposit three undoped films at varying chamber starting pressures after pump down commenced using the same recipe as used to fabricate the prior films. Film# 1 has the lowest thickness due to a shorter deposition (3 hours vs 7 to 8 hours). The detailed film properties and compositions with respect to the chamber pressure at the start of the process for each deposited film are presented in table 6.13.

Table 6.13: Film quality and compositional analysis of deposited films.

Films	Chamber Pressure (Torr)	Thickness (nm)	Refractive index	Bandgap (eV)	O (at%)	Ga (at%)	La (at%)	S (at%)
1	$2.0x10^{-6}$	241	2.04	2.52	34.07	16.21	15.14	34.57
2	$3.83x10^{-7}$	1099	2.32	2.69	8.29	20.09	11.65	59.96
3	$3.17x10^{-7}$	1273	2.41	2.39	5.97	21.02	12.23	60.75
Target					5.1	27.48	13.46	53.96

The data clearly indicates that the oxygen concentration in the deposited films depends upon the chamber pressure at the start of the sputtering process largely aligning with the data of figure 6.18. Film #3, deposited at $3.17x10^{-7}$ Torr pressure hasproperties quite close to the target in terms of oxygen content. It is clear that pressures below $4x10^{-7}$ Torr must be reached before commencing sputtering in this system to eliminate gross water contamination. Indeed to attain water

contamination levels comparable to glasses, rather lower starting pressures will be required. This then raises the need for adding in chamber dedicated water vapour cryopumps to selectively remove water at very high rates (up to 150,000 L/s is possible) whilst leaving the sputter gases untouched. This could not however be assessed in the time frame of this project.

Another important question is how the water is incorporated into the film, by surface adsorption/reaction or in the plasma of the sputtering gun? The monolayer formation time of water on substrate was calculated by following impingement rate equations at different starting chamber pressures [375]. It was concluded that a monolayer of water molecules will be deposited in ~0.04 seconds at 3.31×10^{-6} Torr chamber base pressure. However, the deposition of water layer will take ~8 seconds at 4.01×10^{-7} Torr chamber base pressure. In comparison the deposition rate of the GLS film is typically ~0.05 nm/s. So, based on the atomic diameters of Ga, La and S, it is estimated that a GLS monolayer deposition will take ~18s. As the sticking coefficient of water is ~1 [376], it means there is no significant hydrolysis reaction between water and GLS on the surface given the observed reduction in oxygen content at lower starting pressures. A plasma could certainly break water into O and OH, which could then react with the sputtered atoms in GLS to form contamination or quenching centers in the deposited films and this then seems the most likely route.

An erbium doped film was then deposited on a TOx wafer using the GLS target with Er foil *(*0.7 x 0.7 cm^2 size) using the same recipe as used for the prior film # 4 (table 6.9) but at better chamber starting pressure (3.98×10^{-7} Torr). The resultant properties of the fabricated film are presented in table 6.14 below:

Table 6.14: Film quality and compositional analysis of deposited doped film # 4.

Thickness (nm)	Refractive index @ 1550 nm	Bandgap (eV) @1550nm	O (at%)	Ga (at%)	Si (at%)	La (at%)	S (at%)	Er (at%)	Er conc (ions/cm^3)
300	2.36	2.23	7.26	16.88	0.69	15.78	58.40	0.954	0.895×10^{21}
Target			5.1	27.48	0	13.46	53.96	0	

As hoped for, this film had a much lower oxygen concentration as compared to film # 4, which was quite promising. The film was pumped in the as-deposited state with a 1490 nm laser diode at 126.45 kW/cm^2 pump intensity via a lens tipped fibre to study the PL properties at 1550 nm. In the prior as-deposited film # 4, there was no emission. With the reduced oxygen/OH contamination it was possible to measure the lifetime and 1550 nm PL intensity in the as-deposited film. The measured 1/e lifetime, intrinsic radiative lifetime, and PL intensity were 0.316ms, 0.615 ms, and 0.551V respectively at 126.45 kW/cm^2. These numbers are however still inferior to those of the previous annealed films indicating there is still significant water in the films or that the material structure was imperfect. The prior thermal annealing method was therefore applied to the as-deposited films and the results are listed in table 6.15.

Table 6.15:PL properties of annealed film # 4 at different temperatures for 2 hours.

PL properties	As deposited	Annealed at 530°C	Annealed at 550°C
1/e Lifetime (ms)	0.316	0.792	0.611
Radiative lifetime (ms)	0.615	2.131	2.527
PL intensity (V)	0.551	0.75	0.709

Thermal annealing at different temperatures (530°C and 550°C) improved the PL properties of the film and increased the observed green and red emissions visible from the top surface of the film as well, which were getting stronger with increasing pump intensity just like prior annealing analysis (films #3 and #4). However, when the film was annealed at 580°C, no near IR emissions were detected likely because of significant changes in film composition as compared to prior tested films (# 2, # 3, and # 4). Further study is required to re-establish the optimum annealing conditions for an uncontaminated film.

Detection of mid IR emission

After achieving PL in as deposited films and further improvement by annealing at 530°C, mid IR emission detection using the same approaches as discussed in section 6.2.5 were attempted. However, mid IR emission still could not be detected. This tends to imply further improvements are still needed in the vacuum level most ideally by adding in chamber water vapour pumping.

Conclusion:

In following prior research on GaLaS glasses and films, RF magnetron sputtered Er doped GLS films proved capable of incorporating a huge amount of Er without clustering. Good lifetimes of important mid-IR levels were achieved and a rich PL spectrum observed containing transitions previously not observed in GLS. Furthermore, the role of residual water in the vacuum and high sensitivity to OH in sulphide hosts was also highlighted by this work. However, it was also apparent that GLS (and as others in the group also discovered sulphide chalcogenide glasses in general) appear to have a very strong affinity for the incorporation of Hydroxyl groups. Whist progress was made in overcoming this problem in the work discussed in this thesis, further work remains before high performance MIR devices will be possible.

GLS remains a very promising material even after all the challenges encountered. It was not possible to get to the planned end point as due to COVID-19 lockdowns it was not possible to obtain the Er:GLS sputter target in time to undertake experiments. Once this target is received, based on the processes developed in this thesis waveguide amplifier devices can be built and tested at 1550 nm with the prospects of very high gain and saturated output powers. This should clearly be explored as a matter of urgency. To obtain suitable results in the MIR, it is clear that further work on reducing water in the deposition chamber during deposition is key, and the use of dedicated in chamber water vapour pumping needs to be explored as the most likely candidate to resolve the issue.

Chapter 7: Conclusions and Recommendations

7.1 Conclusions

This work was based on improved deposition techniques (sputtering and evaporation) and several host materials with better solubility of rare earth ion plus film consolidation to overcome issues faced in the past. There have been a number of important achievements, which were never nor discussed before. Er ion doped chalcogen films were fabricated using RF sputtering and Co-thermal evaporation based on tellurite and sulphide based host materials.

After deep studies of significant issues in reactive sputtering and custom enhancements to the sputtering system (MFC, water cooling system, monitoring system, oxygen partial pressure control etc), a stable and repeatable process to fabricate high quality undoped and Er doped tellurite films was achieved with the resultant films having apparently the best ever lifetime for Tellurium dioxide.

Rapid Thermal Annealing (RTA) was investigated as a means to consolidate magnetron sputtered Er doped As_2S_3 films to eliminate the incorporation of OH groups by upconverted light observed in prior studies. However, rapid thermal treatments still allowed erbium to thermally cluster at treatment times beyond 2 minutes or temperatures beyond 200^{o}C after 1 minute. Unfortunately this was not sufficient to prevent the OH incorporation. Therefore, the RTA treatment was concluded to be an ineffective solution at preventing green light activated OH induced quenching.

Turning to alternate hosts, then thermal evaporation of GeGaS powder was proven not to be a viable way forward for film formation despite the material's apparently

promising properties. No consistency in composition was observed in the films fabricated at <1100°C and the material remaining in the crucible was pure Ga_2S_3. In contrast flash evaporation was considered a successful strategy to deposit film at 1100°C in less than two minutes, where the final composition of the film ($Ge_{28.49}Ga_{9.99}S_{61.54}$) was quite close to the composition of the used $Ge_{28.5}Ga_{6.2}S_{65.3}$ glass. However, it is hard to control the deposition rate during non PID controlled flash evaporation and it is therefore also difficult to control the thickness of the film. There is a genuine concern that the film is not going to have uniform composition through its depth as again after conclusion of the deposition the crucible contained only pure Ga_2S_3. Given these issues thermal/flash evaporation of GeGaS was not pursued further.

Multiple attempts and the considerable effort expended herein have proved that the co-evaporation of erbium sulphide with a chalcogenide glass is difficult and much more work is required to overcome the issues encountered (which have never been discussed in the literature). At this stage it is still unknown whether co-evaporation is a viable technique without a considerable further research investment.

In following prior research on GaLaS glasses and films, RF magnetron sputtered Er doped GLS films proved capable of incorporating a huge amount of Er without clustering. Good lifetimes of important mid-IR levels were achieved and a rich PL spectrum observed containing transitions previously not observed in GLS. Furthermore, highlighted the role and sensitivity of OH contamination in planar devices. However, it was also apparent that GLS (and as others in the group also discovered sulphide chalcogenide glasses in general) appear to have a very strong affinity for the incorporation of Hydroxyl groups. Whist progress was made in overcoming this problem in the work discussed in this thesis, further work remains before high performance MIR devices will be possible.

7.2 Recommendations for Future Work

From the work performed in this thesis, it is clear that “simple” fixes do not exist around the problems holding back chalcogen glasses in terms of relaising high performance planar MIR emission. Some approaches initially considered promising are now clearly unsuitable, though the materials involved may still have promise with other fabrication methods.

The stable sputtering process developed for the fabrication of doped reactively sputtered tellurite films can now be used to finally and scientifically study the impact of high Er concentrations in pure TeO_2 films and allow the development of processes to match the outstanding performance achieved in highly Er doped pure and multicomponent TeO_2 glasses. This would then allow a high saturated output power optical amplifier to be built on chip, a key technological milestone. It is however clear that further development work around adding dedicated vacuum water vapour pumping is necessary as part of this study to reduce OH incorporation because rare earth lifetimes are significantly affected by OH contamination in particular.

Turning to Er:As_2S_3, RTA cannot solve the porosity problems encountered in magnetron sputtered material and it is clear that magnetron sputtering is not a viable way forward. So it would be recommended to alter the film growth habit by adopting deposition methods such as bias sputtering, Ion Beam Sputtering and secondary ion beam bombardment etc. Each of these has its own merits and compromises and it is not immediately clear which would be preferred. Alternatively, the adoption of an entirely different method is needed. For example, coating a moisture barrier layer on the film as hermetic sealing to protect it could be an option though this is difficult and relatively costly at the device scale. Moving instead to thermal co-evaporation of Er_2S_3 and As_2S_3 also did not

prove to be an easy alternative. Another approach such as E-beam co-evaporation might be viable for the fabrication of erbium sulphide doped films, but requires significant investment in its own right and carries the risk of overheating the substrate.

Moving away from the proven planar integration platform offered by As_2S_3 to other hosts with better rare earth properties still remains an attractive option. For the fabrication of GeGaS films with optimised stoichiometry, it is recommended to move to co-evaporation of GeS_2 and Ga_2S_3 from separate rate-controlled furnaces in the future to get consistent composition. It is estimated that 90% GeS_2 and 10% Ga_2S_3 can be used to fabricate one micron thick uniform films with the required atomic ratio ($Ge_{28.5}Ga_{6.2}S_{65.3}$). It is also recommended to use Pyrolytic Boron Nitride crucibles and baffles for further thermal evaporation process in future because they can withstand high temperature in high vacuum environment. This will then enable a detailed study of the suitability of GeGaS as a rare earth host for MIR devices.

GLS remains a very promising material even after all the challenges encountered. It was not possible to get to the planned end point as due to COVID-19 lockdowns it was not possible to obtain the Er:GLS sputter target in time to undertake experiments. Once this target is received, based on the processes developed in this thesis waveguide amplifier devices can be built and tested at 1550nm with the prospects of very high gain and saturated output powers. This should clearly be explored as a matter of urgency. To obtain suitable results in the MIR, it is clear that further work on reducing water in the deposition chamber during deposition is key, and the use of dedicated in chamber water vapour pumping needs to be explored as the most likely candidate to resolve the issue.

References:

[1] A. B. Seddon, Z. Tang, D. Furniss, S. Sujecki, and T. M. Benson, "Progress in rare-earth-doped mid-infrared fiber lasers," *Opt. Express*, 2010, doi: 10.1364/oe.18.026704.

[2] Biliana Gasharova, "Raman, Conventional Infrared and Synchrotron Infrared Spectroscopy in Mineralogy and Geochemistry: Basics and Applications," ANKA Synchrotron Light Source / Institute for Synchrotron Radiation, Research Center Karlsruhe, Germany, 2008.

[3] A. Kunlun Yan(LPC, "Rare-earth ion doped chalcogenide waveguide amplifiers," Australian National University, 2018.

[4] G. Fox, "The brewing industry and the opportunities for real-time quality analysis using infrared spectroscopy," *Applied Sciences (Switzerland)*. 2020, doi: 10.3390/app10020616.

[5] David Caffey, "Recent Results from Broadly Tunable External Cavity Quantum Cascade Lasers," *Recent Results from Broadly Tunable Extern. Cavity Quantum Cascade Lasers*, 2011.

[6] X. Zhu and N. Peyghambarian, "High-power ZBLAN glass fiber lasers: Review and prospect," *Advances in OptoElectronics*. 2010, doi: 10.1155/2010/501956.

[7] *Solid-State Mid-Infrared Laser Sources*. 2003.

[8] Y. Yao, A. J. Hoffman, and C. F. Gmachl, "Mid-infrared quantum cascade lasers," *Nature Photonics*. 2012, doi: 10.1038/nphoton.2012.143.

[9] X. Liu, R. M. Osgood, Y. A. Vlasov, and W. M. J. Green, "Mid-infrared optical parametric amplifier using silicon nanophotonic waveguides," *Nat. Photonics*, 2010, doi: 10.1038/nphoton.2010.119.

[10] J. Swiderski, "High-power mid-infrared supercontinuum sources: Current status and future perspectives," *Progress in Quantum Electronics*. 2014, doi: 10.1016/j.pquantelec.2014.10.002.

[11] G. Wysocki, R. F. Curl, F. K. Tittel, R. Maulini, J. M. Bulliard, and J. Faist, "Widely tunable mode-hop free external cavity quantum cascade laser for high resolution spectroscopic applications," *Appl. Phys. B Lasers Opt.*, 2005, doi: 10.1007/s00340-005-1965-4.

[12] T. Hausmaninger, I. Silander, and O. Axner, "Narrowing of the linewidth of an optical parametric oscillator by an acousto-optic modulator for the realization of mid-IR noise-immune cavity-enhanced optical heterodyne molecular spectrometry down to 10^−10 cm^−1 Hz^−1/2," *Opt. Express*, 2015, doi: 10.1364/oe.23.033641.

[13] W. Shi, A. Schulzgen, R. Amezcua, X. Zhu, and S.-U. Alam, "Fiber lasers and their applications: introduction," *J. Opt. Soc. Am. B*, 2017, doi: 10.1364/josab.34.00fla1.

[14] L. Sójka *et al.*, "Broadband, mid-infrared emission from Pr3+ doped GeAsGaSe chalcogenide fiber, optically clad," *Opt. Mater. (Amst).*, 2014, doi: 10.1016/j.optmat.2014.01.038.

[15] L. Sojka *et al.*, "Milliwatt-Level Spontaneous Emission Across the 3.5–8 µm Spectral Region from Pr3+ Doped Selenide Chalcogenide Fiber Pumped with a Laser Diode," *Appl. Sci.*, vol. 10, pp. 1–11, 2020.

[16] L. G. and S. D. J. D. Hudson, E. Magi, "1 W diode-pumped tunable Ho31, Pr31-doped fluoride glass fibre laser," *Electron. Lett.*, vol. 47, 2011.

[17] Stuart D. Jackson, “Single-transverse-mode 2.5-W holmium-doped fluoride fiber laser operating at 2.86 mm,” *Opt. Lett.*, vol. 29, 2004.

[18] Stuart D. Jackson, “High-power and highly efficient diode-claddingpumped holmium-doped fluoride fiber laser operating at 2.94 _m,” *Opt. Lett.*, vol. 34, 2009.

[19] W. Tang *et al.*, “High-peak-power mode-locking pulse generation in a dual-loss-modulated laser with BP-SA and EOM,” *Opt. Lett.*, 2017, doi: 10.1364/ol.42.004820.

[20] W. H. Renninger and F. W. Wise, “Fundamental Limits to Mode-Locked Lasers: Toward Terawatt Peak Powers,” *IEEE J. Sel. Top. Quantum Electron.*, 2015, doi: 10.1109/JSTQE.2014.2329936.

[21] C. Wei, H. Shi, H. Luo, H. Zhang, Y. Lyu, and Y. Liu, “34 nm-wavelength-tunable picosecond Ho^3+/Pr^3+-codoped ZBLAN fiber laser,” *Opt. Express*, 2017, doi: 10.1364/oe.25.019170.

[22] J. M. Fedeli and S. Nicoletti, “Mid-Infrared (Mid-IR) Silicon-Based Photonics,” *Proceedings of the IEEE*. 2018, doi: 10.1109/JPROC.2018.2844565.

[23] J. Ari *et al.*, “Rare-earth-doped chalcogenide glasses for mid-IR gas sensor applications,” 2017, doi: 10.1117/12.2251529.

[24] P. Ma *et al.*, “Low-loss chalcogenide waveguides for chemical sensing in the mid-infrared,” *Opt. Express*, 2013, doi: 10.1364/oe.21.029927.

[25] P. Ma *et al.*, “High Q factor chalcogenide ring resonators for cavity-enhanced MIR spectroscopic sensing,” *Opt. Express*, 2015, doi: 10.1364/oe.23.019969.

[26] V. M. Lavchiev and B. Jakoby, “Photonics in the Mid-Infrared: Challenges in Single-Chip Integration and Absorption Sensing,” *IEEE J. Sel. Top. Quantum Electron.*, 2017, doi: 10.1109/JSTQE.2016.2619330.

[27] and H. X. T. Pao Tai Lin, Hojoong Jung, L ionel C. Kimerling, Anu Agarwal, “Low-loss aluminium nitride thin film for mid-infraredmicrophotonics,” *Laser Photonic Rev.*, vol. 8, 2014.

[28] M. S. Yazici, B. Dong, D. Hasan, F. Sun, and C. Lee, “Integration of MEMS IR detectors with MIR waveguides for sensing applications,” *Opt. Express*, 2020, doi: 10.1364/oe.381279.

[29] H. Lin *et al.*, “Mid-infrared integrated photonics on silicon: A perspective,” *Nanophotonics*, vol. 7, no. 2. Walter de Gruyter GmbH, pp. 393–420, 2017, doi: 10.1515/nanoph-2017-0085.

[30] A. Spott *et al.*, “Quantum cascade laser on silicon,” *Optica*, 2016, doi: 10.1364/optica.3.000545.

[31] J. S. Sanghera, L. B. Shaw, and I. D. Aggarwal, “Chalcogenide glass-fiber-based mid-IR sources and applications,” *IEEE J. Sel. Top. Quantum Electron.*, 2009, doi: 10.1109/JSTQE.2008.2010245.

[32] F. Starecki *et al.*, “All-optical carbon dioxide remote sensing using rare earth doped chalcogenide fibers,” *Opt. Lasers Eng.*, 2019, doi: 10.1016/j.optlaseng.2019.06.018.

[33] K. Yan, K. Vu, R. Wang, and S. Madden, “Greater than 50% inversion in Erbium doped Chalcogenide waveguides,” *Opt. Express*, 2016, doi: 10.1364/oe.24.023304.

[34] G. Tao *et al.*, “Infrared fibers,” *Adv. Opt. Photonics*, 2015, doi: 10.1364/aop.7.000379.

[35] C. Calahoo and L. Wondraczek, “Ionic glasses: Structure, properties and classification,” *Journal of Non-Crystalline Solids: X*. 2020, doi: 10.1016/j.nocx.2020.100054.

[36] T. Sandrock, A. Diening, and G. Huber, “Laser emission of erbium-doped fluoride bulk glasses in the spectral range from 27 to 28 ?m,” *Opt. Lett.*, 1999, doi: 10.1364/ol.24.000382.

[37] A. Berrou, C. Kieleck, and M. Eichhorn, “Mid-infrared lasing from Ho^3+ in bulk InF_3 glass,” *Opt. Lett.*,

2015, doi: 10.1364/ol.40.001699.

[38] L. Wetenkamp, G. F. West, and H. Többen, “Optical properties of rare earth-doped ZBLAN glasses,” *J. Non. Cryst. Solids*, 1992, doi: 10.1016/S0022-3093(05)80737-9.

[39] Jackson.S.D, “Singly Ho-doped fluoride fibre laser operating at 2.92 μm,” *Electron. Lett.*, vol. 40, 2004.

[40] S. D. J. Yuen H Tsang, Atalla E El-Taher, Terence A King, “Efficient 2.96 microm dysprosium-doped fluoride fibre laser pumped with a Nd:YAG laser operating at 1.3 microm,” *Opt. Express*, vol. 14, 2006.

[41] and D. J. O. Ori Henderson-Sapir, Jesper Munch, “Mid-infrared fiber lasers at and beyond 3.5 μm using dual-wavelength pumping,” *Opt. Lett.*, vol. 39, 2014.

[42] H. Többen, “CW Lasing at 3.45 μm in Er3+doped Fluorozirconate Fibres,” *Frequenz*, 1991, doi: 10.1515/FREQ.1991.45.9-10.250.

[43] J. Schneider, “<title>Properties of a fluoride fiber laser operating at 3.9 um</title>,” 1996, doi: 10.1117/12.258976.

[44] S. D. Jackson, “Towards high-power mid-infrared emission from a fibre laser,” *Nature Photonics*. 2012, doi: 10.1038/nphoton.2012.149.

[45] Hong-Yu LuoYong-Zhi Wang, “Linearly polarized polarization-maintaining Er3þ-dopedfluoridefiber laser in the mid-infrared,” *J. Electron. Sci. Technol.*, vol. 20, 2021.

[46] C. Xia *et al.*, “Mid-infrared supercontinuum generation to 45 μm in ZBLAN fluoride fibers by nanosecond diode pumping,” *Opt. Lett.*, 2006, doi: 10.1364/ol.31.002553.

[47] M. Liao, X. Yan, G. Qin, C. Chaudhari, T. Suzuki, and Y. Ohishi, “A highly non-linear tellurite microstructure fiber with multi-ring holes for supercontinuum generation,” *Opt. Express*, 2009, doi: 10.1364/oe.17.015481.

[48] S. D. Le *et al.*, “Efficient four-wave mixing in a ultra-highly nonlinear suspended-core chalcogenide fiber,” 2011.

[49] T. M. Monro and H. Ebendorff-Heidepriem, “Progress in microstructured optical fibers,” *Annual Review of Materials Research*. 2006, doi: 10.1146/annurev.matsci.36.111904.135316.

[50] V. Artyushenko, A. Bocharnikov, T. Sakharova, and I. Usenov, “Mid-infrared Fiber Optics for 1 - 18 μm Range,” *Opt. Photonik*, 2014, doi: 10.1002/opph.201400062.

[51] J. Lucas, “Infrared glasses,” *Curr. Opin. Solid State Mater. Sci.*, 1999, doi: 10.1016/S1359-0286(99)00007-8.

[52] V. A. Kamynin *et al.*, “Tm3+-doped tellurite fiber weak signal amplifier at a wavelength of 2.27 μm,” *Results Phys.*, 2021, doi: 10.1016/j.rinp.2021.104512.

[53] E. A. Anashkina, “Laser sources based on rare-earth ion doped tellurite glass fibers and microspheres,” *Fibers*. 2020, doi: 10.3390/FIB8050030.

[54] D. C. Sordillo, L. A. Sordillo, P. P. Sordillo, and R. R. Alfano, “Fourth near-infrared optical window for assessment of bone and other tissues,” 2016, doi: 10.1117/12.2214320.

[55] J. Ma, Z. Qin, G. Xie, L. Qian, and D. Tang, “Review of mid-infrared mode-locked laser sources in the 2.0 μ m-3.5 μ m spectral region,” *Applied Physics Reviews*. 2019, doi: 10.1063/1.5037274.

[56] J. S. Wang, E. M. Vogel, and E. Snitzer, “Tellurite glass: a new candidate for fiber devices,” *Opt. Mater. (Amst).*, 1994, doi: 10.1016/0925-3467(94)90004-3.

[57] 2015. www.npphotonics.com, retrieved April 1, “No Title.” .

[58] R. Stegeman *et al.*, “Tellurite glasses with peak absolute Raman gain coefficients up to 30 times that of fused silica,” *Opt. Lett.*, 2003, doi: 10.1364/ol.28.001126.

[59] O. Mori A, Shikano K, Enbutsu K and N. K. K, “1.5μm band zero-dispersion shifted tellurite photonic crystal fibre with a nonlinear coefficient γ of 675 W−1km−1,” *Proc. ECOC*, 2004.

[60] A. Y. Z. Yu Zhang, Lizhang Xia, Jiale Ding, Chengyan Li, Xinjie Shen, Jun Li, “2.7 μm band enhancement induced by energy transfer in Er3+/Tm3+ co-doped tellurite glass,” *J. Opt. Soc. Am. B*, vol. 38, 2021.

[61] R. El-Mallawany, *Tellurite Glasses Handbook: physical properties and data*. CRC Press, 2002.

[62] K. Vu, S. Farahani, and S. Madden, “980nm pumped erbium doped tellurium oxide planar rib waveguide laser and amplifier with gain in S, C and L band,” *Opt. Express*, 2015, doi: 10.1364/oe.23.000747.

[63] B. D. O. Richards and A. Jha, “Lasers utilising tellurite glass-based gain media,” *Springer Ser. Mater. Sci.*, 2017, doi: 10.1007/978-3-319-53038-3_6.

[64] and C. P. C. Chryssou, F. Di Pasquale, “Er3+ doped channel waveguide amplifiers for WDM systems: A comparison of tellurite, alumina and Al/P silicate materials,” *IEEE J. Sel. Top. Quantum Electron*, vol. 6, no. 114–121, 2000.

[65] S. Dai, C. Yu, G. Zhou, J. Zhang, G. Wang, and L. Hu, “Concentration quenching in erbium-doped tellurite glasses,” *J. Lumin.*, 2006, doi: 10.1016/j.jlumin.2005.04.003.

[66] S. Shen *et al.*, “Tellurite glasses for broadband amplifiers and integrated optics,” *J. Am. Ceram. Soc.*, 2002, doi: 10.1111/j.1151-2916.2002.tb00286.x.

[67] A. Mori, “Tellurite-based fibers and their applications to optical communication networks,” *Journal of the Ceramic Society of Japan*. 2008, doi: 10.2109/jcersj2.116.1040.

[68] Y. Hu *et al.*, “Numerical analyses of the population dynamics and determination of the upconversion coefficients in a new high erbium-doped tellurite glass,” *J. Opt. Soc. Am. B*, 2001, doi: 10.1364/josab.18.001928.

[69] S. M. Khu Vu, “Tellurium dioxide Erbium doped planar rib waveguide amplifiers with net gain and 2.8dB/cm internal gain,” *Opt. Express*, vol. 18, p. 18, 2010.

[70] S. J. Madden and K. T. Vu, “Very low loss reactively ion etched Tellurium Dioxide planar rib waveguides for linear and non-linear optics,” *Opt. Express*, 2009, doi: 10.1364/oe.17.017645.

[71] H. C. Frankis *et al.*, “ Low-loss TeO 2 -coated Si 3 N 4 waveguides for application in photonic integrated circuits ,” *Opt. Express*, 2019, doi: 10.1364/oe.27.012529.

[72] I. Savelli *et al.*, “Mid-infrared 2000-nm bandwidth supercontinuum generation in suspended-core microstructured Sulfide and Tellurite optical fibers,” *Opt. Express*, 2012, doi: 10.1364/oe.20.027083.

[73] D. Lezal, “Chalcogenide glasses - Survey and progress,” *J. Optoelectron. Adv. Mater.*, 2003.

[74] A. R. M.D Sario, G Leggeire, A Luches, M Martino, “Pulsed Laser Deposition of Presedymium doped chalcogenide thin films,” *Appl. Surf. Sci.*, vol. 186, 2002.

[75] N. Abdellaoui *et al.*, “ Tb 3+ doped Ga 5 Ge 20 Sb 10 Se 65-x Te x (x = 0-375) chalcogenide glasses and fibers for MWIR and LWIR emissions ,” *Opt. Mater. Express*, 2018, doi: 10.1364/ome.8.002887.

[76] Shixun Dai, “A Review of Mid-Infrared Supercontinuum Generation in Chalcogenide Glass Fibers,” *Appl. Sci.*, 2018.

[77] H. Lin *et al.*, “Planar chalcogenide glass mid-infrared photonics,” 2014, doi: 10.1117/12.2035688.

[78] M. R. Lamont, B. Luther-Davies, D.-Y. Choi, S. Madden, and B. J. Eggleton, “Supercontinuum generation in dispersion engineered highly nonlinear (γ = 10 /W/m) As_2S_3 chalcogenide planar waveguide,” *Opt. Express*, 2008, doi: 10.1364/oe.16.014938.

[79] T. Negami, “Cu(In,Ga)Se2 thin film solar cells with an efficiency of 18%,” *Sol. Energy Mater. Sol. Cells*, vol. 67, pp. 331–335, 2001.

[80] M. Bayindir *et al.*, “Metal-insulator-semiconductor optoelectronic fibres,” *Nature*, 2004, doi: 10.1038/nature02937.

[81] A. V. Legin, Y. G. Vlasov, A. M. Rudnitskaya, and E. A. Bychkov, “Cross-sensitivity of chalcogenide glass sensors in solutions of heavy metal ions,” *Sensors Actuators, B Chem.*, 1996, doi: 10.1016/S0925-4005(96)01852-7.

[82] B. Gleason, K. Richardson, L. Sisken, and C. Smith, “Refractive Index and Thermo-Optic Coefficients of Ge-As-Se Chalcogenide Glasses,” *Int. J. Appl. Glas. Sci.*, 2016, doi: 10.1111/ijag.12190.

[83] T. Toyoda and M. Yabe, “The temperature dependence of the refractive indices of fused silica and crystal quartz,” *J. Phys. D. Appl. Phys.*, 1983, doi: 10.1088/0022-3727/16/5/002.

[84] “I. H. Malitson, JOSA, Vol. 55, Issue 10, pp. 1205-1208 (1965).”

[85] M. Daimon and A. Masumura, “High-accuracy measurements of the refractive index and its temperature coefficient of calcium fluoride in a wide wavelength range from 138 to 2326 nm,” *Appl. Opt.*, 2002, doi: 10.1364/ao.41.005275.

[86] H. Li *et al.*, “Thermal sensitivity of tellurite and germanate optical fibers,” *Opt. Express*, 2007, doi: 10.1364/oe.15.008857.

[87] A. K. SINGH, “A SHORT OVER VIEW ON ADVANTAGE OF CHALCOGENIDE GLASSY ALLOYS,” *J. Non-Oxide Glas.*, 2012.

[88] M. Dejneka and B. Samson, “Rare-earth-doped fibers for telecommunications applications,” *MRS Bull.*, 1999, doi: 10.1557/S0883769400053057.

[89] L. Huang, S. Shen, and A. Jha, “Near infrared spectroscopic investigation of Tm3+-Yb 3+ co-doped tellurite glasses,” 2004, doi: 10.1016/j.jnoncrysol.2004.08.042.

[90] and A. J. Billy Richards, Yuen Tsang, David Binks, Joris Lousteau, “Efficient 2 um Tm3+-doped tellurite fiber laser,” *Opt. Lett.*, vol. 33, 2008.

[91] S. Tokita, M. Murakami, S. Shimizu, M. Hashida, and S. Sakabe, “Liquid-cooled 24 W mid-infrared Er:ZBLAN fiber laser,” *Opt. Lett.*, 2009, doi: 10.1364/ol.34.003062.

[92] L. Mescia, F. Smektala, and F. Prudenzano, “New trends in amplifiers and sources via chalcogenide photonic crystal fibers,” *International Journal of Optics*. 2012, doi: 10.1155/2012/575818.

[93] S. Balaji, G. Gupta, K. Biswas, D. Ghosh, and K. Annapurna, “Role of Yb3+ ions on enhanced ∼2.9 μm emission from Ho3+ ions in low phonon oxide glass system,” *Sci. Rep.*, 2016, doi: 10.1038/srep29203.

[94] T. W. Allen *et al.*, “Photoluminescence measurements of Er-doped chalcogenide glasses,” *J. Vac. Sci. Technol. A Vacuum, Surfaces, Film.*, 2004, doi: 10.1116/1.1648673.

[95] K. Koughia *et al.*, “Photoluminescence in Er-doped Ge-Ga-Se glasses,” 2005, doi: 10.1016/j.jlumin.2004.09.002.

[96] L. B. Shaw, B. Cole, P. A. Thielen, J. S. Sanghera, and I. D. Aggarwal, “Mid-wave IR and long-wave IR

laser potential of rare-earth doped chalcogenide glass fiber," *IEEE J. Quantum Electron.*, 2001, doi: 10.1109/3.945317.

[97] S. Tanabe, "Rare-earth-doped glasses for fiber amplifiers in broadband telecommunication," *Comptes Rendus Chimie*. 2002, doi: 10.1016/S1631-0748(02)01449-2.

[98] K. A. Shingo Kawai, Hiroji Masuda, Ken-lchi Suzuki, "Ultrawide, 75nm 3-dB galn-band optical amplifier utilizing erbium-doped fluoride fiber and Raman fiber," *Opt. Fiber Commun.*, 1998.

[99] R. M. Percival and J. R. Williams, "Highly Efficient 1.064 um UpconversionPumped 1.47 um Thulium Doped Fluoride Fiber Amplifier," *Electron. Lett.*, vol. 30, 1994.

[100] J. I. Mackenzie, G. S. Murugan, T. Suzuki, Y. Ohishi, A. W. Yu, and J. B. Abshire, "Er-doped Tellurite glasses for planar waveguide power amplifier with extended gain bandwidth," 2012, doi: 10.1117/12.908003.

[101] K. Vu and S. Madden, "2.8dB/cm Internal gain Tellurium dioxide Erbium waveguide amplifiers," 2010, doi: 10.1109/acoft.2010.5929957.

[102] S. Fu *et al.*, "L-band wavelength-tunable fiber laser based on Er3+-doped tellurite fiber," 2020, doi: 10.1364/CLEO_SI.2020.STh1P.4.

[103] K. Kwarkye *et al.*, "Influence of pulse duration and repetition rate on mid-infrared cascaded supercontinuum," *Opt. Lett.*, 2020, doi: 10.1364/ol.401274.

[104] T. S. Saini and and V. R. S. Shilpi Arora, "Far-detuned mid-IR wavelength conversion at 4.05 μm in a tellurium oxide rib waveguide pumped at 1550 nm: Design and analysis," *AIP Adv.*, vol. 11, 2021.

[105] T. Schweizer, D. Brady, and D. W. Hewak, "Fabrication and spectroscopy of erbium doped gallium lanthanum sulphide glass fibres for mid-infrared laser applications," *Opt. Express*, 1997, doi: 10.1364/oe.1.000102.

[106] J. S. Sanghera and I. D. Aggarwal, "Active and passive chalcogenide glass optical fibers for IR applications: A review," *J. Non. Cryst. Solids*, 1999, doi: 10.1016/S0022-3093(99)00484-6.

[107] Eli Margalith, "The OPO goes from concept to commercial tool," *Laser Focus World*, 2000.

[108] H. P. T. Nguyen *et al.*, "Supercontinuum generation in a chalcogenide all-solid hybrid microstructured optical fiber," *Opt. Express*, 2020, doi: 10.1364/oe.394968.

[109] J. Bowman, S R; Shaw, L B; Feldman, B J ; Ganem, "A 7-{micro}m praseodymium-based solid-state laser," *IEEE J. Quantum Electron.*, 1996.

[110] A. B. Seddon *et al.*, "Mid-infrared sources, based on chalcogenide glass fibres, for biomedical diagnostics," 2021, doi: 10.1117/12.2593181.

[111] M. R. Majewski, R. I. Woodward, and S. D. Jackson, "Dysprosium Mid-Infrared Lasers: Current Status and Future Prospects," *Laser and Photonics Reviews*. 2020, doi: 10.1002/lpor.201900195.

[112] D. Xia *et al.*, "On-Chip Broadband Mid-Infrared Supercontinuum Generation Based on Highly Nonlinear Chalcogenide Glass Waveguides," *Front. Phys.*, 2021.

[113] T. Schweizer, D. W. Hewak, D. M. Payne, T. Jensen, and G. Huber, "Rare-earth doped chalcogenide glass laser," *Electron. Lett.*, 1996, doi: 10.1049/el:19960430.

[114] J. S. Sanghera *et al.*, "Development and infrared applications of chalcogenide glass optical fibers," *Fiber Integr. Opt.*, 2000, doi: 10.1080/01468030050058811.

[115] D. W. Hewak *et al.*, "Gallium lanthanum sulphide optical fibre for active and passive applications,"

Electron. Lett., 1996, doi: 10.1049/el:19960199.

[116] H. T. K. Itoh*, H. Yanagita, H. Tawarayama, K. Yamanaka, E. Ishikawa, K. Okada,H. Aoki, Y. Matsumoto, A. Shirakawa, Y. Matsuoka, "Pr3+ doped InF3/GaF3 based fluoride glass fibers and Ga–Na–S glass fibers for light amplification around 1.3 μm," *J. Non. Cryst. Solids*, vol. 256–257, pp. 1–5, 1999.

[117] D. P. S. A. K. Mairaj, C. Riziotis, A. M. Chardon, P. G. R. Smith and and D. W. Hewak, "Nd doped GLS glass laser imprinted channel waveguide," *Appl. Phys. Lett.*, vol. 81, p. 3708, 2002.

[118] S. J. Madden *et al.*, "Long, low loss etched As_2S_3 chalcogenide waveguides for all-optical signal regeneration," *Opt. Express*, 2007, doi: 10.1364/oe.15.014414.

[119] L. Zhang, A. M. Agarwal, L. C. Kimerling, and J. Michel, "Nonlinear Group IV photonics based on silicon and germanium: From near-infrared to mid-infrared," *Nanophotonics*. 2014, doi: 10.1515/nanoph-2013-0020.

[120] K. Yan, K. Vu, and S. Madden, "Internal gain in Er-doped As_2S_3 chalcogenide planar waveguides," *Opt. Lett.*, 2015, doi: 10.1364/ol.40.000796.

[121] M. Y. Gen and Y. I. Petrov, "Disperse Condensates of Metal Vapour," *Russ. Chem. Rev.*, 1969, doi: 10.1070/rc1969v038n12abeh001889.

[122] A. Wucher, "Sputtering: Experiment (Det Kongelige Danske Videnskabernes Selskab, Copenhagen," 2006.

[123] J. Zavadil, D. Lezal, and O. Prochazkova, "Optical characterization of glass materials doped with rare-earth elements," 1999, doi: 10.1117/12.373676.

[124] C. G. and C. M. Camille-Sophie Brès ORCID logo EMAIL logo , Alberto Della Torre ORCID logo , Davide Grassani , Victor Brasch, "Supercontinuum in integrated photonics: generation, applications, challenges, and perspectives," *Nanophotonics*, 2023.

[125] and J. S. S. R. R. Gattass, L. B. Shaw, V. Q. Nguyen, P. C. Pureza, I. D. Aggarwal, "All-fiber chalcogenide-based mid-infrared supercontinuum source," *Opt. Fiber Technol*, 2012.

[126] A. Y. O. HOA PHUOC TRUNG NGUYEN,* KENSHIRO NAGASAKA, TONG HOANG TUAN, THAN SINGH SAINI, XING LUO, TAKENOBU SUZUKI, "Highly coherent supercontinuum in the mid-infrared region with cascaded tellurite and chalcogenide fibers," *Appl. Opt.*, 2018.

[127] M. Klimczak, B. Siwicki, A. Heidt, and R. Buczyński, "Coherent supercontinuum generation in soft glass photonic crystal fibers," *Photonics Res.*, 2017, doi: 10.1364/prj.5.000710.

[128] "G. J. McCarthy and J. J. Rhyne編: The Rare Earths in Modern Science and Technology; Proceedings of the 13th Rare Earth Research Conference, West Virginia, 1977, Plenum Press, New York and London, 1978, xv+629ページ, 25.5×17.5cm, 16,630円.," *Butsuri*, 1980, doi: 10.11316/butsuri1946.35.9.793.

[129] P. Bastock, C. Craig, K. Khan, E. Weatherby, J. Yao, and D. W. Hewak, "Properties of gallium lanthanum sulphide glass," 2015, doi: 10.1364/CLEO_SI.2015.STh1G.1.

[130] X. Y. Qin Xu and M. Z. and RongpingWang, "The ability of Gex Ga4 S96-x chalcogenide glasses dissolving rare earth probed by x-ray photoelectron spectra analysis," *Mater. Res. Express*, vol. 6, 2019.

[131] K. Koughia, M. Munzar, T. Aoki, and S. O. Kasap, "Photoluminescence spectra and lifetimes of 4I 13/2 → 4I 15/2 and 4I 11/2 → 4I 15/2 transitions in erbium doped GeGase and GeGas glasses," 2007, doi: 10.1007/s10854-007-9189-5.

[132] M. Rezvani, A. Yousefi Dizaj, A. Rahimian, and T. Joudi, "The effect of Er on optical and mechanical properties of As2S3 glasses quenched in different media," *Eur. Phys. J. Plus*, 2020, doi: 10.1140/epjp/s13360-020-00502-9.

[133] C. C. Ye, D. W. Hewak, M. Hempstead, B. N. Samson, and D. N. Payne, “Spectral properties of Er3+-doped gallium lanthanum sulphide glass,” *J. Non. Cryst. Solids*, 1996, doi: 10.1016/S0022-3093(96)00203-7.

[134] B. R. Judd, “Optical absorption intensities of rare-earth ions,” *Phys. Rev.*, 1962, doi: 10.1103/PhysRev.127.750.

[135] W. J. Miniscalco, “Erbium-Doped Glasses for Fiber Amplifiers at 1500 nm,” *J. Light. Technol.*, 1991, doi: 10.1109/50.65882.

[136] L. B. Shaw, D. Schaafsma, J. Moon, B. Harbison, J. Sanghera, and I. Aggarwal, “Evaluation of the IR transitions in rare-earth-doped chalcogenide glasses,” 1997, doi: 10.1109/cleo.1997.603102.

[137] D. F. and A. B. S. S.P. Morgan, “Effect ofGlass Purity on the Glass Stability and Physical Properties of Ga-La-S Glasses,” *Proc. 0f101h mt. Symp. Nonoxide Glas.*, 1996.

[138] S. Kasap, K. Koughia, G. Soundararajan, and M. G. Brik, “Optical and photoluminescence properties of erbium-doped chalcogenide glasses (GeGaS:Er),” *IEEE J. Sel. Top. Quantum Electron.*, 2008, doi: 10.1109/JSTQE.2008.921415.

[139] J. N. Munzar, M.; Koughia, K.; Tonchev, D.; Kasap, S. O.; Sakai, T.; Maeda, K.; Ikari, T.; Haugen, C.; Decorby, R.; McMullin, “Influence of Ga on the optical and thermal properties of Er2S3 doped stoichiometric and nonstoichiometric Ge–Ga–Se glasses,” *Soc. Glas. Technnology*, vol. 46, 2005.

[140] Y. Ohishi, *Rare-earth ions in glasses and transitions for optical amplification,” in Optical Fiber Amplifiers: Materials, Devices, and Applications*. 1997.

[141] A. Hrubý, “Evaluation of glass-forming tendency by means of DTA,” *Czechoslov. J. Phys.*, 1972, doi: 10.1007/BF01690134.

[142] D. Furniss and A. B. Seddon, “Thermal Analysis of Inorganic Compound Glasses and Glass-Ceramics,” in *Principles and Applications of Thermal Analysis*, 2008.

[143] J. D. Shephard, R. I. Kangley, R. J. Hand, D. Furniss, and A. B. Seddon, “Analysis of oxide content in gallium lanthanum sulphide (GLS) glasses by infrared absorption spectroscopy,” *Phys. Chem. Glas.*, 2003.

[144] Q. Jiao *et al.*, “Effect of gallium environment on infrared emission in Er3+-doped gallium-antimony-sulfur glasses,” *Sci. Rep.*, 2017, doi: 10.1038/srep41168.

[145] N. & S. Kolimiets, B., Goryunova, “Glassy State in Chalcogenides,” *Publ. House USSR Acad. Sci. Petersbg.*, vol. 450–460, 1960.

[146] T. H. Lee, S. I. Simdyankin, J. Hegedus, J. Heo, and S. R. Elliott, “Spatial distribution of rare-earth ions and GaS4 tetrahedra in chalcogenide glasses studied via laser spectroscopy and ab initio molecular dynamics simulation,” *Phys. Rev. B - Condens. Matter Mater. Phys.*, 2010, doi: 10.1103/PhysRevB.81.104204.

[147] S. D. Pangavhane, P. Němec, V. Nazabal, A. Moreac, P. Jõvári, and J. Havel, “Laser desorption ionization time-of-flight mass spectrometry of erbium-doped Ga-Ge-Sb-S glasses,” *Rapid Commun. Mass Spectrom.*, 2014, doi: 10.1002/rcm.6896.

[148] B. G. Aitken, C. W. Ponader, and R. S. Quimby, “Clustering of rare earths in GeAs sulfide glass,” *Comptes Rendus Chim.*, 2002, doi: 10.1016/S1631-0748(02)01458-3.

[149] Y. Chen *et al.*, “High content Er3+-doped 25La2O3-75Ga2O3 glass: A potential material for high-power lasers or EDWA,” *J. Alloys Compd.*, 2020, doi: 10.1016/j.jallcom.2020.155477.

[150] L. Gomes *et al.*, “Energy level decay and excited state absorption processes in erbium-doped tellurite glass,” *J. Appl. Phys.*, 2011, doi: 10.1063/1.3651399.

[151] K. Yoshimoto, Y. Ezura, M. Ueda, A. Masuno, and H. Inoue, “2.7 μm Mid-Infrared Emission in Highly Erbium-Doped Lanthanum Gallate Glasses Prepared Via an Aerodynamic Levitation Technique,” *Adv. Opt. Mater.*, 2018, doi: 10.1002/adom.201701283.

[152] C. Koughia, C. Craig, D. W. HEWAKa, and S. Kasap, “Further studies of radiation trapping in Er3þ doped chalcogenide glasses,” *Opt. Mater. (Amst).*, vol. 87, 2019.

[153] S. Ramachandran and S. G. Bishop, “Excitation of Er emission by host glass absorption in sputtered films of Er-doped Ge10As40Se25S25 glass,” *Appl. Phys. Lett.*, vol. 73, 1998.

[154] K. A. Cerqua-Richardson, J. M. McKinley, B. Lawrence, S. Joshi, and A. Villeneuve, “Comparison of nonlinear optical properties of sulfide glasses in bulk and thin film form,” *Opt. Mater. (Amst).*, 1998, doi: 10.1016/S0925-3467(97)00142-0.

[155] J. FickE.J. KnystautasA. VilleneuveF. SchiettekatteS. RoordaK.A. Richardson, “High photoluminescence in erbium-doped chalcogenide thinÆlms,” *J. Non. Cryst. Solids*, vol. 272, 2000.

[156] C. Meneghini and A. Villeneuve, “As_2S_3 photosensitivity by two-photon absorption: holographic gratings and self-written channel waveguides,” *J. Opt. Soc. Am. B*, 1998, doi: 10.1364/josab.15.002946.

[157] A. Polman, “Erbium implanted thin film photonic materials,” *J. Appl. Phys.*, 1997, doi: 10.1063/1.366265.

[158] W. J. Miniscalco and R. S. Quimby, “General procedure for the analysis of Er^3+ cross sections,” *Opt. Lett.*, 1991, doi: 10.1364/ol.16.000258.

[159] J. S. E Desurvire, “Evaluation of 4I15/2 and 4I13/2 Stark-level energies in erbium-doped aluminosilicate glass fibers,” *Opt. Lett.*, 1990.

[160] A. Fuchs, J. Fick, V. Balan, C. Vigreux, and A. Pradel, “Photoluminescence and waveguiding in sputtered films of Er-doped chalcogenide glasses,” 2004, doi: 10.1117/12.545740.

[161] J. A. Frantz, J. S. Sanghera, L. B. Shaw, G. Villalobos, I. D. Aggarwal, and D. W. Hewak, “Sputtered films of Er3+-doped gallium lanthanum sulfide glass,” *Mater. Lett.*, 2006, doi: 10.1016/j.matlet.2005.11.028.

[162] K. Yan, R. Wang, K. Vu, R. Elliman, K. Belay, and B. Luther-Davies, “Photoluminescence in er-doped Ge-As-Se chalcogenide thin films,” 2011, doi: 10.1364/ome.2.001270.

[163] and B. L.-D. R. P. Wang, D. Bulla, A. Smith, T. Wang, “Structure and physical properties of GexAsySe1-x-y glasses with the same mean coordination number of 2.5,” *Appl. Phys.*, vol. 109, 2011.

[164] and B. L.-D. A. Prasad, C. J. Zha, R. P. Wang, A. Smith, S. Madden, “Properties of GexAsySe1-x-y glasses for all-optical signal processing,” *Opt. Express*, vol. 16, 2008.

[165] and S. O. K. Z. G. Ivanova, K. Koughia, D. Tonchev, J. C. Pivin, “Photoluminescence in Er-implanted amorphous Ge-S-Ga thin films,” *J. Optoelectron. Adv. Mater.*, vol. 7, pp. 1271–1276, 2005.

[166] J. A. Frantz, L. B. Shaw, J. D. Myers, K. J. Ewing, and J. S. Sanghera, “Mid-IR emission in erbium-doped gallium lanthanum sulfide glass integrated optic waveguides,” 2014, doi: 10.1109/SUM.2014.36.

[167] V. Nazabal *et al.*, “Luminescence at 2.8 μm: Er3+-doped chalcogenide micro-waveguide,” *Opt. Mater. (Amst).*, 2016, doi: 10.1016/j.optmat.2016.06.009.

[168] S. Normani, J. , Geofrey Louvet, Emeline Baudet, Marek Bouška, F. Starecki, Y. L. , Jean-Louis Doualan4, Y. Messaddeq, and P. N. & V. N. Jean-LucAdam, “Comparative study of Er3+-doped Ga-Ge-Sb-S thin flms fabricated by sputtering and pulsed laser deposition,” *Sci. Rep.*, vol. 10, 2020.

[169] V. Moizan *et al.*, “Er3+-doped GeGaSbS glasses for mid-IR fibre laser application: Synthesis and rare earth spectroscopy,” *Opt. Mater. (Amst).*, 2008, doi: 10.1016/j.optmat.2008.01.005.

[170] W. Ryba-Romanowski, “Effect of temperature and activator concentration on luminescence decay of erbium-doped tellurite glass,” *J. Lumin.*, 1990, doi: 10.1016/0022-2313(90)90036-B.

[171] S. B. R. Reisfeld, “No Title,” vol. 22, p. 123, 1975.

[172] S. Shen, M. Naftaly, and A. Jha, “Tungsten-tellurite - A host glass for broadband EDFA,” *Opt. Commun.*, 2002, doi: 10.1016/S0030-4018(02)01309-3.

[173] in: B. D. B. (Ed. . G.F. Imbush, “Advances inNonradiative Processes in Solids,” *Plenum Press. NewYork*, p. 261, 1991.

[174] S. O. T. Nakai, Y. Noda, T. Tani, Y. Mimura, S. Sudo, “No Title,” *OSA TOPS*, vol. 25, p. 82, 1998.

[175] M. F. R. Rollia,, M. Montagna, S. Chaussedent, A. Monteil, V.K. Tikhomirov, “Erbium-doped tellurite glasses with high quantumefficiency and broadband stimulated emissioncross section at 1.5lm,” *Opt. Mater. (Amst).*, vol. 21, 2003.

[176] H. L. Z. Pan, S.H. Morgan, K. Dyer, A. Ueda, “No Title,” *J. Appl.Phys*, vol. 79, 1996.

[177] “M. Dejneca, B. Samson,” *MRS Bull.*, vol. 24, 1999.

[178] P. R. Ehrmann and J. H. Campbell, “Nonradiative energy losses and radiation trapping in neodymium-doped phosphate laser glasses,” 2002, doi: 10.1111/j.1151-2916.2002.tb00223.x.

[179] Y. Yan, A. J. Faber, and H. de Waal, “Luminescence quenching by OH groups in highly Er-doped phosphate glasses,” *J. Non. Cryst. Solids*, 1995, doi: 10.1016/S0022-3093(94)00528-1.

[180] M. Arnaduov, “No Title,” *Phys. Chem. Glas.*, vol. 127, p. 48, 1986.

[181] T. A. A. de A. and L. K. Cacho, V. D. Del, Davinson Mariano da Silva, “Fabrication of Yb3+/Er3+ codoped Bi2O3–WO3–TeO2 pedestal type waveguide for optical amplifiers,” *Opt. Mater. (Amst).*, 2014.

[182] S. E. Motorin, V. V. Dorofeev, B. I. Galagan, S. E. Sverchkov, V. V. Koltashev, and B. I. Denker, “Study of absorption and IR-emission of Er3+, Dy3+, Tm3+ doped high-purity tellurite glasses,” 2018, doi: 10.1088/1757-899X/347/1/012038.

[183] J. Huang, L. Zhang, L. Xia, X. Shen, W. Wei, and W. You, “Highly efficient ~3.4 μm emission of Er3+-doped TeO2 based glasses via resonant energy transfer and multi-phonon relaxation processes,” *Opt. Mater. (Amst).*, 2020, doi: 10.1016/j.optmat.2020.110387.

[184] S. M. Pietralunga *et al.*, “High-contrast waveguides in sputtered pure TeO,_2 glass thin films,” *Opt. Express*, 2008, doi: 10.1364/oe.16.021662.

[185] S. Shen, B. Richards, and A. Jha, “ Enhancement in pump inversion efficiency at 980 nm in Er 3+ , Er 3+ /Eu 3+ + and Er 3+ /Ce 3+ doped tellurite glass fibers ,” *Opt. Express*, 2006, doi: 10.1364/oe.14.005050.

[186] M. Lanata, M. Feré, D. Pieeinin, S. M. Pietralunga, and M. Martinelli, “Sputtered tellurite glass thin films for planar optical devices,” 2008, doi: 10.1109/ICTON.2008.4598696.

[187] R. Stępień, R. Buczyński, D. Pysz, and I. Kujawa, “Supercontinuum generation in microstructured tellurite glass fiber,” 2011, doi: 10.1117/12.896284.

[188] R. R. Alfano, *The supercontinuum laser source: The ultimate white light, third edition*. 2016.

[189] P. Wang *et al.*, “Tellurite Glass and Its Application in Lasers,” in *Advanced Functional Materials*, 2020.

[190] J. H. V. Price *et al.*, “Supercontinuum generation in non-silica fibers,” *Opt. Fiber Technol.*, 2012, doi: 10.1016/j.yofte.2012.07.013.

[191] C. Lin and R. H. Stolen, “New nanosecond continuum for excited-state spectroscopy,” *Appl. Phys. Lett.*,

1976, doi: 10.1063/1.88702.

[192] A. B. Seddon, “Mid-infrared (IR) - A hot topic: The potential for using mid-IR light for non-invasive early detection of skin cancer in vivo,” *Phys. Status Solidi Basic Res.*, 2013, doi: 10.1002/pssb.201248524.

[193] A. Mukherjee, S. Von Der Porten, and C. K. N. Patel, “Standoff detection of explosive substances at distances of up to 150m,” *Appl. Opt.*, 2010, doi: 10.1364/AO.49.002072.

[194] S. Dupont, C. Petersen, J. Thøgersen, C. Agger, O. Bang, and S. R. Keiding, “IR microscopy utilizing intense supercontinuum light source,” *Opt. Express*, 2012, doi: 10.1364/oe.20.004887.

[195] Upendra N. Singh; Gelsomina Pappalardo, “Lidar Technologies, Techniques, and Measurements for Atmospheric Remote Sensing VII,” *SPIE*, vol. 8182, 2011.

[196] https://www.nktphotonics.com/, “SC Commercially.”

[197] Jacek Swiderski, “High-power mid-infrared supercontinuumsources: Current status and future perspectives,” *Prog. Quantum Electron.*, vol. 38, 2014.

[198] D. Jain and O. Bang, “High power mid-infrared fiber based supercontinuum sources: Current status and future perspectives,” 2018, doi: 10.1364/cleopr.2018.th3d.5.

[199] P. M. Moselund, C. Petersen, L. Leick, J. S. Dam, P. Tidemand-Lichtenberg, and C. Pedersen, “Highly stable, all-fiber, high power ZBLAN supercontinuum source reaching 4.75 μm used for nanosecond mid-IR spectroscopy,” 2013, doi: 10.1364/assl.2013.jth5a.9.

[200] J.-C. Gauthier *et al.*, “Mid-IR supercontinuum from 24 to 54 μm in a low-loss fluoroindate fiber,” *Opt. Lett.*, 2016, doi: 10.1364/ol.41.001756.

[201] T. Cheng *et al.*, “Mid-infrared supercontinuum generation spanning 20 to 151 μm in a chalcogenide step-index fiber,” *Opt. Lett.*, 2016, doi: 10.1364/ol.41.002117.

[202] C. R. Petersen *et al.*, “Increased mid-infrared supercontinuum bandwidth and average power by tapering large-mode-area chalcogenide photonic crystal fibers,” *Opt. Express*, 2017, doi: 10.1364/oe.25.015336.

[203] J. Haas and B. Mizaikoff, “Advances in Mid-Infrared Spectroscopy for Chemical Analysis,” *Annual Review of Analytical Chemistry*. 2016, doi: 10.1146/annurev-anchem-071015-041507.

[204] X. Feng, P. Horak, and F. Poletti, “Tellurite glass fibers for mid-infrared nonlinear applications,” *Springer Ser. Mater. Sci.*, 2017, doi: 10.1007/978-3-319-53038-3_9.

[205] T. Cheng, L. Zhang, X. Xue, D. Deng, T. Suzuki, and Y. Ohishi, “Broadband cascaded four-wave mixing and supercontinuum generation in a tellurite microstructured optical fiber pumped at 2 μm,” *Opt. Express*, 2015, doi: 10.1364/oe.23.004125.

[206] P. Domachuk *et al.*, “Over 4000 nm bandwidth of mid-IR supercontinuum generation in sub-centimeter segments of highly nonlinear tellurite PCFs,” *Opt. Express*, 2008, doi: 10.1364/oe.16.007161.

[207] S. Kedenburg *et al.*, “High repetition rate mid-infrared supercontinuum generation from 13 to 53 μm in robust step-index tellurite fibers,” *J. Opt. Soc. Am. B*, 2017, doi: 10.1364/josab.34.000601.

[208] I. Savelii *et al.*, “Suspended core tellurite glass optical fibers for infrared supercontinuum generation,” *Opt. Mater. (Amst).*, 2011, doi: 10.1016/j.optmat.2011.05.010.

[209] K. Richardson, D. Krol, and K. Hirao, “Glasses for Photonic Applications,” *Int. J. Appl. Glas. Sci.*, 2010, doi: 10.1111/j.2041-1294.2010.00008.x.

[210] B. I. Denker *et al.*, “Rare-earth ions doped zinc-tellurite glass for 2 ÷ 3 μm lasers,” *Appl. Phys. B Lasers Opt.*, 2018, doi: 10.1007/s00340-018-7107-6.

[211] J.S.WangE.M.VogelE.Snitzer, “Telluriteglass:a newcandidateforfiberdevices,” *Opt. Mater. (Amst).*, vol. 3, pp. 187–203, 1994.

[212] B. Burtan *et al.*, “Influence of rare earth ions on the optical properties of tellurite glass,” *Acta Phys. Pol. A*, 2011, doi: 10.12693/APhysPolA.120.579.

[213] P. Klocek and M. Dekker, *Handbook of Infrared Optical Materials*. 1991.

[214] David H. Titterton; Mark A. Richardson; Robert J. Grasso; Harro Ackermann; Willy L. Bohn, “Technologies for Optical Countermeasures X; and High-Power Lasers 2013: Technology and Systems,” *SPIE*, vol. 8898, 2013.

[215] M. Liao, C. Chaudhari, G. Qin, X. Yan, T. Suzuki, and Y. Ohishi, “Tellurite microstructure fibers with small hexagonal core for supercontinuum generation,” *Opt. Express*, 2009, doi: 10.1364/oe.17.012174.

[216] S. J. Madden and K. T. Vu, “High-Performance Integrated Optics with Tellurite Glasses: Status and Prospects,” *Int. J. Appl. Glas. Sci.*, 2012, doi: 10.1111/ijag.12002.

[217] P. Zhou *et al.*, “High-gain erbium silicate waveguide amplifier and a low-threshold, high-efficiency laser,” *Opt. Express*, 2018, doi: 10.1364/oe.26.016689.

[218] Jonathan D. B. Bradley and Markus Pollnau, “Erbium-doped integrated waveguide amplifiers and lasers,” *Laser photonic Rev*, vol. 5, 2011.

[219] K. T. Vu, “Fabrication and characterisation of tellurite planar waveguides,” 2012.

[220] and M. N. A. Jha, S. Shen, “Structural origin of spectral broadening of 1.5-mm emission in Er3-doped tellurite glasses,” *Am. Phys. Soc.*, vol. 62, 2000.

[221] S. Abedrabbo, B. Lahlouh, and A. T. Fiory, “Analytical study of thermal annealing behaviour of erbium emission in Er2O3-sol-gel silica films,” *J. Phys. D. Appl. Phys.*, 2011, doi: 10.1088/0022-3727/44/31/315401.

[222] “https://sci-soft.com/product/filmtek-4000/.” .

[223] F. P. Xian Feng, Peter Horak, “Tellurite glass fibers for mid-infrared nonlinear applications,” *Springer Ser. Mater. Sci.*, pp. 213–239, 2017.

[224] “https://serc.carleton.edu/research_education/geochemsheets/techniques/EPMA.html.” .

[225] K. Vu and S. Madden, “Tellurium dioxide Erbium doped planar rib waveguide amplifiers with net gain and 28dB/cm internal gain,” *Opt. Express*, 2010, doi: 10.1364/oe.18.019192.

[226] S. Brovelli *et al.*, “Efficient 1.53 μm erbium light emission in heavily Er-doped titania-modified aluminium tellurite glasses,” *J. Non. Cryst. Solids*, 2007, doi: 10.1016/j.jnoncrysol.2007.02.052.

[227] and M. N. A. Jha, S. Shen, “Structural origin of spectral broadening of 1.5-um emission in Er3-doped tellurite glasses,” *Am. Phys. Soc.*, vol. 62, p. 6215, 2000.

[228] R. M. M. T. F. M. J. F. M. F. B. Gonzalo, “Er3þ-dopedfluorotellurite thinfilm glasses with improvedphotoluminescence emission at 1.53mm,” *J. Lumin.*, vol. 170, pp. 778–784, 2016.

[229] N. Sathish *et al.*, “Effects of concentration and thermal annealing on the optical activation of Er implanted into GaN layers,” 2012, doi: 10.1080/10420150.2012.686111.

[230] M. Fukushima, N. Managaki, M. Fujii, H. Yanagi, and S. Hayashi, “Enhancement of 1.54-μm emission from Er-doped sol-gel SiO 2 films by Au nanoparticles doping,” *J. Appl. Phys.*, 2005, doi: 10.1063/1.1990257.

[231] H.-W. Pan *et al.*, “Thickness-dependent crystallization on thermal anneal for titania/silica nm-layer

composites deposited by ion beam sputter method," *Opt. Express*, 2014, doi: 10.1364/oe.22.029847.

[232] R. Morea. MiguelT.T. Fernandez. MatéF.J. FerrerC. MaffiotteJ. FernandezR. BaldaJ. Gonzalo, "Er3þ-dopedfluorotellurite thinfilm glasses with improvedphotoluminescence emission at 1.53mm," *J. Lumin.*, vol. 170, 2016.

[233] I. Jlassi, H. Elhouichet, and M. Ferid, "Thermal and optical properties of tellurite glasses doped erbium," *J. Mater. Sci.*, 2011, doi: 10.1007/s10853-010-4820-x.

[234] H. Sun, X. Huang, X. Lian, and G. Wang, "Discrepancies in the microstructures of annealed Cu-Zr bulk alloy and Cu-Zr alloy films," *Materials (Basel).*, 2019, doi: 10.3390/ma12152467.

[235] "Handbook of advanced dielectric, piezoelectric and ferroelectric materials," *Mater. Today*, 2008, doi: 10.1016/s1369-7021(08)70258-x.

[236] Z. Ma, Z. Yu, Y. Yang, and J. Sun, "Crystallization and electroluminescence performance of the Er-doped polycrystalline Gd3Ga5O12 nanofilms fabricated by atomic layer deposition on silicon," *J. Lumin.*, 2022, doi: 10.1016/j.jlumin.2021.118544.

[237] O. Durante *et al.*, "Emergence and evolution of crystallization in tio2 thin films: A structural and morphological study," *Nanomaterials*, 2021, doi: 10.3390/nano11061409.

[238] B. L. Jiang, H. T. Li, M. L. Cai, Q. U. Miao, and B. Yang, "Effect of annealing temperature on crystallization process of Al, Cu, Ni induced Si films," *Jinshu Rechuli/Heat Treat. Met.*, 2010.

[239] G. Reiter, "Unstable Thin Polymer Films: Rupture and Dewetting Processes," *Langmuir*, 1993, doi: 10.1021/la00029a031.

[240] A. Sharma, "Relationship of Thin Film Stability and Morphology to Macroscopic Parameters of Wetting in the Apolar and Polar Systems," *Langmuir*, 1993, doi: 10.1021/la00027a042.

[241] K. Kargupta, A. Sharma, and R. Khanna, "Instability, Dynamics, and Morphology of Thin Slipping Films," *Langmuir*, 2004, doi: 10.1021/la035016s.

[242] F. F. Zhang, W. J. Zhang, J. Yuan, D. D. Chen, Q. Qian, and Q. Y. Zhang, "Enhanced 2.7 μm emission from Er3+ doped oxyfluoride tellurite glasses for a diode-pump mid-infrared laser," *AIP Adv.*, 2014, doi: 10.1063/1.4870581.

[243] F. Chen, T. Wei, X. Jing, Y. Tian, J. Zhang, and S. Xu, "Investigation of mid-infrared emission characteristics and energy transfer dynamics in Er3+ doped oxyfluoride tellurite glass," *Sci. Rep.*, 2015, doi: 10.1038/srep10676.

[244] A. MiguelR. MoreaJ. GonzaloM.A. ArriandiagaJ. FernandezR. Balda, "Near-infrared emission and upconversion in Er3þ-dopedTeO2–ZnO–ZnF2glasses," *J. Lumin.*, vol. 140, 2013.

[245] M. Koide, K. Matusita, and T. Komatsu, "Viscosity of fluoride glasses at glass transition temperature," *J. Non. Cryst. Solids*, 1990, doi: 10.1016/0022-3093(90)90327-I.

[246] B. Neuhaus, T. Schmid, and J. Riedel, "Collection management and study of microscope slides: Storage, profiling, deterioration, restoration procedures, and general recommendations," *Zootaxa*, 2017, doi: 10.11646/zootaxa.4322.1.1.

[247] G. Greeuw and J. F. Verwey, "The mobility of Na+, Li+, and K+ ions in thermally grown SiO2 films," *J. Appl. Phys.*, 1984, doi: 10.1063/1.334256.

[248] M. J. Li; S. Honkanen; W. J. Wang; ... et. al, "Potassium and silver ion-exchanged dual-core glass waveguides with gratings," *Appl. Phys. Lett.*, 1991.

[249] S. Manning, "A study of Tellurite glasse for electro-optic optical fibre devices," 2011.

[250] S. M. Borah, “Direct Current Magnetron Glow Discharge Plasma Characteristics Study for Controlled Deposition of Titanium Nitride Thin Film,” *J. Mater.*, 2013, doi: 10.1155/2013/852859.

[251] L. Agazzi, K. Wörhoff, and M. Pollnau, “Energy-transfer-upconversion models, their applicability and breakdown in the presence of spectroscopically distinct ion classes: A case study in amorphous Al2O3:Er3+,” *J. Phys. Chem. C*, 2013, doi: 10.1021/jp4011839.

[252] A. Anders, “Tutorial: Reactive high power impulse magnetron sputtering (R-HiPIMS),” *J. Appl. Phys.*, 2017, doi: 10.1063/1.4978350.

[253] K. Strijckmans, R. Schelfhout, and D. Depla, “Tutorial: Hysteresis during the reactive magnetron sputtering process,” *J. Appl. Phys.*, 2018, doi: 10.1063/1.5042084.

[254] F. Chen, S.-W. Wang, L. Yu, X. Chen, and W. Lu, “Control of optical properties of TiN_xO_y films and application for high performance solar selective absorbing coatings,” *Opt. Mater. Express*, 2014, doi: 10.1364/ome.4.001833.

[255] B. L.-D. Duk Yong Choi, Steve Madden, Andrei Rode, Rongping Wang, “Advanced processing methods for As2S3 Waveguide Fabrication,” *IEEE*, 2006.

[256] A. Zakery and S. R. Elliott, “Optical properties and applications of chalcogenide glasses: A review,” *Journal of Non-Crystalline Solids*. 2003, doi: 10.1016/j.jnoncrysol.2003.08.064.

[257] Qi Chen, “ARSENIC TRISULFIDE ON LITHIUM NIOBATE WAVEGUIDES FOR NONLINEAR INFRARED OPTICS.”

[258] W. S. Rodney, I. H. Malitson, and T. A. King, “Refractive Index of Arsenic Trisulfide,” *J. Opt. Soc. Am.*, 1958, doi: 10.1364/josa.48.000633.

[259] A. Zakery, “Low loss waveguides in pulsed laser deposited arsenic sulfide chalcogenide films,” *J. Phys. D. Appl. Phys.*, 2002, doi: 10.1088/0022-3727/35/22/304.

[260] M. Asobe, T. Kanamori, K. Naganuma, H. Itoh, and T. Kaino, “Third-order nonlinear spectroscopy in As2S3 chalcogenide glass fibers,” *J. Appl. Phys.*, 1995, doi: 10.1063/1.359256.

[261] Z. Jafari and F. Emami, “Strip/slot hybrid arsenic tri-sulfide waveguide with ultra-flat and low dispersion profile over an ultra-wide bandwidth,” *Opt. Lett.*, 2013, doi: 10.1364/ol.38.003082.

[262] X. Song, W. Tan, W. T. Snider, X. Xia and C. K. Madsen, “Gain Improvement of Er-Ti:LiNbO3 Waveguide Amplifi er by an As2 S3 Overlay Waveguide,” *IEEE Photonics J.*, vol. 3, pp. 686–695, 2011.

[263] P. Kylemark, P. O. Hedekvist, H. Sunnerud, M. Karlsson, and P. A. Andrekson, “Noise characteristics of fiber optical parametric amplifiers,” *J. Light. Technol.*, 2004, doi: 10.1109/JLT.2003.822152.

[264] B. A. V. Lyubin, M. Klebanov, B. Sfez, “Photoluminescence and photodarkening effect in erbium-dopedchalcogenide glassy films,” *Mater. Lett.*, vol. 58, pp. 1706–1708, 2004.

[265] D. Y. Choi, S. Madden, D. Bulla, R. Wang, A. Rode, and B. Luther-Davies, “Thermal annealing of arsenic tri-sulphide thin film and its influence on device performance,” *J. Appl. Phys.*, 2010, doi: 10.1063/1.3310803.

[266] A. D. Bristow, N. Rotenberg, and H. M. Van Driel, “Two-photon absorption and Kerr coefficients of silicon for 850-2200 nm,” *Appl. Phys. Lett.*, 2007, doi: 10.1063/1.2737359.

[267] C. M. Schwarz *et al.*, “Processing and properties of arsenic trisulfide chalcogenide glasses for direct laser writing of 3D microstructures,” 2014, doi: 10.1117/12.2042809.

[268] A. Zakery, Y. Ruan, A. V. Rode, M. Samoc, and B. Luther-Davies, “Low-loss waveguides in ultrafast laser-deposited As_2S_3 chalcogenide films,” *J. Opt. Soc. Am. B*, 2003, doi: 10.1364/josab.20.001844.

[269] N. S. Abdel-Moneim, C. J. Mellor, T. M. Benson, D. Furniss, and A. B. Seddon, “Fabrication of stable, low optical loss rib-waveguides via embossing of sputtered chalcogenide glass-film on glass-chip,” *Opt. Quantum Electron.*, 2015, doi: 10.1007/s11082-014-9917-z.

[270] W. C. Tan *et al.*, “Characterization and Optical Properties of Erbium doped As2S3 Films Prepared by Multi-layer Magnetron Sputtering,” *arXiv*. 2018.

[271] H. Hiramatsu, W. S. Seo, and K. Koumoto, “Electrical and Optical Properties of Radio-Frequency-Sputtered Thin Films of (ZnO)5In2O3,” *Chem. Mater.*, 1998, doi: 10.1021/cm980173b.

[272] J. Fick, É. J. Knystautas, A. Villeneuve, F. Schiettekatte, S. Roorda, and K. A. Richardson, “High photoluminescence in erbium-doped chalcogenide thin films,” *J. Non. Cryst. Solids*, vol. 272, no. 2–3, pp. 200–208, 2000, doi: 10.1016/S0022-3093(00)00119-8.

[273] M. Knadel, R. A. Viscarra Rossel, F. Deng, A. Thomsen, and M. H. Greve, “Visible-Near Infrared Spectra as a Proxy for Topsoil Texture and Glacial Boundaries,” *Soil Sci. Soc. Am. J.*, 2013, doi: 10.2136/sssaj2012.0093.

[274] H. K. Kim, C.-C. Li, X. M. Fang, G. Nykolak, and P. C. Becker, “<title>Er-doped silicate glass films prepared by co-sputtering for optical amplifiers</title>,” 1994, doi: 10.1117/12.175265.

[275] M. Rančić, “High Resolution Spectroscopy of Erbium Doped Solids,” 2018.

[276] A. Polman, D. C. Jacobson, D. J. Eaglesham, R. C. Kistler, and J. M. Poate, “Optical doping of waveguide materials by MeV Er implantation,” *J. Appl. Phys.*, 1991, doi: 10.1063/1.349234.

[277] Y. Chen *et al.*, “Comparison of magnetron sputtering and ion beam sputtering on dispersive mirrors,” *Appl. Phys. B Lasers Opt.*, 2020, doi: 10.1007/s00340-020-07431-6.

[278] T. Sabapathy, A. Ayiriveetil, A. K. Kar, S. Asokan, and S. J. Beecher, “Direct ultrafast laser written C-band waveguide amplifier in Er-doped chalcogenide glass,” *Opt. Mater. Express*, 2012, doi: 10.1364/ome.2.001556.

[279] T. Y. Ivanova, A. A. Man’shina, A. V. Kurochkin, Y. S. Tver’yanovich, and V. B. Smirnov, “Non-radiative energy transfer from Er3+ ions to the electronic states of the chalcogenide glass matrix,” 2003, doi: 10.1016/S0022-3093(03)00422-8.

[280] Y. S. T. T Yu Ivanova, A A Manshina, A V Povolotskiy and S.-K. L. and Y.-S. Hsieh, “Erbium mediated photoconductivity of Ga-Ge-S-Se: Er(3+) chalcogenide glasses,” *J. Phys. D. Appl. Phys.*, vol. 41, 2008.

[281] Y. SUN *et al.*, “Suppression of photo-induced effects in chemically stoichiometric Ge26.67Ga8S65.33 glasses,” *Opt. Mater. Express*, vol. 11, 2021.

[282] and K. V. A. P. Khan, A. R. Barik, E. M. Vinod, K. S. Sangunni, H. Jain, “Coexistence of fast photodarkening and slow photobleaching in Ge19As21Se60 thin films,” *Opt. Express*, vol. 20, 2012.

[283] S. R. E. A. Zakery, “Optical properties and applications of chalcogenideglasses: a review,” *J. Non Cryst. Solids*, vol. 330, 2003.

[284] “https://chem.libretexts.org/Courses/Franklin_and_Marshall_College/Introduction_to_Materials_Characterization__CHM_412_Collaborative_Text/Spectroscopy/Energy-Dispersive_X-ray_Spectroscopy_(EDS).”

[285] J. Fu *et al.*, “Structure and optical properties of GeGaS films deposited by thermal evaporation,” *Phys. B Condens. Matter*, 2012, doi: 10.1016/j.physb.2012.03.031.

[286] P. N. Kumta and S. H. Risbud, “Rare-earth chalcogenides - an emerging class of optical materials,” *Journal of Materials Science*. 1994, doi: 10.1007/BF00975057.

[287] F. Chen, Q. Yu, B. Qiao, T. Xu, S. Dai, and W. Ji, “Investigations of structure and nonlinear optical properties of gold doped germanium-gallium-sulfur chalcogenide glasses,” *J. Non. Cryst. Solids*, 2015, doi: 10.1016/j.jnoncrysol.2015.01.004.

[288] J.M. MerinoF. RuedaR. Diaz, “Flash evaporation of chalcogenide thin Films,” *Thin Solid Films*, 2000.

[289] R. D. L. Kristensen, S. N. Sahu, and D. Haneman, “Flash evaporation of CuInSe2 films,” *Sol. Energy Mater.*, 1988, doi: 10.1016/0165-1633(88)90015-9.

[290] Alan Bukham, “WHY GOLD SPITS DURING EVAPORATION,” *Materion.* .

[291] T. and H. M. Katsuyama, “Infrared Optical Fibres,” *Adam Hilger IOP Publ. Ltd*, 1989.

[292] and I. D. Sanghera, J. S., V. Q. Nguyen, P. C. Pureza, R. E. Miklos, F. H. Kung and Aggarwal., “Fabrication of long lengths of low-loss IR transmitting As40S(60-x)Se-x glass fibers,” *J. L ightwave Tech*, 1996.

[293] and I. D. A. Sanghera J. S., “Infrared Fiber Optics,” *Boca Raton, FL CRC Press.*, 1998.

[294] Y. D. West, T. Schweizer, D. J. Brady, and D. W. Hewak, “Gallium lanthanum sulphide fibers for infrared transmission,” *Fiber Integr. Opt.*, 2000, doi: 10.1080/01468030050058802.

[295] J. A. Frantz, L. B. Shaw, J. S. Sanghera, and I. D. Aggarwal, “Waveguide amplifiers in sputtered films of Er3+-doped gallium lanthanum sulfide glass,” *Opt. Express*, 2006, doi: 10.1364/oe.14.001797.

[296] R. J. Curry, S. W. Birtwell, A. K. Mairaj, X. Feng, and D. W. Hewak, “A study of environmental effects on the attenuation of chalcogenide optical fibre,” *J. Non. Cryst. Solids*, 2005, doi: 10.1016/j.jnoncrysol.2004.12.013.

[297] T. Schweizer, D. W. Hewak, B. N. Samson, and D. N. Payne, “Spectroscopic data of the 18-, 29-, and 43-μm transitions in dysprosium-doped gallium lanthanum sulfide glass,” *Opt. Lett.*, 1996, doi: 10.1364/ol.21.001594.

[298] A. K. Mairaj, R. J. Curry, and D. W. Hewak, “Chalcogenide glass thin films through inverted deposition and high velocity spinning,” *Electron. Lett.*, 2004, doi: 10.1049/el:20040307.

[299] A. Barnier, S., M. Guittard, M. P. Pardo, A. M. Loireau-Lozach, J. Flahaut, P. Porcher and J. Livage, “Glass forms in the Ga S -La S and Ga S -La O systems,” *Mater. Res. Bull.*, vol. 3, 1983.

[300] and N. F. B. Kang, I., T. D. Krauss, F. W. Wise, B. G. Aitken, “Femtosecond measurement of enhanced optical nonlinearities ofsulfide glasses and heavy-metal-doped oxide glasses,” *J. Opt. Soc. Am. B*, vol. 12, 1995.

[301] and D. N. P. T. Schweizer, D.J. Brady, B.N. Samson, D.W. Hewak, “PROGRESS TOWARDS MID-INFRARED FIBRE LASERS IN RARE-EARTH DOPED GALLIUM LANTHANUM SULPHIDE GLASS FOR GAS SENSING AND REMOTE SENSING,” *Opto Electron. Res. Cent.*

[302] and R. I. L. Samson, B. N., T. Schweizer, D. W. Hewak, “Properties of dysprosium doped GaLaS fibre amplifiers operating at 1.3 microns,” *opt Lett.*, 1997.

[303] K. P. J. D. W. Hewak, J. A. Medeiros Neto, B. Samson, R. S. Brown and and D. N. P. J. Wang, E. Taylor, R. I. Laming, G. Wylangowski, “Quantum-Efficiency of Praseodymium Doped Ga:La:S Glass for 1.3 pm Optical Fibre Amplifiers,” *IEEE PHOTONICS Technol. LEITERS*, vol. 6, 1994.

[304] T. Schweizer, D. W. Hewak, B. N. Samson, and D. N. Payne, “Spectroscopy of potential mid-infrared laser transitions in gallium lanthanum sulphide glass,” *J. Lumin.*, 1997, doi: 10.1016/S0022-2313(96)00387-0.

[305] B. Claudet, V. V. Sokolov, B. A. Kolesov, L. A. Sheludyakova, and I. Y. Filatova, “Rare-earth-doped lanthanum-gallium-sulfide-oxide glasses as new optically operated materials,” *J. Opt. A Pure Appl. Opt.*,

2007, doi: 10.1088/1464-4258/9/4/001.

[306] M. Petrovich, “Gallium lanthanum sulphide glasses for near-infrared photonic applications,” 2003.

[307] R. Asal, P. E. Rivers, and H. N. Rutt, “Gallium-lanthanum sulphide films for waveguide devices,” *Conf. Proc. - Lasers Electro-Optics Soc. Annu. Meet.*, 1996.

[308] K. S. Albarkaty, E. Kumi-Barimah, C. Craig, D. Hewak, G. Jose, and J. Chandrappan, “Erbium-doped chalcogenide glass thin film on silicon using femtosecond pulsed laser with different deposition temperatures,” *Appl. Phys. A Mater. Sci. Process.*, 2019, doi: 10.1007/s00339-018-2286-x.

[309] D. J. Brady, T. Schweizer, J. Wang, and D. W. Hewak, “Minimum loss predictions and measurements in gallium lanthanum sulphide based glasses and fibre,” *J. Non. Cryst. Solids*, 1998, doi: 10.1016/S0022-3093(98)00801-1.

[310] A. Anders, “Physics of arcing, and implications to sputter deposition,” 2006, doi: 10.1016/j.tsf.2005.07.228.

[311] G. Demetriou *et al.*, “Refractive index and dispersion control of ultrafast laser inscribed waveguides in gallium lanthanum sulphide for near and mid-infrared applications,” *Opt. Express*, 2016, doi: 10.1364/oe.24.006350.

[312] R. P. Wang, S. J. Madden, C. J. Zha, A. V. Rode, and B. Luther-Davies, “Annealing induced phase transformations in amorphous As2S 3 films,” *J. Appl. Phys.*, 2006, doi: 10.1063/1.2353787.

[313] V. Balan, “Verres de chalcogènures pour l’optique intégrée,” *PhD thesis, Univ. Montpellier II, Fr.*, 2003.

[314] K. Yan, B. Khu Vu, Zhiyong Yang, Rongping Wang, Sukanta Debbarma, and L.-D. and S. Madden, “Emission properties of erbium-doped Ge-GaSe glasses, thin films and waveguides for laser amplifiers,” *Opt. Matrerals Express*, vol. 4, 2014.

[315] N. V. U. M.S. Sajna, Sunil Thomas, K.A. Ann Mary, Cyriac Joseph, P.R. Biju, “Spectroscopic properties of Er3þ ions in multicomponent tellurite glasses,” *J. Lumin.*, vol. 159, 2015.

[316] Y. S. Tver’yanovich, “Concentration Quenching of Luminescence of Rare-Earth Ions in Chalcogenide Glasses,” *Glas. Phys. Chem.*, 2003, doi: 10.1023/A:1023407125519.

[317] C. Yu, S. Dai, G. Zhou, J. Zhang, L. Hu, and Z. Jiang, “The effect of OH groups on the spectroscopic properties of erbium-doped tellurite glasses,” *Sci. China, Ser. E Technol. Sci.*, 2005, doi: 10.1360/102005-38.

[318] J. jia Zhang *et al.*, “Enhanced mid-infrared emission of non-oxide erbium doped fluorochloride glass,” *Optoelectron. Lett.*, 2020, doi: 10.1007/s11801-020-9178-y.

[319] W. Wang, L. Mao, J. Liu, and S. Xu, “Glass-forming regions and enhanced 2.7 μm emission by Er3+ heavily doping in TeO2–Ga2O3–R2O (or MO) glasses,” *J. Am. Ceram. Soc.*, 2020, doi: 10.1111/jace.17217.

[320] J. FickE.J. KnystautasA. VilleneuveF. SchiettekatteS. RoordaK.A. Richardson, “High photoluminescence in erbium-doped chalcogenide thin films,” *J. Non Cryst. Solids*, vol. 272, 2000.

[321] C. Vigreux-Bercovici, A. Pradel, A. Fuchs, and J. Fick, “Effect of annealing on the photoluminescence in sputtered films of Er-doped chalcogenide glasses,” 2006.

[322] t and M. B. W Q. Shi, M. Bass, “Effects of energy transfer among Er3 ions on the fluorescence decay and lasing properties of heavily doped Er: Y 3AI5 012,” *J.Opt.Soc.Am.*, vol. 7, 1990.

[323] G. N. Van Den Hoven, E. Snoeks, A. Polman, C. Van Dam, J. W. M. Van Uffelen, and M. K. Smit, “Upconversion in Er-implanted Al2O3 waveguides,” *J. Appl. Phys.*, 1996, doi: 10.1063/1.361020.

[324] R. M. Almeida, A. C. Marques, R. Cabeça, L. Zampedri, A. Chiasera, and M. Ferrari, “Photoluminescence

of erbium-doped silicate sol-gel planar waveguides," *J. Sol-Gel Sci. Technol.*, 2004, doi: 10.1023/B:JSST.0000048010.74400.f0.

[325] Z. Pan, S. H. Morgan, A. Loper, V. King, B. H. Long, and W. E. Collins, "Infrared to visible upconversion in Er3+-doped-lead-germanate glass: Effects of Er3+ ion concentration," *J. Appl. Phys.*, 1995, doi: 10.1063/1.359436.

[326] X. Zhang, Z. Chen, and J. Qiu, "Mechanistic investigation of upconversion luminescence in Er3+-doped BaCl2, BaF2 and NaYF4 phosphors," *Mater. Chem. Phys.*, 2015, doi: 10.1016/j.matchemphys.2015.05.003.

[327] R. Li, D. Furniss, H. Bagshaw, and A. B. Seddon, "Decisive role of oxide content in the formation and crystallization of gallium-lanthanum-sulfide glasses," *J. Mater. Res.*, 1999, doi: 10.1557/JMR.1999.0351.

[328] T. SCHWEIZER *et al.*, "VISIBLE UPCONVERSION IN RARE-EARTH DOPED GALLIUM LANTHANUM SULPHIDE BASED GLASSES," *Res. Gate*, 1998.

[329] E. Preda, M. Stef, G. Buse, A. Pruna, and I. Nicoara, " Concentration dependence of the Judd–Ofelt parameters of Er 3 + ions in CaF 2 crystals ," *Phys. Scr.*, 2009, doi: 10.1088/0031-8949/79/03/035304.

[330] D. A. Ravagli, N. G. Boetti, F. A. Guzman Cruz, G. A. Alzaidy, D. Pugliese and D. M. and D. W. Hewaka, "Structural and spectral characterisation of Er3+ and Nd3+ doped Ga-La-S-Se glasses," *RSC Adv*, vol. 8, 2018.

[331] K. S. R. K. R. Z.G.Ivanova, J. Zavadil, "Compositional trends in low-temperature photoluminescence of heavily Er-dopedGeS2–Ga2S3glasses," *J. Non Cryst. Solids*, vol. 357, 2011.

[332] V. V. Halyan and I. A. Ivashchenko, "Mechanism of Photoluminescence in Erbium-Doped Chalcogenide," in *Luminescence - OLED Technology and Applications*, 2020.

[333] B.-C. Hwang, S. Jiang, T. Luo, J. Watson, G. Sorbello, and N. Peyghambarian, "Cooperative upconversion and energy transfer of new high Er^3+- and Yb^3+–Er^3+-doped phosphate glasses," *J. Opt. Soc. Am. B*, 2000, doi: 10.1364/josab.17.000833.

[334] I. V. Kityk *et al.*, "NIR and visible luminescence features of erbium doped Ga2S3–La2S3 glasses," *J. Non. Cryst. Solids*, 2018, doi: 10.1016/j.jnoncrysol.2018.03.024.

[335] V. K. Bogdanov, "Energy exchange processes in erbium-doped fluoride glasses," 1999.

[336] X. T. Zhang *et al.*, "Room-temperature blue luminescence from ZnO:Er thin films," *Thin Solid Films*, 2002, doi: 10.1016/S0040-6090(02)00356-5.

[337] V. I. Kalinchuk, V. G. Katyshov, and T. V. Shestakova, "Resolution of overlapping luminescence bands by measurement of time-resolved spectra," *J. Appl. Spectrosc.*, 1991, doi: 10.1007/BF00662417.

[338] H. S. Chin and L. S. Chao, "The effect of thermal annealing processes on structural and photoluminescence of zinc oxide thin film," *J. Nanomater.*, 2013, doi: 10.1155/2013/424953.

[339] M. TortelloS. ColonnaM. BernalJ. GomezM. PaveseC. NovaraF. GiorgisM. MaggioG. GuerraG. SaraccoR.S. GonnelliA. Fina, "Effect of thermal annealing on the heat transfer properties of reducedgraphite oxideflakes: A nanoscale characterization via scanningthermal microscopy," *Carbon N. Y.*, vol. 109, pp. 390–401, 2016.

[340] D. Y. Choi, S. Madden, D. Bulla, A. Rode, R. Wang, and B. Luther-Davies, "SU-8 protective layer in photo-resist patterning on As2S3 film," *Phys. Status Solidi Curr. Top. Solid State Phys.*, vol. 8, no. 11–12, 2011, doi: 10.1002/pssc.201000741.

[341] S. Ghazali, S. Jamar, N. Noordin, and K. M. Tan, "Properties of Controlled-Release-Water-Retention Fertilizer Coated with Carbonaceous-g-Poly(acrylic acid-co-acrylamide)Superabsorbent Polymer," *Int. J.*

Chem. Eng. Appl., 2017, doi: 10.18178/ijcea.2017.8.2.646.

[342] "(https://pdf.directindustry.com/pdf/hamamatsu-13622.html)."

[343] "http://www.teledynejudson.com/prods/Documents/InAs_shortform_Mar2003.pdf#search=J12TE4%2D3CN%2DR01M." .

[344] C. D. Tran and G. H. Gao, "Characterization of an erbium-doped fiber amplifier as a light source and development of a hear-infrared spectrophotometer based on the EDFA and an acoustooptic tunable filter," *Anal. Chem.*, 1996, doi: 10.1021/ac9600262.

[345] J. Normani, Simone, Geofrey Louvet, Emeline Baudet, Marek Bouška, Y. M. Starecki, Florent, Jean-Louis Doualan, Yannick Ledemi, and P. N. & V. N. Jean-LucAdam, "Comparative study of Er3+-doped Ga-Ge-Sb-S thin flms fabricated by sputtering and pulsed laser deposition," *Sci. Rep.*, vol. 10, p. 7997, 2020.

[346] D. Drouin, A. R. Couture, D. Joly, X. Tastet, V. Aimez, and R. Gauvin, "CASINO V2.42 - A fast and easy-to-use modeling tool for scanning electron microscopy and microanalysis users," *Scanning*, 2007, doi: 10.1002/sca.20000.

[347] J. Requejo-Isidro, A. K. Mairaj, V. Pruneri, D. W. Hewak, M. C. Netti, and J. J. Baumberg, "Self refractive non-linearities in chalcogenide based glasses," *J. Non. Cryst. Solids*, 2003, doi: 10.1016/S0022-3093(02)01798-2.

[348] O. G. Pompilian *et al.*, "Pulsed laser deposition of rare-earth-doped gallium lanthanum sulphide chalcogenide glass thin films," *Appl. Phys. A Mater. Sci. Process.*, 2014, doi: 10.1007/s00339-014-8359-6.

[349] J. Normani, Simone, Geofrey Louvet, Emeline Baudet, Marek Bouška, F. Starecki, Y. L. , Jean-Louis Doualan4, Y. Messaddeq, and P. N. & V. N. Jean-LucAdam, "Comparative study of Er3+-doped Ga-Ge-Sb-S thin flms fabricated by sputtering and pulsed laser deposition," *Sci. Rep.*, vol. 10, 2020.

[350] G. C. Xie *et al.*, "Effect of In-doping on the Optical Constants of ZnO Thin Films," 2012, doi: 10.1016/j.phpro.2012.03.614.

[351] D. W. Hewak *et al.*, "Chalcogenide glasses for photonics device applications," 2010.

[352] "Royston Paynter, "XPS Theory."

[353] S. J. Kerber, J. J. Bruckner, K. Wozniak, S. Seal, S. Hardcastle, and T. L. Barr, "The nature of hydrogen in x-ray photoelectron spectroscopy: General patterns from hydroxides to hydrogen bonding," *J. Vac. Sci. Technol. A Vacuum, Surfaces, Film.*, 1996, doi: 10.1116/1.579947.

[354] T. L. Barr, *Modern ESCA : the principles and practice of X-Ray photoelectron spectroscopy*. 1994.

[355] G. B. and D. Briggs, *High Resolution XPS of Organic Polymers*. 1992.

[356] J. Xie *et al.*, "Controllable disorder engineering in oxygen-incorporated MoS2 ultrathin nanosheets for efficient hydrogen evolution," *J. Am. Chem. Soc.*, 2013, doi: 10.1021/ja408329q.

[357] Q.-H. Wu, M. Liu, and W. Jaegermann, "Erratum to 'X-ray photoelectron spectroscopy of La0.5Sr0.5MnO3,'" *Mater. Lett.*, 2005, doi: 10.1016/j.matlet.2004.12.060.

[358] Y. Cai *et al.*, "Easy incorporation of single-walled carbon nanotubes into two-dimensional MoS2 for highperformance hydrogen evolution," *Nanotechnology*, vol. 25, 2014.

[359] M. L. Qi-Hui Wu, T and W. Jaegermann, "X-ray photoelectron spectroscopy of La0.5Sr0.5MnO3," *Mater. Lett.*, vol. 59, 2005.

[360] J. P. H. Li *et al.*, "Understanding of binding energy calibration in XPS of lanthanum oxide by: In situ

treatment," *Phys. Chem. Chem. Phys.*, 2019, doi: 10.1039/c9cp04187g.

[361] "https://www.jp.xpssimplified.com/elements/gallium.php." .

[362] G. Cossu, G. M. Ingo, G. Mattogno, G. Padeletti, and G. M. Proietti, "XPS investigation on vacuum thermal desorption of UV/ozone treated GaAs(100) surfaces," *Appl. Surf. Sci.*, 1992, doi: 10.1016/0169-4332(92)90219-N.

[363] "https://www.thermofisher.com/au/en/home/materials-science/learning-center/periodic-table/lanthanide-rare-earth/lanthanum.html)."

[364] "https://srdata.nist.gov/xps/EngElmSrchQuery.aspx?EType=PE&CSOpt=Retri_ex_dat&Elm=La."

[365] "https://www.jp.xpssimplified.com/elements/lanthanum.php." .

[366] "https://www.jp.xpssimplified.com/elements/erbium.php." .

[367] E. M. and J. P. Wightman, "Determination of the Concentration of SurfaceHydroxyl Groups on Metal Oxide Films by aQuantitative XPS Method," *Surf. interface Anal.*, vol. 26, 1998.

[368] V. V. H. Y. K. A. I. H. K. D. O. T. P. V. V. Bulik, "Electronic structure and optical properties of (Ga70La30)2S300and(Ga69.75La29.75Er0.5)2S300single crystals, novel light-converting materials," *Phys. B Condens. Matter*, vol. 544, 2018.

[369] A. L. Strizik, T. Wagner, V. Weissova, J. Oswald, K. Palka and C. K. and S. O. K. L. Benes, M. Krbal, R. Jambor, "Solution-processed Er3+-doped As3S7 chalcogenide films: optical properties and 1.5 lm photoluminescence activated by thermal treatment," *J. Mater. Chem. C*, vol. 5, 2017.

[370] M. F. Hssen Fares, iIfa JlassiS. HraiechS., "Radiative parameters of Nd3+-doped titanium and tungsten modified tellurite glasses for 1.06 μm laser materials," *J. Quant. Spectrosc. Radiat. Transf.*, vol. 147, 2014.

[371] X. L. and X. G. Jiajia Zhang , Xiaosong Zhang, Lan Li, Shaohua Wu, Hao Yin, "Enhanced mid infrared emission of erbium doped fluoro-zinc glassceramics," *Mater. Res. Express*, vol. 6, 2019.

[372] S. D. Jackson, M. Pollnau, and J. Li, "Diode pumped erbium cascade fiber lasers," *IEEE J. Quantum Electron.*, 2011, doi: 10.1109/JQE.2010.2091256.

[373] "https://www.idealvac.com/Brooks-Cryogenics-CTI-Cryo-Torr-10-Vacuum-Pump/pp/P109174." .

[374] Dieter Muller, "HOW CRYOPUMPS WORK: A DETAILED GUIDE ON THEIR USE," 2020. .

[375] E.Al-Dmour, "Fundamentals of Vacuum Physics and Technology," *CERN*, 2017.

[376] U. Education, "Repetition: Physical Deposition Processes."